Beach cusps in a low-energy lake environment

Relating hydrodynamics to coastal feature formation at the Houtribdijk

T. van Meurs

TUDelft   Delft
University of
Technology

Beach cusps in a low-energy lake environment

Relating hydrodynamics to coastal feature formation at the Houtribdijk

By

T. (Tom) van Meurs

in partial fulfillment of the requirements for the degree of

Master of Science
in Hydraulic Engineering

at the Delft University of Technology,
to be defended publicly on November 10, 2020.

Thesis committee:	Prof. dr. ir. S.G.J. (Stefan) Aarninkhof,	Chairman, TU Delft
	Ir. A.M. (Anne) Ton,	TU Delft
	Prof. dr. ir. A.J.H.M. (Ad) Reniers,	TU Delft
	Prof. dr. ir. J.A. (Dano) Roelvink	UNESCO-IHE

Cover photo: Bureau Start the Future, 2020, commissioned by Rijkswaterstaat

Preface

This thesis is the final part of the Master of Science program Hydraulic Engineering of the Delft University of Technology. I am grateful for the support and the readiness of all people I have met during my thesis, you have been very motivating.

To start, many thanks to Anne Ton, my supervisor during the thesis and part of my graduation committee. She was the one who introduced me to the wonderfully complex topic of low-energy environments. Without her insightful feedback this thesis would not have had the depth and structure it now has. Thanks for always having the time to discuss any difficulties that I ran into.

Next, I would like to thank my other committee members. Prof. Stefan Aarninkhof, thank you for being my chairman and making me realize the bigger picture, thereby helping me generalize my study. This is what made it a more relatable part of the knowledge of these environments. Prof. Ad Reniers, thank you for referring me to the state-of-the-art theory and numerical model, you provided me the tools to give my thesis that much more depth. I would also like to thank Prof. Dano Roelvink, for having made the innovate open source model ShorelineS and helping me understand it. Applying the model gave me much more insight in the processes involving high-angle waves.

Also, thanks to all the people working together at project LakeSIDE, some of whom I was lucky to have met in person despite the COVID-19 pandemic. Thanks to Rinse Wilmink working at Rijkswaterstaat WVL, for always being ready to help and bringing me into contact with other people involved in this project.

Finally, I would like to thank my parents for always being ready to help me with whatever I needed, thank you for bearing with me as I went into way too much detail at the dinner table.

Tom van Meurs

Delft, November 2020

Summary

In the recent decades, the threat of rising sea levels has become more and more prevalent. Coastal, as well as inland regions, are being affected by the consequences of keeping sea water out, while at the same time preventing river discharge from flooding our hinterland. Dikes are often an important part of flood safety networks. In the Netherlands, one such dike, the Houtribdijk, separates two main fresh-water bodies and provides a road connection between the provinces of Noord-Holland and Flevoland.

At the beginning of 2019, construction of nature-based sandy shores along large parts of the dike was finished. These sandy shores are an integrated part of the dike, contributing to flood safety. Unavoidable perturbations of the waterline, leftovers from construction, were seen to evolve into cusp-like shapes in a matter of months. Later, it was even found that stormy conditions could change the shape of features on the scale of days.

The construction of sandy shores in an inland lake was a novelty. The wave damping function of beaches in general is proven, but not yet in this scenario. Environments like these are less exposed to hydrodynamic forcing and less energetic, resulting in them being generally less studied. Despite this, low-energy environments like these are highly morphologically variable, and sensitive to changes in wave climate.

To expand our knowledge on low-energy environments, the goal of this thesis is to find out the causes of the formation of the beach cusps and their morphodynamic behavior on the sandy shores of the Houtribdijk. A major part of this was classifying the system and finding the physical processes responsible. Physical processes, in this context, are the interaction between waves, flow and morphology.

A literature study was performed, from which it followed that the possible cause is instabilities due to high-angle waves. The theory indicates that waves that approach the beach under an acute angle of incidence will cause the growth of perturbations. On top of that, studies have shown that low-energy environments like ours typically experience steep, erosive, waves that refract less (as compared to common open ocean coasts).

Further classification included the distinction between calm and stormy conditions, to isolate hydrodynamics that are the likely cause for morphological change. Subsequently, we used field measurements to find the position of our waterline. This led to quantifying our beach cusps based on their numbers, horn positions, wavelengths, amplitudes, and shape asymmetry ('leaning' of the cusps). We derived a micro scale conceptual model (single cusps), which is based on the existing theory of high-angle waves. For example (Figure 1-1), when most waves arrive at the beach from the left we expect the cusp to move and 'lean' to the right (in the direction of the waves), and grow in amplitude.
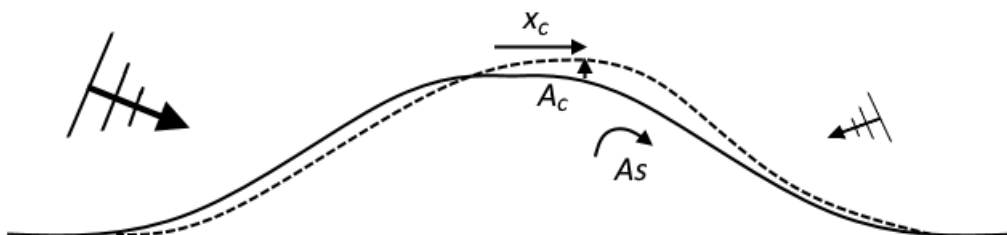
Figure 1-1: Conceptual model for cusps influenced by waves. Arrows on the side indicate that most waves arrive from the left. Morphological change is quantified by horn position (x_c), amplitude (A_c), and shape asymmetry (As).

Summary

Expanding the conceptual model to the macro scale (entire stretches of beach) allowed us to find representative hydrodynamic conditions that were considered responsible for the measured morphological changes. Here, it was found that increase in the number of cusps was mostly caused by high-angle waves. Similarly, the shape asymmetry and horn position generally changed to reflect leaning in the direction of the waves (i.e. to the right if waves came from the left). Changes in amplitudes would sometimes be inconsistent with the conceptual model, but wavelengths were predicted qualitatively correct. Cases where hydrodynamics were relatively constant in time (apart from the wave conditions), were seen to be most consistent with our conceptual model.

The data analysis indicated that cusp development is steered by the high-angle wave mechanism. However, it was also found that our low-energy environment is complex. Other processes, like water level fluctuations, were found to sometimes explain discrepancies between conceptual model and field measurements, but not always. Consistent with literature on low-energy environments, it seems that calm conditions have insufficient power to cause morphological change. Instead, it seems the waterline inherits its features from 'higher'-energy (stormy) events.

To expand on our findings, the numerical model ShorelineS was applied. This model is specifically designed to reproduce instabilities caused by high-angle waves. The simulation results seemed to agree well with our conceptual model, which was to be expected, as they are based on the same theory. However, like for the data analysis, amplitudes and shape asymmetry of the model simulations would occasionally be inconsistent with measured changes in these quantities. This, combined with the data analysis, led to the conclusion that the high-angle wave mechanism is an important process during stormy conditions, but our environment could be dominated by other processes during calmer periods.

Altogether, the stormy conditions, shape of the cross-shore profile, steep and erosive waves, and large nearshore wave incidence angles are all characteristic of our low-energy environment. Studies have linked all of these characteristics to the formation of coastal features. For the Houtribdijk specifically, this has led to the regular emergence and dissipation of small beach cusps, often found along the larger, more persistent cusps.

From the waterlines analyzed in our study, we found that there was a slight retreat (10 to 20 m in eight months). However, due to the waterline defined at an elevation close to the average water level, and the transition from winter to summer water levels in the analyzed period, it is yet unclear if there is structural retreat. The larger, more persistent, cusps can be seen to slowly migrate Southward (approximately 20 to 30 m in eight months). It seems that net longshore sediment transport is therefore small, but a more in-depth analysis will be required to establish volume distributions due to the development of the coastal features.

To conclude, it seems wave forcing certainly contributes to morphological change, but it is likely not the sole process responsible. The horns of the cusps may move and 'lean' in the general direction where the waves are going. The number of cusps may increase for high-angle waves and decrease for low-angle conditions. Initial construction of the sandy shores left larger and more prominent cusps, of which the horns could be reshaped by stormy conditions. Like the smaller cusps that would often emerge and dissipate under the influence of waves, these horns could reshape on timescales in the order of days. The larger cusps themselves could, over the course of months, be seen to slowly migrate in the dominant wave direction. All in all, lake environments like the IJsselmeer have many properties that literature has linked to three-dimensional coastal features (e.g. beach cusps). Despite the low-energy aspect, these environments have proven to have a very dynamic morphology, and it seems that sandy shores in a low-energy lake environment are very likely to develop coastal features.

Samenvatting

In recente decennia is de bedreiging van zeespiegelstijging meer en meer heersend geworden. Zowel aan de kust als landinwaarts, worden steeds meer gebieden beïnvloed door de gevolgen van het buiten houden van zeewater, terwijl men tegelijkertijd het overstromen van de rivieren in het achterland probeert te voorkomen. Dijken zijn vaak een belangrijk deel van het waterveiligheidsnetwerk. Eén zo'n dijk in Nederland, de Houtribdijk, scheidt twee waterlichamen en biedt een wegverbinding tussen de provincies Noord-Holland en Flevoland.

Aan het begin van 2019 was de aanleg van 'nature-based' zandige versterkingen van grote delen van de dijk afgerond. Deze zandige kusten vormen een integraal deel van de dijk, waar ze bijdragen aan waterveiligheid. Onvermijdelijke verstoringen van de waterlijn, overblijfselen van de aanleg, veranderden zichtbaar in gepiekte vormen in een kwestie van maanden. Later kwam men er zelfs achter dat stormachtige omstandigheden de vorm van pieken in een kwestie van dagen konden veranderen.

De aanleg van zandige kusten aan een binnenmeer was nieuw. De golfdempende functie van een strand is bewezen, maar nog niet in deze situatie. Omgevingen als deze zijn minder blootgesteld aan de hydrodynamica en minder energetisch, wat ertoe heeft geleid dat ze over het algemeen minder bestudeerd zijn. Desondanks zijn deze laag-energetische omgevingen erg morfologisch variabel en gevoelig voor veranderingen in het golfklimaat.

Om onze kennis van laag-energetische omgevingen uit te breiden, is het doel van deze thesis het achterhalen van de oorzaken van de vorming van strandpieken en hun morfodynamische gedrag op de zandige kusten van de Houtribdijk. Een groot deel hiervan was de classificering van het systeem, en het vinden van de fysieke processen die verantwoordelijk waren. In deze context zijn fysieke processen de interactie tussen golven, stroming, en morfologie.

Er is een literatuurstudie verricht, waaruit volgde dat de mogelijke oorzaak golven die onder een hoge hoek op het strand aankomen is. De theorie geeft aan dat deze 'hoge-hoek' golven de groei van verstoringen veroorzaken. Daarbovenop hebben studies aangetoond dat laag-energetische omgevingen, zoals de onze, golven ervaren die stijl en erosief zijn, en weinig refractie ervaren (in vergelijking met kusten aan de open oceaan).

Verdere classificering bevatte het onderscheid tussen rustige en stormachtige omstandigheden, zodat we de hydrodynamica konden isoleren die waarschijnlijk de oorzaak was van morfologische veranderingen. Vervolgens gebruikten we velddata om de positie van de waterlijn te vinden. Dit leidde tot kwantificering van het gepiekte strand, gebaseerd op het aantal pieken, de positie van de punten, hun golflengtes, amplitudes, en de asymmetrie van de vormen (het 'leunen' van de pieken). We leidden een conceptueel model af voor de micro schaal (enkele strandpieken), gebaseerd op de bestaande theorie van hoge-hoek golven. Bijvoorbeeld (Figuur 1-2), wanneer de meeste golven van links op het strand aankomen verwachten we de piek naar rechts te bewegen en 'leunen' (in de richting van de golven), en de amplitude te groeien.
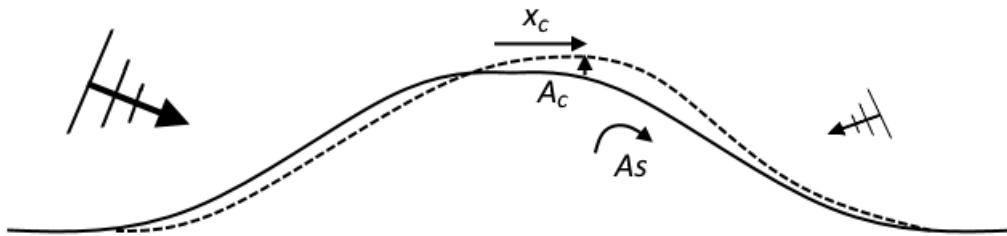
Figuur 1-2: Conceptueel model voor kustpieken beïnvloed door golven. Pijlen aan de zijkanten geven aan dat de meeste golven van links komen. Morfologische verandering is gekwantificeerd door piek positie (x_c), amplitude (A_c), en vorm asymmetrie (As).

Het conceptueel model werd uitgebreid naar de macro schaal (hele strandsecties), zodat representatieve hydrodynamische condities gevonden konden worden die geacht werden verantwoordelijk te zijn voor de gemeten morfologische veranderingen. Hier vonden we dat toename in het aantal pieken grotendeels veroorzaakt werd door hoge-hoek golven. Evenzo bleken veranderingen van de asymmetrie van de vormen en de posities van de punten over het algemeen overeen te komen met de richting van de golven (d.w.z. naar rechts als golven van links komen). Veranderingen in amplitudes waren soms inconsistent met ons conceptuele model, maar golflengtes werden kwalitatief correct voorspeld. Situaties waar de hydrodynamica in de tijd relatief constant bleef (afgezien van het golfklimaat) bleken het meest consistent met ons conceptueel model te zijn.

De data-analyse gaf aan dat ontwikkeling van het gepiekte strand gestuurd wordt door het hoge-hoek mechanisme. Echter, we ontdekten ook dat onze laag-energetische omgeving complex is. Andere processen, zoals fluctuaties in het waterniveau, konden soms de tegenstrijdigheden tussen het conceptueel model en de veldmetingen verklaren, maar niet altijd. Het bleek, overeenkomende met de literatuurstudie, dat rustige omstandigheden onvoldoende kracht hadden om morfologische veranderingen te veroorzaken. In plaats daarvan bleek de waterlijn overblijfselen te vertonen van 'hoger'-energetische (stormachtige) gebeurtenissen.

Uitbreidend op onze bevindingen pasten we het numerieke model ShorelineS toe. Dit model is specifiek ontworpen om verstoringen door het hoge-hoek mechanisme te kunnen nabootsen. De resultaten van de simulaties bleken overeen te komen met ons conceptuele model, wat te verwachten was, gezien ze op dezelfde theorie gebaseerd zijn. Echter, zoals met de data-analyse, bleken amplitudes en vorm asymmetrie van de model simulaties soms inconsistent te zijn met de gemeten veranderingen in deze hoeveelheden. Dit, in combinatie met de data-analyse, leidde tot de conclusie dat het hoge-hoek mechanisme belangrijk is tijdens stormachtige omstandigheden, maar onze omgeving tijdens rustigere omstandigheden overheerst zou kunnen worden door andere processen.

Alles bij elkaar zijn de stormachtige omstandigheden, vorm van het dwarsprofiel van het strand, steile en erosieve golven, en grote invalshoeken van de golven nabij de kust allemaal kenmerkend voor onze laag-energetische omgeving. Studies hebben al deze kenmerken verbonden met het ontstaan van kustvormen. Specifiek voor de Houtribdijk heeft dit geleid tot het regelmatig verschijnen en verdwijnen van kleine pieken, die men vaak vond aan de grotere, persistente pieken.

Op basis van de waterlijnen gevonden in onze studie, vonden we een kleine terugtrekking van de waterlijn (10 tot 20 m in acht maanden). Echter, vanwege de definitie van de waterlijn op een hoogte dicht bij het gemiddelde waterniveau, en de overgang van winter- naar zomerpeil in de geanalyseerde periode, is het nog onduidelijk of er structurele terugtrekking is. De grotere, meer persistente, strandpieken migreren langzaam naar het zuiden (ongeveer 20 tot 30 m in acht maanden). Het lijkt daardoor dat netto sediment transport langs de kust klein is, maar een meer diepgaande analyse zal nodig zijn om volumeverdelingen als gevolg van de ontwikkeling van de kustvormen te bepalen.

Ter conclusie blijken hoge-hoek golven zeker bij te dragen aan morfologische veranderingen, maar zijn waarschijnlijk niet het enige verantwoordelijke proces. De punten van de strandpieken kunnen bewegen en 'leunen' in de algemene beweegrichting van de golven. Het aantal strandpieken kan toenemen onder invloed van hoge-hoek golven, en afnemen bij lage-hoek condities. De aanleg van de zandige versterking liet grotere en prominentere pieken achter, waarvan de punten hervormt konden worden door stormachtige condities. Zoals de kleinere pieken die regelmatige ontstonden en dissipeerden onder de invloed van golven, konden de punten vervormen op een tijdsschaal in de orde van dagen. De grotere pieken migreerden zelf in de loop van maanden in de dominante golfrichting. Alles bij elkaar hebben meer-omgevingen zoals het IJsselmeer veel eigenschappen die de literatuur heeft verbonden aan driedimensionale kustvormen (zoals de strandpieken). Ondanks het laag-energetische aspect hebben deze omgevingen laten zien dat ze een erg dynamische morfologie hebben, en bleek het ontwikkelen van dergelijke vormen aan zandige kusten in laag-energetische omgevingen zeer waarschijnlijk.

Table of contents

List of figures

List of figures

List of tables

1 Introduction

The topic of coastal protection is becoming more and more relevant, especially with regards to climate change and the predicted sea level rise. No matter what the exact consequences will be, flood safety will have an increasing impact on many peoples' lives. Countries like The Netherlands are even more so at risk, being located in a delta area and a large portion of it below sea level. Expanding knowledge on the way coastal defenses may prevent flooding is therefore an ongoing field of research.

1.1 Background and relevancy

The overarching topic of the thesis concerns a project commissioned by Rijkswaterstaat (the Dutch Directorate-General for Public Works and Water Management). The Houtribdijk (see Figure 1-2), is a coastal defense structure situated in between the cities of Lelystad and Enkhuizen and separates the IJsselmeer and Markermeer fresh-water lakes. Originally, the Houtribdijk was intended to be a dike, protecting the proposed, but never realized, Markerwaard polder. Since this plan was cancelled, it now serves as a dam between the two water bodies.

The dike was reinforced with a nourishment of roughly 10 million cubic meters of sand (Rijkswaterstaat, n.d.). This was done to keep the dike up to code (safety standards as described in the Dutch 'Waterwet'). Using sandy shores as flood protection in a lake without tides is a novelty. Its construction completed in March of 2019, however, due to strong winds blowing some of the sand onto the nearby provincial road, the sandy shore had been partly covered with coarser material and grass. This led to the current state of the Houtribdijk, see Figure 1-1, which shows that features that look like beach cusps have emerged at the location of the Houtribdijk. The topic of the thesis concerns expanding knowledge and answering questions regarding the formation of these cuspate features.

Figure 1-1: Aerial photo of the Houtribdijk case location including the coastal features (Janssens, 2019).
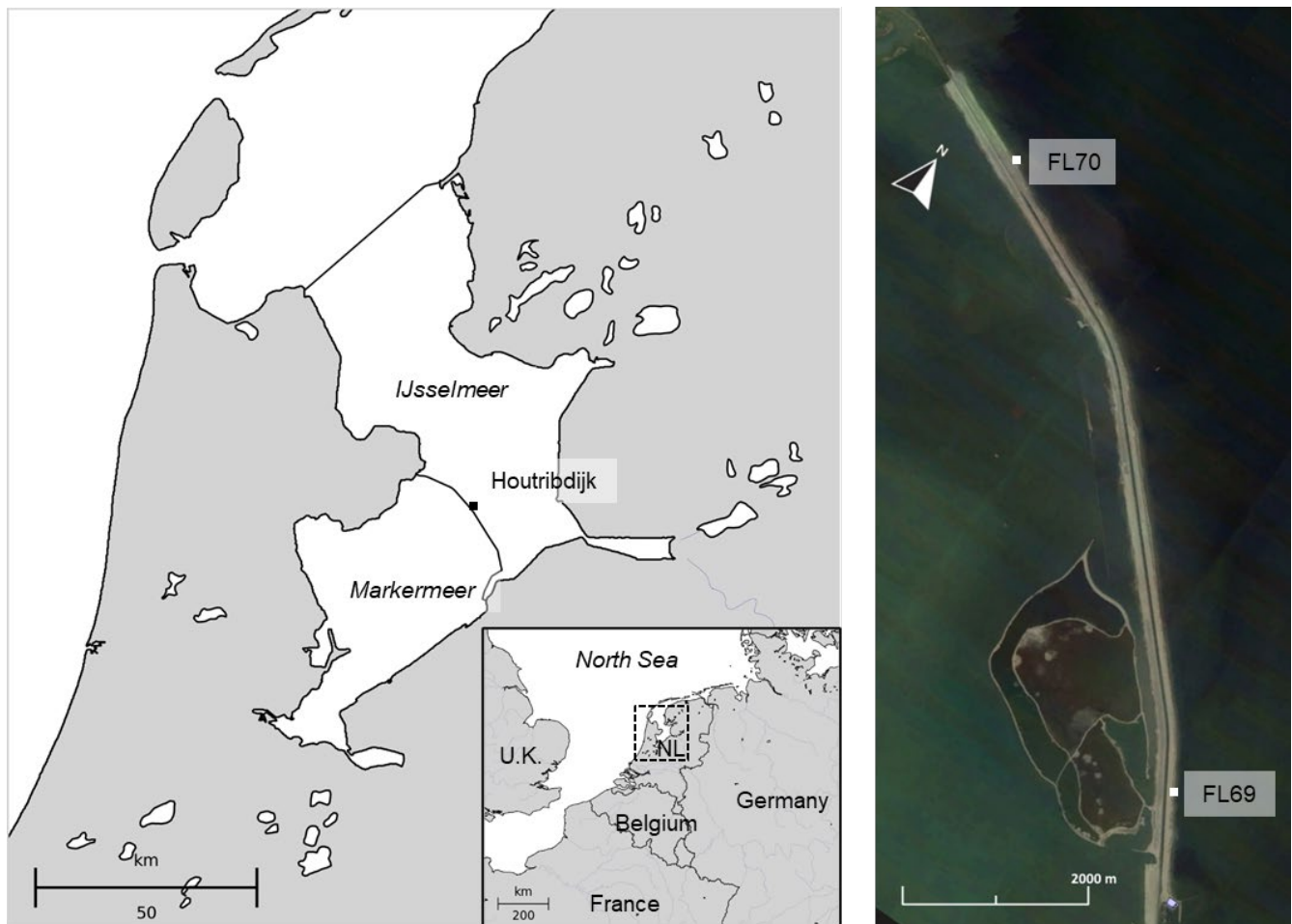
Figure 1-2: Location of the Houtribdijk on the map (Google, n.d.).

The intent of the thesis is expanding existing knowledge in the field of Coastal Engineering, being part of the LakeSIDE (Lake Shore Interconnecting Defense and Environment) project. LakeSIDE is financed by Rijkswaterstaat and partly executed by Delft University of Technology. LakeSIDE is part of the research and monitoring program by Rijkswaterstaat, aimed at expanding knowledge on "efficient and effective management and maintenance of sandy reinforcements" (Ton, 2019).

1.2 Problem statement

Since the Houtribdijk's main function is flood safety, its structural integrity is paramount. Elaborating the understanding of the wave damping effect of sandy reinforcements helps coastal engineers in the design of coastal defense structures, as reducing loads decreases the probability of failure. Understanding the physical processes that lead to the formation of the characteristic coastal features is the first step in understanding the impact they have on the sandy shores. Physical processes in this context are considered the interaction between waves, flow (hydrodynamics) and morphology (morphodynamics).

The most exposed and energetic coasts are historically studied the most. As such, the coasts of short-fetch or low-energy environments are much less studied (Lorang et al., 1993; Nordstrom & Jackson, 2012). Reports on the field pilot at the Markermeer side of the Houtribdijk affirm the lack of knowledge of 'low-energy' (lake) environments (Steetzel et al., 2017; Ton et al., 2019). Environments like these have a high variability in coastal morphology and may be sensitive to changes in wave climate (Wright & Short, 1984). We may apply models, but since this application of sandy shores is new, validation

may be difficult. Finding a model that will accurately predict the formation of the coastal features therefore poses another challenge.

1.3   Research questions

The main goal of the thesis is expanding our current knowledge of low-energy environments. Here, we specifically focus on understanding the physical process that drives the beach cusps. This in turn will help us understand the morphodynamic behavior of the cusps and what this means for the sandy shores on the IJsselmeer side of the Houtribdijk. In the search for the physical process behind the feature formation, the focus is the interaction between morphology and hydrodynamics.

The main research question is defined as follows:

What are the causes of the formation of the beach cusps and their morphodynamic behavior on the sandy shores of the Houtribdijk?

Which may be answered by elaboration of the following sub-questions:

1. What knowledge of beach cusps formation in low-energy environments exists in literature?

    A. What are the characteristic shape and dimensions of beach cusps?
    B. Which physical processes are used to explain the formation of beach cusps?

2. What classification may be assigned to the beach cusps at the Houtribdijk?

    A. Which hydrodynamic processes are responsible for the formation of beach cusps?
    B. Which morphodynamic processes contribute to the formation of beach cusps?

3. How can we simulate the morphodynamics of beach cusps at the Houtribdijk?

    A. Which numerical model may be used to substantiate the processes causing beach cusps?
    B. Which numerical model may be used to reproduce the morphodynamics?
    C. What combination of calibration settings may be used to represent the beach cusps best?
    D. What differences and similarities do the model show when validating with other periods in time?

4. How does the morphodynamics of beach cusps influence the sandy shore of the Houtribdijk?

    A. What morphodynamic behavior of the beach cusps can be used to assess volume distributions?
    B. What are the effects of volume distributions on the sandy shores?

1.4   Reading guide

Below, we provide an overview of the topics discussed in this thesis report, and where to find them.

- **Theoretical background:**
  Contains the literature study, which is mostly focused on answering the first research question. We start with the definitions used in our report (Section 2.1). Information on physical processes we suspect are relevant to the formation of the coastal features may be found in Section 2.2. To follow this topic, we elaborate on ways to reproduce the morphodynamics of the coastal features using numerical models, in Section 2.3. Lastly, in Section 2.4 we describe the process

of wave angle of incidence in relation to small scale morphological changes, based on the theory in the preceding sections.

- **Methodology:**
  We explain the approach taken to answer our research questions. To start, Section 3.1 includes the general outline of this approach, providing an overview of the steps taken in the following chapters. In Sections 3.2 and 3.3 some more in-depth descriptions of our methods are given for the hydrodynamics and morphodynamics, respectively.

- **Hydrodynamics:**
  Using what we learned from the theoretical background, we classified our environment based on the hydrodynamics. In Section 4.1 we describe how this was done based on nearshore wave refraction and by making a distinction between 'calm' and 'stormy' conditions. Next, in Section 4.2 we use a couple of parameters found during our literature study to make a first estimate of the relation between the hydrodynamics and the morphology of the beach cusps. The last part, Section 4.3, provides an overview of the results of the hydrodynamic classification of our environment. This section partly answers the research question regarding finding the hydrodynamic process responsible for the formation of beach cusps.

- **Morphodynamics:**
  This chapter is started with an overview of orthogonal photos and satellite imagery in Section 5.1. Using measurement data, the waterline position was located (Section 5.2), and the cusps were quantified (Section 5.3). A conceptual model, based on the theoretical background, was expanded to the scale of the entire stretch of coast (macro scale, Section 5.4). This conceptual model was applied to derive representative hydrodynamic conditions in Section 5.5. In Section 5.6, these results were interpreted and used to answer the research question concerning the classification of the beach cusps at the Houtribdijk.

- **Numerical modeling:**
  In this chapter we try to substantiate our findings using the numerical model ShorelineS. But first, requirements for our model are elaborated in Section 6.1, as found from our data analysis. Subsequently, we describe how we set-up and calibrated our model in Section 6.2. Results of our simulations, and the comparison with our data analysis, may be found in Section 6.3. We will elaborate more on these results, relating them back to our research question concerning the simulation of the morphodynamics of beach cusps, in Section 6.4.

Many other topics were also treated, but did not end up in the main report. These topics will be included in the appendices and referenced whenever relevant.

2 Theoretical background

The focus of this chapter is providing the theory on which most of the methodology and results of this report are based. As such, the first research question is elaborated here. In Section 2.1 we define what we mean by beach cusps and describe what quantification exists in literature. Research question 1A is then partly answered, with the rest of the quantification described in the conceptual model of Section 2.4. The physical processes from question 1B are mostly investigated in Sections 2.2 and 2.3, where we describe concepts and model applications found in literature.

2.1 Definitions

The following paragraphs elaborate on the definitions found in literature, which were subsequently used in this report.

2.1.1 Beach cusps

Werner & Fink (1993) use the general term 'beach cusp' to describe the coastal features we observe. They show that beach cusps can be simulated by the 'self-organizing' process (see Section 2.2.1) of local swash flow and feedback from morphology. Goodfellow & Stephenson (2005) suggest breaking waves, longshore currents, and a highly variable wave climate (both in magnitude and direction) as the general cause for change in morphology. A review paper by Coco & Murray (2007) describes both 'beach cusps' and 'cuspate' features, the former being small scale (spacing of order 10's m) and the latter being large scale (spacing order of km's). Explanations given are related to swash zone flow excursion and high-angle wave instabilities (see Section 2.2.3), respectively. Falqués et al. (2017) and Mujal-Colilles et al. (2019) likewise describe spacing in the order of 10's m. Ashton & Murray (2006a) describe features emerging due to high-angle waves as 'cuspate' (spacing same order of magnitude). More recent model simulations by Daly et al. (2019) use both 'beach cusps' and 'cuspates' to describe the same feature. Here, the features are initiated by processes in the surf and swash zone, controlled by wave asymmetry and skewness. Subsequent development of the features is attributed to positive feedback from the morphology ('self-organization').

In short, most recent studies on the topic describe these features as originating from 'self-organizing' processes, as opposed to 'forcing templates'. Since the physical process behind the coastal feature formation is precisely what we are looking for, the only sure difference between 'beach cusps' and 'cuspates' is their dimensions. Therefore, the term 'beach cusp' will be used to describe the coastal features observed at the Houtribdijk.

2.1.2 Low-energy environments

Low-energy beaches are generally characterized by low significant wave heights, though the exact definition of such beaches is not clear (Goodfellow & Stephenson, 2005). Jackson et al. (2002) found that definitions often include significant wave heights or storm wave heights. Specifically, low-energy environments experience little to no influence of tides, as tidal energy is generally expected to inhibit the growth of coastal features. A paper on the field pilot at the Markermeer side of the Houtribdijk, by Steetzel et al. (2017), mentions that the lack of tide is indeed the cause of more or less permanent profile change (no profile recovery).

Commonly, beaches are classified by their current morphodynamic regime, or beach state, that is evaluated with the dimensionless fall velocity (Wright & Short, 1984). However, this classification may not apply to low-energy beaches due to their variability (Goodfellow & Stephenson, 2005). Low-energy environments are sometimes referred to as fetch-limited environments because the wind generates small waves that are steep, erosive and less affected by refraction (Jackson et al., 2002). The term fetch-limited is often used when wave conditions were unknown, and these conditions have to be derived from wind data, as originally described by Bretschneider (1964).

They refract less because they are low and short, meaning they are affected by bottom friction only relatively close to the shore. A fetch-limited environment is characterized by an undeveloped wind wave climate. Both reflective and intermediate beach states are expected to show a combination of three-dimensional features (Wright & Short, 1984).

Due to the clear criteria of Jackson et al. (2002), and to be consistent in what is meant by the term 'low-energy', the following criteria are used (Jackson et al., 2002): (1) Significant wave height H_s less than 0.25 m, (2) wave height during storm set-up H_{ss} less than 0.50 m, (3) a narrow beach with a width less than 20 m and (4) the beach must contain features inherited from higher energy events. Also, since we already have accurate measurement data available, it makes sense to use the term 'low-energy' instead of 'fetch-limited'.

2.1.3 Submerged platform

Studies have observed a sort of platform (mildly sloped bathymetry in the cross-shore profile) just seaward of the shoreline (Goodfellow & Stephenson, 2005; Jackson et al., 2002; Mujal-Colilles et al., 2019). The field pilot on the Markermeer side of the Houtribdijk shows such a cross-shore shape as well (Ton et al., 2019). Beach measurements have shown that they are also found at the IJsselmeer side, see Figure 2-1. Such a physical feature will be referred to as 'platform' or 'terrace' in this document. More recently, Ton et al. (2020) suggest that the elevation of the platforms (at the Markermeer side) will reach a dynamic equilibrium, given relatively constant conditions and sufficient time. Based on the figure below, the third low-energy criterium (previous section), a beach face width of less than 20 m, is already fulfilled.
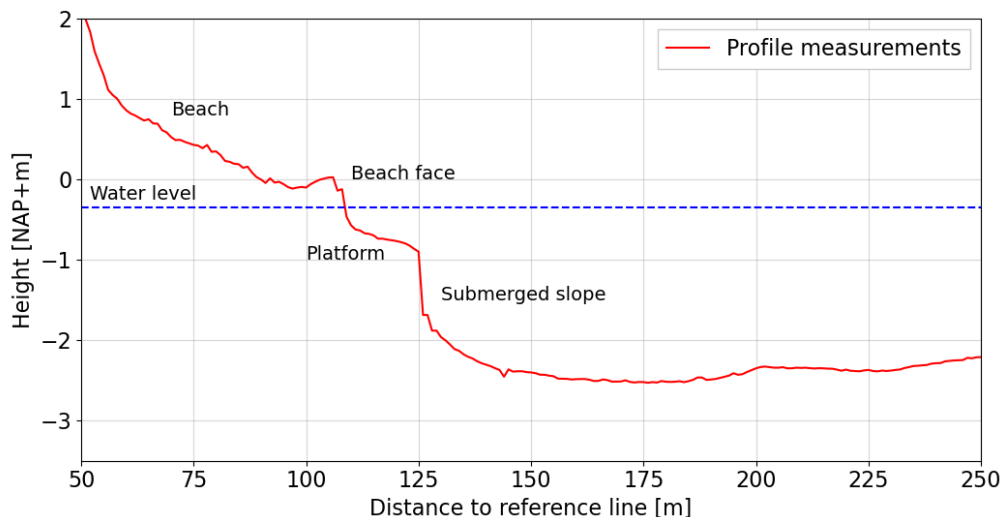
Figure 2-1: Transect measurement of November 2019 near location FL69 (at km 59.950).

2.1.4 Wave climate parameters

A study on high-angle wave instability classifies several emerging coastal features, namely sand waves, spits and capes, based on two parameters (Ashton & Murray, 2006a). However, these parameters were not explicitly defined. Based on their analysis, it is assumed that they used the following formulation, where φ is defined as the angle of the approaching wave to the shore-normal (see Figure 2-2). The first parameter (U) is the number of high-angle 'unstable' waves ($45° < \varphi < -45°$) with respect to the total number of onshore travelling waves. Another parameter is the directional asymmetry (A) in the wave climate, indicated by the proportion of rightward travelling waves ($\varphi > 0$, as seen from the plan view) to the total number of onshore travelling waves. The study additionally shows that these parameters were derived with assumptions that indicate the beach had enough time to adapt to the hydrodynamics. This means they are not meant for shoreline changes on small time-scales, like storms. A short explanation of the model they used in their study is presented in Section 2.3.1.

For parameter U lower than 0.5 we should not see high-angle wave instabilities. Parameter A larger than 0.5 means there are more waves travelling to the right, a value of 0.5 means that we expect no net longshore sediment transport. Right-travelling waves for the case of the Houtribdijk are the waves originating from the North, left-travelling waves originate from the South-East.
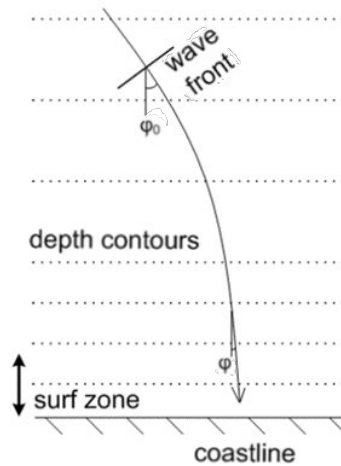
Figure 2-2: Schematic view of wave angle of incidence, from Bosboom & Stive (2015), with the offshore (φ_0) and nearshore (φ) wave angle of incidence.

2.2 Beach cusp physics

As mentioned in the introduction, most studies focus on the more energetic high-energy coasts. Nevertheless, some studies have investigated the physical processes behind coastal features in low-energy environments. Below, we have gathered some of the theories that seemed most applicable to the beach cusps at the Houtribdijk.

2.2.1 Paradigm shift

According to Coco & Murray (2007), the world of nearshore morphodynamics is governed by two major paradigms. The first is commonly named a 'forcing template', or 'forced' response. Here, it is assumed that the hydrodynamics or underlying geology imprint their response on the unconsolidated sands. As such, sediment is not considered an explicit process, but instead a consequence of hydrodynamic conditions, where often nonlinearities and feedbacks are neglected. The second paradigm is usually referred to as 'self-organization', or 'free' response. As visible in Figure 2-3, the coupling between morphology and hydrodynamics is acknowledged. Due to processes like nonlinear interactions and dissipation, such an application seems especially relevant in the nearshore environment. It may lead to the preference for complex system research, instead of (numerically) solving of the conservation equations for mass and momentum. Coco & Murray (2007) also suggests that relatively simple interactions (feedback loops between morphology and hydrodynamics) may lead to complex patterns or features (e.g. bars, beach cusps, spits). Additionally, Mujal-Colilles et al. (2019) hint at the necessity to analyze the bathymetry, currents and waves in order to confirm self-organization.
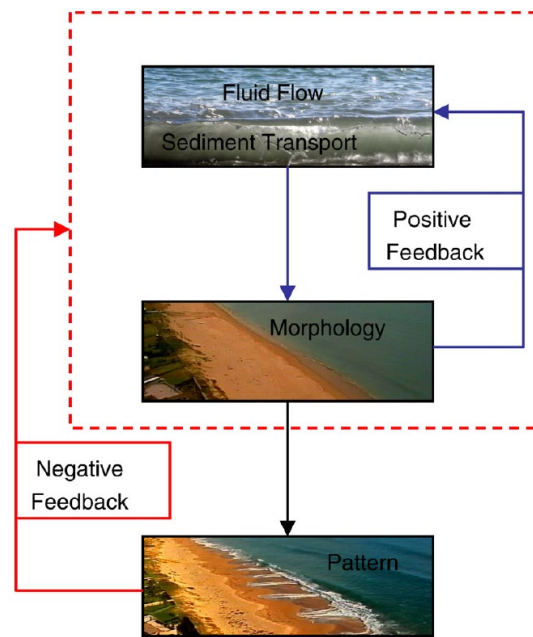
Figure 2-3: Schematized principle of self-organization, from Coco & Murray (2007).

For many years, the forcing template seemed to be the best explanation for any hydro- and morphodynamic system, due to its dependence on conserved quantities. However, the past few decades have seen more focus on self-organization (Bosboom & Stive, 2015). Even though this approach is sensitive to input parameters (e.g. hydrodynamic conditions and initial bathymetry), it can reproduce complex coastal features. This ability may prove useful in verifying physical processes.

2.2.2 Cross-shore

Typical nearshore processes include the distinction between summer and winter conditions (Bosboom & Stive, 2015). These are respectively linked to low-energy and high-energy conditions. Typically, this means calm or stormy, respectively. During calm conditions and under the influence of tides, beaches are expected to slowly evolve towards the reflective beach state (Wright & Short, 1984). High-energy events ('reset' events) are expected to move sediment from the upper shoreface to the lower shoreface, moving the beach state towards a dissipative (higher) state.

Similarly to tides, other long waves (e.g. infragravity waves) are expected to provide the mechanism that leads to possible shoreward return of sediment and is characteristic for dissipative beaches (Goodfellow & Stephenson, 2005; Wright & Short, 1984). The presence of such waves can give insight in the processes leading to the changing morphology. To find long waves, a spectral analysis might be a useful tool.

Relating back to the description of low-energy environments, the IJsselmeer seems to agree with the calm (summer) conditions. Low-energy beaches are therefore expected to evolve towards the reflective beach state. Bosboom & Stive (2015) mention that this state is characterized by (among other things) relatively steep slopes and a narrow beach face. So far, Figure 2-1 seems to fit this description.

2.2.3 Longshore

Characteristic length-scales, like the spacing of beach cusps, may be related to the swash zone flow excursion (Coco et al., 1999; Werner & Fink, 1993). However, data on this quantity is yet unavailable. It is our understanding that this is the same process that is now commonly described as transport due to set-up differences. These set-up differences cause longshore sediment transport due to the presence of a dominant wave direction different from the shore normal. Considering a longshore uniform bathymetry, most alongshore sediment transport formulae predict a maximum when waves approach at offshore angles of approximately 45° to the shore normal

(Ashton & Murray, 2006b). Several studies explain the instabilities in the beach when the wave angle of attack is too large (Ashton et al., 2001; Ashton & Murray, 2006a; Coco & Murray, 2007). Of those studies, the study by Ashton et al. (2001) assumes that for high-angle wave instabilities, cross-shore transport is less important than longshore. They additionally mention that the maximum longshore transport angle of 45° may correspond to a breaking wave angle of 10°.

Figure 2-4 illustrates this process, starting with an initial perturbation (time 1). The assumption here, is that there is a longshore uniform bathymetry, such that refraction is constant in the longshore direction. Theoretically, the set-up differences cause longshore differences in erosion and deposition. High-angle waves cause counterclockwise and clockwise rotation of the shoreline at the left and right inflection points (at vertical dashed-dotted line, time 2), respectively. Change in orientation of the beach may lead to positive feedback, causing a 'hump' to grow, or negative feedback, causing it to stabilize (dissipate). The creation of a 'shadow zone' may eventually lead to spit-like formations (time 3 through 5).
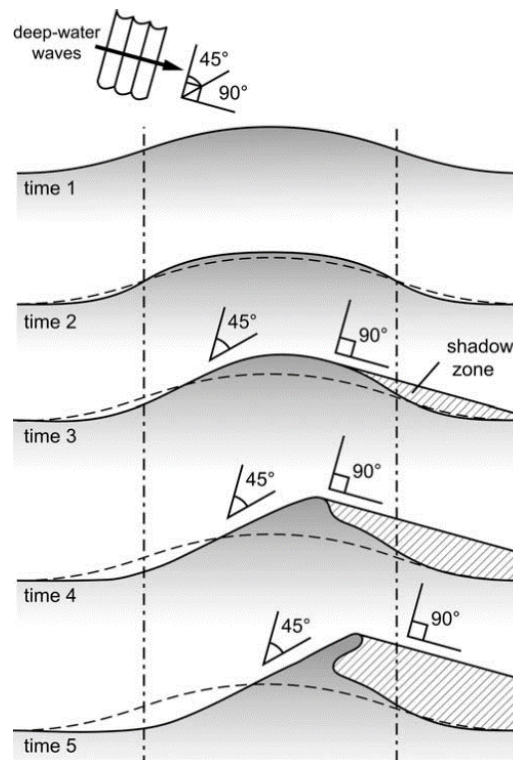
Figure 2-4: Temporal evolution of a perturbation as a result of high-angle wave attack, from Ashton & Murray (2006a).

A recent study on the morphology of the Marker Wadden shows that the response of the beach is very much dependent on the orientations of the beach and respective wave attack (Ton et al., 2020). The Markermeer side of the Houtribdijk has hardly started showing development of coastal features, comparing Figure 2-5 and Figure 2-6 to the cover photo of this report. The former experiences wave attack angles close to the shoreline normal. At the IJsselmeer side, this hints at the process of high-angle wave instability causing three-dimensional shapes. This dominance of high-angle waves may mean that the transport of sediment also moves in this longshore direction.

Figure 2-5: Drone photo of the Markermeer side of the Houtribdijk (Bureau Start the Future, 2020).

Figure 2-6: Drone photo of Trintelzand, on the Markermeer side of the Houtribdijk (Bureau Start the Future, 2020).

So, it seems that the self-organizing approach can explain the growth of instabilities (e.g. coastal features) and is considered the state-of-the-art. However, recent developments as reviewed by Falqués et al. (2017) indicate that not only high-angle waves cause instabilities. They mention the angle of wave attack used to assess whether a wave is high-angle or not should be taken at the depth of closure. Additionally, even low-angle waves may lead to instabilities when the beach is steep and wave heights are relatively small. Similarly, a study on simulating beach cusp formation mentioned that a large spreading of the wave directions may prevent the formation of beach cusps, due to smoothing of the perturbations (Daly et al., 2019).

The study on sand waves, by Falqués et al. (2017), makes the distinction between three locations where either the alongshore sediment transport rates, breaking wave heights or relative wave angle (i.e. angle to the shore normal) are maximum. Growth of the sand waves was observed when the maximum of sediment transport was located on the same side of the features as where the dominant wave direction originated. For waves that are less refractive (and resulting wave front stretching) the maximum in breaking wave heights tend to be on the updrift side of the features, leading to instabilities. Their analysis explains that the competition between destabilizing gradients in breaking wave heights and stabilizing gradients in relative wave angles leads to the critical value of approximately 42°.

2.2.4 Morphology

High-energy storm events can cause sediment loss, as erosive high waves can transport material seaward of the wave base (Jackson et al., 2002). This also means that these events may cause the formation of coastal features that are not generally associated with a low-energy environment. Another study, for a strong-wind bay environment, showed that the beach experiences a 'bimodal' behavior, alternating between reflective (low-energy) and dissipative (high-energy) states

(Goodfellow & Stephenson, 2005). This study suggests that high-energy infragravity waves and the high variability in wind conditions are responsible for the dynamic response of the beach. They indicate that such an environment rarely reaches an equilibrium, and that the absence of swell (or tide) causes the beach to retain its shape caused by storms.

From the study by Ton et al. (2019), we expect sediment to deposit at the edges of the platform until it is situated below the wave base. Any erosion of the beach face after this point will be lost beyond the platform. Additionally, the platforms will likely reach an equilibrium once they are wide enough to reduce the wave height at the waterline to approximately zero, which implies no more erosion of the beach face.

Since platform development is expected to be erosion driven, it is likely that sediment sorting is of importance (Ton et al., 2019). Lorang et al. (1993) have found that coarser sediment tends to stay at the shoreline, while finer sediment is transported offshore. Their study even shows that sediment transport over the platform can lead to bar formation. However, Ton et al. (2019) note that none of the sources precisely explain the process behind the development. One study, concerning a fetch-limited environment experiencing episodes of strong winds, has found high-energy events to cause onshore movement of bars (Goodfellow & Stephenson, 2005). Cross-shore dimensions seem to be similar to that of the Houtribdijk. The onshore migration hints at negative feedback in the system, preventing the permanent loss of sediment in cross-shore direction. If these environments can be related to the Houtribdijk, this may suggest the existence of an equilibrium cross-shore profile.

2.3   Numerical modeling of beach cusps

Some of the studies from the previous sections have applied numerical models to see what their capabilities are in reproducing more complex coastal features. They have used models to verify the writers' assumptions (e.g. physical process). To be able to make a smooth transition from data analysis to model simulations during the thesis, we have explored the way models were applied in these studies. This section provides some background information on the way models have been applied in the past up to the current state of the art.

2.3.1   History

An early model study by Werner & Fink (1993) used self-organization to model beach cusps. Their model uses a simplified coupled flow, simulating sediment transport and morphology change. Their conclusion was that current data on beach cusps is insufficient to distinguish between model results of forced or free response principles. They also argue that edge waves provide an initial perturbation, that evolves the morphology through positive feedback and later stabilizes it through negative feedback.

A common problem under one-line models is a so-called 'erosion waves', numerical artifacts that occur when waves approach at an angle larger than approximately 45°. Ashton et al. (2001) elaborate on the interaction between hydro- and morphodynamics by including a condition that applies upwind discretization at locations with high-angle waves, thus preventing erosion waves. They also mention that most previous studies on this interaction were aimed at coastal features with dimensions in the order of those of the surf zone. In order to make prediction on larger scales, they created a numerical model that is able to take into account high-angle waves, see Figure 2-7. Their assumptions were, that on larger scales, sediment transport gradients in the alongshore direction cause shoreline evolution. So, smaller scale morphological changes are assumed to be absorbed in the general trend of shoreline evolution. Therefore, the model is not suitable for modeling short-term episodic events (e.g. storms).
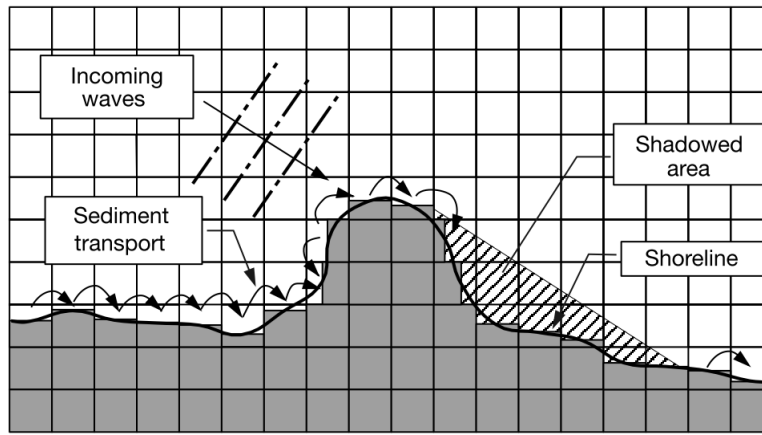
Figure 2-7: Plan view of the one-line model set-up, from Ashton et al. (2001).

In Figure 2-8 the result of a simulation of this model is given, indicating the evolution from initial perturbations to beach cusps. Although spatial and temporal scales are much bigger than we observe at the beaches of the IJsselmeer, the physical process may act in a similar way. The paper where this figure is explained elaborates that model results are scalable with wave height and period.

In a continuation of their study, Ashton & Murray (2006a) investigated their wave climate parameters (Section 2.1.4) using this simple model. The analysis of the model simulations have led to an easy classification of coastal features as a function of U and A (Figure 2-9).
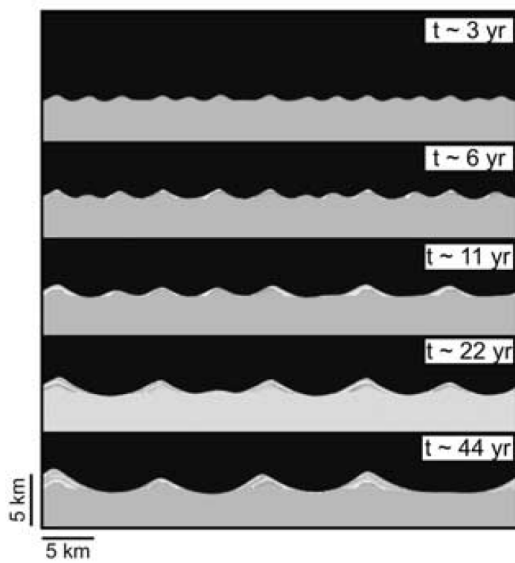
Figure 2-8: Model simulation plan-view development of beach cusps, from Ashton & Murray (2006a).
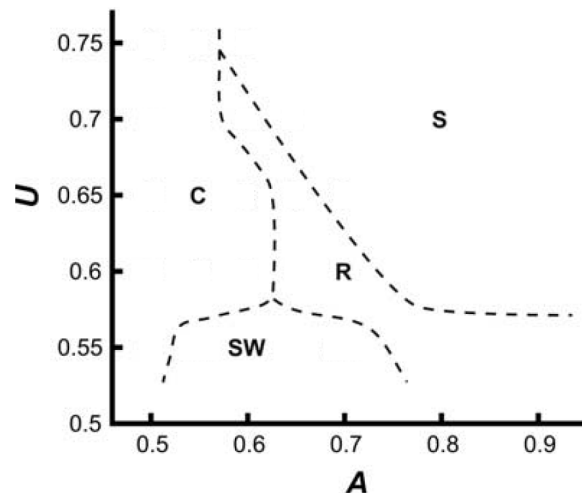
Figure 2-9: Wave climate parameters and expected beach shapes (C: Cusps, SW: Sand waves, R: Reconnecting spits, S: Flying spits), adapted from Ashton & Murray (2006a). Here, U is the ratio of high-angle waves, and A is the wave climate asymmetry.

2.3.2 State of the art

The recent model study by Daly et al. (2019) shows that the non-hydrostatic version of XBeach may be used to model beach cusps. Their goal was to reproduce a coastal accretive event at Nha Trang, Vietnam, and to investigate the sensitivity of cusp dimensions by varying boundary conditions. Their simulations made use of wave transformation (skewness and asymmetry in the surf and swash zone), groundwater flow (in- and exfiltration in swash zone) and optimized model settings for bed friction, bed slope effects, dilatancy and Darcy flow permeability.

Roelvink et al. (2020) created a model named ShorelineS, which elaborates on the model by Ashton et al. (2001). ShorelineS is a one-line model which, similarly, applies an upwind correction when high-angle waves approach the coastline. This, in combination with a vector-based grid system, allows for the modeling of complex shapes. However, small-scale events are not yet considered. It takes wave shadowing into account, makes use of an overwash mechanism for spits

or barriers and allows for merging or splitting of coastal features. The power of this model comes from it being computationally inexpensive (due to the simple mechanics) and that it can simulate beach response to both low- and high-angle waves. The model gains its light-weight aspect from the fact that it models the line around Mean Sea Level (MSL), as opposed to the top of the active profile, allowing for a simplified computation.

To summarize, it seems the current state of the art for multi-dimensional models requires non-hydrostatic calculations to model beach cusps. For one-line modeling, a vector-based grid system may be used to accurately predict complex shapes.

2.4   Conceptual model

To create an objective way of comparing morphological changes and to find hydrodynamic conditions that explain them, a conceptual model was set-up. From the previously explained theory on high-angle wave instabilities, we describe the influence of wave incidence angles on a local scale. This section serves to bring together the sought-after quantification of the beach cusps and the physical concepts we can use to explain them (research question 1). It is included in this chapter, since it is mostly a rephrasing of the prevailing theory on high-angle wave instabilities.

The process described in Section 2.2.3 has led to five cases, shown in Figure 2-10 and Figure 2-11. The theory is based on wave angles of incidence being the sole driver of morphological change. This means that wave height and period are constant. The first figure shows the growth of a 'bump' under the influence of several combinations of high-angle waves. The second figure shows the bump dissipating, or shrinking, due to the damping effect of low-angle waves. Due to the small scales we are currently looking at, this description is referred to as 'micro scale' in the rest of this thesis.

The cases are based on the conservation of sediment volume. Using the wave climate parameters described in 2.1.4, high-angle wave cases correspond to $U = 1$ and low-angle wave cases to $U = 0$. The asymmetry of the wave climate is assigned based on Figure 2-9.

Case A: A symmetric and high-angle wave climate ($A \cong 0.5$) leads to a symmetrical growth of the bump. This means that there is no change in alongshore position (x_c) and no change in shape asymmetry (As). The bump will move seaward, meaning its amplitude (A_c) increases and the wavelength (L_c) decreases.

Case B: An asymmetric high-angle wave climate ($0.5 < A \leq 0.8$), with a preference for waves coming from the left. Since there is still forcing from both sides, the amplitude is expected to increase. However, the dominant direction will cause displacement to the right and an increase in shape asymmetry. Following the balance of volume, we expect the wavelength to stay roughly the same.

Case C: A nearly fully asymmetric high-angle wave climate ($0.8 < A \leq 1.0$), where waves only approach from the left. This unidirectional forcing is expected to prevent the growth of the bump itself, instead causing eroded parts of the shape to 'skip' over the tip. Initially, this sediment will deposit in the shadow-zone, later it will likely cause spit-like features. The amplitude therefor stays more or less the same, but displacement will be to the right, and shape asymmetry and wavelength will increase.

Case D: A symmetric low-angle wave climate ($A \cong 0.5$) leads to a symmetrical dissipation of the bump. This will cause the opposite response as case A; a decrease in amplitude and increase in wavelength. However, the alongshore position and shape asymmetry will likewise stay the same.

Case E: An asymmetric low-angle wave climate ($0.5 < A \leq 1.0$), with some or all waves coming from the left. Since dissipation is expected to be dominant, we expect all degrees of wave climate asymmetry leading to more or less the same change in quantities. This means a decrease in amplitude, a displacement to the right, and an increase in shape asymmetry and wavelength.
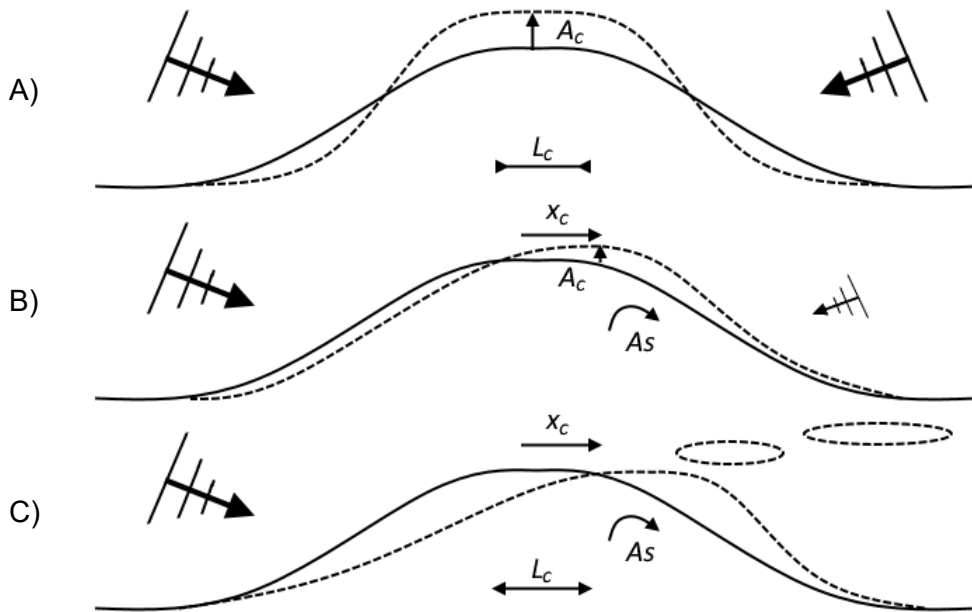
Figure 2-10: Conceptual model perturbation under influence of high-angle waves (A: Symmetrical wave climate, B: Asymmetrical wave climate with most waves coming from the left, C: Asymmetrical wave climate with all waves coming from the left). Quantities indicated are the longshore position of the cusp horn (x_c), its amplitude (A_c), wavelength (L_c), and shape asymmetry (As).
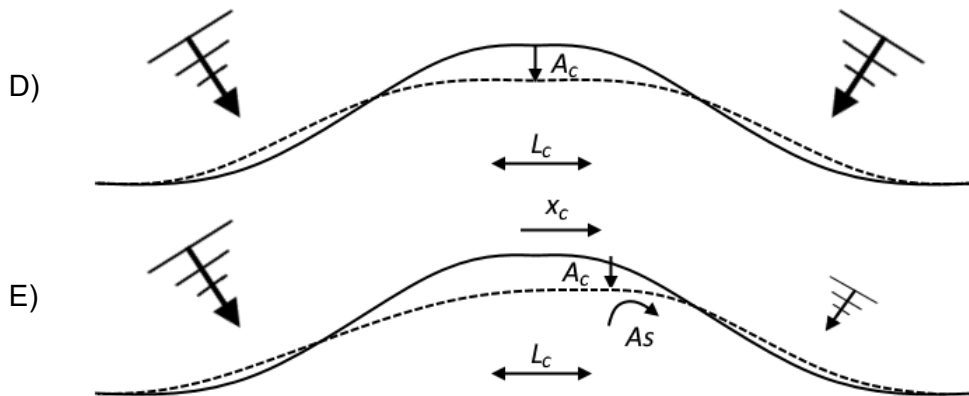
Figure 2-11: Conceptual model perturbation under influence of low-angle waves (D: Symmetrical wave climate, E: Asymmetrical wave climate with most waves coming from the left). Quantities indicated are the longshore position of the cusp horn (x_c), its amplitude (A_c), wavelength (L_c), and shape asymmetry (As).

3 Methodology

An approach on how to classify the beach cusps at the Houtribdijk (research question 2) is presented in this chapter. One of the goals of this study, was to find the physical processes responsible for the formation of beach cusps at the sandy shore of the IJsselmeer. Section 3.1 concerns the general approach, providing the steps we took to answer our research questions. Sections 3.2 and 3.3 concern more detailed descriptions of some of the steps in our general outline.

3.1   Approach outline

The morphodynamics on the IJsselmeer side of the Houtribdijk are the focus of this thesis. Literature suggests that the wave climate causes shoreline instabilities. The theoretical background has introduced several concepts and theories used to classify beach cusps. It has helped us to answer research question 1. To answer the rest, we started with the assumption that the main driving force in shoreline development is high-angle wave instabilities. The general outline of our approach is described below, of which some steps are elaborate in more detail in the rest of this chapter.

- To begin classifying the beach cusps at the Houtribdijk, Chapter 4 concerns the classification of the hydrodynamics. A distinction between calm and stormy conditions was made (see Section 3.2), and various properties of our environment were related to theory. Such properties thereby helped us to with research question 2A. In Appendix B, some more theories from the theoretical background were tested on our environment, to find out which of the physical processes would be applicable to our case. In a way, this expands on research question 1B.
- In Section 3.3.1, we explain how we used topography and bathymetry data to find the exact position of the waterlines for most of the measurement periods. The results may be found in Section 5.2. From this waterline we were able to quantify beach cusps properties (e.g. wavelength, amplitude, position of the horn and asymmetry), which is explained in Section 3.3.2. Results of this quantification are given in Section 5.3, which has helped us answer question 2B.
- How we translated the conceptual model to a macro scale is explained in Section 3.3.3, based on the theory of high-angle wave instabilities (the growth and dissipation of a local perturbation under the influence of waves). This meant that the micro scale (Section 2.4) was extrapolated to macro scale coastline changes.
- We applied the conceptual model to data, per measurement period and location, to find representative hydrodynamic conditions. Section 5.5 presents a collection of conditions that were (mostly) able to explain changes in the waterline of the respective period. Morphological changes explained in this way were used to substantiate the claim that high-angle waves are the primary cause.
- Section 5.6 contains an overview of the results. In other words, we summarized what change in the morphology can be explained by the investigated hydrodynamic conditions. This section therefore contains a conclusion where we presented possible answers to questions 2A and 2B.
- Physical processes that were applied in the data analysis, in combination with what was learned from the literature study, were collected to form a list of model requirements (Section 6.1). From this, the definitive choice of numerical model was made, answering question 3A.
- How we set-up and calibrated the numerical model is elaborated in Section 6.2. This meant that the model was set to best represent refraction, using the available offshore and nearshore wave data. This method was assumed to best represent the physics previously found, answering question 3C.

- For each of the periods evaluated in the data analysis, their representative hydrodynamic conditions were applied to the model. This led to a number of modeled coastlines, that were each compared to the actual measured coastline. The results may be found in Section 6.3, where we presented an answer to research question 3D. In Section 6.4 we additionally discuss question 3B, which is mostly answered in the recommendations of Section 9.2.
- Lastly, we evaluated all the results to assess whether we could objectively assign wave forcing as the dominant process. We have done this in the form of a discussion in Chapter 7, where we tried to definitively answer research questions 2 and 3. Although not explicitly investigated, we have presented answers to research question 4 as well. With this, we have formulated our answer to the main research question, to the extent of the knowledge acquired during our analyses.

3.2   Hydrodynamics

To start our classification, we first analyzed the hydrodynamics. A description of the available data may be found in Appendix A.1. Results of the method below may be found in Chapter 4.

What we learned from the theoretical background, was that often a distinction between low-energy and high-energy conditions may help classification. For this reason, and what was found in Appendix B, we split up the hydrodynamic data in two types of conditions, to reflect both low-energy and 'higher'-energy conditions. These conditions were referred to as 'calm' and 'stormy'.

This was done for the period between March 2019 and September 2020, using the measurement data from the STB at location FL69 (370 m offshore), since this dataset was the most complete. A peak-over-threshold method was applied with a minimum wave height of 0.25 m, conforming to the low-energy definitions of Section 2.1.2. A minimum storm duration of 4 hours was prescribed. Periods of stormy conditions found in this way were also considered valid to conditions measured by other measurement equipment.

3.3   Morphodynamics

Next part in the classification, is analyzing morphological changes and relating them to the hydrodynamics. Steps relevant to this process are elaborated below. The results of these methods are mostly found in Chapter 5. Data used was available from measurements by the contractor and Shore. The contractor was Combinatie Houtribdijk, a collaboration between dredging engineering companies Boskalis and Van Oord, see Appendix A.2. Shore is a monitoring company that have been measuring the sandy shore since November 2019. Information on the available data may be found in Appendix A.2.

3.3.1   Waterline analysis

In the literature, studies were often focused on changes in the waterline to visualize coastal features. To gain insight in longshore processes, an analysis was performed that located the waterline using the measured topography and bathymetry. This analysis shows the shape of the beach cusps. Available point data as supplied by the contractor and Shore were used in the original analysis. However, due to aliasing problems it was found that the measurements by the contractor could not be used to find coastal features (i.e. the transect spacing was too big to discern cusp shapes). The periods in between Shore's measurements, the ones we used in our analyses, were often referred to by 'morphological periods' in this thesis. Finding the waterline was done using a Python script applying the approach below. Results of this waterline analysis may be found in Section 5.2.

1. A reference elevation is specified, for which we determined the coordinates of the waterline. This elevation was determined by taking the average of the second half of the preceding measurement period (using STB data). A representative wave height during calm conditions of

0.15 m was then added, to somewhat represent the elevation at which both calm and stormy condition waves attack the beach.

2. A z-margin was prescribed, which sets a range above and below the reference elevation where the script looks for available data. This margin was set at 5 cm, which was sufficient to reproduce a waterline, due to the large amount of data.

3. To filter the data from the last step, the x-direction kilometering is split up in 950 segments, setting our resolution to 1.0 m in the longshore direction. Here, each segment is filtered for the data point that has the largest y-value and is therefore most 'seaward'. We chose the largest y-value, instead of an average, because choosing the latter often produced waterline coordinates in the wrong areas (as checked using the orthogonal photos). This was caused by the small shallow areas on the landward side of the berm, because when water levels approached the top of the berm, this would create two coordinates within the z-margin. For example, in Figure 3-1, taking an average y-position at km 59.730 would result in a waterline positioned landward of the actual waterline.
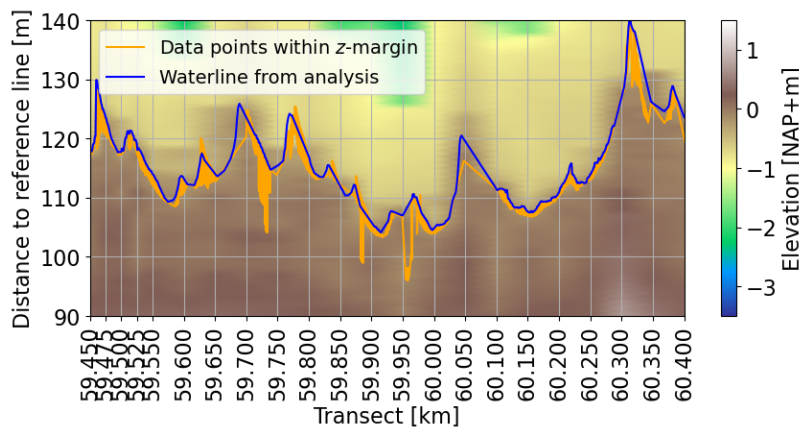
Figure 3-1: Example of waterline analysis results including data points within z-margin (November 2019, location FL69).

3.3.2 Beach cusp quantification

The waterline from the analysis above was used to quantify the beach cusps. This was done in the steps described below. The quantification was done using the four variables described in Section 2.4: Longshore coordinate (x_c), wavelength (L_c), amplitude (A_c) and shape asymmetry (As). Results of this quantification may be found in Section 5.3.

1. The first step is finding and recording the coordinates of the coastal features. The applied method is looking for the longshore coordinate of the feature (x_c) corresponding to a cross-shore coordinate that is larger than the neighboring data points. If found, the value is saved and called a 'horn'. Subsequent minima in between the peaks are named 'bays'. To prevent every small ripple in the waterline from being recorded as a cusp, we applied some restrictions. One was a prominence, which is a minimum vertical distance between the peak and the lowest bay, set at 0.1 m. The other was a minimum longshore bay-to-bay distance of 5 m.

2. Secondly, the wavelength is defined as the distance between the bays around a horn. Most of the beach cusps are oriented differently from the average beach orientation. To get the wavelength, and most of the other measures, we rotate the beach cusps towards the average beach orientation (see Figure 3-2).

3. Thirdly, we defined the amplitude as half the y-distance between the orientation corrected horn and bay locations (see Figure 3-2). We take this rotated cusp, since the vertical coordinates of the bays can differ much, especially if a cusp is far from parallel to the average beach orientation.

4. Lastly, the shape asymmetry was defined as the ratio of cusp surface areas (see Figure 3-3). This is the area to the left of the alongshore peak coordinate (A_1) with respect to the total cusp area (A_{tot}), formulated as $As = A_1/A_{tot}$. In other words, an asymmetry lower than 0.5 indicates hanging to the left, higher than 0.5 hanging to the right, and exactly 0.5 would imply symmetry.
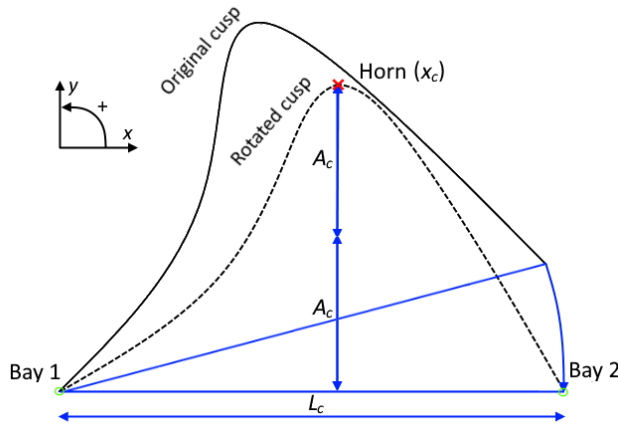
Figure 3-2: Definition of horn position (x_c), wavelength (L_c) and amplitude (A_c) of a beach cusp.
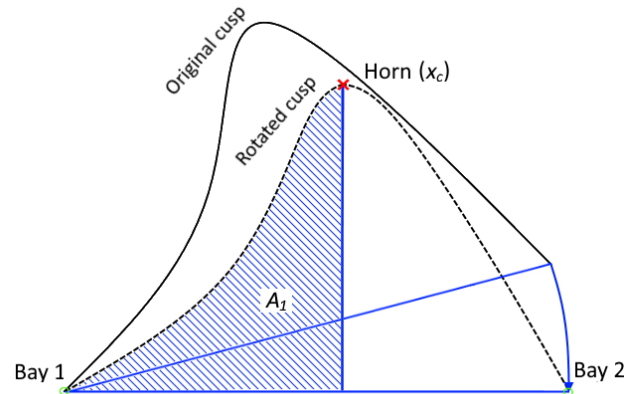
Figure 3-3: Definition of the shape asymmetry of a beach cusp, with A_1 the area left of the horn position (x_c).

3.3.3 Conceptual model

The theoretical conceptual model (see Section 2.4) could now be used to relate morphological change to the hydrodynamics. We quantified the number of beach cusps N_c, average wavelength of the cusps $\bar{L}_c$, average amplitude of the cusps $\bar{A}_c$ and the average shape asymmetry $\overline{As}$ for each period (as measured by Shore). The average amplitude was weighted by the wavelength of the cusps, such that it would not change erratically when the number of cusps changed. The shape asymmetry was weighted by the amplitudes of the cusps for the same reason. Knowledge from this quantification, and from observations, have led to an expansion of the conceptual model concerning the morphological change we expect to occur on the macro scale (Section 5.4).

Considering the description of large-scale morphological change, we compared the change in the quantities to the hydrodynamic conditions in the respective period. Conditions that could explain the morphological change according to our expectations were then considered representative for the development of beach cusps. So, conditions that best fit with our conceptual model were selected. If multiple conditions seemed reasonable, the most recent one was considered representative or they were combined and considered a single representative condition. Results of this application may be found in Section 5.5 and Appendix E. In the former, the representative hydrodynamic conditions were presented by a single, averaged, value. Conclusions regarding our findings may be found in Section 5.6.

4 Hydrodynamics

In literature, the process of high-angle wave instabilities was considered a major process in driving morphological change. Therefore, classifying our environment based on this hydrodynamic process will be our first step towards finding the cause of the formation of beach cusps along the Houtribdijk. In Section 4.1 we analyze hydrodynamic data to assess whether our waves are typically less refractive than common on open ocean coasts (from here on simply named 'less refractive'), and to make a distinction between low- and 'higher'-energy conditions. Literature stated that both are considered relevant classifications in lake environments. Next, in Section 4.2, we apply the wave climate parameters of Section 2.1.4 (U and A) to our data, to make an early classification of the coastal features. Finally, Section 4.3 includes an overview of the hydrodynamics per 'morphological period' (the periods in between measurements by Shore). In this section we also return to the criteria for low-energy environments (Section 2.1.2), so that we may better classify our system. We also started on an answer to the following research question:

> *2A: Which hydrodynamic processes are responsible for the formation of beach cusps?*

4.1   Classification

In the following sections we elaborate on the classification of our environment. We do this first based on refraction, which was considered important in the theoretical background due to the suspected forcing by high-angle waves. Next, we make a distinction between 'calm' and 'stormy' conditions, based on our method described in Section 3.2. It is argued by literature that the morphology is strongly influenced by higher-energy events. As such, this distinction will allow us to isolate higher-energy conditions, which will help us relating the hydrodynamics to the morphodynamics and brings us closer to finding the driving force behind the formation of beach cusps.

Classifying the features based on the hydrodynamics is mostly done using offshore measurement data, due to most prevailing coastal dynamics theories being related to offshore wave conditions. For this reason, we would prefer data that is least affected by shoaling and refraction. Additional information on the available data may be found in Appendix A. The complete timeseries of hydrodynamic measurements is included for location FL69, FL70 and FL70C in Appendix C.

Measurements of the STB's may be considered more accurate than the ADV's, due to the latter's pressure sensors occasionally getting clogged (V. Vuik, personal communication, July 15, 2020). Relations between the data are included in Appendix A.3. Since we expect wave forcing to be the dominant process, we try to use data on wave properties from one source (e.g. all from the ADV), choosing the consistency between data over possible inaccuracies. Water levels, often considered separately, were taken from the STB due to a larger accuracy.

4.1.1   Refraction

From the theoretical background (Section 2.1.2) we expect that environments like this experience waves that refract less. We can compare directional data from offshore to nearshore locations to verify this. Figure 4-1 and Figure 4-2 show the relation between wave directions at the offshore and nearshore ADV's of both location FL69 and FL70. The red dashed line indicates the beach orientation. Within these lines, waves are moving towards the beach. The green dashed line indicates the 45° critical value.

The horizontal velocities measured by the ADV's are used to determine the direction of wave orbital velocities (applying linear wave theory). Knowing that the wave crests and troughs have opposite velocities, the water level from pressure measurement can be used to find the direction of the waves.

We see that especially wave heights (H_{m0}) above 0.25 m have a strong correlation. Relating back to the theoretical background, the figures also show that for those waves an offshore wave angle of approximately 45° almost always corresponds to a nearshore wave angle larger than 10°. Since they seem to be less refractive, it is likely that these are short and steep wind-waves. Due to the strong correlation for stormy conditions, we expect that especially these waves are most influential in morphological change.
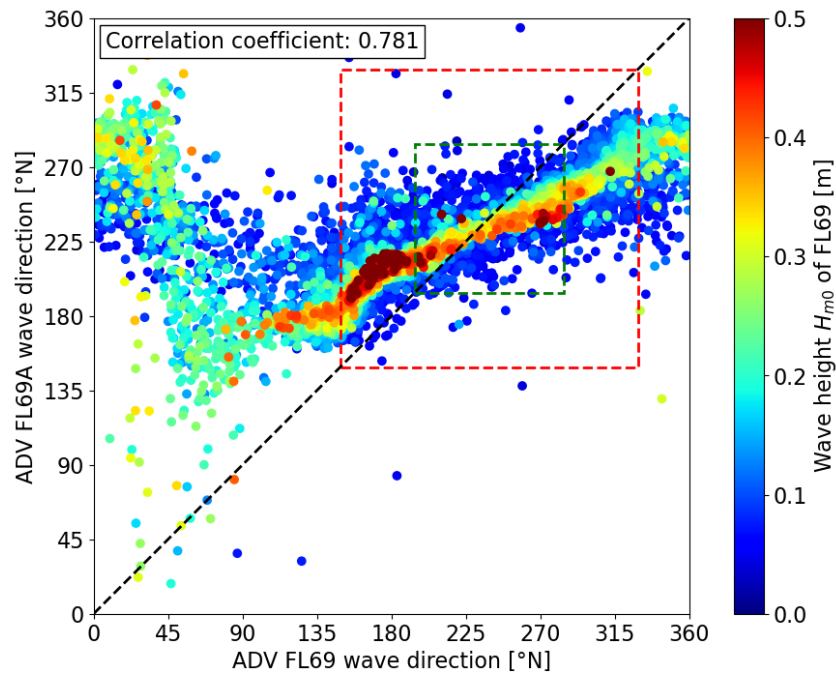
Figure 4-1: Comparison of offshore and nearshore ADV wave directions at FL69.
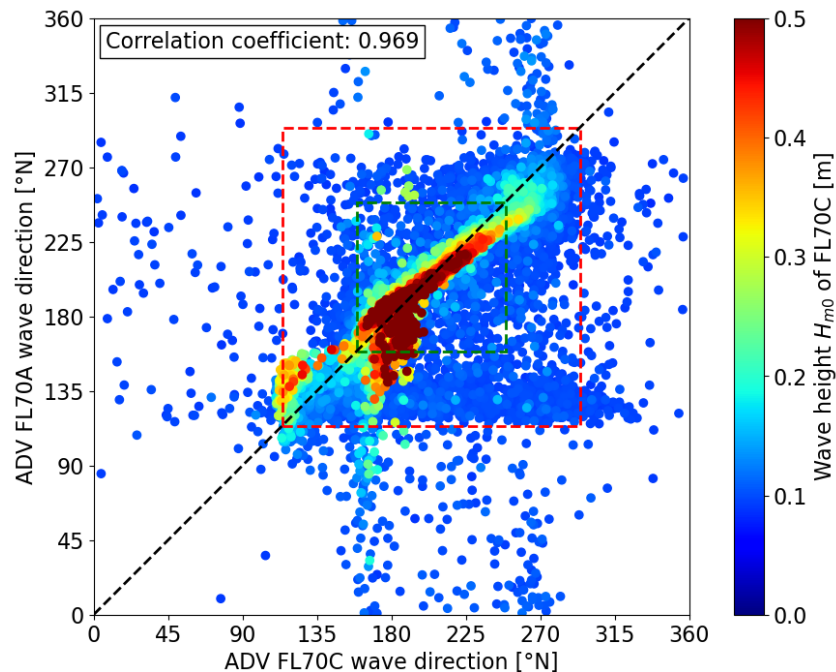
Figure 4-2: Comparison of offshore and nearshore ADV wave directions at FL70.

4.1.2 Stormy conditions

The results of the storm analysis for last February and March (during which storm Ciara occurred, indicated by a yellow shading) are given in Figure 4-3. Wave climates of the entire period for location FL69, FL70 and FL70C may be found in Appendix C. For location FL70 we mostly used data from FL70C, despite it being a nearshore location, because it was the most offshore location there that included wave directional data. This choice was elaborated further in Appendix A.3.

In the figure, we included both ADV (blue) and STB (yellow) data for comparison. The figure indicates the periods where stormy conditions occurred with a red line. In the bottom graph, the waves are indicated in the direction they are going (blue), with parts that coincide with stormy conditions (red). In this graph, the beach is indicated by a solid red line, in between which the waves are considered approaching the beach. The shore-normal angle is indicated by a solid green line, and the dashed green line indicates the 45° critical angle (border between low- and high-angle waves).

We see that the conditions we call stormy, occur on a regular basis. Additionally, we see that in those conditions wave directions tend to form a more structured path, seen by the red line in the bottom graph often being less scattered. This was coupled to the dominance of wind during these conditions, which was elaborated in some detail in Appendix B.1. Due to this dominance, we see many stormy conditions either going offshore, or partly approaching the beach under a low- or high-angle. Calmer conditions, however, seem to be more frequently high-angle.
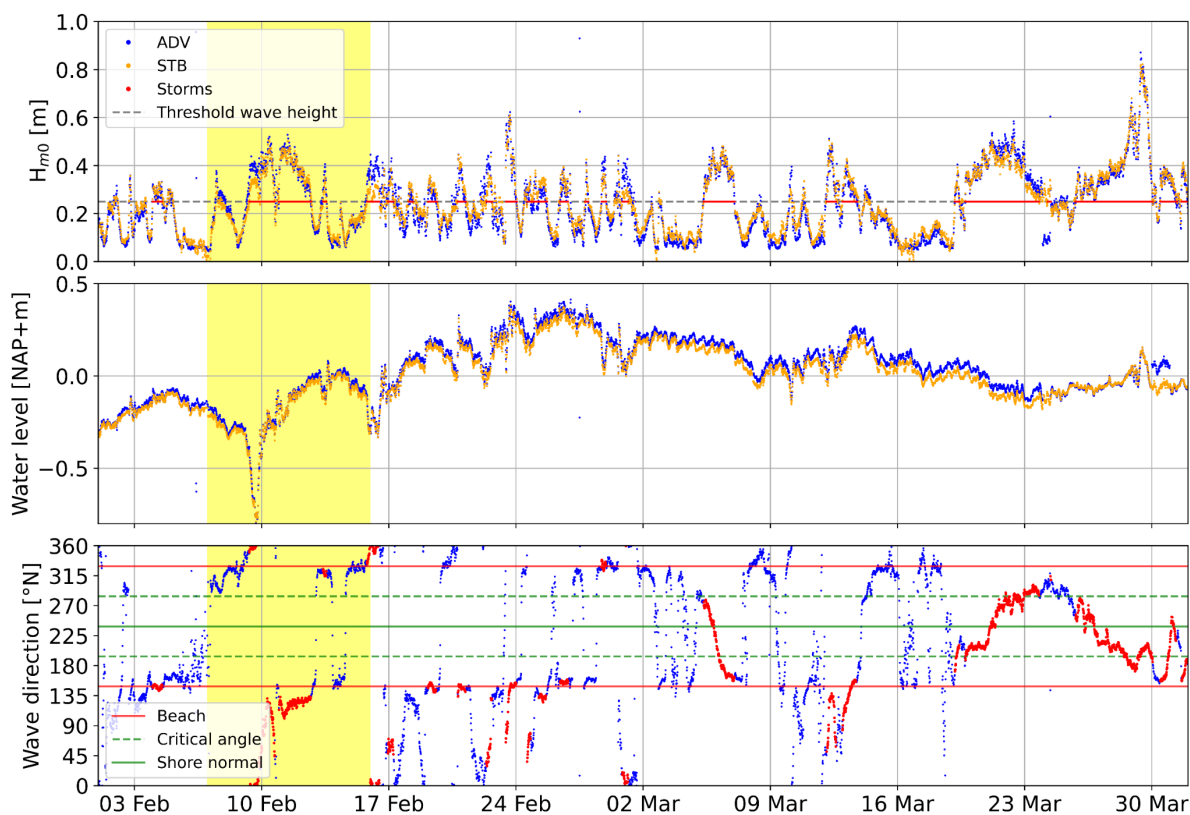
Figure 4-3: Hydrodynamic measurement data at location FL69 for February and March 2020.

Analyzing the ADV data for both calm and stormy periods has resulted in average values for the spectral wave height (H_{m0}), spectral wave period (T_{m01}), peak period (T_p), and wave direction (coming from, ϕ_m), as given in Table 4-1 for location FL69. The analyzed period was from June 22nd 2019 to September 1st 2020. This was done for location FL70C as well, shown in Table 4-2, but for the period of October 2nd 2019 to June 10th 2020 (due to data availability).

Comparing these tables, we see a significant difference between calm and stormy conditions, with more than a factor 2 difference om wave height. Considering the quadratic relation of wave height to energy ($E = \rho g H^2/8$), doubling the wave height (stormy conditions) may therefore result in four times the potential for transport; $E = \rho g (2H)^2/8 = \rho g H^2/2 = 4E$. The difference in wave periods is less, with only a fraction increase for stormy conditions. Computing the wave steepness using the definition $s = 2\pi H_{m0}/(g T_{m01}^2)$, we arrive at the last column. This shows that during stormy conditions, waves are steeper than during calm conditions.

Table 4-1: Average wave properties for the ADV at location FL69.

Conditions	Wave height H_{m0} [m]	Wave period T_{m01} [s]	Peak period T_p [s]	Mean direction* (coming from) ϕ_m [°N]	Wave steepness s [-]
Calm	0.14	1.66	1.87	47	0.03
Stormy	0.35	2.09	2.47	28	0.05
Overall	0.20	1.77	2.06	39	0.04

Table 4-2: Average wave properties for the ADV at location FL70C.

Conditions	Wave height H_{m0} [m]	Wave period T_{m01} [s]	Peak period T_p [s]	Mean direction* (coming from) ϕ_m [°N]	Wave steepness s [-]
Calm	0.12	1.50	1.93	46	0.03
Stormy	0.32	2.27	2.68	12	0.04
Overall	0.17	1.72	2.15	34	0.04

*: Mean directions can be misleading, as in the next section we will show that there is often a large spread in directions.

The average of the five largest wave heights at FL69 is 0.84 m, with an average peak period of 3.0 s. Despite this, the average values in the tables seem to conform to the wave height criteria of the definition of low-energy environments in Section 2.1.2. We fulfilled (1) overall wave heights less than 0.25 m (0.20 m for FL69 and 0.17 m for FL70), and (2) wave heights during stormy conditions less than 0.50 m (0.35 m and 0.32 m). This means that, when considering the average wave properties of calm and stormy conditions, our environment can be classified as low-energy.

4.2 Wave climate parameters

The literature study has led us to a couple of parameters (U and A), representing the ratio of high-angle waves and wave climate directional asymmetry (respectively, see Section 2.1.4). These parameters were presented in a study, where they were used to classify coastal features. The data so far (see Figure 4-3 and Appendix C) shows that many waves approach the beach from an angle close to the shore parallel. Additionally, we have a drone photo from February 2020, showing completely shore parallel wave directions (Figure 4-4). To find out if high-angle wave instabilities are the dominant cause of beach cusp formation, we may want to apply the wave climate parameters to our environment. The result of this may indicate that beach cusp development is indeed related to the presence of high-angle waves.
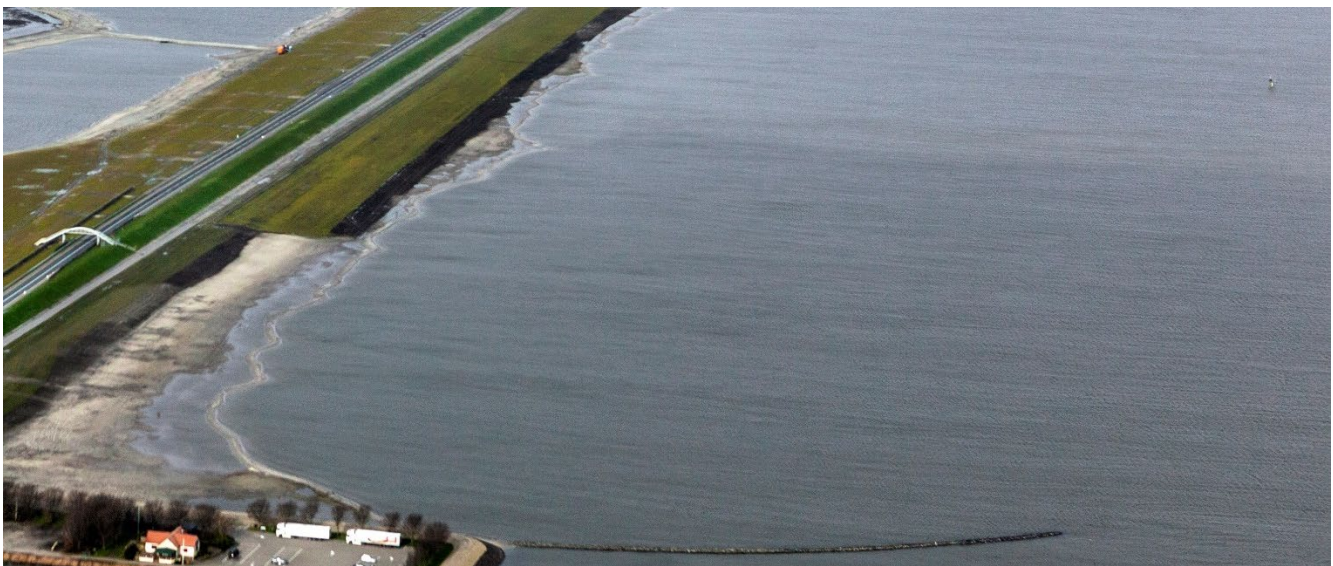
Figure 4-4: Aerial photo near location FL69, taken on 22nd February 2020 (Bureau Start the Future, 2020).

One way to evaluate the wave climate parameters, is by creating wave roses. Figure 4-5 and Figure 4-6 show such roses. We have used the wave directional data of the ADV at location FL69 for the period June 22nd 2019 to August 31st 2020. In Figure 4-7 and Figure 4-8 we show the data at location FL70C for the period October 2nd 2019 to June 10th 2020. When showing wave roses, the bars indicate the direction where the waves are coming from, instead of the direction they are moving to. The colors indicate the range for the wave heights and the height of the bars indicate what percentage of the total number of wave records they represent. The beach orientation is presented as a solid red line, with the beach on the South-Eastern side and the beach normal in solid green. The dashed green lines indicate the critical wave incidence angle of 45°. The legend is only shown in the first figure, the colors in all figures indicate the same ranges.
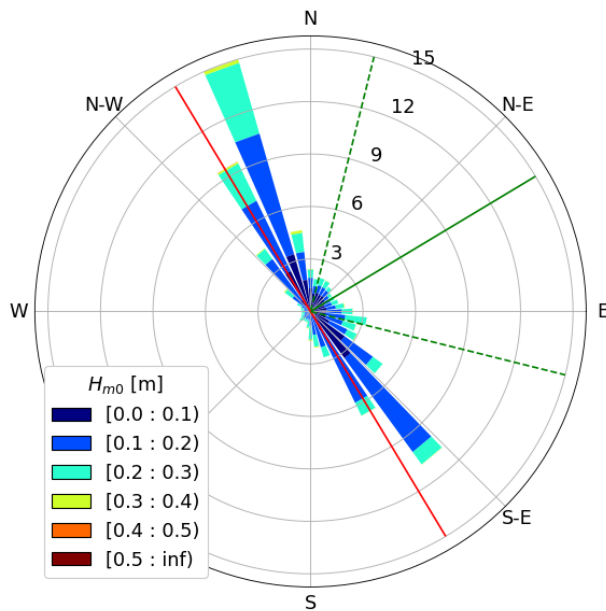
Figure 4-5: Wave rose for FL69 during calm conditions, from 22 June 2019 to 31 August 2020. Bars indicate wave origins.
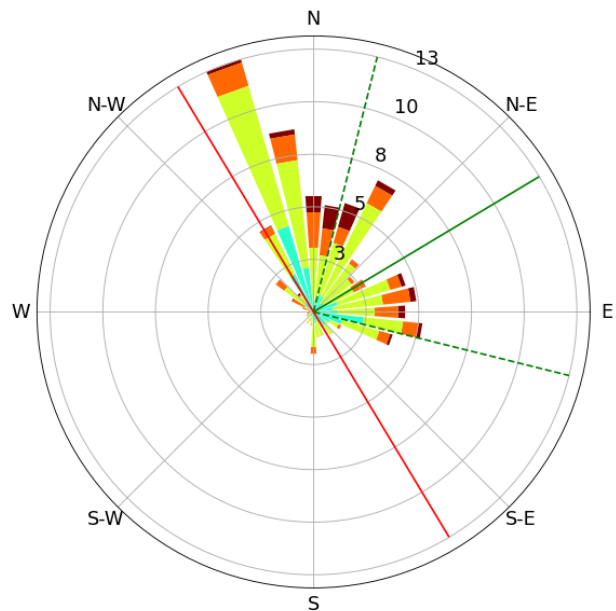
Figure 4-6: Wave rose for FL69 during stormy conditions, from 22 June 2019 to 31 August 2020. Bars indicate wave origins.

23
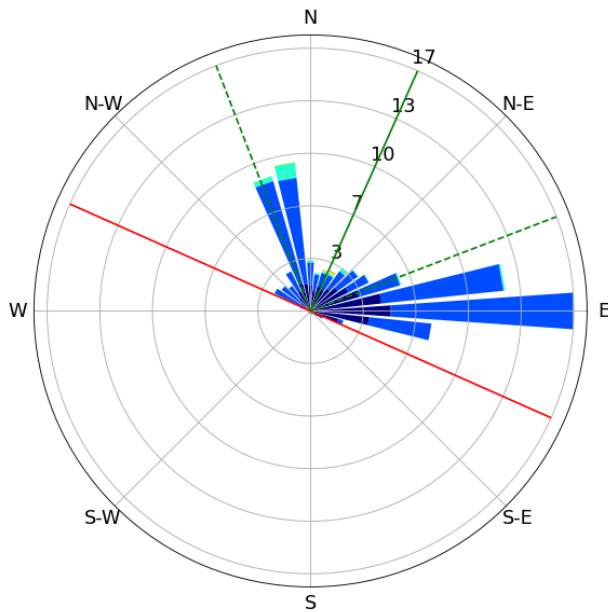
Figure 4-7: Wave rose for FL70C during calm conditions, from 22 June 2019 to 31 August 2020. Bars indicate wave origins.
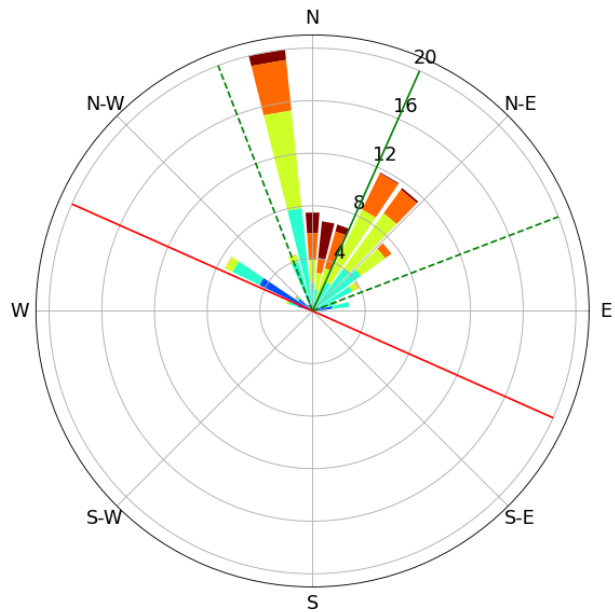
Figure 4-8: Wave rose for FL70C during stormy conditions, from 22 June 2019 to 31 August 2020. Bars indicate wave origins.

Similar to Section 4.1.1, the wave roses in combination with the aerial photo show that waves indeed often approach from high angles. Applying the definitions for the wave angles given in Section 2.1.4 and neglecting waves that appear to travel offshore, values for U and A are computed and shown in Table 4-3. The value given for A is followed by the direction that is considered the wave origin.

Table 4-3: Wave climate parameters at locations FL69 (22 June 2019 to 31 August 2020) and FL70C (2 October 2019 to 10 June 2020), with the ratio of high-angle waves (U) and the wave climate asymmetry (A).

Location	Conditions	U [-]	A [-]
FL69	Calm	0.76	0.52 (N)
	Stormy	0.52	0.65 (N)
FL70C	Calm	0.57	0.62 (SE)
	Stormy	0.18	0.58 (N)

In Figure 4-9 we show how these values fit in the results of the paper by Ashton & Murray (2006a). Calm conditions at FL69 would lead to beach cusps, while stormy conditions would lead to sand waves. At FL70C, calm conditions would similarly lead to beach cusps. However, stormy conditions at FL70C should theoretically result in a stable coast ($U < 0.5$, majority of low-angle waves) and thus dissipation of the coastal features.
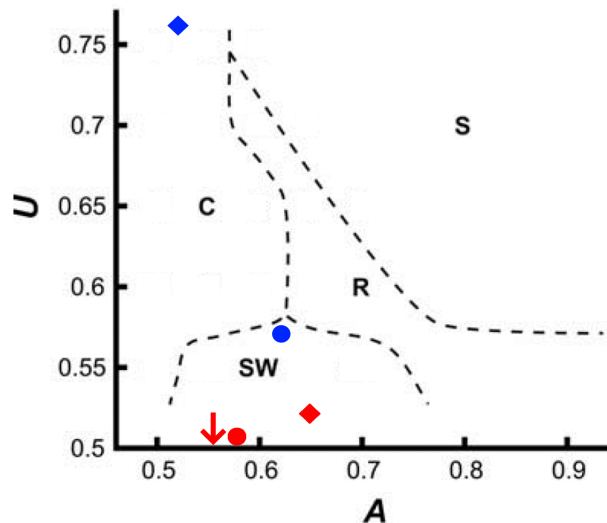
Figure 4-9: Classification of coastal features during calm (blue) and stormy (red) hydrodynamic conditions, for locations FL69 (diamond) and FL70 (circle), adapted from Ashton & Murray (2006a). Classification is a function of the ratio of high-angle waves (U) and the wave climate asymmetry (A).

Based on these parameters, it seems that high-angle waves are likely the cause of the formation of our beach cusps. Despite these parameters indicating whether a coastline would show the growth of coastal features, they are likely less accurate when looking at local events (e.g. singly stormy events). This was indicated in the theoretical background, where Ashton & Murray (2006a) explained that a coastline must have had enough time to adapt to the hydrodynamics. Nevertheless, this simplification of the hydrodynamics suggests that high-angle waves are, at least partly, the cause of the morphological changes.

4.3   Overview and conclusion

To summarize this chapter, we have included an overview of the hydrodynamics we suspect are relevant to finding the physical process that drives the beach cusp formation. We also relate back to the low-energy environment criteria mentioned in the theoretical background (Section 2.1.2), and conclude on our findings concerning the hydrodynamics.

Table 4-4 and Table 4-5 contain typical values associated with the analyzed periods for the respective locations (FL69 and FL70C), so that we may better characterize the system. The columns indicate the average values of the spectral wave height (H_{m0}), stormy wave height (H_{ss}), spectral wave period (T_{m01}), peak period (T_p), and water level (h). We also indicated the dominant wave directions (coming from, θ). The last two columns are the relative amount of high-angle waves (U) and wave climate asymmetry (A), as elaborated in Section 2.1.4.

Some periods were dominated by stormy conditions, which was determined visually from the timeseries of the respective location. In the tables, these periods are indicated by a gray background color. We only show the hydrodynamics corresponding with Shore's measurement periods, since these were used in the data analysis of the next chapter. The complete timeseries are given in Appendix C.

The average wave height during stormy conditions is larger, with a slightly larger stormy wave height as well. A similar relation may be observed with the wave periods. For location FL69, the preference for high-angle waves is in the unstable regime ($U > 0.5$) regardless of the period, even though on average values are lower in stormy periods. Conversely, at location FL70 we see that during periods of stormy conditions we are mostly in the stable regime ($U < 0.5$).

The target levels of the IJsselmeer are between NAP -0.10 and -0.30 m in the summer, and NAP -0.25 m in the winter. The periods of stormy conditions, as indicated in the table, were all found during the summer water levels (or transition to).

Table 4-4: Summary of hydrodynamic quantities characterizing the respective period at location FL69, with wave height (H_{m0}), stormy wave height (H_{ss}), spectral wave period (T_{m01}), peak wave period (T_p), water level (h), dominant wave origin (θ), ratio of high-angle waves (U), and wave climate asymmetry (A).

Period	H_{m0} [m]	H_{ss} [m]	T_{m01} [s]	T_p [s]	h [NAP+m]	θ [°N]	U [-]	A [-]
November to December	0.16	0.30	1.65	2.01	-0.33	160, 280	0.75	0.63 (SE)*
December 2019 to January 2020	0.16	0.31	1.57	1.77	-0.25	160, 320	0.89	0.75 (SE)*
January to February	0.20	0.35	1.68	1.86	-0.14	150, 340	0.92	0.56 (SE)*
February to March	0.22	0.37	1.78	2.04	-0.06	160, 210, 295, 30	0.57	0.51 (N)*
March to May	0.25	0.39	1.91	2.25	0.03	340, 20, 80	0.54	0.71 (N)*
May to July	0.23	0.39	1.86	2.26	-0.12	340, 30	0.59	0.70 (N)*

Table 4-5: Summary of hydrodynamic quantities characterizing the respective period at location FL70C, with wave height (H_{m0}), stormy wave height (H_{ss}), spectral wave period (T_{m01}), peak wave period (T_p), water level (h), dominant wave origin (θ), ratio of high-angle waves (U), and wave climate asymmetry (A)..

Period	H_{m0} [m]	H_{ss} [m]	T_{m01} [s]	T_p [s]	h [NAP+m]	θ [°N]	U [-]	A [-]
November to December	0.14	0.26	1.63	2.05	-0.32	350, 45, 90	0.45	0.61 (SE)*
December 2019 to January 2020	0.12	0.26	1.49	1.88	-0.24	350, 90	0.64	0.72 (SE)*
January to February	0.13	0.21	1.55	1.94	-0.15	300, 350, 90	0.68	0.54 (N)*
February to March	0.17	0.29	1.70	2.11	-0.06	350, 20, 90	0.42	0.58 (SE)*
March to May	0.22	0.35	1.88	2.31	0.05	0, 40	0.22	0.60 (N)*
May to July	0.22	0.37	1.90	2.35	-0.13	350, 40	0.13	0.62 (N)*

*: Wave climate asymmetry implies more waves coming from the North (N), or the South-East (SE).

Considering wave climate asymmetry, there seems to be a preference for waves coming from the North during periods of stormy conditions (summer water levels), and waves coming from the South-East during calmer periods (winter water levels).

It seems that the periods of winter water levels show more high-angle waves (larger U), and the periods of summer water levels less so (lower U). The dominance of high-angle waves during calm conditions was also visible in the wave roses of Section 4.2. Additionally, it was found that wave directions are very dependent on wind directions (see Appendix B.1).

Relating back to the low-energy criteria mentioned in Section 2.1.2, it seems we mostly fulfill (1) average significant wave heights H_s less than 0.25 m, and (2) wave height during storm set-up H_{ss} less than 0.50 m. Some additional analyses substantiating this classification may be found in Appendix B. The third criterium, a narrow beach face, was already fulfilled in Section 2.1.3. We discuss the last criterium, evidence of features inherited by storm events, in Section 5.6.

To conclude, and couple back to our research question (on how to classify the beach cusps), it seems that our system may be considered a low-energy environment. We have found that during winter water levels (calm conditions), we see more high-angle waves than during the summer water levels (stormy conditions). The latter was coupled to the larger variation in wave directions, due to the dominance of wind forcing, which also resulted in the waves coming mostly from the North. These waves can generally be considered steep and short, meaning that they are less affected by refraction, and thus (despite often being low-angle) have the potential to approach the beach at a relatively high angle (even in the nearshore). These waves (that refract less) have been linked to the formation of beach cusps, with the physical driver being high-angle wave instabilities.

5 Morphodynamics

In this chapter we focus on the way the hydrodynamics can explain the morphological changes. To start, Section 5.1 is dedicated to presenting a first view of what changes we can observe from photos alone. The next step is the definition of the waterline (Section 5.2). Quantification of the beach cusps, so that we may objectively assess changes, is done in Section 5.3. The conceptual model used to find the relation between the hydrodynamics and morphological change is described in Section 5.4. The results of applying this model may be found in Section 5.5. Here, we present an overview of the results, where we show some of the cases that are explained by high-angle wave instabilities. This section closes with a summary of the hydrodynamic conditions found representative for the measured morphological change. Lastly, in Section 5.6 we answer the following research questions:

2.   *What classification may be assigned to the beach cusps at the Houtribdijk?*

A: *Which hydrodynamic processes are responsible for the formation of beach cusps?*
B: *Which morphodynamic processes contribute to the formation of beach cusps?*

5.1 Observations

Before delving into the data analysis, we show some of the photos (either orthogonal or satellite) we have of the beaches both locations FL69 and FL70. For each case we include the wave roses of the preceding period, to show what the hydrodynamics looked like. A short description is given that tries to relate the hydrodynamic conditions to the observed morphological change. The intent is that the reader gets a clearer picture of the actual observed change, and how this study approaches the problem of finding the cause. Therefore, we also included thoughts on the cause of the morphological change, not solely observations. These qualitative descriptions will be used as input in formulating the conceptual model.

The figures in this section combine wave roses with orthogonal photos and satellite imagery. Wave roses are shown for both calm and stormy conditions, where the numbers on the axis reflect the total number of 15-minutes wave records in the respective period. They are oriented to the beach (red), so that one may easily see whether waves approach under a low (inside green dashed lines) or high angle (outside green dashed lines). The solid green line indicates the shore normal.

Both locations (FL69 and FL70) described below, include a figure showing the bathymetry as interpolated from the topography and bathymetry measurements. Each is rotated, so that we see a horizontal beach with the transects on the x-axis. The y-axis denotes the cross-shore distance to the reference line used in Shore's measurements. This reference line corresponds to the top of the original revetment of the Houtribdijk. Descriptions on those measurements, as well as a figure showing the entire IJsselmeer side of the Houtribdijk, may be found in Appendix A.2. Larger versions of the orthogonal photos and satellite images may be found in Appendix D.

5.1.1 Location FL69

As could be seen from the elevation plots of Section A.2, this area is characterized by a mostly shallow offshore bathymetry between 2.0 to 3.0 m deep. Notably, the left part (North-Western) is deeper than the rest of the area (see Figure 5-1). As we learned from our hydrodynamic classification and the theoretical background, this deeper part is therefore more likely to experience waves that refract less.
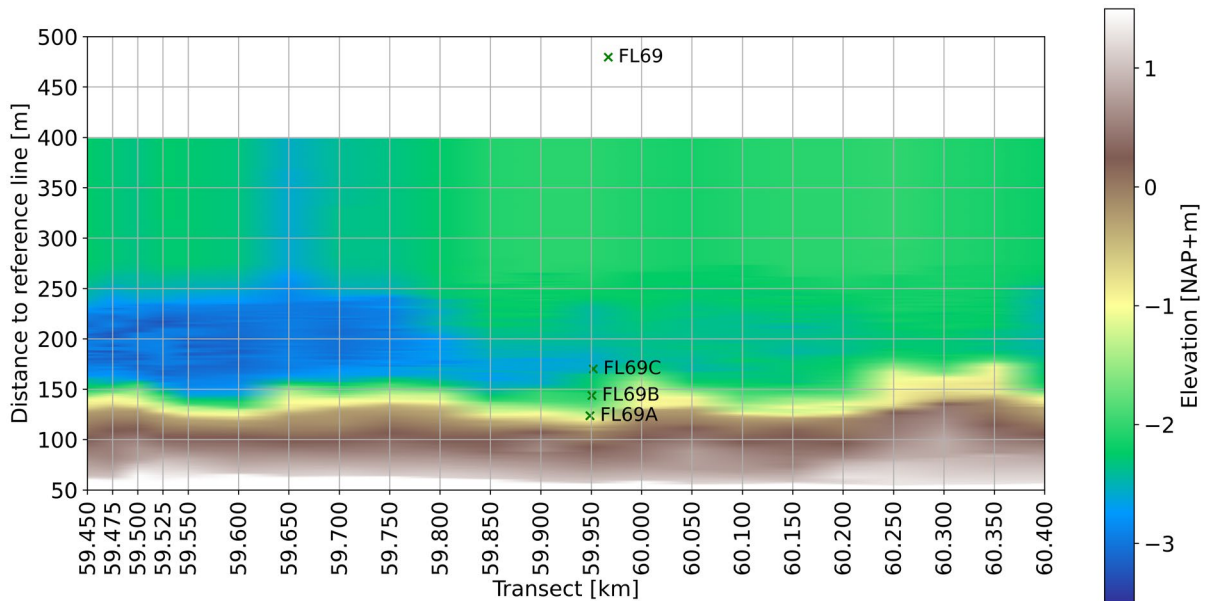
Figure 5-1: Close-up of location FL69 at the as-built measurement.

22 June to 28 July 2019

Figure 5-2 below shows three satellite images of location FL69 from 22 and 29 June 2019. At the top of the figures two wave roses are included representing calm and stormy conditions, respectively. The *y*-axis of the photos shows the distance to the reference line as used by Shore.

Data from the ADV at the offshore location shows that the first four days between (A) and (B) were either calm or stormy, but both arrive at the beach under a low angle form the East. The last three days show stormy conditions approaching the beach under a high angle from the North. The first three weeks of the period from (B) to (C) have nearly exclusively been storms from the North, arriving at a high angle. The last week consisted mostly of low-angle waves, both calm and stormy conditions.

Despite these conditions, from (A) to (B) the beach seems to be in relatively the same shape. For example, looking at the features at km 59.690, 60.060 and 60.320, we see no significant change in amplitude. Looking closely, we might see that features are slightly more pronounced, but nothing that would suggest the apparent stormy conditions. Examining the hydrodynamic conditions from (B) to (C) hints at case B of the micro scale conceptual model (moderately asymmetric high-angle wave climate). However, the low-angle waves of the last week may have prevented the growth in amplitude and displacement of the horn.
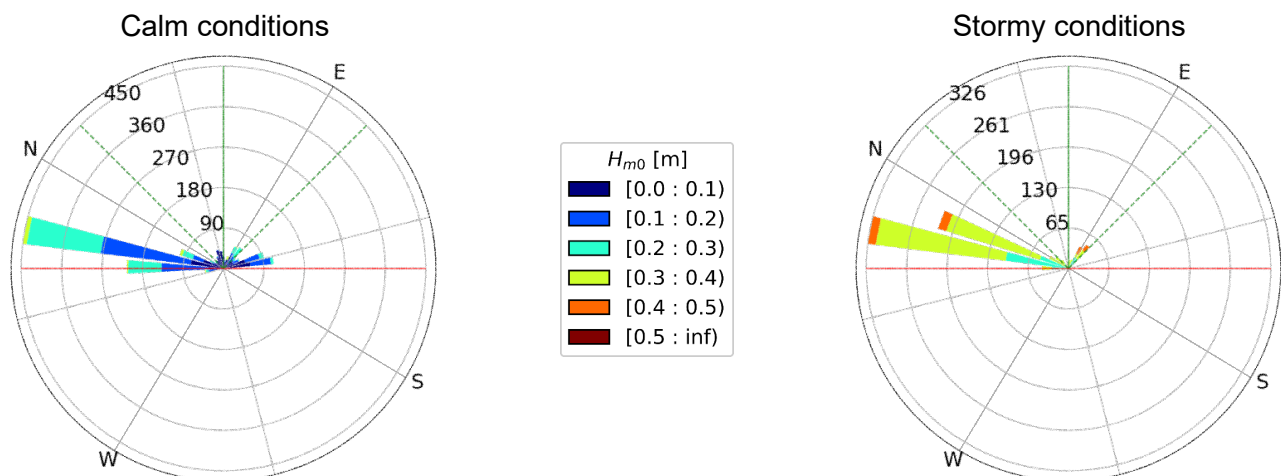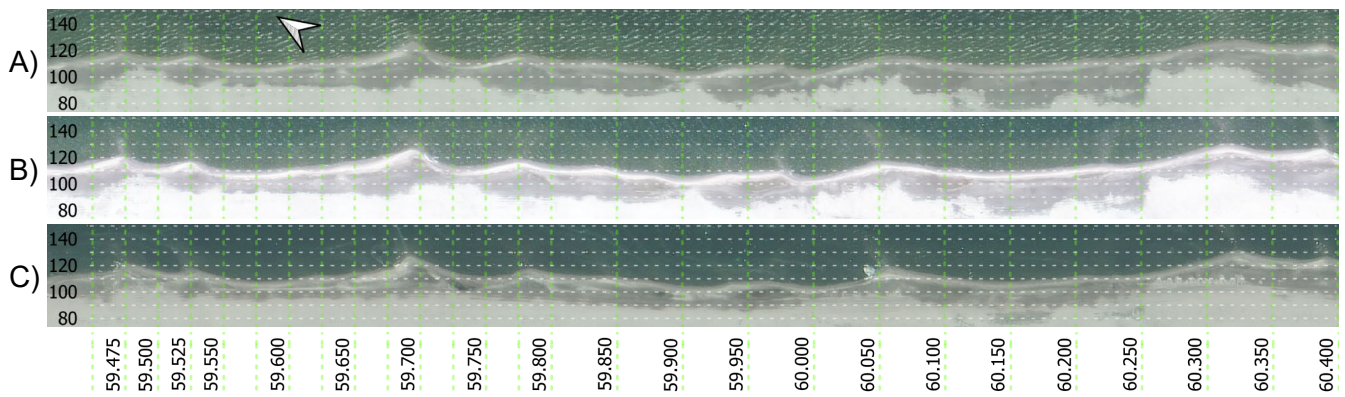
Figure 5-2: Comparison of beaches at FL69, with photos of (A) 22 and (B) 29 June, and (C) 28 July 2019.

28 July to 19 September 2019

The period from (D) to (E) in Figure 5-3 is characterized mostly by waves originating from the North, where most of them are concentrated in the last three weeks. The water levels were about 10 cm lower at (D), but the occasionally stormy conditions were often accompanied by set-up.

Many of them also appear to be 'leaning' towards the right now. This combination of forcing seems to have resulted in a significant increase in amplitude at most of the more prominent cusps (e.g. at km 59.475, 59.525, 59.700, 59.870, 60.060 and 60.320). Despite these changes, the positions of the horns seem to be more or less the same. The morphological changes seem to agree with the micro scale conceptual model (case B), seeing as the perturbations (cusps) seem to have grown. However, our model suggests that horns will be displaced, which is not what we observed.
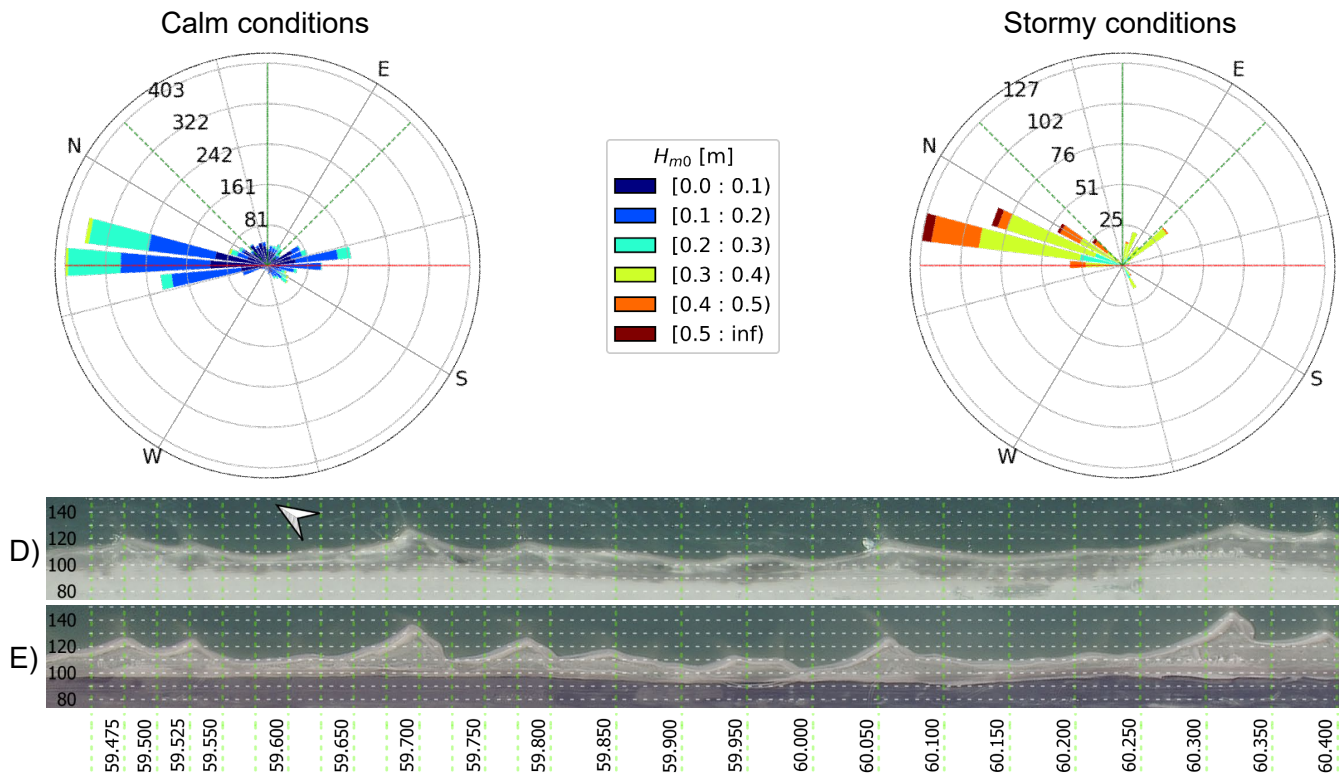
Figure 5-3: Comparison of beaches at FL69, with photos of (D) 28 July and (E) 19 September 2019.

16 November to 14 December 2019

Period (F) to (G) in Figure 5-4 has seen high-angle waves, both calm and stormy conditions, from both the North and South-East. Some of the stormy conditions were even on the low-angle side, coming

30

from the East. The last couple weeks before (H) mostly consisted of high-angle waves approaching from the South-East. Of the three stormy conditions in this last period, two were accompanied by a reduced water level and originated from the South-East. The other storm originated from the North and was accompanied by an increase in water level.

An interesting feature is the apparent spits that have started to form at approximately km 59.680 and 60.320. From the wave climate parameters of Section 4.2, we were not expecting this. The combination of wave attack from both sides is expected to have been the cause for the more symmetric shapes in (G), which seemingly also grew in amplitude. The fact that most waves came from the South-East is potentially why the cusps at (H) seem to be leaning more to the left than at (G). Seeing as the spits seem to grow Northward, it seems likely that forcing in this direction was dominant.

Some other interesting features seen mostly in photo (G), are the smaller features that look like sand waves (e.g. between km 60.060 and 60.220). From the theory we understand that high-angle waves may create new instabilities, which is likely what we see here. It seems strange that high-angle conditions in the period from (G) to (H) seem to have dissipated them. Possibly the storm from the North, with an increased water level, has worked to dissipate the cusps.
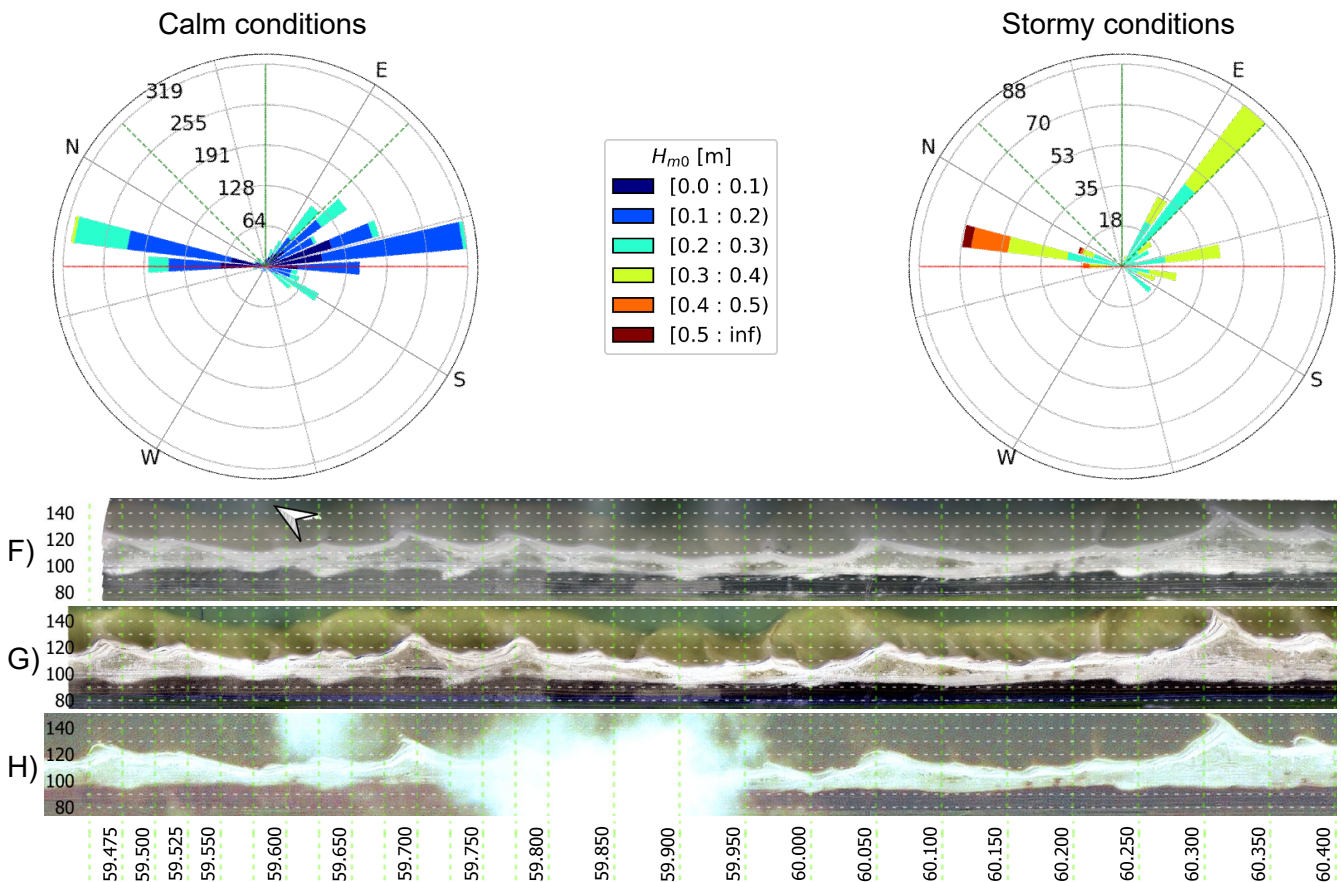
Figure 5-4: Comparison of beaches at FL69, with photos of (F) 16 November, (G) 4 and (H) 14 December 2019.

1 April to 25 May 2020

The first period of Figure 5-5, from (I) to (J), has seen half low-angle storms, and half high-angle storms from the North. The period from (J) to (K) was under the influence of a wave climate coming from the North, some high-angle, but mostly low-angle. Stormy conditions in the second weekend of May occurred with a water level set-up, combined with an angle of incidence around the critical angle of 45°.

The figure shows that the first period does not experience significant growth of amplitudes, with the exception of the cusp at km 60.320. However, there does seem to be some movement to the right, especially between km 59.450 and 59.550. Especially the bay to the right of cusp 60.320 seems to have been filled in during this period. From period (J) to (K), the amplitudes have decreased slightly and there is some additional displacement to the right.
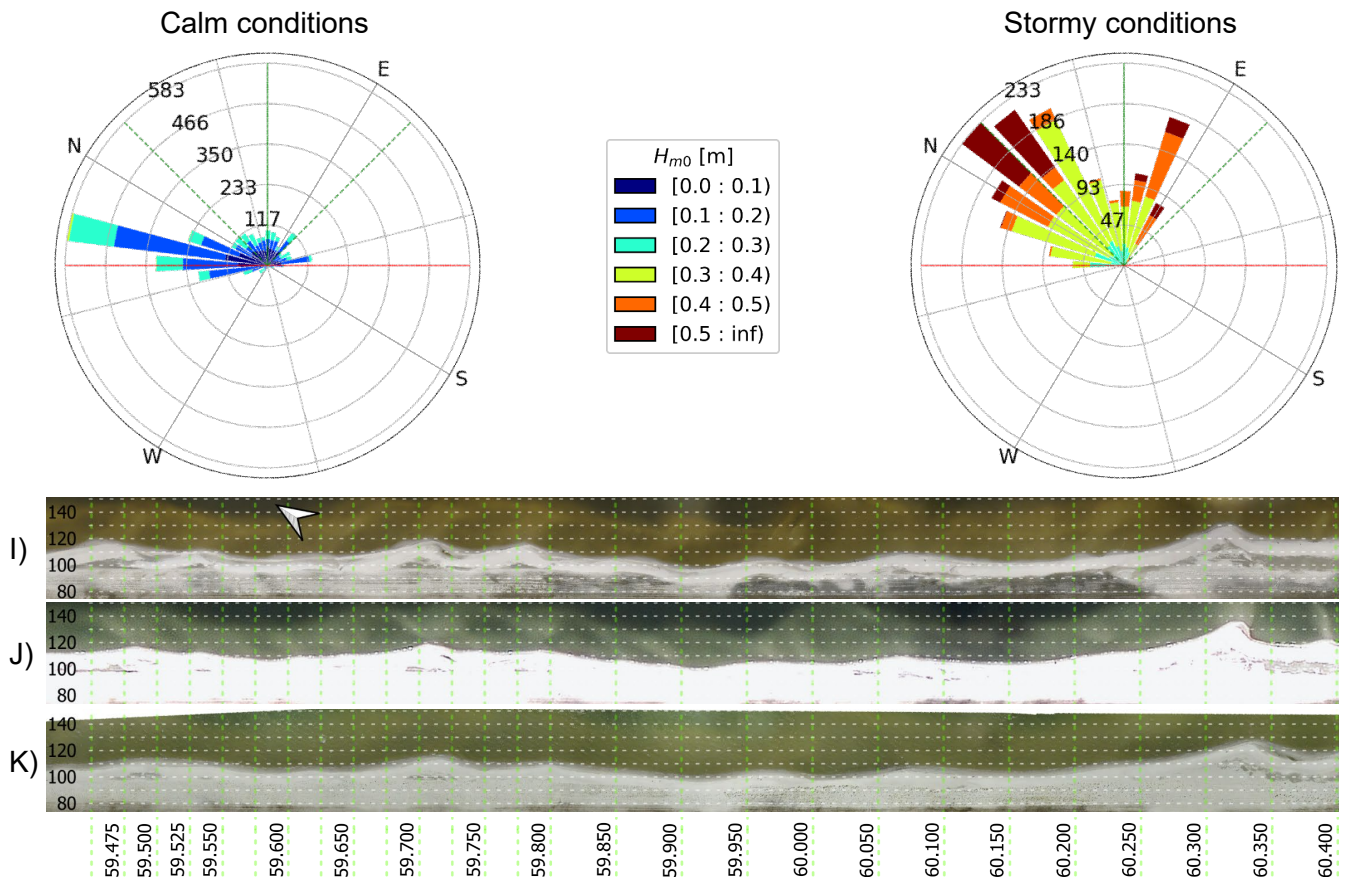
Figure 5-5: Comparison of beaches at FL69, with photos of (I) 1 and (J) 26 April, and (K) 25 May 2020.

5.1.2 Location FL70

The offshore bathymetry at location at FL70 is mostly deeper than FL69, reaching depths of 3.0 to 3.5 m (see Figure 5-6). Similar to the deeper parts of FL69, the sandy shores may experience waves that refract less. Since data for the ADV at FL70C was only available from October 2019 onwards, we could not compare the same early periods as for location FL69.
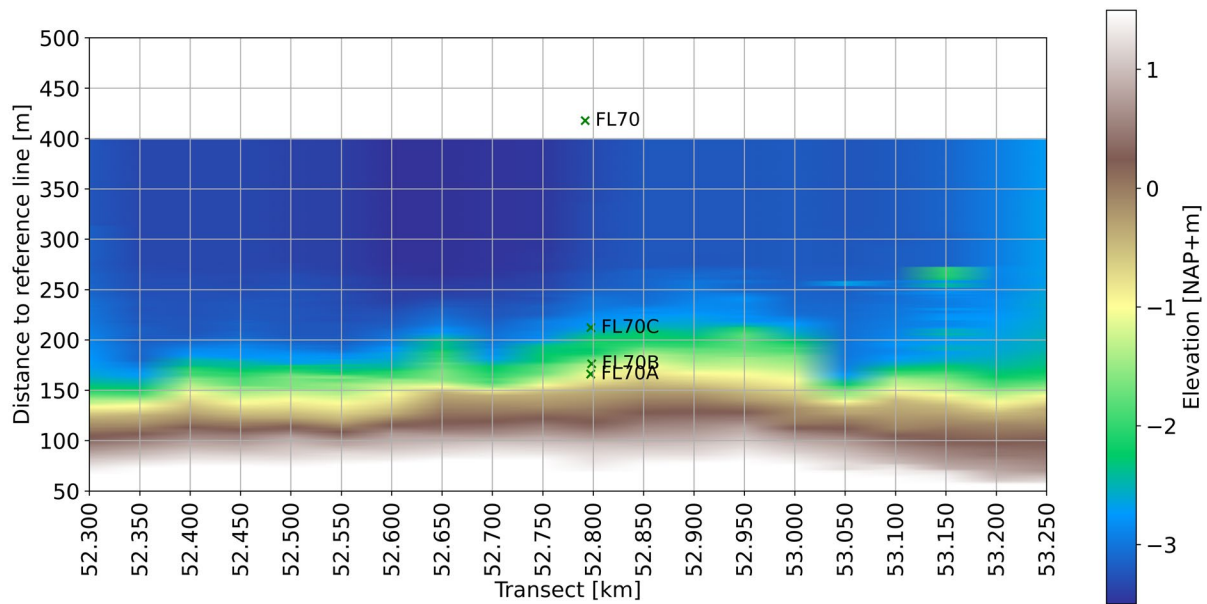
Figure 5-6: Close-up of location FL70 at the as-built measurement.

16 November 2019 to 16 January 2020

Periods (L) to (M) in Figure 5-7 mostly show either low-angle stormy conditions, or high-angle calm conditions. From (M) to (N) there were almost exclusively high-angle calm conditions. Only three stormy low-angle events occurred. Water levels fluctuated on an approximately weekly basis in a range of 20 cm.

The high-angle calm conditions seem to conform to the theory, as we see a general increase in amplitude at features along the Eastern half (right side). The coastline seems to have damped out, but this might also be caused by the water level being on the higher end of the range at the time of the photo (N). All in all, this entire period seems to be rather dynamic, but with no clear wave conditions that can explain them.
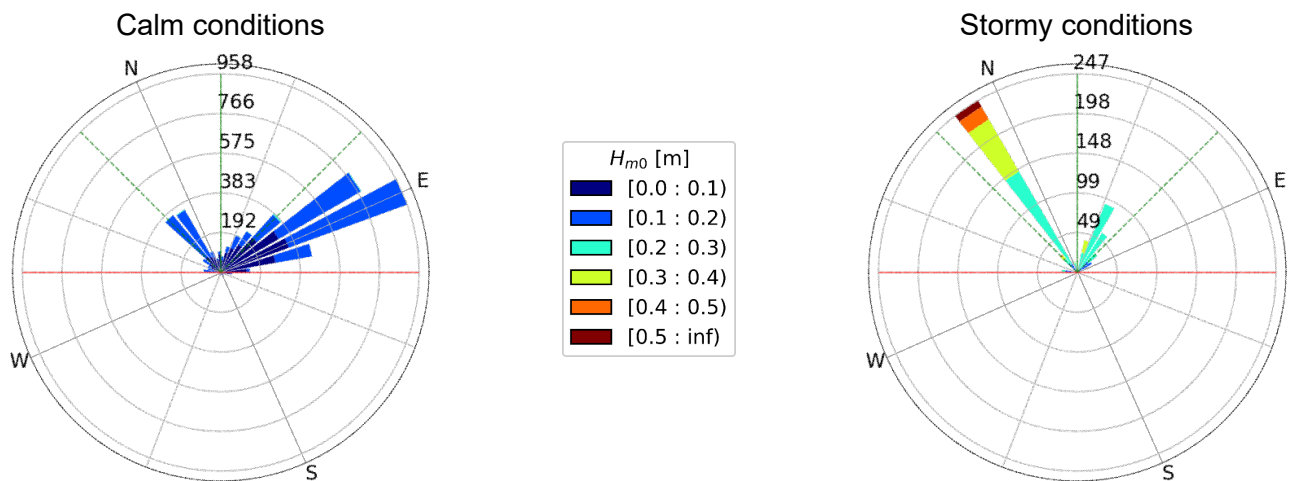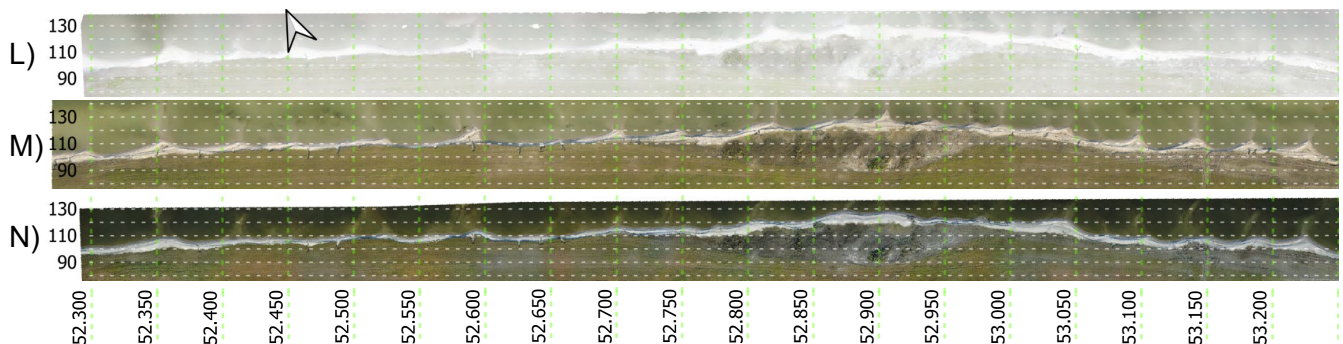
Figure 5-7: Comparison of beaches at FL70, with photos of (L) 16 November, (M) 4 December 2019 and (N) 16 January 2020.

24 March to 1 April 2020

Even though this period is short, some interesting things happened here. In Figure 5-8, from period (O) to (P) we saw some low-angle calm conditions from the East, followed by low-angle stormy conditions. One stormy event lasting several days in the middle of this period came from a high-angle (North-West). This period ended with stormy conditions approaching under a low-angle from the East. From (P) to (Q) the beach experienced high-angle calm conditions from the East for the first two days, followed by a low-angle storm from the same direction the last day. There was a general downward trend of the water level here, falling by about 25 cm.

The cusps seem to have decreased significantly in amplitude in only a few days. In this time, the spits we can vaguely see at km 52.860 and 53.030 seem to have completely disappeared. Similarly, other 'arching' features (e.g. at km 52.320 and 52.560) have seemingly been dissipated as well.

A possible explanation for this, could be an emergence of underlying bathymetry due to the decreasing water levels, which were not damped out by the low-angle storm at the end. Other explanations may be that calm conditions are underestimated at this location, or that we are dealing with low-angle wave instabilities (Section 2.2.3), both of which can be explained by waves that refract less as a result of a deeper bathymetry.

Seeing as the last day experienced a similar stormy condition as occurred at the end of period (O) to (P), we do not suspect low-angle wave instabilities. Instead, this case seems to hint at a previously unexposed elevation of the beach, now being forced by low-angle waves, finally starting to dissipate the cusps. This last explanation seems to conform to the fourth criteria in Section 2.1.2, stating that low-energy beaches inherit features from higher-energy events.
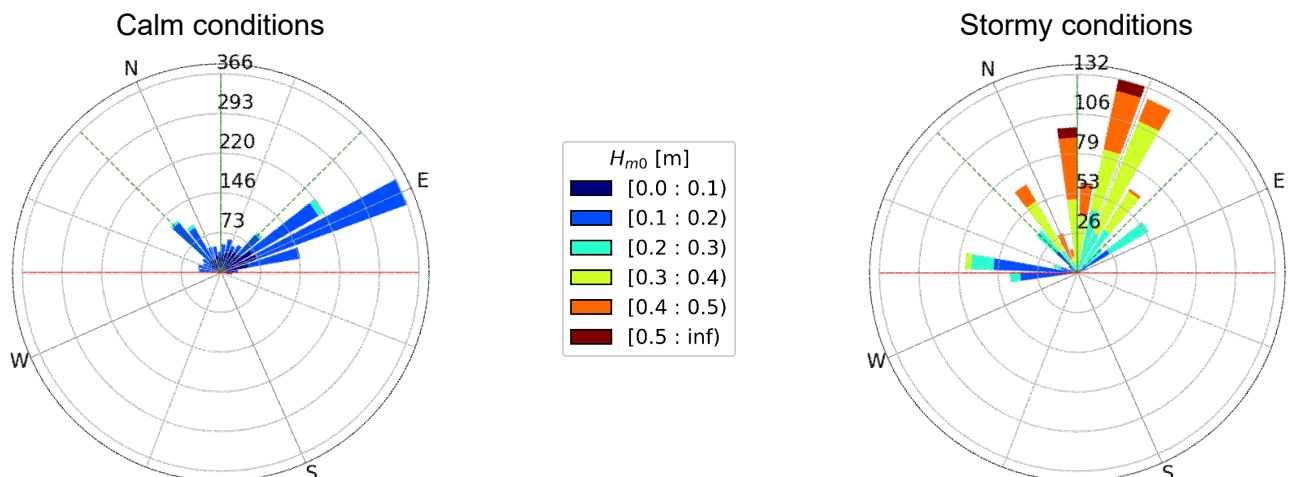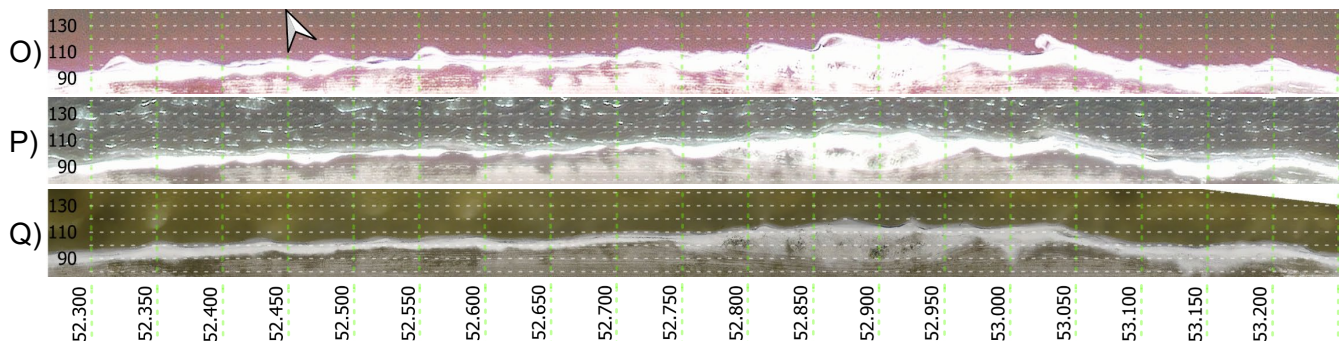
Figure 5-8: Comparison of beaches at FL70, with photos of (O) 24 and (P) 27 March, and (Q) 1 April 2020.

25 May to 17 July 2020

Since ADV data at location FL70C was only available until 10 June 2020, we supplemented the rest of this period with data from the ADV at FL69. A high correlation during stormy conditions is given as argument (as shown in Appendix A.3).

For the entire period shown in Figure 5-9, water levels were more or less constant. From (R) to (S) the beach seems to have experienced almost exclusively low-angle stormy conditions from the North. Next, period (S) to (T) shows some high-angle wave conditions, either from the North-West or the East. The last week of this period, however, consisted of calm and stormy conditions approaching at the critical angle of 45°.

These first conditions may have decreased the amplitude of the more prominent cusps at km 52.350, 52.530 and 52.600. Under influence of the conditions from (S) to (T), amplitudes seem to have increased slightly, leading to the suspicion that the high-angle conditions are responsible, despite the (questionable) low-angle conditions in the last week.
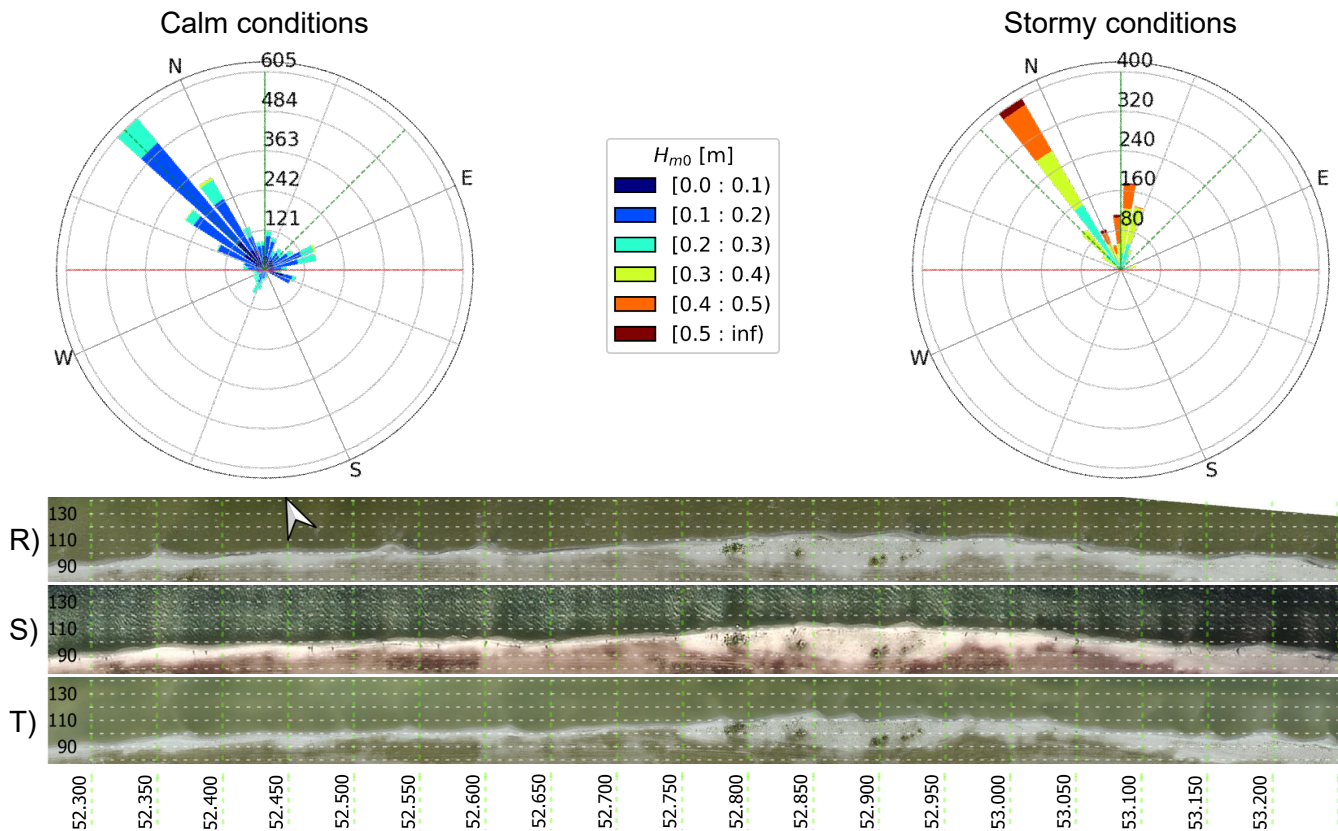
Figure 5-9: Comparison of beaches at FL70, with photos of (R) 25 May, (S) 21 June and (T) 17 July 2020.

5.2 Waterline results

The first step in the method described in Section 3.3.1 involved determining a reference elevation, as shown in Table 5-1. These were determined using the STB data, taking the average of the second half of the preceding period, and adding 0.15 m. This method was chosen since it resulted in the least amount of manual corrections to the waterline.

Table 5-1: Reference water levels used in the waterline analysis.

Measurement data	Water level [NAP+m]	
	FL69	FL70
16 November 2019 (T0)	-0.35	-0.32
4 December (T1)	-0.31	-0.30
16 January 2020 (T2)	-0.26	-0.25
28 February (T3)	-0.01	-0.02
1 April (T4)	-0.04	-0.02
25 May (T5)	-0.12	-0.14
17 July (T6)	-0.12	-0.14

Applying the second step to the topography and bathymetry measurements, and after some corrections, we arrive at the waterline. In Figure 5-10 and Figure 5-11, the waterline (blue) from the analysis is used together with the interpolated grid to visualize the development of the beach. Similar to previous figures, the x-axis indicates the transect and the y-axis denotes the cross-shore distance to Shore's reference line. The horns of the beach cusps are indicated by a red cross, the bays with a green cross. We define beach cusps, or other coastal features, as the shapes between bays.

Comparing the figures, we clearly see that the waterline at location FL69 is much less horizontal, implying larger cusps. At this location we can also distinguish some cusps that persist throughout time (e.g. km 59.700, 59.775, 60.050 and 60.300). These prominent cusps were previously observed in Section 5.1. They seem to be slowly migrating to the right (South), having moved approximately 20 to 30 m in the analyzed period (eight months). Also, the platforms at location FL70 seem to be wider, and the depths offshore of these platforms is generally larger. More information on the elevations and measurements may be found in Appendix A.2.
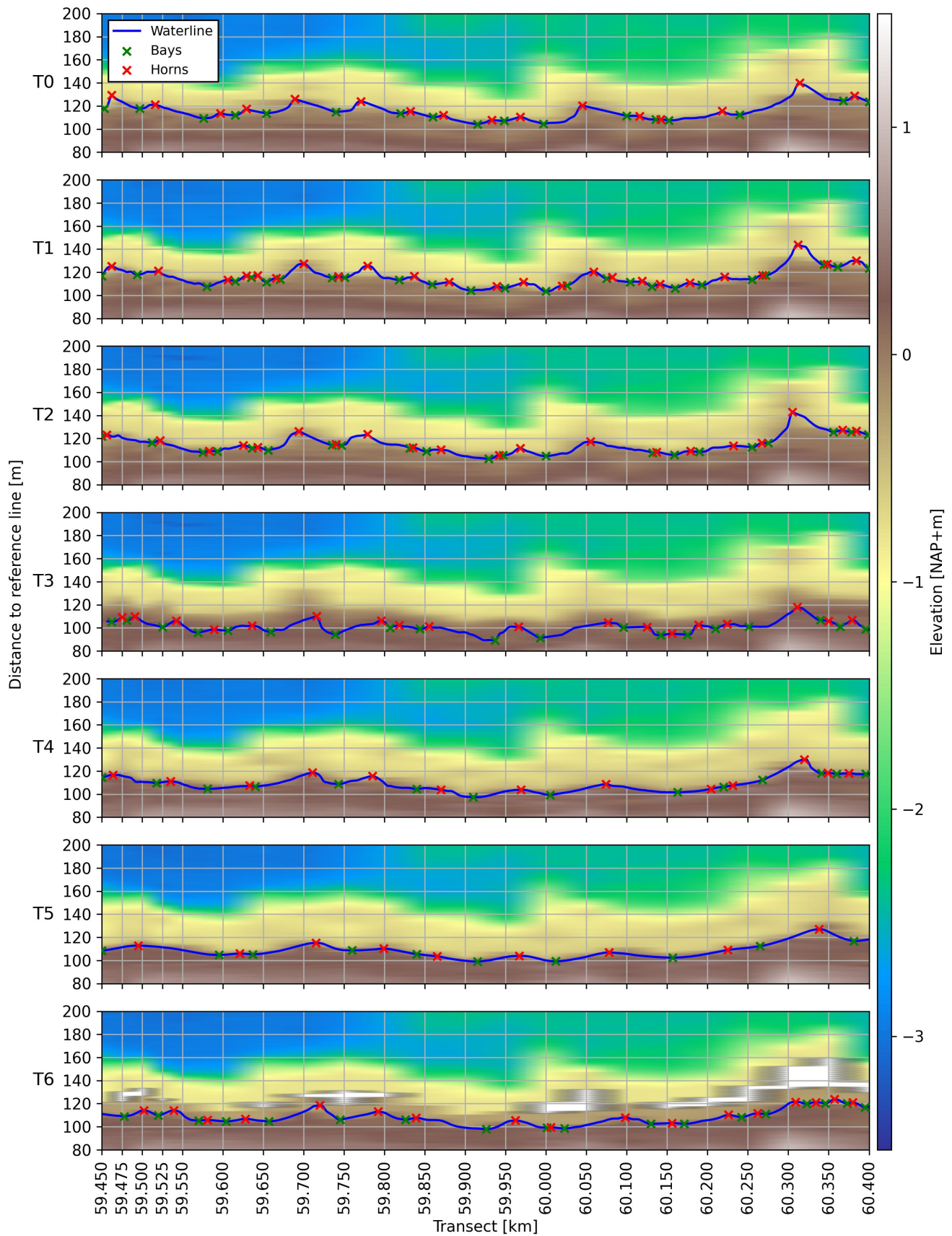
Figure 5-10: Interpolated beach and bathymetry, including waterline position, at location FL69.
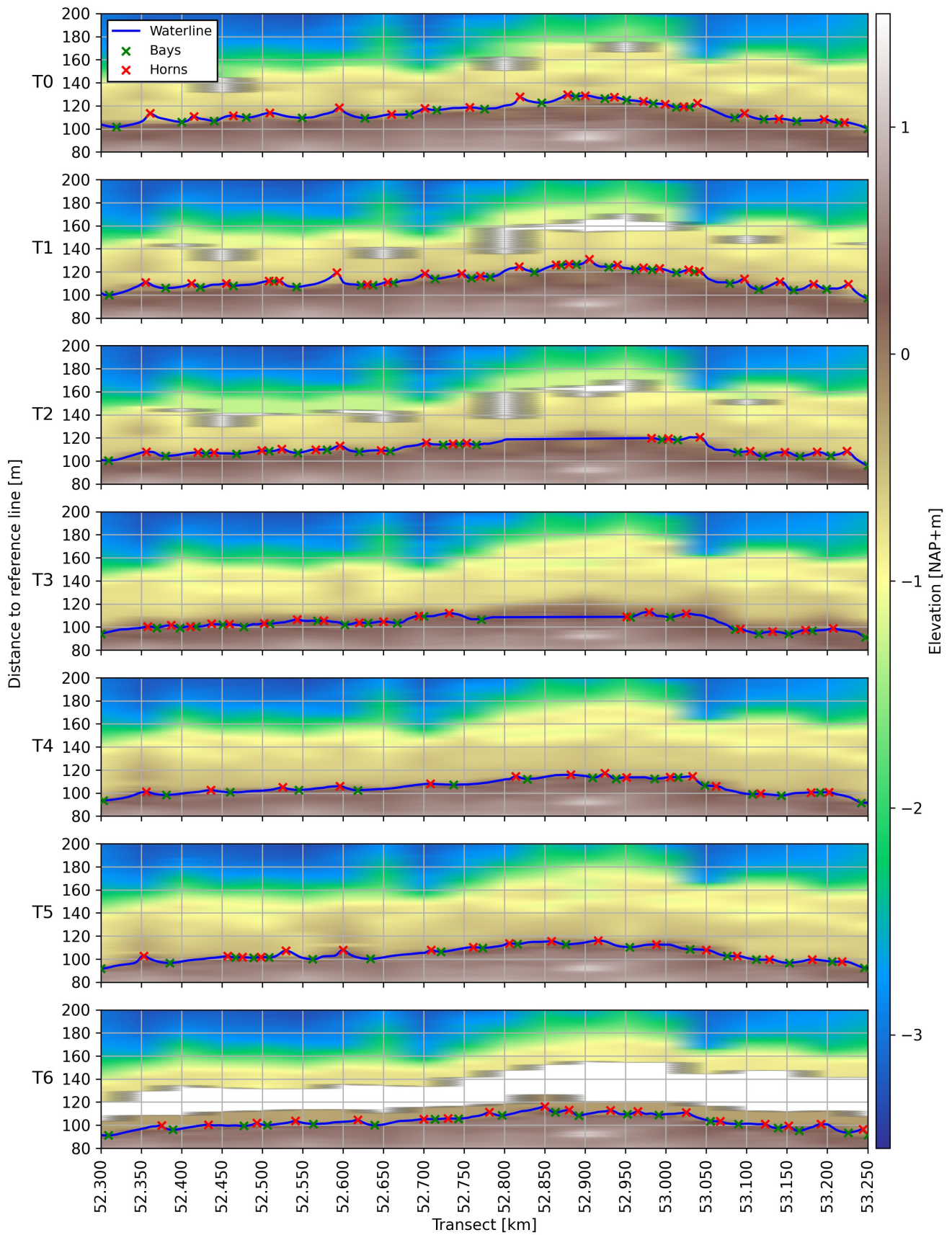
Figure 5-11: Interpolated beach and bathymetry, including waterline position, at location FL70.

5.3 Beach cusp quantification

The waterlines shown in the previous section were processed to quantify each of the beach cusps (each shape between two green crosses). Applying the method described in Section 3.3.2, we were able to find quantities that describe the size and shape of each beach cusp.

The result of this quantification is shown in Figure 5-12 and Figure 5-13, per location, per measurement period. Here, the first plot shows the number of beach cusps (N_c), the second the length (L_c), the third the amplitude (A_c) and the last the shape asymmetry (As). Top values indicate maximum values found for the respective period, bottom values the minimum, and middle values (dotted) the average.

Most notably, we see that the number of cusps is much more variable at location FL69 than at FL70. Wavelengths are similarly smaller at FL70, and maxima are significantly larger at FL69. However, the minimum wavelengths are more or less the same at both locations. Another significant difference is the larger amplitudes at location FL69, with often a factor 2 difference between the averages and maxima of FL70. Minima of amplitudes are in the same order of magnitude at both locations. The same holds for the range of asymmetries, where values at FL70 are only slightly lower than at FL69.

Relating back to the periods of stormy conditions shown in Table 4-4 (Section 4.3, February onwards), it seems that for location FL69 the range of amplitude significantly decreased. This coincides with the periods of rising water levels, as the summer target levels are now in effect, leading to a change in the elevation of the analyzed waterlines. At location FL70, this change in amplitude is visible to a lesser degree.

During these periods of stormy conditions, the average asymmetry at location FL69 has gone up slightly. This is consistent with the literature on high-angle wave influences (Section 2.4), where a dominance of Northern stormy conditions would theoretically lead to moving of the horns in the direction of the waves (towards the South-East). Even though location FL70 also experienced these Northern stormy conditions, the dominance of low-angle conditions (as found in Table 4-5) may explain why these trends in asymmetry are not so clear here.
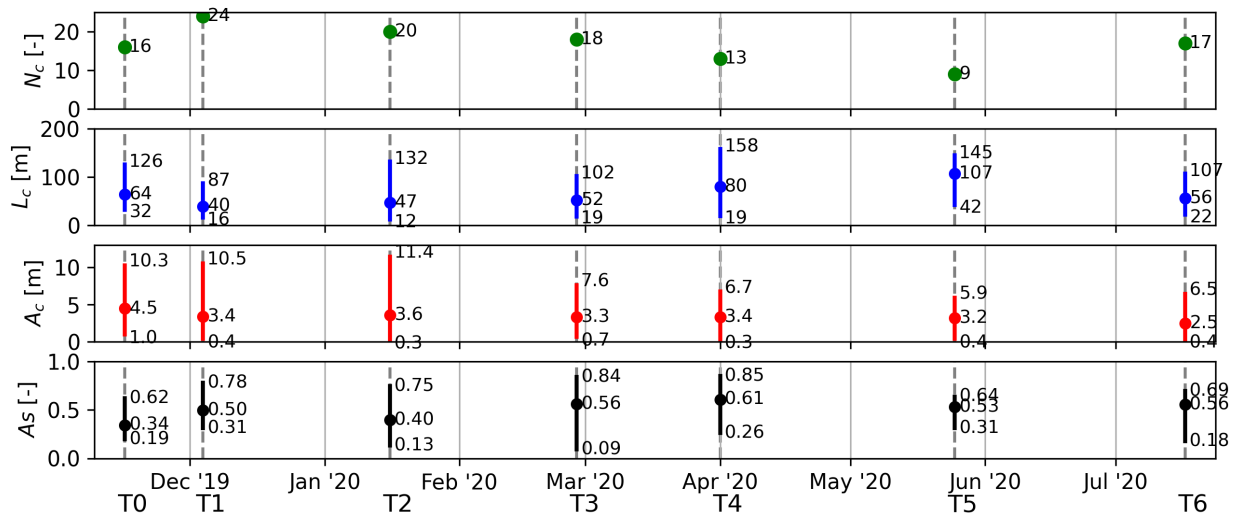
Figure 5-12: The variation of beach cusp quantities at location FL69 over time, with the number of cusps (N_c), their wavelengths (L_c), amplitude (A_c), and shape asymmetry (As).
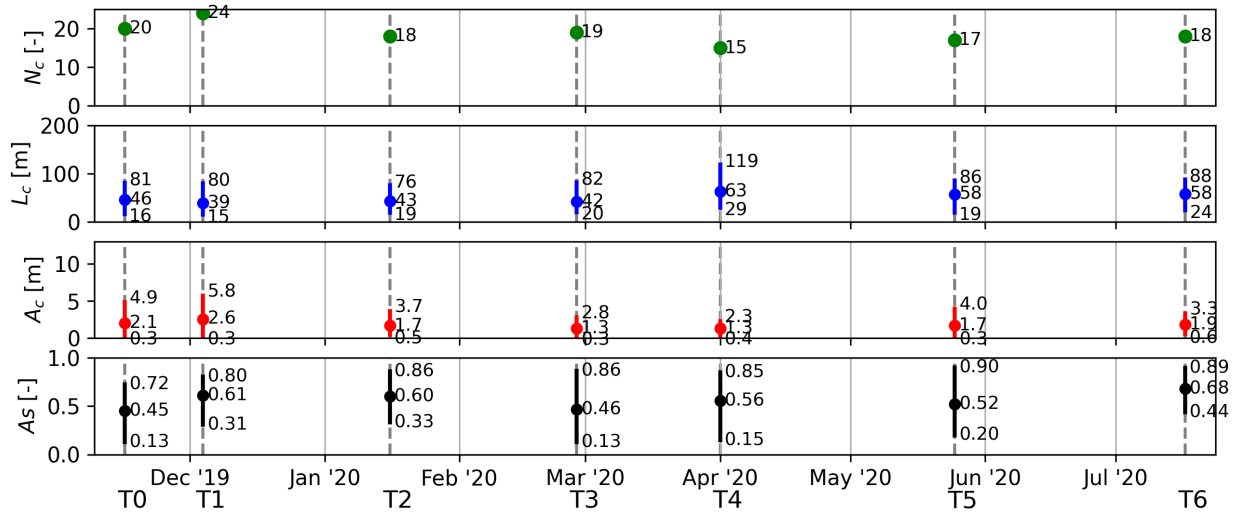
Figure 5-13: The variation of beach cusp quantities at location FL70 over time, with the number of cusps (N_c), their wavelengths (L_c), amplitude (A_c), and shape asymmetry (As).

As mentioned in Section 5.2, location FL69 has a number of cusps that have persisted for over a year, which can be seen by comparing photo (U) to (V) and (W) in Figure 5-14. The first of the photos is a satellite image of approximately one month after construction. The cusps at roughly km 59.700, 59.775, 60.050 and 60.300 were evaluated individually, indicated in the figure by a red arrow. As far as we know, the persistent cusps are remnants of the initial construction of the sandy shores. Over the course of a year, they can be seen to move southward, but the cross-shore location of the horns is more or less the same. A similar quantification as above is done for these individual cusps, of which the results may be found in Section 5.5.2.
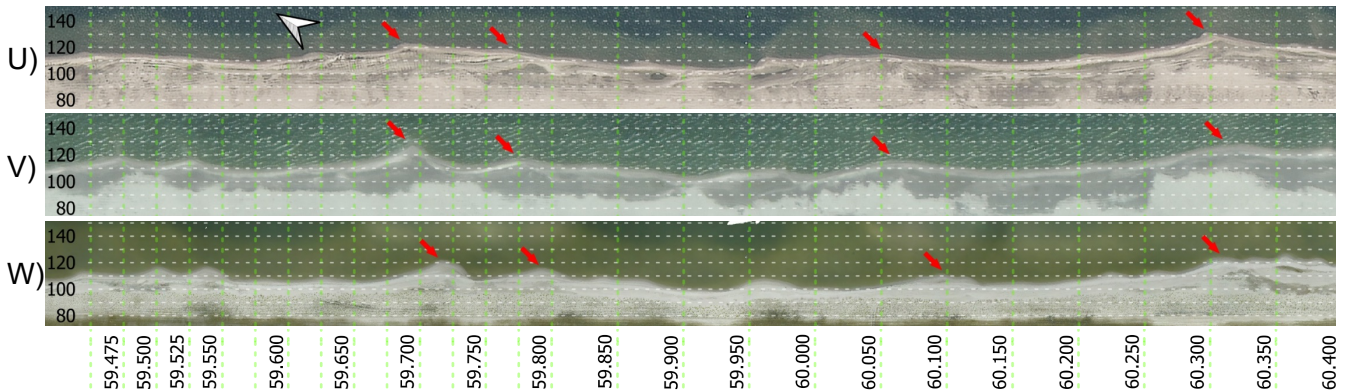
Figure 5-14: Comparison of beaches at FL69, with photos of (U) 24 March, (V) 22 June 2019 and (V) 17 July 2020.

5.4 Conceptual model

In Section 2.4 of the theoretical background, we described the development of a shoreline bump in the form of a conceptual model for the micro scale. We explained what quantities can be used to classify these bumps as beach cusps in our methodology (Section 3.3). The previous sections have served to find the waterline and determine the number of cusps (N_c), their wavelengths (L_c), amplitudes (A_c) and shape asymmetry (As).

We defined our general research hypothesis in Section 5.4.1. To find a link between the hydrodynamics and the changes in the quantities above, we have expanded the micro scale conceptual model of Section 2.4. The resulting macro scale conceptual model describes the morphological changes of larger stretches of coast. In Section 5.4.2 we describe this macro scale and in Section 5.4.3 we elaborate on the influence of water level variations.

5.4.1 Hypothesis

Using what we learned from the analysis of the hydrodynamics conditions (Chapter 4), observations, and beach cusp quantification (preceding sections), it seems likely that high-angle waves are involved in morphological changes. This suspicion is backed by most recent studies found in the literature study (Chapter 2). Therefore, we have formulated our general hypothesis as follows:

The formation of the coastal features is the result of an asymmetrical wave climate with a clear preference for high-angle waves. This causes the sediment to deposit at the peaks of small perturbations, which subsequently grow due to the resulting sediment transport (by existing theory on S-φ transport relations). An initial perturbation is unavoidably made during construction, which quickly grows due to the interaction between the hydrodynamic forcing and the morphology (positive feedback). After some time, the perturbation will grow into more prominent beach cusps and slowly start stabilizing (negative feedback).

5.4.2 Macro scale

To apply our conceptual model on a macro scale, we theorized the evolution of averaged values of the quantities mentioned in Section 2.4. This was based on observations, where it was often the case that a change in wave climate influenced the amplitude of the cusps, the horn positions, and the shape asymmetry (leaning of the feature). The waterline analysis itself has shown that also the number of cusps quickly changes under influence of the hydrodynamics.

Shore mentioned that change of beach morphology can occur in the order of days, as was noticed when topography measurements were once done a few days apart (R. de Zeeuw, personal communication, July 1, 2020). Measurements done with the LiDAR and by walking with a GPS device have shown significant difference in a matter of four days, where they concluded morphological change to have a time-scale of days (Shore Monitoring & Research BV., 2020b).

An (extreme) example of this for location FL70 is given in Figure 5-15 (previously shown in Figure 5-8). From period (X) to (Y) there was a storm perfectly shore-normal, with a visible decrease in number and amplitude of cusps in a matter of days. The observed change corresponds to our expectations; waves approaching under a low angle lead to dissipations of the cusps. However, we did not expect this to occur within the span of three days.
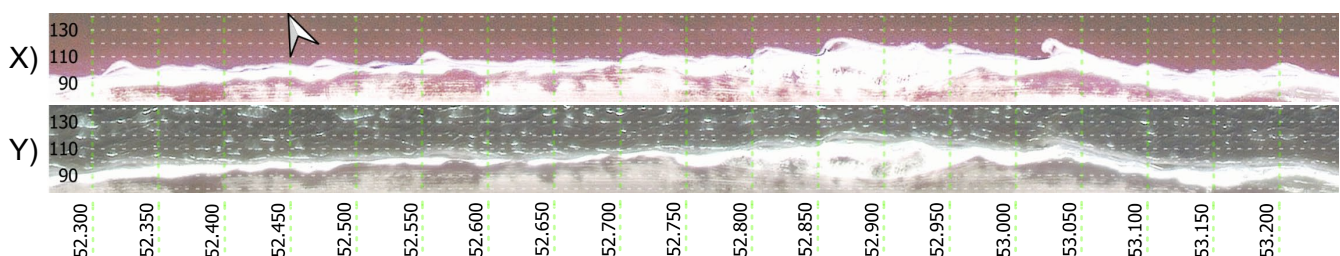
Figure 5-15: Comparison of beaches at FL70 in 2020, with a (X) satellite image of 24 March and (Y) satellite image of 27 March.

A concept we use to substantiate the observations, is that a sudden change in wave climate will lead to a strong response in the form of change in wavelength or amplitude. How different this wave climate is from before, will determine the magnitude of the change. We use what we learned from theory, stating that low-energy beaches inherit features from higher-energy events, to assume that stormy conditions will leave their 'mark' on the beach. We therefore expect these stormy conditions, being much different from preceding calm conditions, to be the primary source of morphological change.

Another concept we use, is the theory that states that transport is higher when waves have a relative angle of incidence of around 45° (critical angle). Continuing the concept above, we expect that the first

instabilities start to form at locations where relative angles are on the high-angle side of this critical angle. Since little volume is required to form those smaller instabilities, we expect the first response of the beach to be an increase in number of cusps.

Combining these two concepts, we theorize the following in relation to macro scale morphological change. Based on the findings by Shore and Figure 5-15, we thought it wise to describe these in short-term (order of days) and long-term (order of weeks to months). Since quantifying the rate of morphological change is difficult, we focus on qualitative changes.

- When the wave climate changes to more high-angle waves, the short-term response would be an increase in number of cusps, as small instabilities start to form along the coastline. This translates to a decrease in the average wavelength and amplitude. As high-angle conditions continue, the long-term response would eventually be an increase in these quantities, as the smaller cusps start being absorbed into the larger cusps.
- Conversely, a change to more low-angle waves would result in the short-term increase in average wavelength and amplitude, because the number of cusps is expected to decrease (smaller cusps are 'easier' to dissipate). As the stabilizing low-angle wave conditions continue, the long-term response would be a further increase in the average wavelength, and a decrease in the average amplitude as the larger cusps slowly dissipate as well.

These theorized morphological changes are summarized in Table 5-2 below. The variables in the table are the number of cusps (N_c), their average wavelength ($\bar{L}_c$), and average amplitude ($\bar{A}_c$). The signs and colors indicate an increase ('+', green), or decrease ('-', red) of the respective morphological quantity.

Table 5-2: Macro scale conceptual model, overview of theorized changes of the number of cusps (N_c), their average wavelength ($\bar{L}_c$), and their average amplitude ($\bar{A}_c$), under influence of different hydrodynamic forcing.

Case		N_c	$\bar{L}_c$	$\bar{A}_c$
High-angle waves	Short-term	+	-	-
	Long-term	-	+	+
Low-angle waves	Short-term	-	+	+
	Long-term	-	+	-

In addition to the theorized changes in number of cusps, wavelength, and amplitude, we also assess the changes in shape asymmetry. As discussed in Section 4.3, there seems to be a relation between the wave direction and the shape asymmetry and horn position of the cusps, referred to as 'leaning'. Considering the beach as the horizontal, we therefore expect the shape asymmetry to increase if more waves come from the left, and decrease if more come from the right. This is the same theorization as presented for the micro scale conceptual model of Section 2.4.

5.4.3 Water level variations

One other process that was included in the macro scale conceptual model, was the influence of water level variations. On open ocean coasts, tidal influences are normally expected to prevent the growth of features (Sections 2.1.2). A reason for this, is that wave action is distributed vertically on the beach profile. Having no water level variations therefore means that all wave action is focused on a small vertical range of the profile. The criteria of low-energy environments stating that the beach inherits features from higher-energy events, is based on this process.

Therefore, we expect water level variations, if any, to reduce any increase in beach cusp amplitude or wavelength caused by high-angle waves. This has led to the following additions to the conceptual model:

- If representative (or dominant) hydrodynamic conditions force the beach at roughly the same elevation as the measured waterline, the conceptual model as described in the previous section is applicable.
- When these conditions are accompanied by a decreased water level, we expect the lower elevations to experience most of the wave action in the following way:
  - For high-angle wave forcing, we expect the horns to move offshore, and the bays to move landward (increase in amplitude). Near horns we say this increase in amplitude of the lower elevation that will likely not be visible when water levels rise again (because they will be submerged). Near the bays we say an increase in amplitude to be visible in all elevations up to the top of the berm. We assume the steep beach face (see cross-shore profile in Section 2.1.2) means that erosion of the lower parts will lead to the same results at higher elevations.
  - For low-angle wave forcing, we expect the horns to move landward, and the bays to move offshore, leading to a dissipation of the cusps (decrease in amplitude). The reverse of the above is then assumed. The decreased amplitude near the horns will be visible at all elevations above, while the decreased amplitude near the bays is visible only at the elevation experiencing wave action.
- Whenever such conditions coincide with an increased water level, the beach experiences wave action at a higher elevation. The last observation of Section 5.1.1 hints at the damping effect of such a case. We assume the following effects:
  - For high-angle waves, the increased amplitude near the horns will be visible at lower elevations (as water levels return to normal), because material will sink downwards. The increased amplitude near the bays will likely only be visible at the elevation experiencing the wave action.
  - For low-angle waves, the decreased amplitude near the horns will only show itself at the elevation attacked by the waves. The decreased amplitude near the bays will also be visible at the lower elevations.

The theorized effects of changes in water level are summarized in Table 5-3 below. The variables in the table are amplitude near the cusp horns ($A_{c,horn}$), and the amplitude near the cusp bays ($A_{c,bay}$). The signs and colors indicate an increase ('+', green), constant value ('=', yellow), or decrease ('-', red) of the respective amplitude.

Table 5-3: Overview of theorized changes of horn amplitudes ($A_{c,horn}$), and bay amplitudes ($A_{c,bay}$), under influence of changes in water level.

Water level	High-angle		Low-angle	
	$A_{c,horn}$	$A_{c,bay}$	$A_{c,horn}$	$A_{c,bay}$
Constant	+	+	-	-
Decrease	=	+	-	=
Increase	+	=	=	-

5.5 Conceptual model results

In previous sections we have found the waterline per morphological period for each of the locations (FL69 and FL70). Then we analyzed these waterlines to find several quantities, namely the number of cusps (N_c), their wavelength (L_c), amplitude (A_c) and shape asymmetry (As). Subsequently, the conceptual model from the theoretical background was expanded to be applicable to the scale of the entire waterline.

Now, the final step is to apply this conceptual model, so that we may find the hydrodynamic conditions responsible for the morphological change. The macro scale part of the model (previous section) was

applied to the whole beach segments at both location FL69 and FL70. Additionally, the cusps at 59.700, 59.775, 60.050 and 60.300 are evaluated using the micro scale part of the conceptual model (Section 2.4). Some of the most convincing findings are presented in this section, while its entirety may be found in Appendix E. We end with an overview of the representative hydrodynamic conditions.

5.5.1 Macro scale

Due to an often asymmetrical wave climate, the cusps in the examples below correspond to case B (moderately asymmetrical) or C (fully asymmetrical) of the micro scale model. Since our hypothesis is aimed at high-angle wave instabilities, we will focus the results below on high-angle conditions.

FL69: 16 November to 4 December 2019 (T0 to T1)

When comparing the waterlines of T0 and T1 in Figure 5-16 with each other, we found that the average shape asymmetry increased from 0.35 to 0.51 (the cusps were more symmetrical). The number of cusps increased from 16 to 24 and, subsequently, the average wavelength and amplitude decreased.

Considering these changes in quantities, we expect a high-angle wave climate from the North. It was found that in the five days preceding the waterline measurement of T1, most hydrodynamic conditions were high-angle, originating from the North. Assuming these conditions as representative fully explains the macro scale changes of the beach.
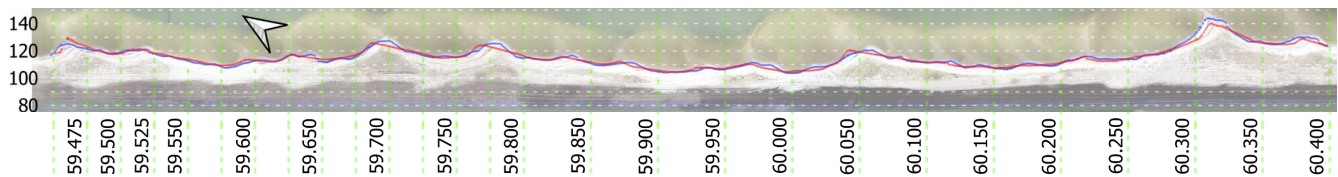
Figure 5-16: Comparison of waterlines at FL69, for the period 16 November (red) to 4 December 2019 (blue).

FL69: 25 May to 17 July 2020 (T5 to T6)

In Figure 5-17, the waterlines of T5 (red) and T6 (blue) show that the shape asymmetry on average has increased slightly, from 0.53 to 0.56, meaning they are 'leaning' slightly more to the right. Most prominently, however, is the significant increase in number of cusps from 9 to 17. This is also visible in the average wavelength and amplitude, which both decreased.

The last one and a half weeks before T6 had shown almost exclusively high-angle waves originating from the North. This period is therefore assumed to be representative of the hydrodynamic forcing. However, an increase in water level in this representative period has previously been observed to yield damped responses, due to a different elevation experiencing wave action. This means that the theorized effect of water level variations was likely not relevant to this case. Nonetheless, the change in the waterline seems to be conform the macro scale conceptual model.
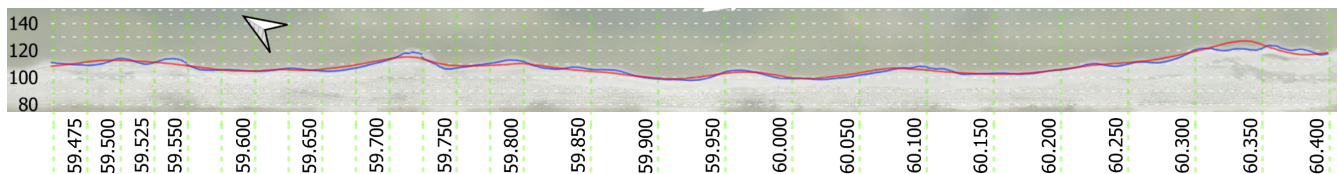
Figure 5-17: Comparison of waterlines at FL69, for the period 25 May (T5, red) to 17 July 2020 (T6, blue).

FL70: 1 April to 25 May 2020 (T4 to T5)

An example of morphological change at a short time-scale, is what happened between T4 (red) and T5 (blue) in Figure 5-18. The shape asymmetry decreased slightly from 0.56 to 0.52 and the number of cusps increased from 15 to 17. Average wavelengths subsequently decreased, as did the average amplitude.

These changes are not exceedingly large. However, the suspected hydrodynamics only lasted for two and a half days, and many cusps seem to have been displaced. Taken together, this hints at potentially considerable change if exposure to these conditions is sufficiently long. This case, however, is not fully explained by our conceptual model, since we expected the shape asymmetry to increase instead of decrease.
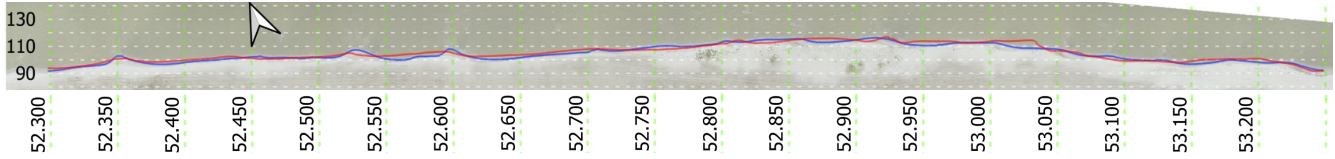
Figure 5-18: Comparison of waterlines at FL70, for the period 1 April (T4, red) to 25 May 2020 (T5, blue).

5.5.2 Micro scale

The cusp at km 59.700 is presented as an example in Figure 5-19. An overview of all four of the cusps may be found in Appendix F. In contrast to the micro scale conceptual model in Section 2.4, we have not included the wavelength as part of the analysis. The reason is that this quantity was found to vary a lot over time, due to the emergence of smaller cusps on top of the larger, persistent cusps. This proved it difficult to objectively assess this quantity.

Characteristic of all the cusps in the figure, is that their peaks displaced to the right over the analyzed period. This displacement presents itself in the change in shape asymmetry, which has generally increased. Also, they all decreased in amplitude over the period of approximately February to June 2020. These changes seem to suggest a persistent dominance of low-angle waves (case E of the micro scale model). The fact that these waves mostly originated from the North, presented itself in the cusps mostly 'leaning' towards the right in this period. The final measurements of July once again show an increase in amplitude. These changes are on average consistent with wave forcing from the North (case B/C).
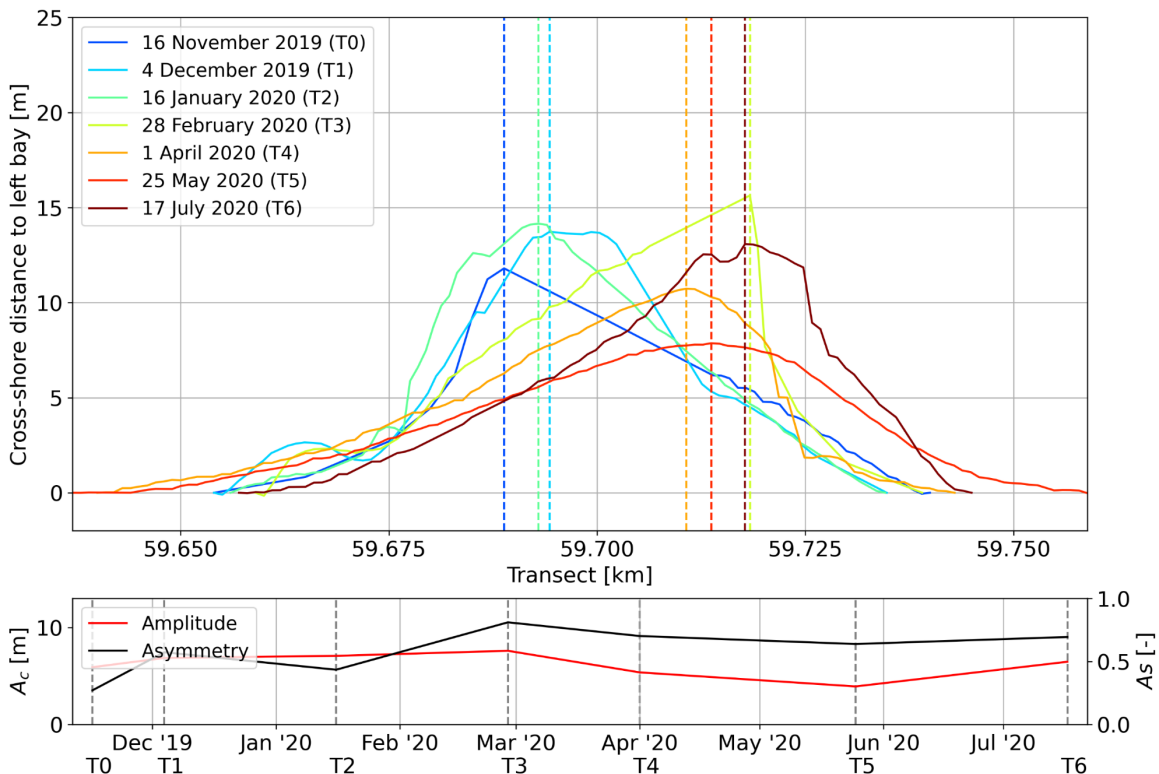
Figure 5-19: Evolution of local prominent cusp at km 59.700 of location FL69.

5.5.3 Representative hydrodynamics

By applying the conceptual model, described above and in Appendix E, we have formulated the hydrodynamics conditions that may be considered representative for the morphological periods. Values for the wave heights (H_{m0}), peak periods (T_p) and offshore directions (wave origins; nautical, ϕ_0, and local, $\phi_{0,loc}$) are presented as averages in Table 5-4 and Table 5-5 for locations FL69 and FL70, respectively. Local angles are defined using the convention in Figure 5-20. The last column indicates whether these conditions were high-angle (HA) or low-angle (LA).

For the period T2 to T3, during the transition from winter to summer water levels, we were unable to find representative conditions. Instead, we evaluated T2 and T3 with T4, so that we may still use and draw conclusions from this period.

Table 5-4: Overview representative hydrodynamic conditions for location FL69, with the wave height (H_{m0}), peak wave period (T_p), nautical offshore wave angle (ϕ_0), and local offshore wave angle ($\phi_{0,loc}$).

Period	H_{m0} [m]	T_p [s]	ϕ_0 [°N]	$\phi_{0,loc}$ [°]	Type
T0 to T1	0.15	2.25	337	82	HA
T1 to T2	0.28	2.44	87	-28	LA
T2 to T3	n.a.	n.a.	n.a.	n.a.	n.a.
T2 to T4	0.38	2.74	50	9	LA
T3 to T4	0.38	2.74	50	9	LA
T4 to T5	0.36	2.69	30	29	LA
T5 to T6	0.17	2.33	350	69	HA

Table 5-5: Overview representative hydrodynamic conditions for location FL70, with the wave height (H_{m0}), peak wave period (T_p), nautical offshore wave angle (ϕ_0), and local offshore wave angle ($\phi_{0,loc}$).

Period	H_{m0} [m]	T_p [s]	ϕ_0 [°N]	$\phi_{0,loc}$ [°]	Type
T0 to T1	0.17	2.38	347	37	LA
T1 to T2	0.17	2.38	344	40	LA
T2 to T3	n.a.	n.a.	n.a.	n.a.	n.a.
T2 to T4	0.35	2.89	38	14	LA
T3 to T4	0.40	2.92	11	13	LA
T4 to T5	0.12	1.91	323	61	HA
T5 to T6	0.18	2.37	348	36	LA
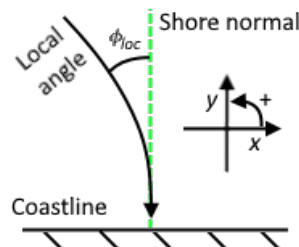
Figure 5-20: Definition local wave angle of incidence (ϕ_{loc}), being the offshore wave angle of incidence normalized by the beach orientation.

5.6 Conclusion

We used our methods described in Chapter 3 to find the waterline, quantify beach cusps, and find the corresponding hydrodynamics. Quantities like the number of cusps (N_c), their wavelength (L_c), amplitude (A_c) and shape asymmetry (As) were used to objectively assess morphological change. The conceptual model, both on the macro and micro scale, was used to find the hydrodynamic conditions responsible.

A summary of the macro scale results is presented below in Table 5-6, with a complete picture included in Appendix E. The results of the micro scale changes at location FL69 are summarized in Table 5-7. Evolution of these cusps over time may be found in Appendix F. The table is meant to show the reader which cases can reasonably be linked to wave processes ('W') described in the conceptual model. The distinction between low-angle ('LA') and high-angle ('HA') forcing is indicated as well.

A 'v' (green) indicates that the found hydrodynamics agree with the conceptual model (e.g. three or all quantities change as expected), an 'x' (red) indicates no representative conditions could be found. A '?' (yellow) means that only one or two quantities agreed with the conceptual model. In any case, we refer to the respective section in Appendix E to see what the exact inconsistencies were. Additionally, we checked if taking into account water level variations ('L') could explain the change. If the hydrodynamics agreed with the morphological change, the latter was not necessary, and the table cell is left empty. If there were any discrepancies, we included an evaluation of the water level mechanism.

Table 5-6: Overview of macro scale cases where representative hydrodynamics explain morphological change, with 'W' the wave angle mechanism, and 'L' the water level mechanism.

Period	FL69			FL70		
	Forcing	W	L	Forcing	W	L
T0 to T1	HA	v		HA	v	x
T1 to T2	LA	v		LA	?	v
T2 to T3	LA	x	?	HA	x	?
T2 to T4	LA	v		LA	v	
T3 to T4	LA	v	?	LA	v	
T4 to T5	LA	v	v	HA	?	x
T5 to T6	HA	v		LA	v	x

Table 5-7: Overview of micro scale cases where representative hydrodynamics explain morphological change, with 'W' the wave angle mechanism, and 'L' the water level mechanism.

Period	59.700		59.775		60.050		60.300	
	W	L	W	L	W	L	W	L
T0 to T1	v		v		v		?	x
T1 to T2	v	?	v	?	v		v	?
T2 to T3	v		v	?	v	?	v	
T2 to T4	v		v		v		v	
T3 to T4	?	x	?	x	?	x	v	
T4 to T5	v	?	v	?	v	?	v	?
T5 to T6	v		v	x	v		?	?

It has become clear that the macro scale approach can, in many cases, explain the large-scale development of the beach and mostly link the hydrodynamics to the morphology. This is primarily the case for location FL69, and slightly less so for FL70. On the micro scale, it seems that results agree in a similar way. Reasoning from the macro scale to the representative hydrodynamics included several assumptions. Relating these hydrodynamics back to the micro scale has therefore substantiated our assumptions, since they would then agree with the prevailing theory of high-angle wave instabilities.

On the macro scale, we have seen that dominant wave directions can be linked to changes in asymmetry and horn position. Despite some wrongly predicted asymmetries, it seems that cusps are generally 'leaning' in the direction of forcing. Also, high- and low-angle wave conditions seem to increase and decrease the number of cusps, respectively. As an exception, at FL70 the number of cusps has been predicted wrongly a few times. Wavelengths were seen to always be predicted correctly, however. Lastly, despite some errors in the prediction of amplitudes, they mostly seem to change according to the theory of the conceptual model of Section 5.4.

The persistent cusps can be seen to change their shape over time, where satellite images indicated their slow migration southward. Looking at the waterlines found in Section 5.2, it seems that these larger cusps have moved approximately 20 to 30 m in eight months. This coincides with the stormy periods showing mostly waves originating from the North, and the theory that horns move and shape asymmetry changes in the same direction as the waves are going (Section 4.3). Mostly the periods between February (T3) and June (T5) have shown less pronounced features. Most representative hydrodynamic conditions during these months were classified as low-angle cases. Despite these conditions being low-angle, this period had experienced record wave heights. Additionally, water levels in the summer are artificially kept higher, leading to a previously unexposed elevation of the beach now being subject to wave forcing. The two processes of low-angle waves and water level variations combined may have contributed to visually less features, despite the wave conditions being classified as stormy.

Location FL69 seems to be most consistent with the conceptual model, especially when considering cases with little water level difference between the start and end of the period (T0 to T1, T1 to T2 and T5 to T6). However, large water level variations seem to sometimes cause unexpected responses. Especially for location FL70, we could not explain morphological changes based on water level fluctuations. In the theoretical background we described the possibility of low-angle wave instabilities, relating to steep beach faces and waves that are less refractive. This might prove to be the solution for some of the unexplained cases at location FL70, where some low-angle conditions may have led to a high-angle response of the waterline.

Considering the hypothesis that high-angle waves lead to unstable coastal features like beach cusps, it seems the conceptual model (based on the theory of high-angle wave instabilities) can in many cases explain morphological changes. Inclusion of the concept that smaller cusps contain less volume, and therefore more easily emerge or dissipate (Section 5.4.2), seems to fit this theory well. Additionally, it seems that including water level variations may explain some of the discrepancies, but definitely not all. Due to a lack of time, we have not investigated other processes that may explain the occasional inconsistency between conceptual model and measurements, but we have elaborated on some of them in the discussion of Chapter 7 and recommendations of Chapter 9.

The fourth criteria for low-energy environments (Section 2.1.2) described that features are inherited by storm events. The effects of water level fluctuations, together with the concept that representative stormy conditions result in the measured morphological changes, seem to fulfill this criterium. This, despite the fact that most of the cases studied involved low-angle wave forcing. However, no matter the directional forcing, most cases seem to give results conform the conceptual model. Assuming this means the conceptual model is correct, we can conclude that the concept of morphological change due to high-angle waves has a lot of credibility. In the discussion (Section 7.1), we elaborate some more on this topic.

To conclude, our results so far show that high-angle wave instabilities are definitely part of the process that shapes the beach cusps. Additionally, the suspected influence of water level variations can possibly explain some of the uncertain cases. Both of these processes were substantiated by literature described in the theoretical background. The conceptual model we applied seems to relate the hydrodynamics to the morphological change rather well. With these results, we seem to have mostly answered research questions 2A and 2B and confirmed our hypothesis (Section 5.4.1). To further substantiate our answers, we show the application of a numerical model in the next chapter.

6 Numerical modeling

Our next step is to provide more evidence that the beach cusp development at the Houtribdijk is driven by high-angle wave instabilities, through use of a numerical model. In Section 6.1, we describe what our model should be capable of, in the form of a list of requirements. We also choose the most fitting model in this section, and describe some assumptions made in the model and how we deal with them. The next section (Section 6.2) concerns how we set-up the model, describing parameters, calibration, and the input of our representative hydrodynamics. In Section 6.3 we show the results of the simulations for a few representative cases, with all of them together included in Appendix H. Finally, we present a conclusion of our findings in Section 6.4. The conclusion at the end of this chapter will elaborate on the relevant research questions, 3A through D:

> 3.   *How can we simulate the morphodynamics of beach cusps at the Houtribdijk?*
>
> A: *Which numerical model may be used to substantiate the processes causing beach cusps?*
> B: *Which numerical model may be used to reproduce the morphodynamics?*
> C: *What combination of calibration settings may be used to represent the beach cusps best?*
> D: *What differences and similarities do the model show when validating with other periods in time?*

6.1   Choice of numerical model

From the literature study, we found that many models are able to represent low-energy environments to a certain extent. Roelvink et al. (2020) have found that most can either reproduce the shoreline shape (Ashton et al., 2001), or accurately quantify the transport rates, but rarely both. Below, we have rephrased what our data analysis has taught in the form of a list of requirements:

- Due to the expected emergence of shoreline instabilities, a model that includes the mechanism described by Ashton et al. (2001) may be useful. This mechanism, the upwind correction, allows for the growth of high-angle wave instabilities without creating so-called 'erosion waves' (i.e. numerical discretization artifacts).
- The model preferably includes wave transformation processes, like shoaling, refraction, diffraction and breaking. It may be useful if the model settings can be changed to include or exclude these processes.
- The model should be able to simulate various hydrodynamic conditions (e.g. calm and stormy conditions).
- Interaction between hydro- and morphodynamics is essential. This also means that the model preferably considers sediment characteristics (e.g. grain size d_{50}) and is able produce self-organized results. As described in literature (Section 2.2.1), we would like a model whose change in morphology is initiated by the hydrodynamics, and subsequently stabilized by the emerging shape of the beach.
- To sufficiently visualize even small-scale coastal features, a model that has a large range of spatial steps (grid sizes) may be useful.
- Due to the limited time available for the thesis, a commercially available or open-source model is preferable.
- If choosing a brute-force approach, the model should be able to accept a topography or waterline file as initial conditions, such that the (first) measurements of the bathymetry and beach can be included. This will, in a way, serve as the definition of an initial perturbation. The model should additionally be able to accept a wave time-series in this case.

- If choosing a schematized approach, the model should be able to accept a simple (planar) beach topography as initial condition. In this case, the model should be able to run with schematized hydrodynamic conditions.

From the literature study we may conclude that, when considering most recent models, we either have one that is mostly applicable at scales larger than the cusps at the IJsselmeer (Ashton & Murray, 2006a), or a non-hydrostatic computationally expensive model, which likely requires a lot of expertise (Roelvink et al., 2020). ShorelineS was the most suitable and was chosen due to the limited time available (we focused on data analysis) and the aim of finding the physical process, as opposed to precisely predicting coastline change. This recently published model by Roelvink et al. (2020) fulfills the posed requirements best. Additional properties and characteristics of ShorelineS, as well as an elaboration of the self-organizing aspect of the model, may be found in Appendix G.

6.2   Model set-up

Simulations were run using the representative hydrodynamics found in Section 5.5 (and Appendix E). An elaboration of the model input, including calibration parameters, may be found at the end of this section, in Section 6.2.2.

The current version of the model includes the option to automatically choose a time-step, which improves stability and optimizes runtime. However, this means the hydrodynamic conditions as determined using the conceptual model can only be applied in a schematized way (i.e. by average wave directions, heights, and periods). This required us to combine the brute-forced waterline initial conditions, with schematized hydrodynamic conditions. This contradicts our requirements, however, the conceptual model was derived using schematized hydrodynamics as well, so this contradiction was left unattended.

The model uses a Cartesian coordinate system in its input files, but converts this to a longshore (s) and cross-shore (n) coordinate system. Change in n is computed through the hydrodynamic forcing and the chosen transport formulation. After the effect of other processes are applied (Roelvink et al., 2020), the coordinates are converted back to Cartesian in order to update the waterline position. Several of the model settings are elaborated below.

Wave properties like wave heights, peak periods, and directions, as well as the nearshore water depth depend on the scenario. Other model parameters are kept constant, either due to model restrictions, or because of our application of the model (finding the physical process). Similarly, the transport formulation KAMP (Table G-1) was chosen. It is argued that this formulation contains most of the relevant physics, e.g. refraction, grain size, profile slope, water density and grain density. The KAMP transport formulation also has a set of two calibration parameters (α; factor for point of breaking, γ; breaking coefficient with 5% breaking waves). Since we focus on verifying the high-angle wave mechanism, instead of precisely predicting coastline evolution, we leave them at their default values ($\alpha = 1.8$ and $\gamma = 0.72$). A brief overview of simulations using other transport formulations may be found in Appendix G.2. An overview of the input parameters is given in Table 6-1, where we also indicated what values we used as default in our modeling.

Table 6-1: Overview of ShorelineS model parameters, including the default values used in the modeling of locations FL69 and FL70.

Variable	Description	Usage	Default value	
			FL69	FL70
S.Hso	Significant wave height [m]	Computation of the automatic time-step, refraction, and longshore transport.	-	-
S.tper	Peak wave period [s]	Computation of the automatic time-step, refraction, and longshore transport (for CERC2 and KAMP).	-	-
phiw	Wave direction [°]	Computation of the automatic time-step, refraction, and longshore transport. Also used to find shadowed coastline sections, the application of the upwind correction and to determine the direction a spit may develop.	-	-
S.ds0	Initial space-step [m]	Create the initial coastline from an input file and to add or remove grid points, if deviating to far from this value. Also used to compute the automatic time-step and longshore transport rate.	2.0	2.0
S.d	Active profile height [m]	Compute the automatic time-step and determine the change in cross-shore direction from the transport rate.	0.8	0.7
S.ddeep	Offshore water depth [m]	Calculate refraction for an alongshore uniform bathymetry.	2.3	2.7
S.dnearshore	Nearshore water depth [m]	Calculate refraction for an alongshore uniform bathymetry. Used to calibrate the model (see Section 6.2.1).	-	-
S.spit_width	Critical width of spit [m]	To determine whether a spit may form at a coordinate s.	2.0	2.0
S.rhow	Density of water [kg/m³]	Computation of the automatic time-step and longshore transport (CERC2 and KAMP).	1,000	1,000
S.rhos	Density of sand [kg/m³]	Computation of the automatic time-step and longshore transport (CERC2 and KAMP).	2,650	2,650
S.tanbeta	Mean profile slope [-]	Computation of the automatic time-step and longshore transport (KAMP).	0.046	0.022
S.d50	Median grain diameter [m]	Computation of the automatic time-step and longshore transport (KAMP).	$3.0*10^{-4}$	$3.5*10^{-4}$

The initial space step was chosen based on a value in the same order of magnitude as the average amplitudes (as found in Section 5.3). The spit width was chosen as the same value, following a measurement of the width of the spit that was visible at km 60.320 on the orthogonal photos of November up to February (Appendix D, T0 up to T3).

The active profile height and offshore water depth were chosen per location, based on the bathymetry data at the transect where the hydrodynamic measurements were performed. The cross-shore profiles for both locations are included in Appendix A.1 for reference. The active profile height was defined as the vertical distance between the top of the berm and the edge of the platform. The offshore water depths were taken at locations FL69 and FL70C, respectively. Lastly, the mean profile slope was defined in between the berm and the edge of the platform.

The density of sand was left at the default value, the density of water was changed to that of fresh water. The median grain diameters were taken as the average from several samples taken after

construction of the sandy shores. Additionally, Neumann boundary conditions were applied, allowing for transport across the boundaries. We assumed these boundary conditions to be valid, since time-scales were observed to be short (Section 5.4.2), implying sufficient sediment availability.

6.2.1 Refraction calibration

The linear profile assumption previously explained is not realistic for our environment (see Figure 2-1). The equilibrium and alongshore uniform bathymetry assumptions are also not quite valid. This stems from the fact that the distances from the closure depth to the berm and edge of the platform are not equal and that measurements have shown that the edge of the platform roughly follows the waterline.

The model contains a nearshore water depth variable, which is used to indicate the depth at which waves start refracting. Since wave direction was found to be of high importance to morphological change, and wave data from offshore to nearshore is readily available for both locations, we found that we could calibrate the model's nearshore water depth to accurately reflect refraction. This was done in the following two steps:

1. Data for refraction from location FL70C to FL70A is available for most of the analyzed morphological periods (periods in between Shore's measurements). This was not the case for location FL69, but we did have data outside these periods. For this available data, the relation between the wave directions of the offshore and nearshore locations were fitted with a third-degree polynomial, using the least squares method. For the cases where refraction was unknown (no nearshore data was available), this curve was used to predict the nearshore wave angle of incidence.
2. Next, the relation used to compute nearshore wave angles for a longshore uniform bathymetry (Snel's law, implemented in the model) was reverse calculated. The input in this case is the offshore water depth, offshore wave angle and the nearshore wave angle. The output (the nearshore water depth) was used as the calibration parameter for refraction.

This method allows us to look past the linear profile assumption. However, there are several other assumptions that may not be valid for the case of the Houtribdijk. The first, is the assumption that the distances from the average water level to the platform elevation and to the top of the swash berm are equal. An elaboration of this profile assumption, and how we may correct it, is presented in Appendix G.5. The second, is the assumption of longshore uniform bathymetry, which is only discussed in Sections 7.2 and 9.2. Lastly, by leaving breaking wave parameters α and γ at their default values (see previous section), we seem to assume that the propagation from nearshore to breaking conditions is of minor importance. Since we only applied the model to qualitatively reproduce the physical process, we left these inaccuracies to our recommendations. However, a brief look at what the influence of the γ-parameter is, may be found in Appendix G.6.

Example nearshore calibration

Applying the method described above to location FL69, we first found the relation between the offshore and nearshore wave directions. This relation is shown in Figure 6-1, and was used to predict nearshore wave directions, if none were available.
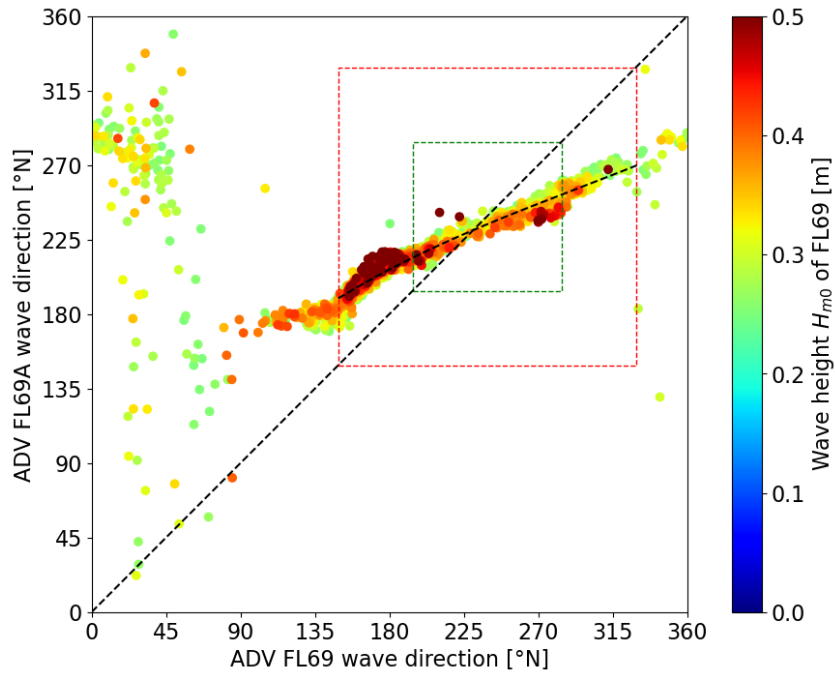
Figure 6-1: Relation between wave directions at FL69 and FL69A.

Retracing the steps that ShorelineS takes to compute nearshore wave directions, we can now reverse calculate the nearshore water depth using the equations below (sourced from ShorelineS, originally implemented in code in the model).

$$d_n = \frac{g[-\log(1-B)]^{0.8}}{\omega^2}$$

With:

$$B = \left[\frac{\sin(\phi_{n,loc})}{\sin(\phi_{0,loc})}\right]^{2.5}\left[1 - \exp\left(-\left[\omega\sqrt{\frac{d_0}{g}}\right]^{2.5}\right)\right]$$

Where:

- d_n [m]: Nearshore water depth for model calibration.
- d_0 [m]: Offshore water depth, taken as the water depth at the offshore measurement location.
- g [m/s²]: Gravitational acceleration (= 9.81 m/s²).
- ω [1/s]: Angular frequency, defined as $\omega = 2\pi/T_p$, with peak period T_p [s].
- $\phi_{n,loc}$ [°]: Local nearshore wave direction, defined as $\phi_{n,loc} = \phi_n - \theta$, with:
  - ϕ_n [°N]: Nearshore wave direction.
  - θ [°N]: Beach orientation.
- $\phi_{0,loc}$ [°]: Local offshore wave direction, defined as $\phi_{0,loc} = \phi_0 - \theta$, with:
  - ϕ_0 [°N]: Offshore wave direction.

Figure 6-2 shows an example of the result of this computation. Here we show the nearshore water depth as function of the local nearshore wave direction, for a local offshore wave angle of 75° and offshore water depth of 2.3 m.
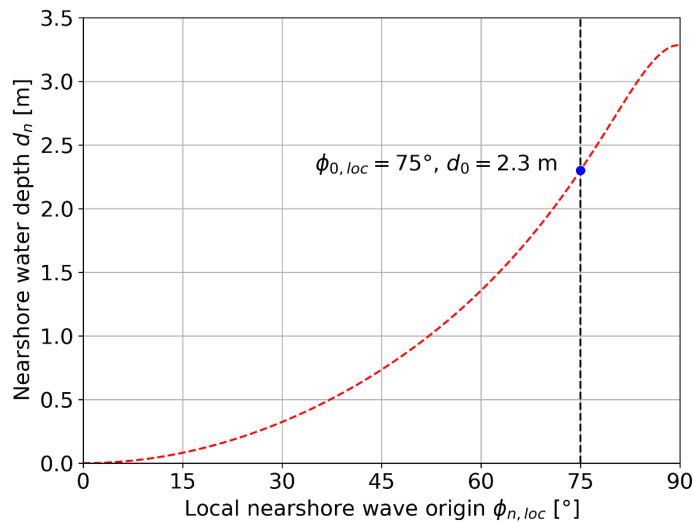
Figure 6-2: Example of ShorelineS refraction calibration function from offshore to nearshore at location FL69.

6.2.2 Model input

Input for the model simulations is described in Table 5-4 and Table 5-5 for locations FL69 and FL70, respectively. These consist mostly of the representative hydrodynamic conditions found in Section 5.5, with the wave height (H_{m0}), peak periods (T_p) and offshore directions (wave origins; nautical, ϕ_0, and local, $\phi_{0,loc}$). Local angles were previously defined using the convention in Figure 5-20. The runtime of each simulation is based on the total duration of the representative hydrodynamics as found from the measurement data. Results of the calibration described in the previous section are given in the last column (d_n). Results of these simulations are elaborated in the next section. The simulation for period T2 to T3 was omitted since we were unable to find representative conditions. Instead, we compared T2 and T3 to T4 in order to fill the gap in results.

Table 6-2: Overview ShorelineS input for location FL69, with wave height (H_{m0}), peak wave period (T_p), nautical wave origin (ϕ_0), local wave origin ($\phi_{0,loc}$), and nearshore water depth (d_n).

Period	Runtime [days]	H_{m0} [m]	T_p [s]	ϕ_0 [°N]	$\phi_{0,loc}$ [°]	d_n [m]
T0 to T1	3.7	0.15	2.25	337	82	0.76
T1 to T2	1.2	0.28	2.44	87	-28	0.52
T2 to T4	8.6	0.38	2.74	50	9	3.02
T3 to T4	8.6	0.38	2.74	50	9	3.02
T4 to T5	4.8	0.36	2.69	30	29	0.56
T5 to T6	8.6	0.17	2.33	350	69	0.57

Table 6-3: Overview ShorelineS input for location FL70, with wave height (H_{m0}), peak wave period (T_p), nautical wave origin (ϕ_0), local wave origin ($\phi_{0,loc}$), and nearshore water depth (d_n).

Period	Runtime [days]	H_{m0} [m]	T_p [s]	ϕ_0 [°N]	$\phi_{0,loc}$ [°]	d_n [m]
T0 to T1	2.9	0.17	2.38	347	37	1.31
T1 to T2	2.0	0.17	2.38	344	40	1.32
T2 to T4	4.5	0.35	2.89	38	14	2.10
T3 to T4	6.2	0.40	2.92	11	13	2.18
T4 to T5	2.1	0.12	1.91	323	61	0.92
T5 to T6	9.1	0.18	2.37	348	36	1.31

6.3   Results

Beach cusp development in the conceptual model (Section 5.4) was described by the theoretical background, the concept of feature inheritance under stormy conditions, and that smaller cusps tend to emerge faster due to their lower volume requirement. Applying this conceptual model has led us to representative hydrodynamics (Section 5.5.3). In order to reinforce our hypothesis that high-angle wave instabilities are dominant, we applied a numerical model that can reproduce this process.

All the results together may be found in Appendix H. The micro scale conceptual model of Section 2.4 was additionally tested by several ShorelineS simulations, the results of which may be found in Appendix G.1. In the following section, we elaborate the comparison of the ShorelineS simulations results with the results of the data analysis of the previous chapter.

6.3.1   Comparison with data analysis

To substantiate the results from the data analysis, we compared the modeling results of the various morphological periods with the waterlines derived from the bathymetric measurements. The examples below are for the same periods as show for the conceptual model results in Section 5.5.1. These are the results that represent the process of high-angle wave instabilities best.

Representative hydrodynamic conditions, as found after applying the conceptual model, should lead to qualitatively similar results when applied as input to the model. These conditions were previously mentioned and can be found in Section 6.2.2. The offshore wave height (H_{s0}) and direction (ϕ_0) are indicated in the figures of the results presented below, using the convention previously shown in Figure 5-20. In the figures presented in this section, the red lines indicate the starting period, the initial condition of the model (e.g. the waterline at T0). The blue line represents the waterline of the next period (e.g. at T1). The black line, including the yellow shading, indicate the model results.

FL69: 16 November to 4 December 2019 (T0 to T1)

In Figure 6-3 we see that this period experienced an increase in number of cusps, average amplitude, and average asymmetry, while the average wavelength decreased. Combined, this seems to mostly correspond to the theorized short-term exposure to high-angle waves coming from the North, considering our conceptual model.

Measured amplitudes at T1 (blue) had decreased conform our macro scale expectations (Section 5.5.1). However, the amplitude in the modeling results increased, which is in contrast to both the conceptual model and the theory on water level fluctuations (Section 5.4.3). A possible explanation may be that we simulated the forcing for too long (3.7 days was considered representative), leading to a long-term response of the modeled waterline, while in reality the water level fluctuations may have damped this response.

Despite the change in amplitude, the other cusp quantities all seem to agree with our conceptual model as well as our measured changes. Most notably the asymmetry is reproduced qualitatively rather well, which is visible by the leaning of the horns in the direction of the waves.
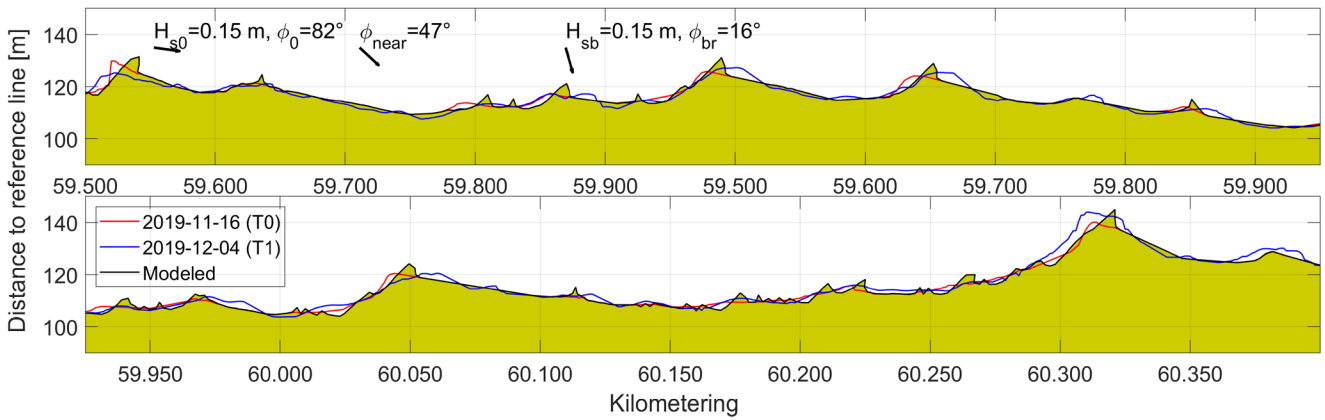
Figure 6-3: Comparison of waterlines at location FL69, for the period 16 November (T0, red) to 4 December 2019 (T1, blue), with the modeled waterline (black).

FL69: 25 May to 17 July 2020 (T5 to T6)

The total number of cusps increased significantly, as seen in Figure 6-4. The average asymmetry increased as well, but the average wavelength and amplitude decreased. These qualitative changes fully correspond to the theorized short-term exposure to high-angle waves coming from the North, as per macro scale conceptual model.

The measured morphological changes of T6 (blue) were qualitatively the same as the modeled quantities. However, the large number of instabilities we see in the figure are not observed in reality, although their dimensions are in the same order of magnitude as seen in the observations (e.g. Figure 5-4 in Section 5.1.1). Despite the long runtime (8.6 days), the response seems to be short-term, which might be explained by the fact that the forcing was intermittent.

Also, even though the average amplitude decreased, we see the emergence of a lot of cusps with smaller amplitudes and large asymmetries. This corresponds very well with the conceptual model, but less with the actual measured morphological changes.
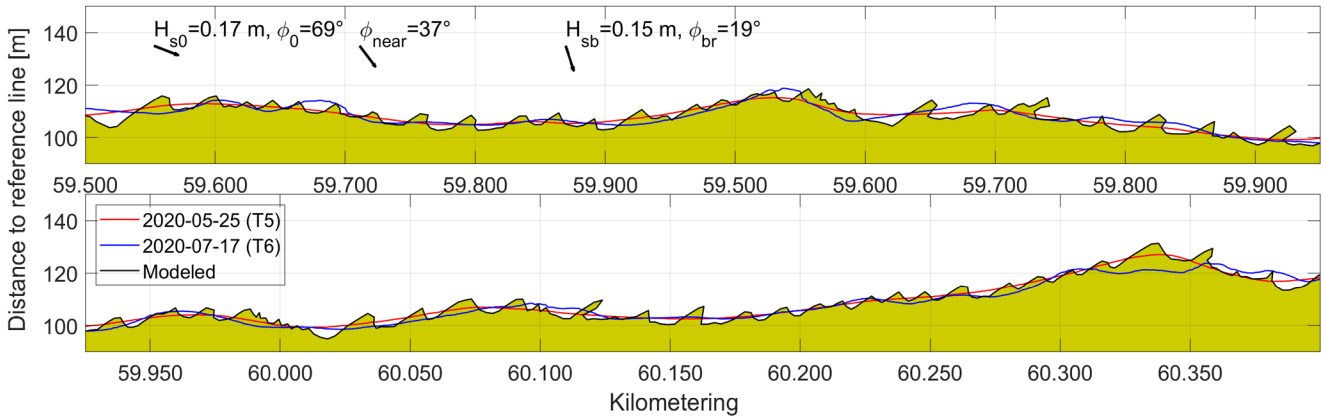
Figure 6-4: Comparison of waterlines at location FL69, for the period 25 May (T5, red) to 17 July 2020 (T6, blue), with the modeled waterline (black).

FL70: 1 April to 25 May 2020 (T4 to T5)

The next period is shown in Figure 6-5, which saw an increase in number of cusps, their average amplitude, and their average asymmetry. In this period the average wavelength had decreased. This partly corresponds to the theorized short-term exposure to high-angle waves from the North, considering our conceptual model.

Both the modeled and the measured amplitudes increased in this period, while our conceptual model indicated this should decrease. Assuming that the development was in the process of going from

short-term to long-term, this simulation seems to represent the conceptual model relatively well. Similar to the previous case, the number of cusps seems to have drastically increased, despite the short runtime (2.1 days).
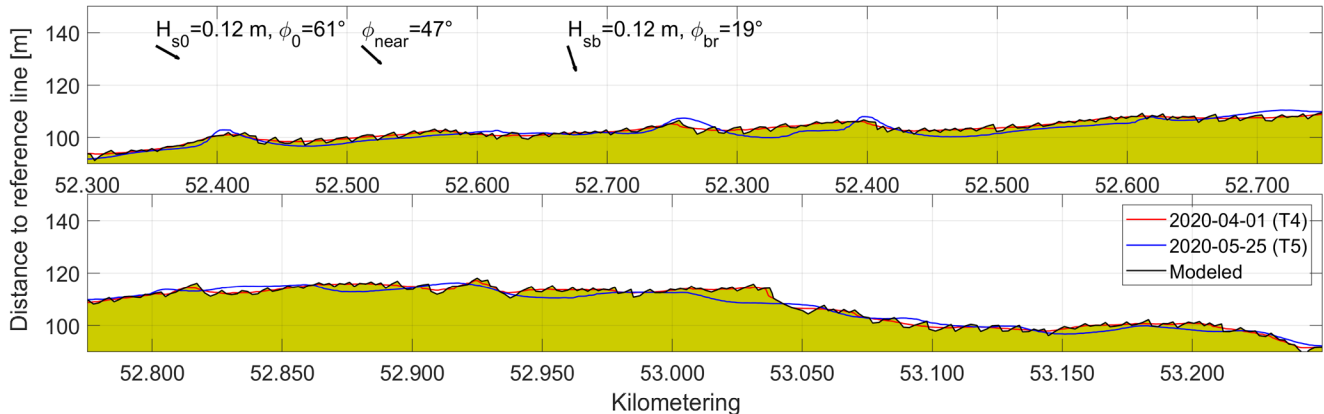
Figure 6-5: Comparison of waterlines at location FL70, for the period 1 April (T4, red) to 25 May 2020 (T5, blue), with the modeled waterline (black).

6.4 Conclusion

To finalize our study towards determining the cause of the beach cusps along the Houtribdijk, we conclude with an overview of the modeling results. Modeling was done using ShorelineS, which was specifically chosen to model the process of high-angle wave instabilities. Table 5-6 of Section 5.6 is repeated, but with the addition of an evaluation of the simulation results (as given in the previous section and Appendix G).

The overview is given in Table 6-4, where 'SM' indicates the cases where ShorelineS produced qualitatively similar results as the measured morphological changes (Section 5.3), and 'SC' indicates the cases where simulation results conform to the theory of our conceptual model (Section 5.4). Results are rated from 'v' (green), meaning three or all morphological quantities change as expected, to 'x' (red), meaning none of them do. A '?' (yellow) means that one or two of the quantities are consistent and the rest are not.

As an example of our evaluation, we take the high angle case of period T5 to T6 at location FL70. Here, the modeled waterline did not fully agree with the measured morphological changes. The model predicted there to be one less cusp, while measurements indicated there was one more. The model also predicted an increase in wavelength, while measurements indicated this to remain more or less constant. These two differences have led us to evaluate 'SM' as uncertain. However, the morphological changes from this simulation did conform fully to the macro scale case of the conceptual model which was used to find the representative hydrodynamics. So, given the same input, the model and the theory both arrived at the same qualitative results, meaning our evaluation of 'SC' is positive.

Table 6-4: Overview of macro scale cases where ShorelineS explains morphological change, with 'W' the wave angle mechanism, 'L' the water level mechanism, 'SM' the evaluation of the model results to the measured morphological changes, and 'SC' the evaluation of the model results to the macro scale conceptual model.

Period*	FL69					FL70				
	Forcing	W	L	SM	SC	Forcing	W	L	SM	SC
T0 to T1	HA	v		v	v	HA	v		v	v
T1 to T2	LA	v		v	v	LA	?	v	?	v
T2 to T4	LA	v		v	v	LA	v		?	?
T3 to T4	LA	v		v	v	LA	v		v	v
T4 to T5	LA	v		v	v	HA	?	x	v	v
T5 to T6	HA	v		v	v	LA	v		?	v

*: Since we were unable to find hydrodynamic conditions responsible for period T2 to T3, this part was omitted and comparisons of T2 and T3 to T4 were used to fill the gap in our results.

Considering the ability of ShorelineS to predict the measured morphological changes, the results show that many cases were predicted qualitatively correct. At FL70, these cases were mostly periods that showed little change in water levels, while at FL69 these changes did not influence the evaluation. Additionally, nearly all results are consistent with the predictions from the macro scale conceptual model.

The more in-depth results, included in Appendix H, show that most discrepancies between model results and measured changes are found with the amplitude and shape asymmetry. A comparison between the simulation results and the conceptual model itself shows the same occasional inconsistency. The number of cusps and wavelengths are mostly qualitatively correct, with the exception of the cases where the conceptual model also predicted it wrongly (Section 5.6 and Appendix D). Also, most simulation results visually show that 'leaning' of the cusps is reproduced well. High-angle cases seem to have been predicted qualitatively correct in all cases, while low-angle cases seem to have some discrepancies (at location FL70).

Some of the differences between the simulation results include exaggerated dissipation of cusps in case of low-angle conditions, and sometimes the emergence of a significant number of instabilities during high-angle conditions. This, however, might be solved by additional calibration, which was not the focus of our study. Some recommendations on how to achieve better quantitative results, are included in Section 9.2.

Relating back to the research questions, it seems reasonable to conclude that ShorelineS is, for our environment, a suitable model to reproduce the physics of beach cusps, even at our small spatial and temporal scales. We have found that by calibrating the model to refraction, simulations showed qualitatively similar results. In some exceptional cases, they even produced results quantitatively in the same order of magnitude as the measurements.

Taken together, the results of both this chapter and Chapter 5 seem to confirm that high-angle waves are the likely cause of beach cusp formation at the IJsselmeer side of the Houtribdijk. The results of the data analysis and modeling simulations seem to agree well with the hypothesis of Section 5.4.1, which states that initial response of the waterline is quick, and eventually resulting in a more stable waterline in the shape of cusps (or sometimes spits).

7 Discussion

Before drawing our conclusion, we first assess our application of the data analysis and numerical modeling. Below, we reflect on our methodology and try to answer our research questions. Most of this will be based on the results of Chapters 5 and 6.

7.1 Data analysis

Most of our research consisted of the data analysis, which is why we reflected on it below. Topics discussed include the low-energy classification, measurement data, our results, and uninvestigated processes that may be relevant to our classification of the beach cusps.

The theoretical background suggested a distinction between low- and 'higher'-energy conditions, where the latter are denoted as the cause of coastal features. Applying the same distinction, in the form of calm and stormy conditions, seems to have helped us in finding the hydrodynamics representative for the measured morphological changes of the waterline. These hydrodynamics were subsequently linked to morphological changes. All in all, it seems our application conforms to experiences with low-energy environments described in literature.

The usage of wave climate parameters (U and A, Section 4.2) was supported by literature, and showed us what coastal features we could expect on a large scale. However, literature told us that they were less accurate in local applications. It was considered applying the wave climate parameters on a more local scale, but we chose instead to use quantities described in Sections 2.4 and 5.4.2 (wavelength, amplitude, horn position, number of cusps, and shape asymmetry). We argue that these quantities showed a more complete picture of morphological changes and allowed for a better classification.

Over the course of this thesis, a few iterations and adjustments to our approach were performed, each based on new findings. The first was that bathymetric measurements performed by the contractor were insufficient to quantify beach cusps. This was due to the measured transects having a larger spatial distancing than the wavelength of most of the cusps. Next, measurements by Shore enabled us to visualize the cusps with great accuracy, due to grid-based measurements with a step size of 0.25 m. This data was used to perform our data analysis and model simulations.

From the observations (Section 5.1) we found that the time-scale of morphological change was in the order of days. This meant that another iteration in our approach should have been to increase measurement frequency. Considering the time available for this thesis, this last step was not realistic. Moreover, it would have been a costly investment. Instead, we attempted to find representative hydrodynamic conditions, that were then assumed to bridge the gap between measurements. A problem with this method, however, is that we are uncertain of the accuracy. We simply do not know what exact morphological changes occurred in between measurements. It might occasionally have been the case that we applied hydrodynamic conditions to a waterline that was not representative of the actual waterline. We have suggested possible solutions, ways to increase the amount of data on waterline positions, in Section 9.1.

Most of the morphological periods studied (Section 5.5 and Appendix E) involved low-angle waves, despite that we were looking for evidence of high-angle wave instabilities. Even so, with these low-angle cases we have shown that our conceptual model corresponds well with reality. It is argued that this means we also expect the macro scale theory to be a reasonable approximation of morphological changes under high-angle waves.

Our data analysis mostly focused on the wave forcing as the driver of morphological change. Other effects that play a role in morphological change, like wave shadowing, variations due to non-uniform bathymetry, currents, and other exchanges between individual beach cusps, are not included in the conceptual model. The reason for this, apart from lack of time, is that combining those effects would likely create an overly complicated model and retracing the actual cause for morphological change would become difficult. However, more in-depth studying of the exceptions to the conceptual model may provide more insight in the functioning of the system as a whole. A more integrated approach, possibly by means of numerical modeling, can likely help in predicting quantitative changes. This may help us to better answer the third and fourth research questions; simulating the morphodynamics of beach cusps and the effects of an extreme event. Similarly, calm conditions where waves are likely not dominant may still contain answers to the exceptions to our conceptual model. Nevertheless, it seems that our current approach of qualitatively comparing morphological changes (e.g. change in number of cusps, their wavelength, amplitude, and shape asymmetry), enabled us to conclude that high-angle waves definitely play a role in beach cusp development.

Some of the other processes that were investigated to a lesser degree while answering the second research question (classification of the beach cusps), were water level fluctuations and the influence of bathymetry. Those processes were combined with the process of high-angle wave instabilities only when the latter could not fully explain observed morphological changes. Until now, variations in water level were only evaluated through an addition to our conceptual model. However, weekly variability in water levels may be linked to a reduction of the amplitude of the cusps, in a comparable way tidal influences help reduce the formation of coastal features on the open ocean. Similarly, the transition from winter to summer levels (in February) and back still have an unverified effect. The idea that the water level causes different elevations of the beach to be reshaped under the influence of waves is substantiated by literature (beaches inherit features from higher-energy events). We have not explicitly shown these inherited features at different elevations. However, looking at some of the photos of the beach (Appendix D), we may distinguish previous waterlines at elevations just above the mean water level (most noticeable by the shadow they sometimes cast).

The influence of bathymetry might explain some of the cases where measurements were inconsistent with our conceptual model. Relating back to the finding that waves are less refractive, having a deeper bathymetry just offshore of the beach may mean that waves refract even less. This was something visible in the model simulation results, where even low-angle offshore waves would result in breaking waves angles larger than 10° (Section 2.2.3). Whether such breaking angles are accurate is uncertain (see Section 7.2), but measurement data does confirm that nearshore angles are relatively high. Therefore, such conditions might even result in low-angle wave instabilities, as mentioned briefly in the theoretical background (Section 2.2.3). Verifying these suspicions, however, may require a lot more in-depth studying of the interaction between hydro- and morphodynamics at the Houtribdijk, and was not considered necessary to verify that high-angle wave instabilities were dominant.

Another area of interest regarding the underlying bathymetry (and topography), is related to the initial construction of the sandy shores at the Houtribdijk. Due to the artificial nature of these shores, physical processes have not sorted sediment in the way they would in nature. Construction of the sandy shores were performed by pipes carrying a certain range of sediment fractions. These pipes would be positioned at the top of the original Houtribdijk revetment. Each time a certain volume was deposited, they would be moved 24 m and started again (M. Caljouw, personal communication, July 15, 2020). This process may have led to sediment sorting behavior, with a longshore varying distribution of grain sizes. Considering the beach cusps occasionally seem to have a horn-to-horn distance of approximately twice this 24 m (especially at location FL70, see Section 5.1.2), cusp spacing may still be influenced by the initial construction.

7.2   Numerical modeling

From our modeling simulations, we found that we could reproduce changes in the waterline in a qualitative way. Below, we will discuss the results, some of the assumptions, and ways we might improve quantitative results.

One of the requirements of the model is that it applies the principles of self-organization, as suggested by literature. Although we have not explicitly addressed this in Chapter 6, we have included some simulations aimed at showing this principle (see Appendix G.3). There we argue that no matter the initial conditions, smaller cusps will develop. Larger cusps are, as expected, less influenced by the hydrodynamic conditions. The way the model works, is that the smaller cusps emerge in a timescale based on how extreme the hydrodynamic conditions are (more longshore transport). Extreme, in this sense, can be interpreted as how high the waves are, or how high their angle is with respect to the shore normal. These simulation results seem to show similar changes in the shape of the waterline as the simulation results of locations FL69 and FL70 (Section 6.3 and Appendix H). We argue therefore, that despite not having performed a complete sensitivity analysis and given the agreement between the results, ShorelineS is a model very suitable for verifying the high-angle wave mechanism.

Results of the ShorelineS simulations often showed an exaggerated response of the beach in the form of rapid dissipation of cusps, or a large increase in their numbers. Roelvink et al. (2020) mention that we see more small-scale disturbances because of the absence of nearshore wave refraction over a bathymetry that in practice will evolve together with the waterline. We therefore know that our application of Snel's law was too simplified, and a 2D refraction model might provide more accurate predictions. However, to establish high-angle wave instabilities as the dominant process, applying Snel's law was shown to be sufficient.

Other processes, like wave shadowing and interactions between cusps may also mean that ShorelineS is more accurate than our conceptual model. In our conceptual model we implicitly assumed that all cusps are oriented parallel to the average beach orientation, because the way we quantified them required the cusps to be positioned horizontally. In reality they are oriented differently, leading to variations in the start and end (bay to bay) of a cusp. In other words, the beach cusps can exchange sediment back and forth, something the conceptual model does not take into account. Similarly, wave shadowing causes longshore variations in transport as well. Therefore, it is likely that ShorelineS modeling results are more accurate predictions than the conceptual model, despite both having similar difficulties in reproducing some of the measured morphological changes (e.g. amplitude and shape asymmetry). The fact that both have errors in qualitative predictions underlines our suspicion that high-angle wave instabilities are not the sole physical process involved in these changes. However, it also shows that the wave mechanism is definitely of importance.

We were lucky to have nearshore wave angles included in our measurement data, as they allowed us to calibrate ShorelineS using offshore to nearshore refraction. In cases where such data is not available, a deep-water measurement location should be used to perform refraction calculations. Appendix A.3 illustrates that the offshore measurement equipment at FL69 may not always be considered deep water. This is especially the case when stormy conditions are accompanied by a water level set-down. At location FL70 this is less of an issue, since the bathymetry is slightly deeper there. Since we already have nearshore measurements of wave directions, these calculations were not necessary. So, it is argued that not complying with the common deep-water assumption is not an issue in our case.

This calibration from offshore to nearshore comprises a big part of the travelled path of a wave. However, the theoretical background (Section 2.2.3) indicated that the path from nearshore to breaking conditions is also important, especially considering the sudden shift in water depth at the

edge of the platform. In modeling, the KAMP transport formulation was applied, making use of the breaking wave heights and angles. In practice, one would try to calibrate these conditions using calibration parameters (α; factor for point of breaking, γ; breaking coefficient with 5% breaking waves). In Appendix G.6 we showed the simulated response of the beach for $\gamma = 1.5$, which did not yield significantly different results. However, a more in-depth analysis may be useful in making predictions more accurate.

Investigating the path from nearshore to breaking wave refraction in Appendix G.6, has led us to another curiosity. Figure 7-1 and Figure 7-2 show what we use in Snel's law for refraction, with the locations of the deep water (h_d), nearshore (h_n, h_{n1}, and h_{n2}), and breaking water depths (h_{br}). The lengths, L_1 and L_2, indicate the distance from offshore to nearshore, and nearshore to breaking depths, respectively. Snel's law describes that refraction occurs due to gradients in the bathymetry. However, waves cannot instantly change direction, they need some space to 'turn'. Due to the sudden changes in the profile at the Houtribdijk (second figure), waves only get a fraction of their required distance to refract (as compared to the longshore uniform case, first figure). We therefore suspect that refraction is even less than model simulations suggest. This was substantiated by a photo of the beach at location FL69 (Figure 4-4), where we saw that waves (albeit under calm conditions) move almost parallel to the beach, and only refracted really close to the waterline. This would mean that breaking wave angles are even larger than we see from the ShorelineS simulations, which would likely yield even more exaggerated responses of the beach. Correctly implementing this, possibly through a 2D refraction model, would therefore not have helped us in our search for the dominant physical process. However, considering the importance of wave angles, predictive analyses should probably include this mechanism to improve accuracy.
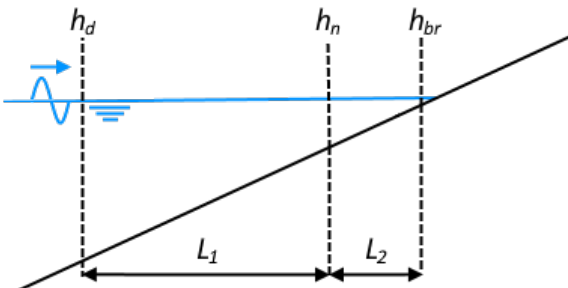
Figure 7-1: Refraction path under linear profile assumptions, with deep water depth (h_d), nearshore water depth (h_n), breaking water depth (h_{br}), and refraction distances (L_1 and L_2).
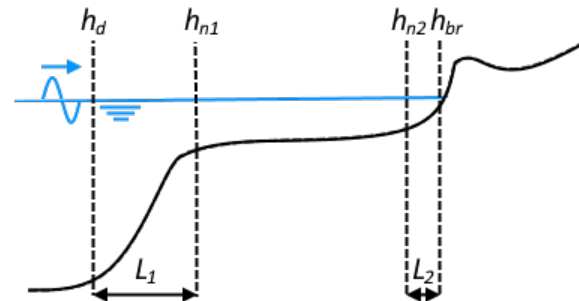
Figure 7-2: Refraction path under logarithmic profile assumptions, with deep water depth (h_d), nearshore water depth (h_{n1} and h_{n2}), breaking water depth (h_{br}), and refraction distances (L_1 and L_2).

On the topic of the influence of the cross-shore profile on our modeling results, ShorelineS assumes that MSL is in the middle of the active profile. Research into the profile on the Markermeer side of the Houtribdijk by Ton et al. (2020) has shown that the profile may not be at an equilibrium elevation yet, so this assumption is likely not valid in our case. We have performed some preliminary simulations that included (1) the complex curvature correction for a linear profile and (2) a logarithmic fit to a representative profile of the IJsselmeer (see Appendix G.5). Since ShorelineS is a one-line model it does not perform calculations of profile adjustment, meaning that these adjustments to the profile only affect the cross-shore change in waterline position. As input we used a wave height of 0.25 m, peak period of 2.51 s, and local wave incidence angle of 82°. These conditions were therefore high-angle, on the border of calm to stormy conditions, and lasted for approximately two days. Initial conditions were the waterline of November 2019 (T0) of location FL69. Results so far show that either profile yields less exaggerated waterline responses (lower amplitudes, less spit-like features) when compared to the response under the default linear non-corrected profile. However, we did see more smaller perturbations. So far, the inclusion of either of the two profiles was not necessary to

substantiate that wave action is a relevant process. However, if we want to predict future development of the waterline, a more accurate representation of the profile may be better.

7.3   Research questions

Together with Chapters 5 and 6, it seems the first three research questions have been answered reasonably well. These three concerned the gathering of relevant knowledge, classifying the beach cusps, and the way we can simulate the morphodynamics of the cusps. The coastal features at the IJsselmeer side of the Houtribdijk have mostly been classified as beach cusps developing due to transport by high-angle waves. We assumed that enough evidence was gathered to confirm that high-angle waves are an important hydrodynamic process. Additionally, the numerical model ShorelineS has provided us a way to further substantiate these claims.

The fourth research question concerns the way we can assess volume distributions, and how we expect this to influence the sandy shore of the Houtribdijk. To try and answer this question, we have performed a preliminary analysis of the cross-shore waterline position (Section 5.2) and the movement of the more persistent cusps (Section 5.5.2 and Appendix F).

The effects of the hydrodynamics on volume distributions were not explicitly investigated. For example, so far it seems that cusps emerge and dissipate under hydrodynamic forcing, but we have little to substantiate any loss of volume. The study on the Markermeer side of the Houtribdijk (Ton et al., 2020) showed that volumes redistribute into the characteristic platform shape (Section 2.1.3), and expectations were that volume transported over the edge is either lost, or used to widen the platform. Figure 7-3 and Figure 7-4 show the waterlines of locations FL69 and FL70, as found in Section 5.2 (but now on top of each other). The slight retreat of the waterline over time (10 to 20 m in eight months) cannot convincingly be used to substantiate these findings, since water levels change over time (influencing the location of the waterline as we defined it), and we are unsure how the waterline relates to volume distributions.
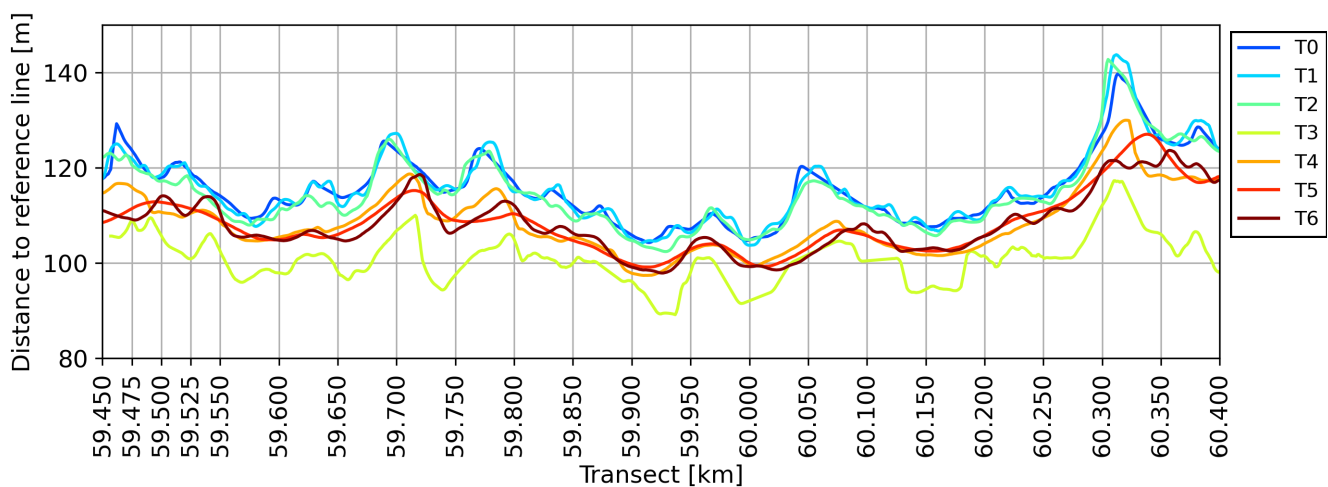
Figure 7-3: Comparison of waterlines at location FL70, for all measurement periods.
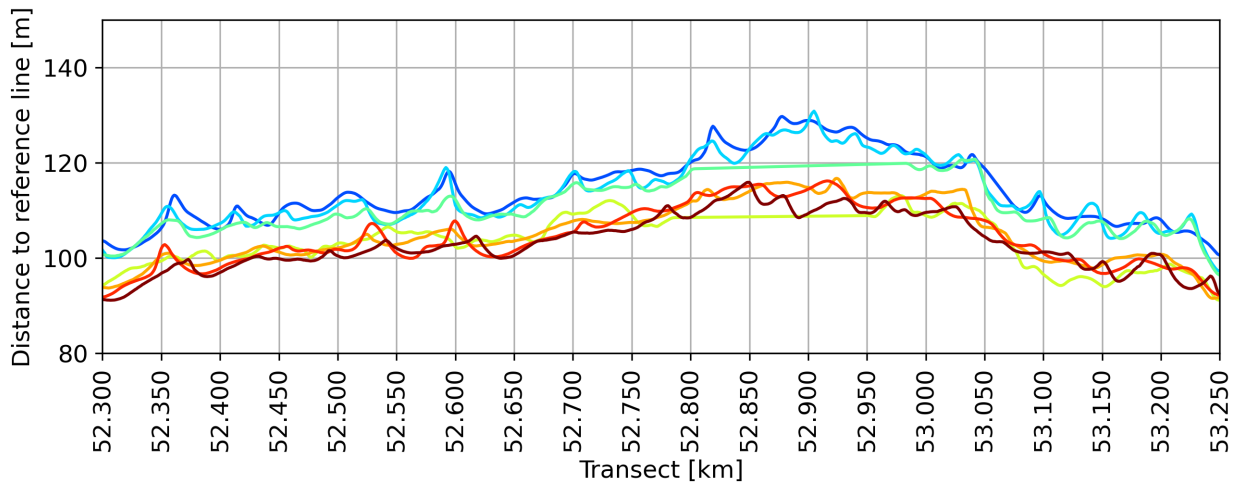
Figure 7-4: Comparison of waterlines at location FL70, for all measurement periods.

Additionally, judging the evolution of the waterline over time based on the orthogonal photos and satellite images (Appendix D), it seems that the waterline is relatively stable. Take into account that the water level from January 2020 onwards was higher, due to the set summer water level. It seems that longshore transport is significant, considering the morphological changes due to high-angle waves. Despite this, it may be the case that transport occurs both ways, which is substantiated by the highly variable hydrodynamics and the persistent cusps (Section 5.1 and Appendix D). These persistent cusps have migrated Southward by approximately 20 to 30 m in eight months. This may mean that our net transport is low, and we have a negligible longshore volume loss. If this is the case, the morphodynamic behavior of the beach cusps has little effect on the sandy shores of the Houtribdijk. However, it is likely wise to investigate these claims further, as we know that environments like these are very complex.

Although the fourth research question does not explicitly mention it, we may be interested in finding out what the consequence of an extreme Northern storm is for volume distributions. Our findings suggest that such conditions (large, high-angle waves) would lead to a very dynamic response of the beach. So far, we have solely seen conditions that are either high-angle, or have a wave height considered stormy, both never at the same time. To gain some insight in this matter, we have performed several simulations (see Appendix G.4). The results show extreme spit formation, features of which we have observed smaller forms at km 60.300 in Appendices D.6 through D.9, and km 53.025 in Appendix D.22. We therefore argue that a more in-depth analysis is advisable, as spits may have the potential to move sediment over the platform edge of the cross-shore profile, leading to permanent volume loss.

To conclude, we know from literature that lakes like these are often wind-dominated, and that waves experienced in these environments are therefore often steep, erosive, and less refractive. Additionally, profile shapes like ours were previously found in similar low-energy environments. A result of this, is waves that break close to the beach, likely under an angle larger than 10°, which is considered extreme in literature. Calm conditions may not have enough potential for morphological change, but stormy conditions were classified as the cause for instabilities in the waterline. Therefore, environments like these are very susceptible to coastal features, with little to no forces that can restore previous states (e.g. tides or other long waves). We therefore suspect that beach cusps, or similar features, are very likely to form in these low-energy environments.

Finally, as discussed in Section 7.1, our study could benefit from an in-depth analysis of other (likely) relevant processes, like currents, water level variations, cross-shore profile development, refraction on

a non-uniform bathymetry, and sediment sorting. This analysis may eventually lead to sufficient knowledge to allow an evaluation of the effects of beach cusps on flood safety. Some ideas on how to achieve this are presented in the recommendations of Chapter 9. Our study has provided an initial view of the behavior and effects of beach cusps, that may be used on the road to understanding the dynamics of sandy shores in low-energy lake environments.

8 Conclusion

The Houtribdijk's main function is flood safety, of which the sandy shores are now an integrated part. Experience regarding the wave damping function of open coast beaches has been researched for years, and is to this day considered well understood. However, applying such a solution in a lake environment was a novelty. The emergence of beach cusps was unexpected, and the observed coastal features were still little understood. Our goal, therefore, was to find out what the causes of these cusps and their morphodynamic behavior are for the sandy shores of the Houtribdijk. A large part of this was to classify them, and find the physical process causing their formation. Below, we conclude on our research.

We found a relation between wave and wind directions during stormy conditions (Section 5.6). This showed that, due to large variability in wind directions, stormy conditions could approach the beach under a large range of angles. This, in contrast to calmer conditions, where waves generally approached under a high-angle. It was due to this variability that stormy conditions were sometimes found to be low-angle, leading to dissipation of the beach cusps, while at other times they were high-angle, leading to the growth of the features. Additionally, during winter water levels (calmer periods) we see that most waves originate from the South-East and are primarily high-angle. During summer water levels (stormy periods) there is a preference for waves originating from the North which can be both high- and low-angle. Waves during these Northern stormy conditions are expected to be more erosive, due to their higher steepness.

Using methods described in Chapter 3 we were able to classify our hydrodynamics, find the waterline, quantify the beach cusps and relate this to representative hydrodynamic conditions. The number of cusps (N_c), their wavelength (L_c), amplitude (A_c) and shape asymmetry (As) were used to objectively assess morphological change. A conceptual model was applied, based on the prevailing theory on high-angle wave instabilities. The representative conditions were linked to morphological changes, through application of this model. Representative hydrodynamics were chosen based on the distinction between 'calm' and 'stormy' conditions, to reflect our expectation that these have different effects on the morphology of the beach cusps. This was done to represent both the low- and 'higher'-energy conditions mentioned in the theoretical background. From theory we suspected that stormy conditions have the most influence on morphology, and from our data analysis it followed that low-energy (calm) conditions likely had insufficient energy to significantly change the waterline.

Our data analysis on the morphological change of the beach cusps suggested that development of the cusps is steered by high-angle wave instabilities. Taking into account that smaller cusps easily emerge and dissipate due to their relatively small volume (Section 5.4.2), we were able to link these high-angle conditions to an increase in the number of cusps. Also, the movement of the horns in the direction of the wave forcing, described as 'leaning' (Section 5.5.2), is mostly consistent with our conceptual model (for both low- and high-angle waves). However, changes in amplitude were occasionally seen to change in contradiction to our expectations.

In some cases, morphological changes unexplained by the high-angle wave mechanism could be understood by analyzing water level fluctuations, but certainly not always. A brief description of the effects of these fluctuations, is that for high-angle waves we expect dissipation of the cusps for wave attack at higher elevations, and growth of features for wave attack at elevations lower than the average water level. The limited number of periods where water level variations could explain morphological change, suggests that there are instances where other processes dominate our system. Nevertheless, cases where the water levels were more or less constant over the examined period

were mostly shown to be very consistent with our conceptual model and confirmed the dominance of high-angle waves.

By applying the numerical model ShorelineS, specifically designed to reproduce instabilities caused by high-angle waves, we were able to create additional evidence to substantiate our findings. The model was proficient in reproducing qualitative changes in cusp shapes described by the conceptual model, although waterline responses were often quantitatively exaggerated (e.g. large increase or decrease in number of cusps). This agreement between simulation and conceptual model results was to be expected, since both were based on the same theory of high-angle wave instabilities. Results show that, like for the conceptual model, ShorelineS simulations corresponds well with the morphological changes from data. On top of that, the numerical model includes other processes, like wave shadowing and sediment exchange between cusps, allowing it to make more accurate predictions than our simple conceptual model.

Our data analysis and model simulations have shown us that our low-energy environment is complex. To a large extent we have confirmed that waves are dominant. By relating the morphological change to the representative hydrodynamics, we have provided evidence that stormy conditions leave their mark on the beach. This coincides with the fourth low-energy criteria (Section 2.1.2), telling us that beaches inherit features from higher-energy events. However, considering some exceptions to this rule, we know that there are additional influential processes. We already mentioned that water level variations are one of them. Another, the steep bathymetry from nearshore to offshore depths, combined with the finding that our waves refract less than they would likely do on open ocean coasts, hints at the possible growth of instabilities under low-angle waves.

In our discussion (Section 7.3), we tried to explain what the expected effects are of a Northern storm (large, high-angle waves) on the sandy shores at the Houtribdijk. Appendix G.4 presents a first glimpse of the expected effects, which could be the formation of extreme spits, possibly leading to permanent loss of sediment volume. However, conclusions regarding this are uncertain, as these results require more in-depth analysis. Despite this, observations definitely suggest the possibility of this happening (km 60.300 in Appendices D.6 through D.9, and km 53.025 in Appendix D.22). Luckily, conditions that are either high-angle, or have a large wave height (but not both), have shown no certain evidence that volume distributions lead to loss of sediment. In the span of our analysis (eight months), we have seen a possible 10 to 20 m retreat of the waterline, and a 20 to 30 m Southward migration of the more persistent cusps. Based on these numbers, we may say that the behavior of the beach cusps does not significantly affect the sandy shores of the Houtribdijk. However, it also seems very advisable to investigate the aforementioned volume distributions in more detail.

Returning to our research questions, it seems we mostly answered the first three. That is, we gathered relevant knowledge from literature, were able to classify the beach cusps, and have found tools (the conceptual model and ShorelineS) that can simulate their morphodynamics. The coastal features at the IJsselmeer side of the Houtribdijk can be classified as beach cusps that emerge and dissipate mostly under the influence of high- and low-angle waves. Despite the likelihood of other processes being of importance, such as water level fluctuations and a non-uniform bathymetry, the high-angle wave instability mechanism plays a definite role in the development of the beach cusps.

The stormy conditions, shape of the cross-shore profile, steep and erosive waves, and large nearshore wave incidence angles are all characteristic of our low-energy environment. Each of these properties has individually been linked to the formation of complex coastal features. Therefore, it seems that such features are very likely to develop in a low-energy environment. In addition, other processes, like currents, water level variations, cross-shore profile development, refraction on a non-uniform bathymetry, and sediment sorting, make our environment even more complex. Therefore, it

will take a lot more to fully understanding the dynamics of sandy shores in a lake environment like the IJsselmeer. However, our results concerning the development of beach cusps is a definite first step in the right direction.

9 Recommendations

Based on the discussion and conclusion, we formulated several recommendations. These will be either related to our methodology, the results of our research, or consist of advice for further research.

9.1 Physical processes

So far, we have investigated the effects of high-angle waves, and to a limited extent the water level fluctuations and bathymetry. Some of the topics below concern ways we may improve our data analysis, so the focus is high-angle wave forcing. The rest of the topics suggest ways we may expand our findings by including other processes.

- The effects of currents were not investigated, even though they may be 0.30 m/s, or higher, at times (see Appendix B.2). We may include the effects of currents by a similar method as we have applied in our study. By that we mean establish a number of representative quantities, like flow velocity and a critical velocity for transport, which may be compared to the same quantities derived for our analysis of wave forcing (e.g. number of cusps, their wavelength, amplitude, and shape asymmetry). We may create a similar layout as given in Appendix E, but including current directions, magnitudes and roses, to help us gain perspective. Given the dominance of wave forcing during stormy conditions we found, such an analysis of currents might be best applied for calm conditions, to explain the inconsistencies between our conceptual model and the measured morphological changes.

- Sediment distributions in the longshore direction have been mentioned in Section 7.1. However, we have not investigated this in detail. Investigating the relation between cusp spacing and these sediment distributions may provide more insight in the less explained morphological changes at location FL70.

- The waterline used in our analysis was determined using a Python script, as specified in our methodology (Section 3.3.1). This approach could lead to relatively fast results, but would more often than not require a lot of manual correction. A more automated approach, by digital processing of orthogonal photos may prove to be more efficient. This would also allow for an analysis of the satellite imagery, and possibly help us substantiate the claim for wave dominance. Should we desire more evidence for our hypothesis that high-angle waves are dominant, we know Shore has previously applied a similar method for determining the waterline, so experience regarding this approach already exists. In addition, Argus monitoring may be applied to gain data on small spatial (e.g. order meters) and temporal (e.g. order days or events) scale. This would, however, likely require considerable investment in comparison with orthogonal photos by drones. Given the distance between the two beach segments (FL69 and FL70 are about 8 km apart along the dike), it may also require two Argus monitoring stations.

- Model simulations using ShorelineS were mostly run on the representative hydrodynamics. No sensitivity analysis was performed to check what quantitative changes occurred under different forcing. For the sake of finding the physical process, and qualitatively checking our conceptual model, this is not a big issue. However, if predictive computations are to be made, a sensitivity analysis may help increase the certainty of the results. Aside from checking the sensitivity to hydrodynamic conditions, the sensitivity to breaking wave parameters (α and γ, see next

section) might prove relevant.

- From the simulations of a Northern storm (large, high-angle waves, see Section 7.3 and Appendix G.4), we suspect that extreme spit formation may occur. Since all of the analyzed high-angle cases had relatively small wave heights ($H_{m0} < 0.25$ m), it would probably be wise to closely monitor a possible high-angle event with a large wave height ($H_{m0} > 0.35$ m). It may be worthwhile to measure and photograph the beach right before, and right after such an event. This would provide additional proof of the dominance of the high-angle wave mechanism, as well as information on sediment volume distributions.

9.2   Predictive analysis

Considering the discussion of the data analysis, concerning measurement frequency and wave dominance, we see that results contain some uncertainty. It seems that waves are an important process reshaping the beach, especially during stormy conditions, but other processes may also play a role. A higher measurement frequency could aid in proving the wave dominance, but may be a less preferable option (considering costs). Therefore, it is recommended to try a more integrated modeling approach.

If we want to specifically model beach cusp development more accurately, a numerical model is recommended that may include currents, variable water levels, variable sediment sizes at the water line, and two-dimensional refraction across a non-uniform bathymetry. This approach would then bridge the gap between finding the physical process and predicting beach cusp evolution. Such an approach might use the modeled waterline of ShorelineS as input alongside the measured waterlines. For example, models like XBeach (e.g. the 2D non-hydrostatic version) may use the waterlines from ShorelineS simulations to predict wave run-up over the cusps, under extreme conditions.

Without resorting to complex process-based models, we made some suggestions related specifically to ways to improve ShorelineS' results. These suggestions are likely exclusively relevant to our environment, because they are all related to the application on our spatial and temporal scales (much smaller than those intended). ShorelineS is meant to be a light-weight model and including the processes below will significantly hamper this purpose, but likely also increase accuracy of modeling results.

- ShorelineS allows for a single value of the active profile height and water depths. The assumption is made that for most coastlines we may assume that sufficient time has passed for an equilibrium to be reached. However, for our case this assumption is less valid. So, making these variables spatially varying, using values from measurements, may improve predictive capabilities of the model.

- The assumption of a longshore uniform bathymetry in the application of ShorelineS is far from the truth in our environment. One may improve the predictive capabilities of the model by coupling a 2D refraction model. ShorelineS already has a module to process refracted wave fields, so this might be implemented with relative ease.

- We explored changing the default profile in ShorelineS to both a curvature corrected linear profile and a logarithmic one (see Section 7.2 and Appendix G.5). A more carefully calibrated profile may increase the accuracy of the longshore sediment transport computation, and therefore improve accuracy of cross-shore grid changes.

- Similarly, the calibration of ShorelineS from nearshore to breaking conditions was not included. In literature, we found that this part of wave modeling may be of importance when studying morphological change. In Appendix G.6 we have briefly elaborated on the influence of the γ-parameter, which seemed to have limited effect on the beach cusp shapes. However, in view of a predictive analysis, we may consider applying calibrated values, as well as applying a calibration of the α-value.

- ShorelineS includes a variable that may be used to set the spreading of the wave directions, which was not used in the simulations of Chapter 6. This spreading would result in slightly damped features, as the wave energy is now used for the growth of instabilities in more than one direction. In Appendix G.3, we applied wave directional spreading based on the averaged measured values at the offshore location of FL69, which probably resulted in more realistic shapes. Considering predictive simulations, it would likely be useful to apply a similar method.

- Grain size distributions were measured after construction of the sandy shores at the Houtribdijk. ShorelineS takes a single value for the median grain size into account, but we may be able to improve predictive capabilities if this quantity could be spatially varied. This would also necessitate field measurement, however, and the added value is as of yet very uncertain.

- Similarly, a way to better visualize the effects of water level variations, without resorting to a computationally intensive model, might be to extend ShorelineS to a multi-line model. This may additionally aid in predicting volume distributions, as were analyzed on the Markermeer side (Ton et al., 2020). We may do this by independently modeling the edge of the platform, the waterline, and the top of the berm. Empirical expressions for the exchange of sediment, based on measurement data, may be added as sources and sinks to the sediment balance equation to couple these three lines.

References

Ashton, A. D., & Murray, A. B. (2006a). High-angle wave instability and emergent shoreline shapes: 1. Modeling of sand waves, flying spits, and capes. *Journal of Geophysical Research: Earth Surface*, *111*(4), 1–19. https://doi.org/10.1029/2005JF000422

Ashton, A. D., & Murray, A. B. (2006b). High-angle wave instability and emergent shoreline shapes: 2. Wave climate analysis and comparisons to nature. *Journal of Geophysical Research: Earth Surface*, *111*(4), 1–17. https://doi.org/10.1029/2005JF000423

Ashton, A. D., Murray, A. B., & Arnault, O. (2001). Formation of coastline features by large-scale instabilities induced by high-angle waves. *Nature*, *414*(6861), 296–300. https://doi.org/10.1038/35104541

Bosboom, J., & Stive, M. J. F. (2015). *Coastal Dynamics I: Lecture notes CIE4305* (0.5). Delft Academic Press.

Bretschneider, C. L. (1964). *Generation of Waves by Wind: State of the Art*. http://resolver.tudelft.nl/uuid:6bc0ec3a-8d52-49d8-a624-22718b58cd4e

Bureau Start the Future. (2020). *[Drone photos of the Houtribdijk]*. Rijkswaterstaat.

Coco, G., & Murray, A. B. (2007). Patterns in the sand: From forcing templates to self-organization. *Geomorphology*, *91*(3–4), 271–290. https://doi.org/10.1016/j.geomorph.2007.04.023

Coco, G., O'Hare, T. J., & Huntley, D. A. (1999). Beach cusps: A comparison of data and theories for their formation. *Journal of Coastal Research*, *15*(3), 741–749.

Daly, C. J., Floc'H, F., Almar, R., & Almeida, L. P. (2019). *Simulating Beach Cusp Formation and the Effect of Wave Forcing*. 502–510. https://doi.org/10.1142/9789811204487_0045

Falqués, A., Ribas, F., Idier, D., & Arriaga, J. (2017). Formation mechanisms for self-organized kilometer-scale shoreline sand waves. *Journal of Geophysical Research: Earth Surface*, *122*(5), 1121–1138. https://doi.org/10.1002/2016JF003964

Fenton, J. D. (1985). A Fifth-Order Stokes Theory for Steady Waves. *Journal of Waterway, Port, Coastal, and Ocean Engineering*, *111*(2), 216–234. https://doi.org/10.1061/(ASCE)0733-950X(1985)111:2(216)

Goodfellow, B. W., & Stephenson, W. J. (2005). Beach morphodynamics in a strong-wind bay: a low-energy environment? *Marine Geology*, *214*(1–3), 101–116. https://doi.org/10.1016/j.margeo.2004.10.022

Google. (n.d.). *[Houtribdijk case locations]*. Retrieved February 17, 2020, from https://www.google.com/maps/@52.6617359,5.3625589,13z

HKV, & Tauw. (2019). *Houtribdijk monitoring and research program: Data report*. Rijkswaterstaat GPO.

Jackson, N. L., Nordstrom, K. F., Eliot, I., & Masselink, G. (2002). 'Low energy' sandy beaches in marine and estuarine environments: a review. *Geomorphology*, *48*(1–3), 147–162. https://doi.org/10.1016/S0169-555X(02)00179-4

Janssens, F. (2019). *[Aerial photo of the Houtribdijk]*. Rijkswaterstaat. https://www.rijkswaterstaat.nl/english/about-us/gems-of-rijkswaterstaat/houtribdijk-reinforcement/index.aspx

References

Kamphuis, J. W. (1991). Alongshore sediment transport rate. *Journal of Waterway, Port, Coastal and Ocean Engineering*. https://doi.org/10.1061/(ASCE)0733-950X(1991)117:6(624)

Lorang, M. S., Stanford, J. A., Hauer, F. R., & Jourdonnais, J. H. (1993). Dissipative and reflective beaches in a large lake and the physical effects of lake level regulation. *Ocean and Coastal Management*, *19*(3), 263–287. https://doi.org/10.1016/0964-5691(93)90045-Z

Mujal-Colilles, A., Grifoll, M., & Falqués, A. (2019). Rhythmic morphology in a microtidal low-energy beach. *Geomorphology*, *334*, 151–164. https://doi.org/10.1016/j.geomorph.2019.02.037

Nordstrom, K. F., & Jackson, N. L. (2012). Physical processes and landforms on beaches in short fetch environments in estuaries, small lakes and reservoirs: A review. *Earth-Science Reviews*, *111*(1–2), 232–247. https://doi.org/10.1016/j.earscirev.2011.12.004

Rijkswaterstaat. (n.d.). *Reinforcement of the Houtribdijk*. Retrieved February 17, 2020, from https://www.rijkswaterstaat.nl/english/about-us/gems-of-rijkswaterstaat/houtribdijk-reinforcement/index.aspx

Rijkswaterstaat. (2019). *Monitoring sandy shores Houtribdijk = Monitoring zandversterking Houtribdijk*. http://publicaties.minienm.nl/documenten/infographic-houtribdijk-sandy-shores-zandige-oevers-monitoring-programme-waves-and-sandy-shores

Roelvink, D., Huisman, B., Elghandour, A., Ghonim, M., & Reyns, J. (2020). Efficient modeling of complex sandy coastal evolution at monthly to century time scales. *Frontiers in Marine Science*, *7*, 1–10. https://doi.org/10.3389/fmars.2020.00535

Shore Monitoring & Research BV. (2020a). *Monitoring Zandige Versterking Houtribdijk 2019 - 2020: Veldrapport T2*. RWS-WVL & RWS-CIV.

Shore Monitoring & Research BV. (2020b). *Monitoring Zandige Versterking Houtribdijk 2019 - 2020: Veldrapport T5*. RWS-WVL & RWS-CIV.

Steetzel, H. J., Goot, F. van der, Fiselier, J., Lange, H. J. de, Penning, W. E., Santen, R. van, & Vuik, V. (2017). Building with Nature Pilot Sandy Foreshore Houtribdijk: Design and Behaviour of a Sandy Dike Defence in a Lake System. *Coastal Dynamics*, *063*.

Ton, A. M. (2019). *LakeSIDE: Research on the banks of the Marker Wadden and Houtribdijk*. https://www.ecoshape.org/en/news/lakeside-research-on-the-banks-of-the-marker-wadden-and-houtribdijk-author-anne-ton-tu-delft/

Ton, A. M., Vuik, V., & Aarninkhof, S. G. J. (2019). *Formation of Sandy Foreshores in Low-Energy Microtidal Environments*. 754–764. https://doi.org/10.1142/9789811204487_0067

Ton, A. M., Vuik, V., & Aarninkhof, S. G. J. (2020). *Sandy beaches in low-energy environments: linking morphological development to hydrodynamic forcing*. *2002*, 1–19.

USACE. (1984). Shore protection manual. In *Coastal Engineering* (Vol. 1, Issues 4th ed., 2 Vol). Dept. of the Army, Waterways Experiment Station, Corps of Engineers, Coastal Engineering Research Center. https://doi.org/10.5962/bhl.title.47829

Werner, B. T., & Fink, T. M. (1993). Beach Cusps as Self-Organized Patterns. *Science*, *260*(5110), 968–971. https://doi.org/10.1126/science.260.5110.968

Wright, L. D., & Short, A. D. (1984). Morphodynamic variability of surf zones and beaches: A synthesis. *Marine Geology*, *56*(1–4), 93–118. https://doi.org/10.1016/0025-3227(84)90008-2

Appendix A: Available data

The processing of data was a big part of our research. Therefore, this appendix is dedicated to the measurement equipment used and what the relations there are between them.

A.1   Hydrodynamics

The Houtribdijk's coastlines are monitored to gain insight in the development of sandy shores and the role of wave loads and currents affecting it. The data is managed by the combination HKV, Tauw and Iv-Infra. Measurements at the Houtribdijk started short after the construction of the sandy nourishment finished over the period from December 2018 to February 2019. In total, project LakeSIDE contains six measurement locations (see Figure A-1). Two of those, namely FL69 and FL70 will be of primary interest for the thesis.

Details of the monitoring and measurements can be found in the field report (HKV & Tauw, 2019). Data related to the hydrodynamics will be sourced from their measurements, unless mentioned otherwise. The beach itself is measured on a regular basis, as mentioned in the data report (Shore Monitoring & Research BV., 2020a). Data related to the morphology of the beach, or aerial photography, is sourced from their measurements and is elaborated in Section A.2.
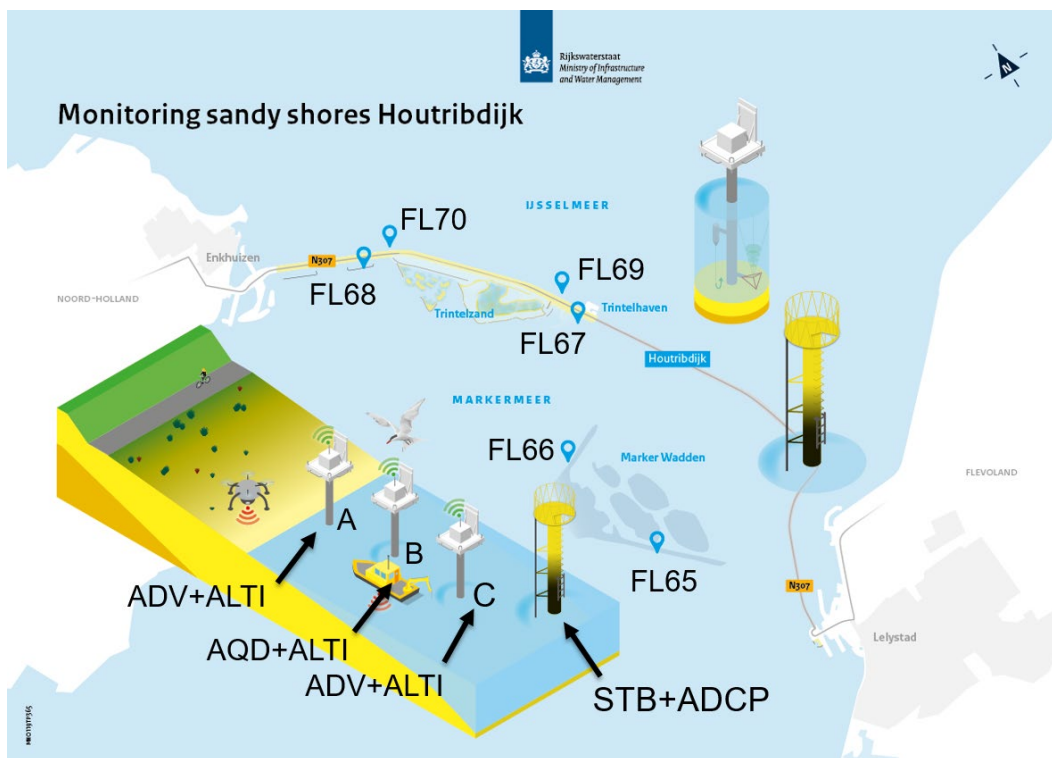
Figure A-1: Measurement locations overview, from Rijkswaterstaat (2019).

Measurement equipment is installed at the locations in Figure A-1 and were commissioned by Rijkswaterstaat. Below, descriptions of the equipment are listed, including the measuring method, frequencies and types of output data (HKV & Tauw, 2019). Table A-1 shows which equipment measures which types of data, indicated in green. The availability of the hydrodynamic measurement data is given in Figure A-2 (up to September).

Appendix A: Available data

- STB (step gauge): Measures water levels (h) via contact sensors with a spacing of 5 cm over a height of 3 m. They have high sampling frequencies (4 Hz), allowing them to additionally provide spectral wave heights (H_{m0}) and wave periods (spectral T_{m01} and peak T_p).
- ADCP (Acoustic Doppler Current Profiler): Positioned near the bed, the devices measure flow at different vertical positions, yielding a vertical velocity profile out of 24 layers (each 25 cm thick). An average value of the three-dimensional velocity vector ($\vec{u}$) given as output every 10 minutes (from bursts of 500 measurements) for each layer.
- ADV (vector Acoustic Doppler Velocimeter): Measures pressure and velocity (in three-dimensions) at a frequency of 4 Hz. Pressure measurements are used to obtain water level fluctuations, and the horizontal velocity vectors are used to compute the orbital velocities of waves (assuming linear wave theory). This data is converted to significant wave heights, periods, directions (ϕ_0) and directional spreading (s_0), as well as water levels. The output is in 15-minute averaged values of these quantities.
- AQD (Aquadopp HR): Comparable to the ADCP, these devices measure pressure and flow near the bottom at a frequency of 4 Hz. They measure 15 layers (each 3 cm thick), allowing for detailed insight in bed load sediment transport. Pressure may be converted to water level fluctuations, wave heights and periods in a similar way as for the ADV. The processed output is in 15-minutes averaged values.
- ALTI (altimeter): Single beam echosounders measuring bed level positions (z_{bed}). These devices measure once per minute, which is the same frequency of the output values. Measurement data occasionally shows wiggles, which represent inaccuracies due to suspended sediment.

Some of the data is automatically processed through a Python scripts, outputting 15-minute averaged values. In the case of significant wave heights, the average of the largest third of the samples is computed for every 15-minute output.

Table A-1: Overview of data type available per measurement equipment, with wave height (H_{m0}), peak wave period (T_p), spectral wave period (T_{m01}), offshore wave angle of incidence (ϕ_0), water level (h), wave directional spreading (s_0), current velocity ($\vec{u}$), and bed elevation (z_{bed}).

Equipment	H_{m0} [m]	T_p [s]	T_{m01} [s]	ϕ_0 [°]	h [NAP+m]	s_0 [°]	$\vec{u}$ [m/s]	z_{bed} [NAP+m]
STB	■	■	■		■			
ADCP							■	
ADV	■	■	■	■	■	■		
AQD	■	■	■		■			
ALTI								■

Figure A-2: Data availability of locations FL69 and FL70 over time.

For the location FL69, the offshore platform (with STB and ADCP, see Figure A-1) is positioned roughly 370 m from the shoreline. Figure A-3 shows the positions of equipment FL69A, FL69B and FL69C (indicated with ADV or AQD, and ALT, in Figure A-1), positioned much closer to the shoreline, at distances of 18, 38 and 66 m, respectively. The offshore platform at location FL70 is situated roughly 290 m offshore. Figure A-4 shows the locations of equipment FL70A, FL70B and FL70C, situated at distances of 35, 48 and 84 m, respectively. The offshore platforms will be referred to as offshore measurement equipment, the others as nearshore.
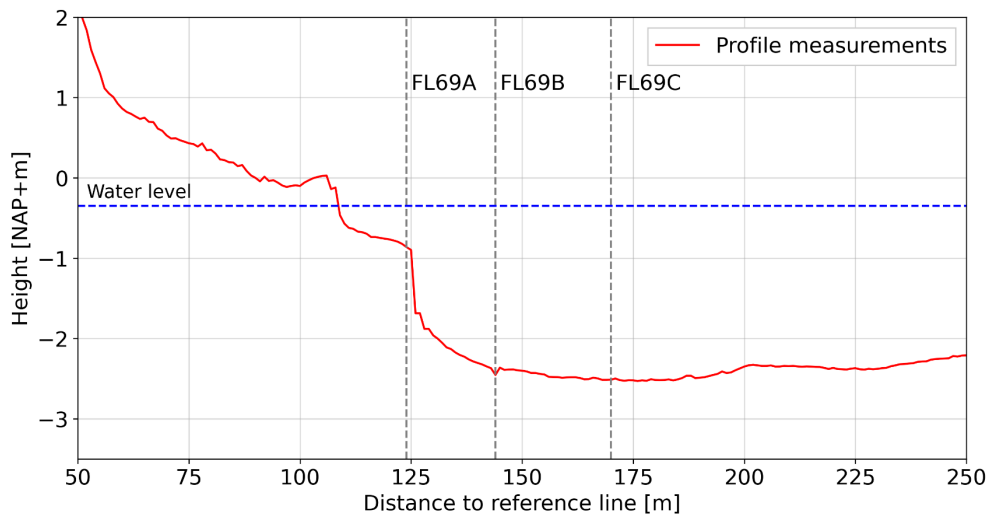
Figure A-3: Cross-shore profile at location FL69, transect 59.950, on 16 November 2019.
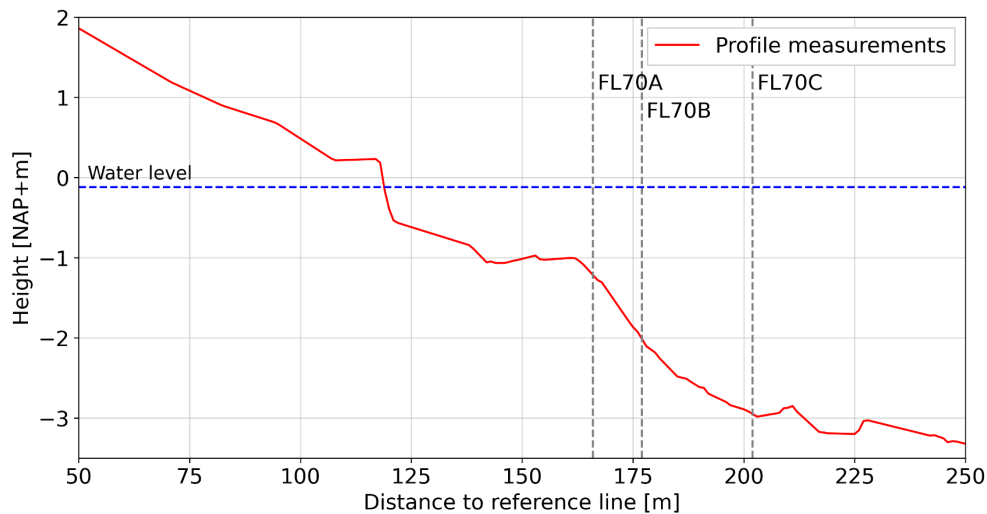
Figure A-4: Cross-shore profile at location FL70, transect 52.850, on 10 October 2019.

A.2   Topography and bathymetry

Measurements of the topography and bathymetry elevations (z) are performed regularly. The field report (Shore Monitoring & Research BV., 2020a) states that transects 52.300 through 53.250 (near FL70, Figure A-1) and transects 59.450 through 60.400 (near FL69) are measured roughly every month. The other transects are measured yearly. Beach and bathymetry measurements have initially been performed by the contractor (Combinatie Houtribdijk, a collaboration between dredging engineering companies Boskalis and Van Oord) up until October 2019.

Shore additionally describes that measurements are done relative to the base station of the GNSS (Global Navigation Satellite System). The topography of the beach is measured using LiDAR from a drone, with a grid-size of 0.25 m. Bathymetry measurements are done using a 3D side-scan echosounder. The overlap between the topography and bathymetry is done by a GPS wheelbarrow, which can reach water depths of around 0.75 m. For the orthogonal photos, the UAV takes photos which are then related to GCP's (Ground Control Points) that have been measured by the GNSS. Shore's measurements, especially considering topography, have a much higher resolution than those done by the contractor.

An overview of the as-built beach and bed elevations is presented in Figure A-5. The figure was made from interpolated measurement data of the contractor. This interpolation concerned creating a grid of 25 m in the longshore direction, and 1 m in the cross-shore direction. Each grid elevation was determined by interpolation of the nearest data points. If less than 10 data points were found, no elevation is recorded. For location FL69 this was performed at the end of December 2018, for location FL70 this was done at the end of February 2019. A list of dates for the other measurements is given in Table A-2. The green crosses indicate the nearshore and offshore locations for the hydrodynamic measurements.

Most notable differences are the larger water depth just offshore at location FL70. A narrow trench of slightly larger water depths may be found along a part of location FL69. To the South of location FL69, we find another deeper area, similar to what was found at location FL70. The rest of the sandy shore seems to be of relatively constant water depth.
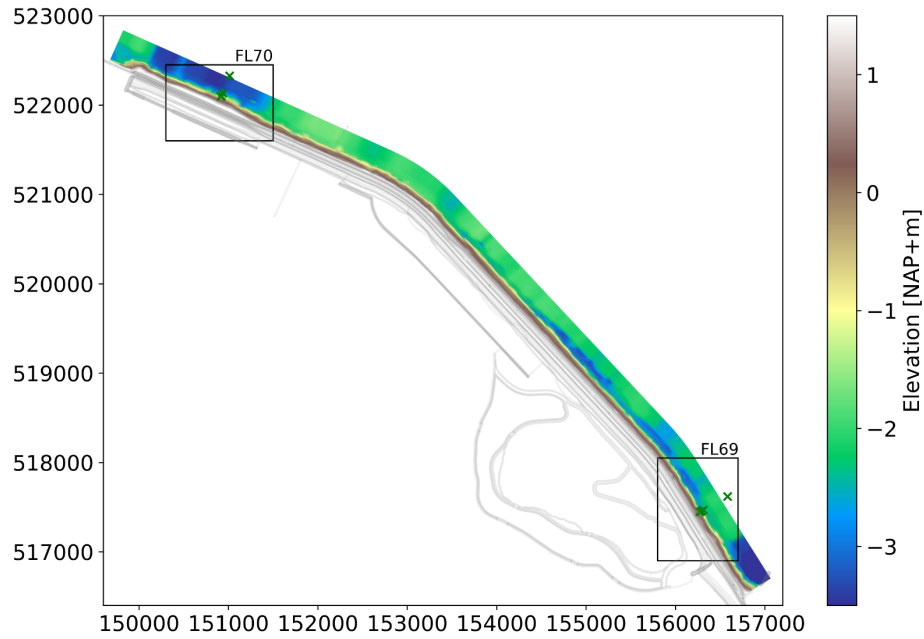
Figure A-5: Overview of the as-built measurements on the IJsselmeer side of the Houtribdijk.

Table A-2: Dates of measurements performed at location FL69 along the IJsselmeer side of the Houtribdijk.

Performed by	Period	Measurement Topography	Bathymetry
Contractor	March 2019	19-3-2019	19-3-2019
	April	3-4-2019	24-4-2019
	May	8-5-2019	7-5-2019
	June	26-6-2019	n.a.
	July	15-7-2019	11-7-2019
	August	29-8-2019	28-8-2019
	September	24-9-2019	3-9-2019
	October	10-10-2019	23-10-2019
Shore	November (T0)	16-11-2019	16-11-2019
	December (T1)	4-12-2019	4-12-2019
	January 2020 (T2)	16-1-2020	16-1-2020
	February (T3)	28-2-2020	28-2-2020
	March (T4)	1-4-2020	1-4-2020
	May (T5)	25-5-2020	26-5-2020
	July (T6)	17-7-2020	15-7-2020

A.3   Correlations

For location FL69, we made use of the offshore ADV data. For location FL70, since there is no offshore ADV, we use data from the ADV at FL70C. To check whether these locations may be considered offshore, a simple calculation for the kd-value was done, of which the formula is given below (Fenton, 1985).

$$kd \approx \frac{\alpha + \beta^2 (\cosh(\beta))^{-2}}{\tanh(\beta) + \beta(\cosh(\beta))^{-2}}$$

With:

$$\alpha = k_0 d = \frac{\omega^2 d}{g} \quad \text{and} \quad \beta = \alpha(\tanh(\alpha))^{-1/2}$$

78

Where:
- o d [m]: Water depth.
- o k_0 [-]: Deep-water wave number.
- o ω [1/s]: Angular frequency, defined as $\omega = 2\pi/T$, with period T [s].
- o g [m/s^2]: Gravitational acceleration (= 9.81 m/s^2).

An overview of kd-values, indicating whether a location may be considered deep ($kd > 3.0$) or shallow ($kd < 0.3$), is given in Table A-3. Values indicate mostly intermediate waters. We did not take into account set-up during stormy conditions. Despite the deep-water assumption being a questionable one, the data selected is still the most offshore we can get. Since there is no other data available, we will continue with the data from the selected locations and include this discrepancy in the discussion.

Table A-3: Values for kd at the ADV's of both locations.

Location	Overall	Calm conditions	Stormy conditions
FL69	2.53	2.74	1.80
FL70C	4.70	5.52	2.61

Figure A-6 shows the relation between the wave heights of the ADV and STB measurements at location FL69. Figure A-7 shows this relation for the STB at FL70 and the ADV at FL69. Figure A-8 shows the relation between the STB's at locations FL69 and FL70. For all these relations, overlapping data was used from the period of June 22nd 2019 to August 31st 2020. The color in the figures indicate the density, the number of 15-minute averaged values per pixel.

Although correlation coefficients are high in all comparisons, large deviation may be observed. Also, the inaccuracies due to device clogging, mentioned at the start of Section 4.1, are visible as outliers in the data. All together we conclude that usage of data should be assessed depending on the application, as would usually be the case.
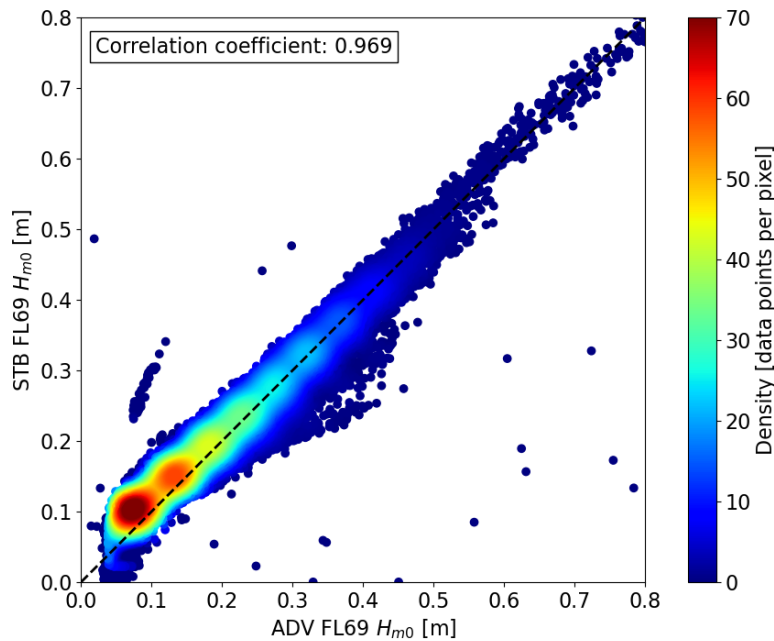
Figure A-6: Relation wave heights of the ADV and STB at FL69.
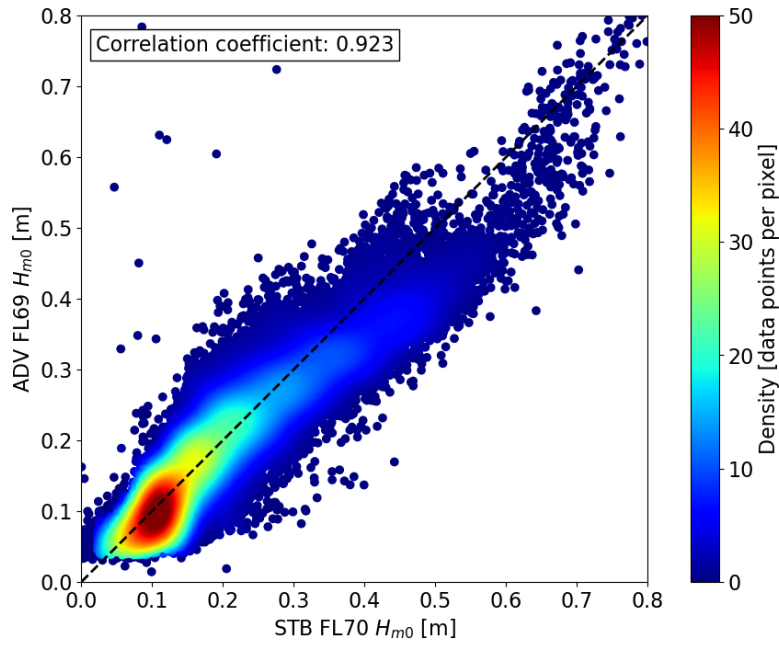
Figure A-7: Relation wave heights of the STB and ADV at FL70 and FL69, respectively.
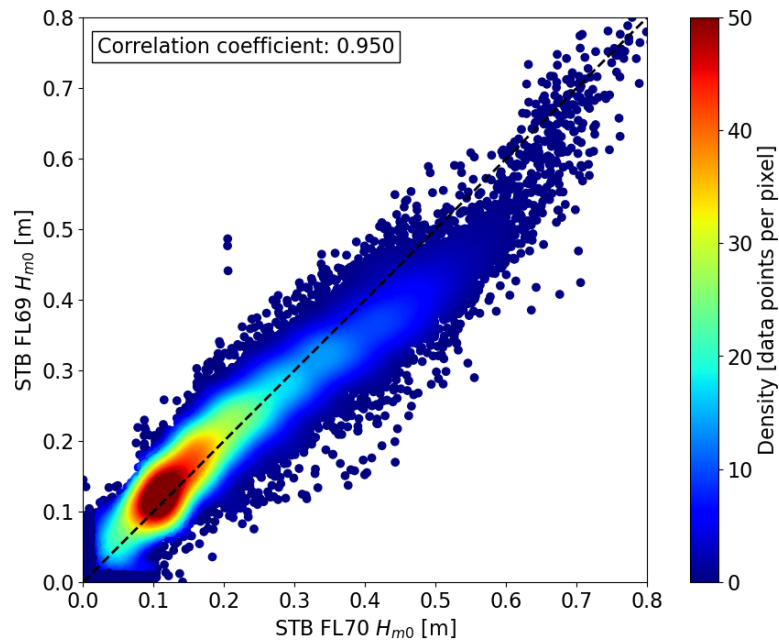
Figure A-8: Relation wave heights of the STB's at FL70 and FL69.

Appendix B: Wind interactions

Due to the absence of tide and swell in the IJsselmeer, most of the observed waves are expected to be generated by the wind. Considering Section 2.1.2, several studies have classified low-energy environments based on the presence of short, steep wind-waves. To substantiate the classification of low-energy environment, we assessed the effects wind has on the hydrodynamics. This was done for both waves and currents (Sections B.1 and B.2, respectively). Additionally, we included an analysis of the wave directional spreading in Section B.3, which underlined our suspicion of wind dominance.

B.1 Wind and wave interactions

Figure B-1 and Figure B-3 show the relation between wind direction, wave direction and wind speed for locations FL69 and FL70C. The dashed red line indicates the beach orientation. Within these lines, wind and waves are moving towards the beach. The green dashed line indicates the 45° critical value. So, within the red and green lines the waves are considered high-angle, inside the green lines they are considered low-angle. The figure for FL69 shows that most wind speeds of 11 m/s and above are coming from the South-West and generate waves that move away from the beach. For location FL70C, these winds are correlated to waves that move towards the beach. However, within the dashed red line of both figures, we see a clear relation between high wind speeds and waves that propagate in the same (or similar) direction. Most notable are the Northern storms that generate higher waves propagating towards the South, as can be seen in Figure B-2.

Figure B-2 and Figure B-4 show the relation between the wind direction, wave direction and wave height. To prevent a cluttered graph, waves smaller than 5 cm are not shown. The figures show that the largest wave heights occur when the wind and wave direction are more or less the same. We also see that the wave direction around the beach parallels is less dependent on wind direction (flatter curve), which means that waves from multiple angles are forced into a single direction. This is likely due to the interaction between wind and currents (see Figure B-6 in the next section). Additionally, the largest waves moving towards the North are smaller than the largest waves moving towards the South-East. This may be explained by a shorter fetch in the South-Eastern direction.
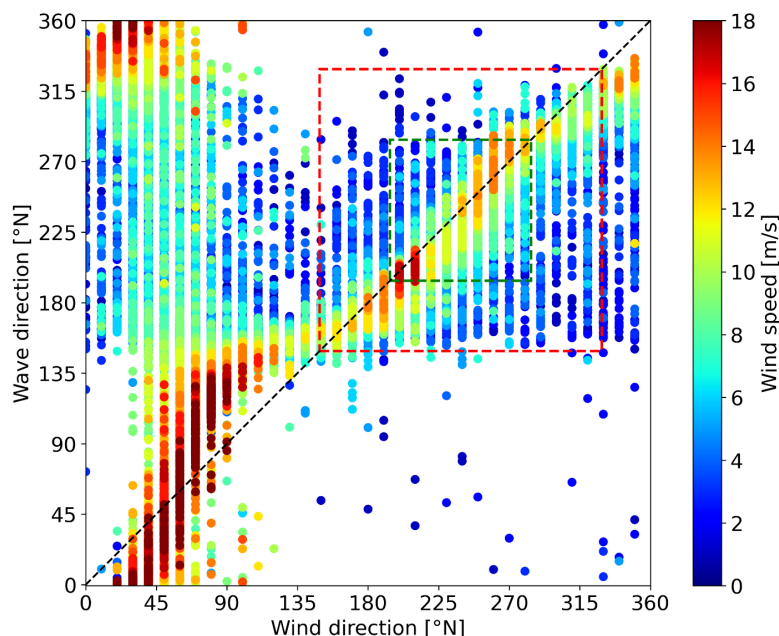
Figure B-1: Relation between wind direction, wave direction and wind speed for location FL69.
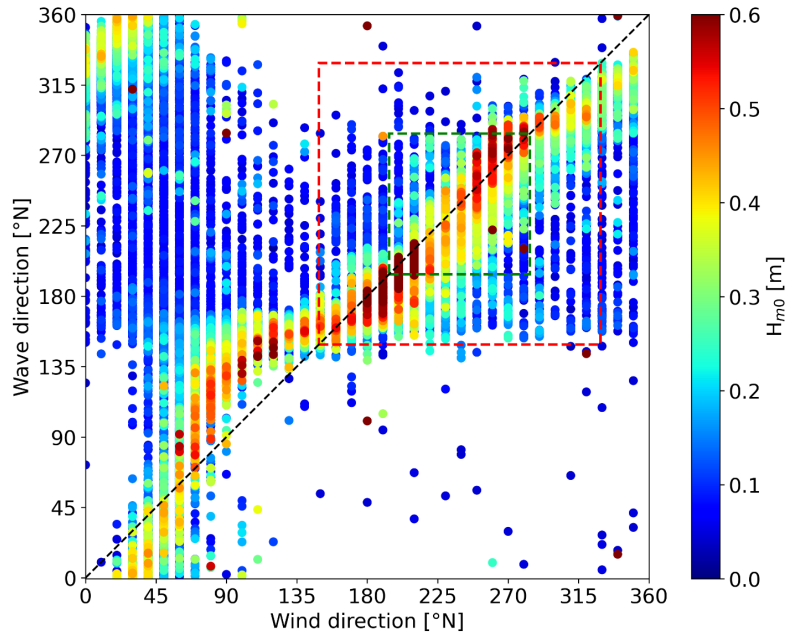
Figure B-2: Relation between wind direction, wave direction and wave height for location FL69.
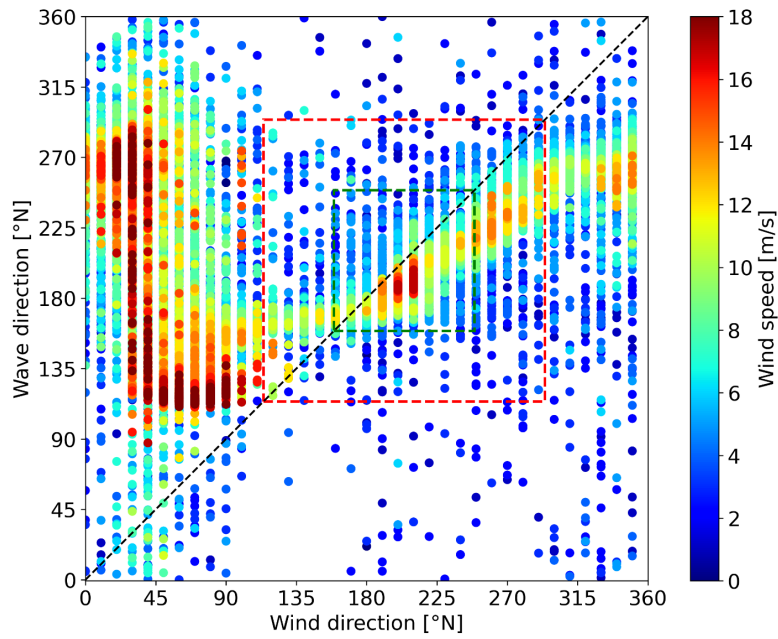
Figure B-3: Relation between wind direction, wave direction and wind speed for location FL70C.
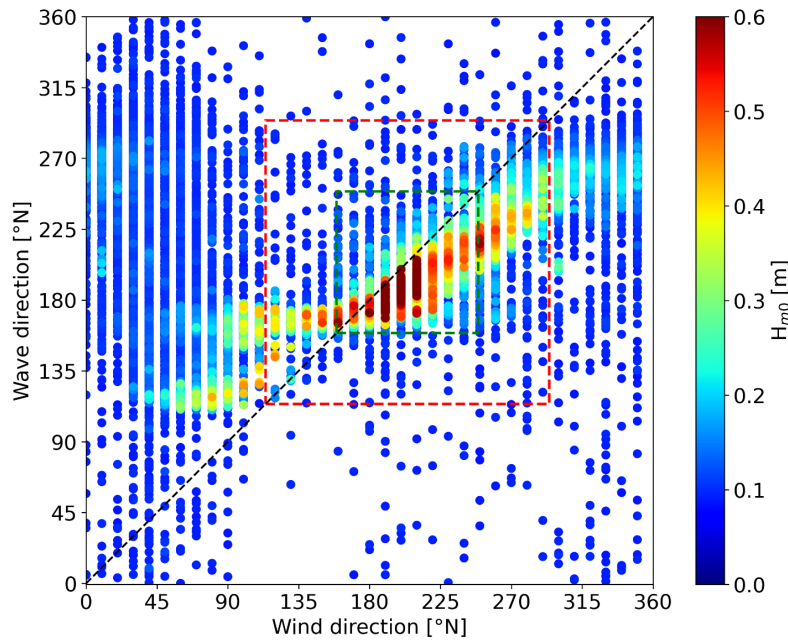
Figure B-4: Relation between wind direction, wave direction and wave height for location FL70C.

Given Figure B-1 and Figure B-2, it seems wind speeds exceeding 11 m/s may give rise to waves larger than approximately 0.25 m, moving in the same direction. This suggests that 'windy' conditions may cause the wave climate to become wind-dominated, whereas calm conditions do not. Considering Section 2.1.2 of the theoretical background, this gives reason to adopt the classification of our environment as mentioned by Jackson et al. (2002). Sections 3.2 and 4.1.2 elaborates on how we made a distinction between 'calm' and 'stormy' conditions in accordance with this classification.

B.2   Wind and current interactions

In Figure B-5 and Figure B-7 we show the relation between wave direction, current direction and wind speed at FL69 and FL70C. Similar to the relation between wind and waves, a relation between wind and currents is clearly noticeable for FL69. A slightly steeper curve in the graph can be explained by focusing of the flow along the coast. For example, wind directions perpendicular and towards the beach can result in flow either going North, or South-East (see also Figure B-6). This seems to be mostly valid for wind speeds of 11 m/s and larger. However, while this also seems to hold for FL70C, we see that wind and currents are more independent, with currents moving mostly parallel to the beach.

Figure B-6 and Figure B-8 show the relation between wind direction, current direction, and current velocity. To reduce clutter in the graph, current velocities lower than 5 cm/s are not shown. This indicates that current velocities are generally increased if the wind is in the same direction, but the wind does not independently control it.
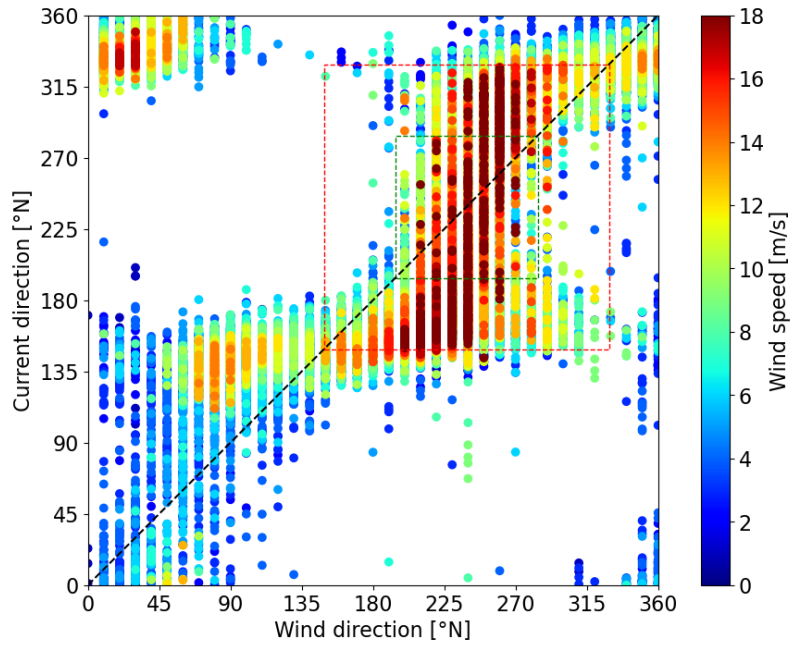
Figure B-5: Relation between wind direction, current direction and wind speed for location FL69.
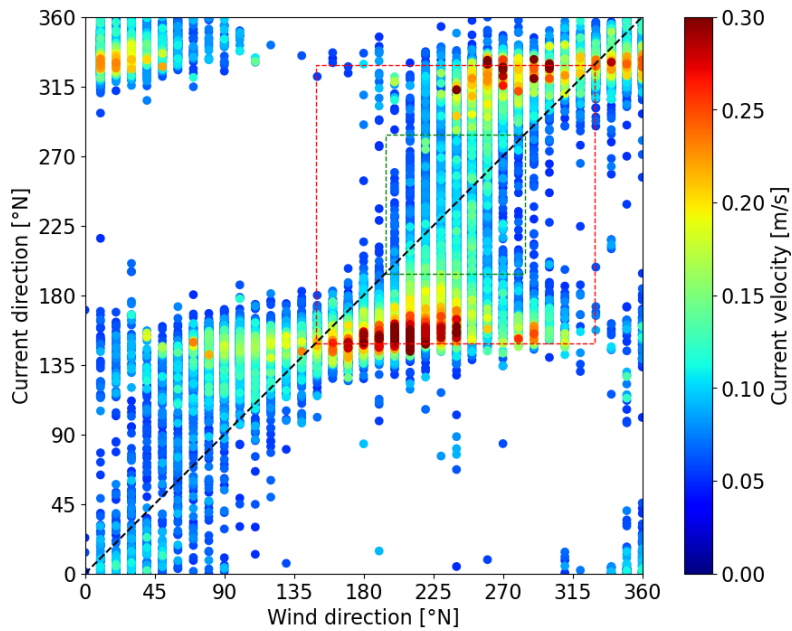
Figure B-6: Relation between wind direction, current direction and current velocity for location FL69.
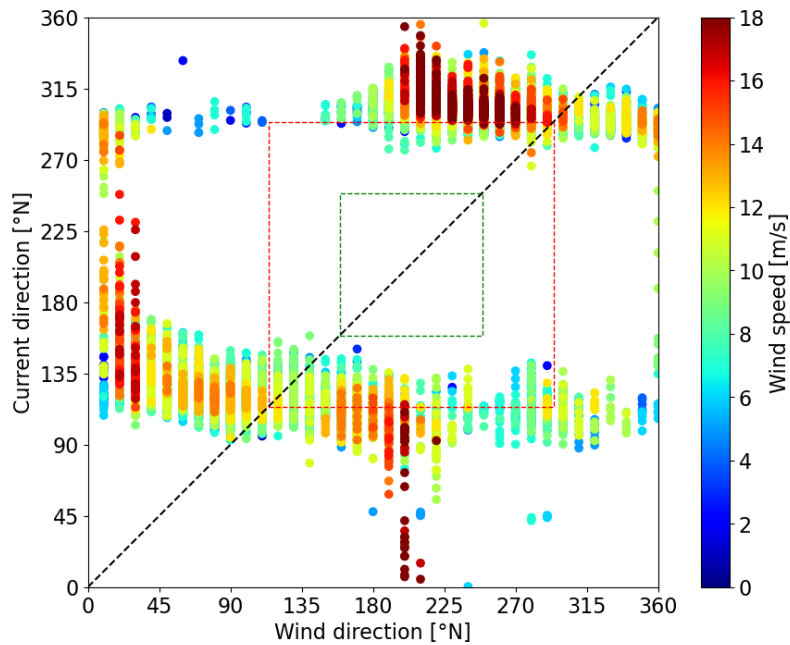
Figure B-7: Relation between wind direction, current direction and wind speed for location FL69.
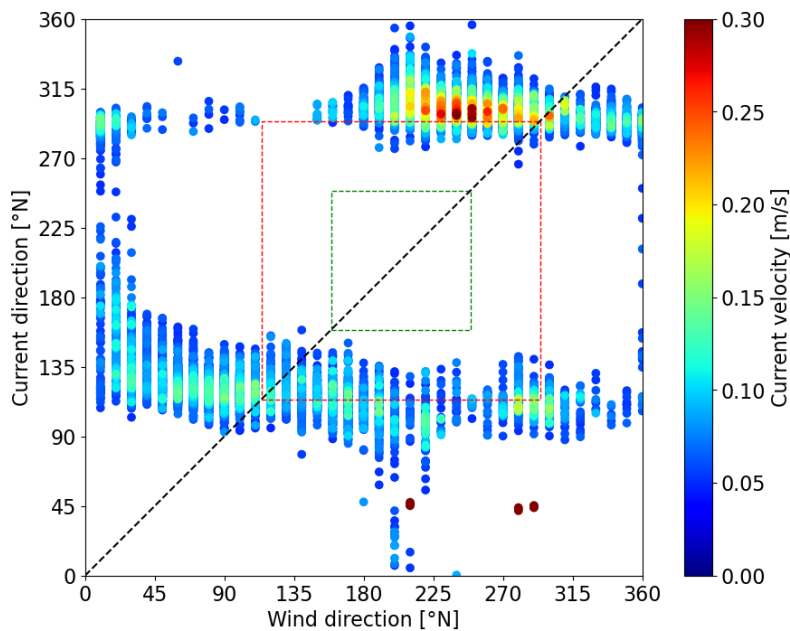
Figure B-8: Relation between wind direction, current direction and current velocity for location FL69.

B.3   Wave directional spreading

A look at the wave directional spreading has provided us insight in the behavior of the wave directions. This was done for the most offshore ADV data (location FL69 and FL70C). Figure B-9 and Figure B-10 show the wave directional spreading as a function of time. The colors indicate whether the data belongs to the previously defined calm or stormy conditions. The color intensity indicates the wave height, as indicated by the color bars on the right. Average values ($\bar{\alpha}$) and standard deviations (σ_α) for the two conditions are given in Table B-1.
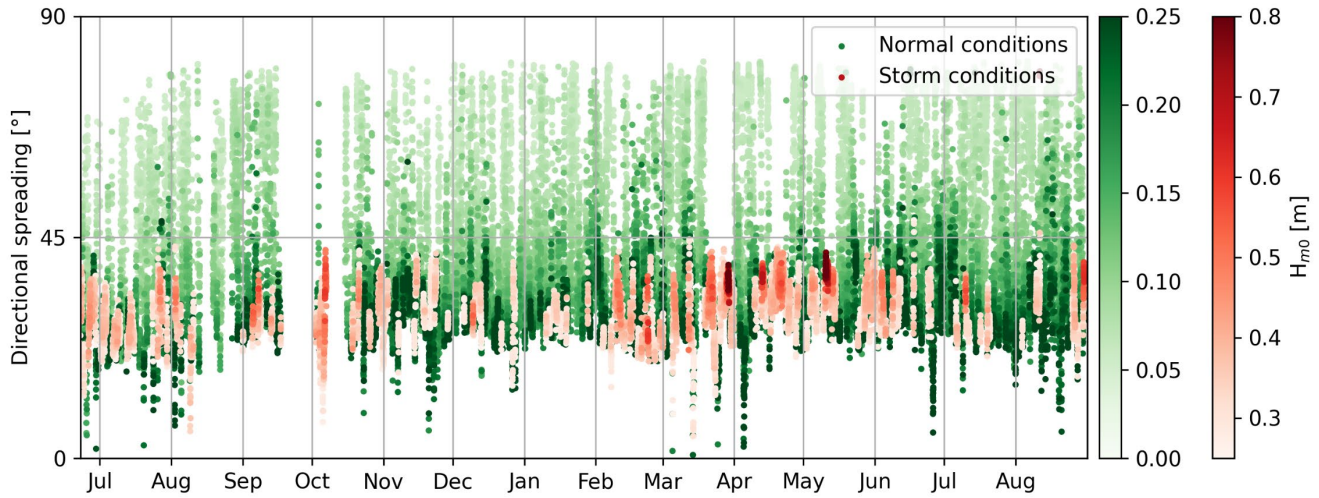
Figure B-9: Wave directional spreading separated in calm and stormy conditions for location FL69.
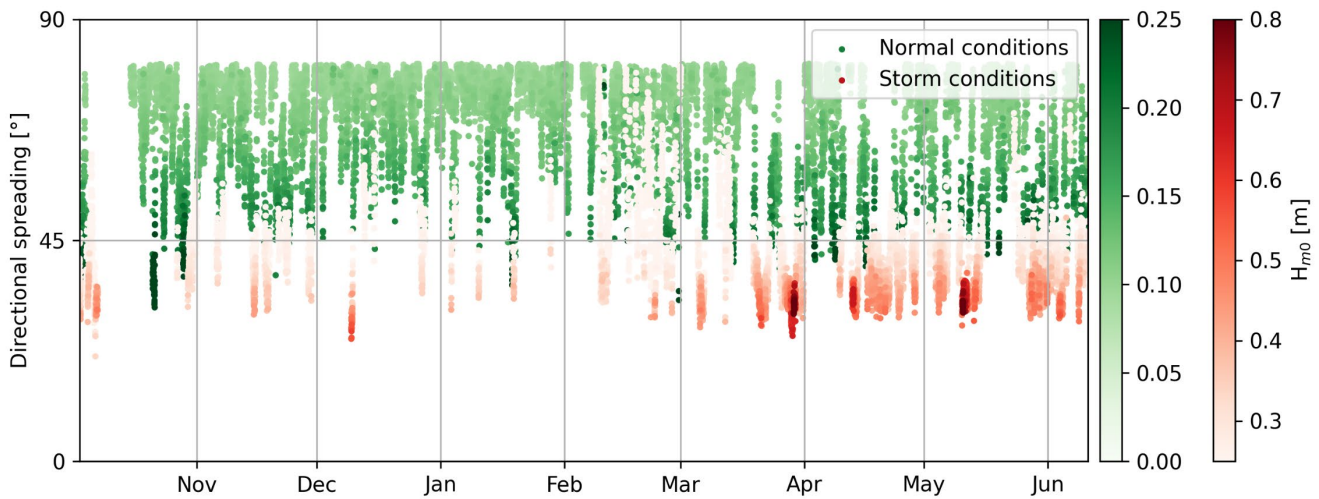
Figure B-10: Wave directional spreading separated in calm and stormy conditions for location FL70C.

Table B-1: Statistics of the wave directional spreading at locations FL69 and FL70C, with average wave direction spreading ($\bar{s}_0$), and standard deviation of the spreading (σ_{s0}).

Location	Conditions	$\bar{s}_0$ [°]	σ_{s0} [°]
FL69	Calm	41	16
	Stormy	30	5
FL70C	Calm	70	10
	Stormy	41	9

A closer look at the vertical streaks of data points indicates an increase in directional spreading and wave height as storms arrive. As wind velocities increase, wave directional spreading at first decreases as we move from calm to stormy conditions, suggesting wind forcing is becoming dominant. Then, as stormy conditions are reached, both directional spreading and wave height steadily increase over the duration of the storm. As wind velocities decrease towards the end of the storm, so do the wave directional spreading and wave height. Finally, when calm conditions are reached, wave directional spreading increases again, suggesting other processes once again dominate the wave dynamics. This seems to substantiate the claim in Section B.1 that stormy conditions are driven by the wind.

Appendix C: Wave climate

C.1   Location FL69
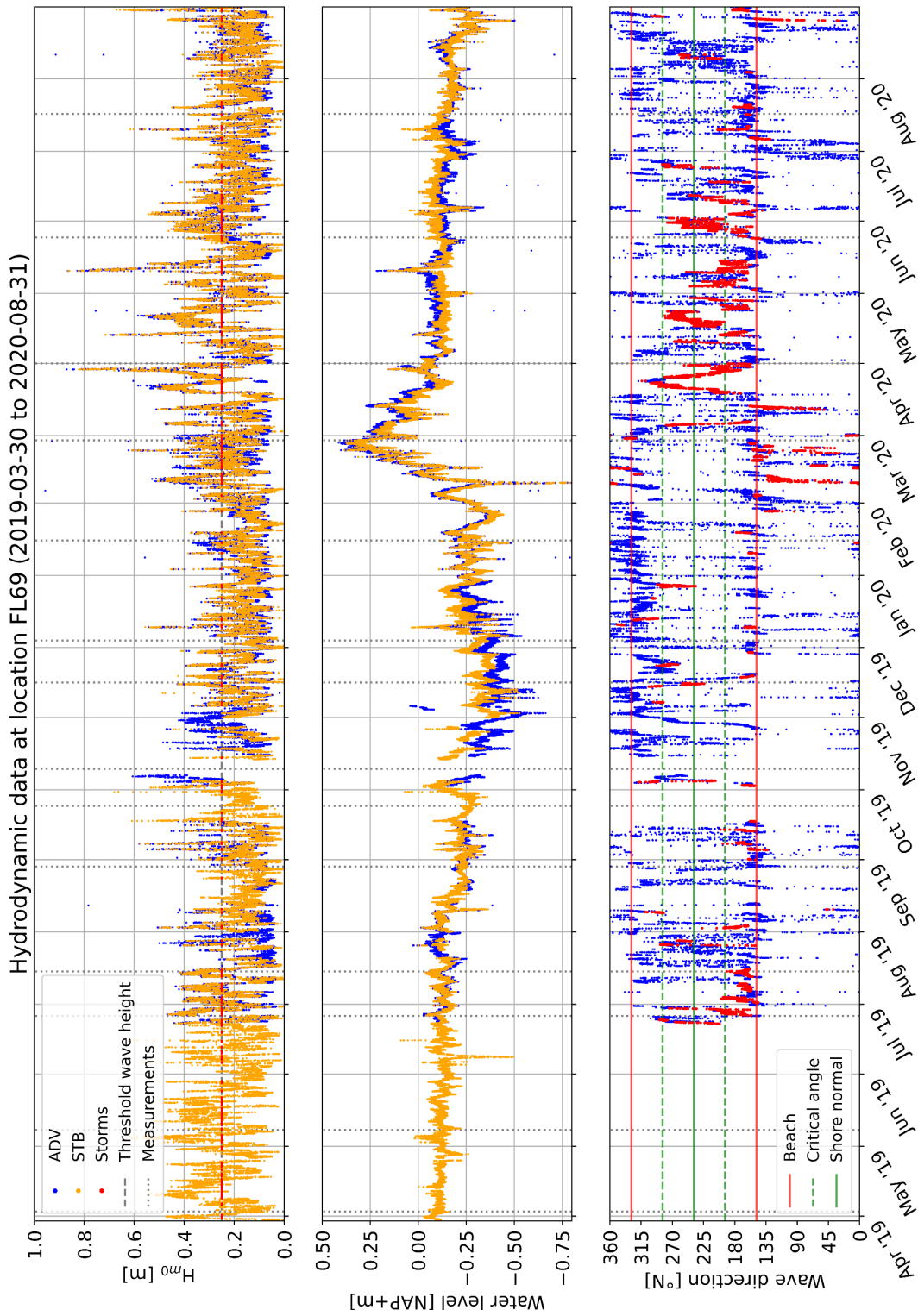
C.2   Location FL70

C.3   Location FL70C

Hydrodynamic data at location FL70C (2019-10-02 to 2020-06-10)
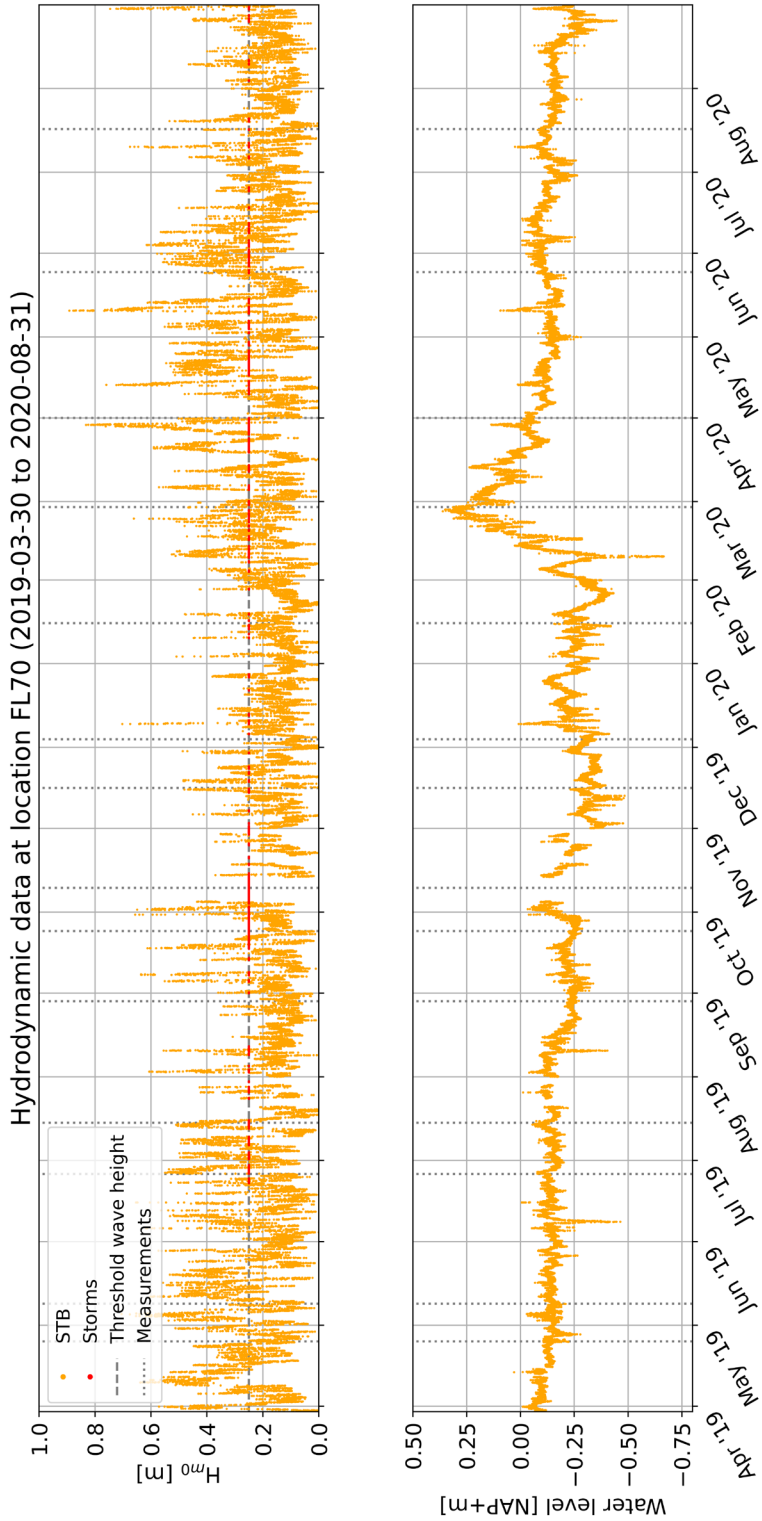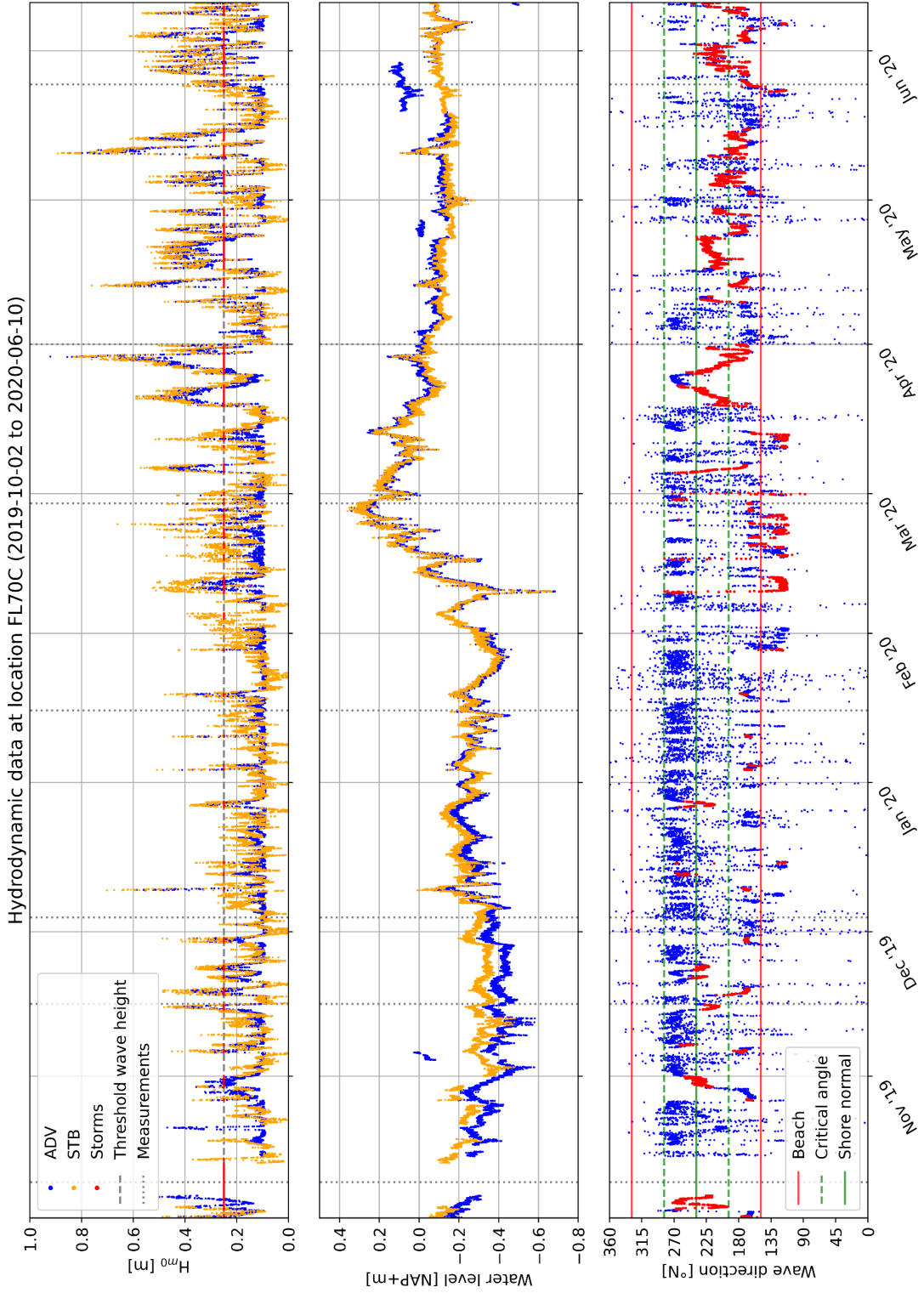
Appendix D: Orthogonal photos and satellite imagery

This appendix includes several satellite images and all the orthogonal photos from both location FL69 and FL70. Satellite images were procured from the Netherlands Space Office (Satellietdataportaal, https://satellietdataportaal.nl/). Orthogonal photos were produced by Shore (Appendix A.2).

D.1 FL69: 24 April 2019 (satellite)
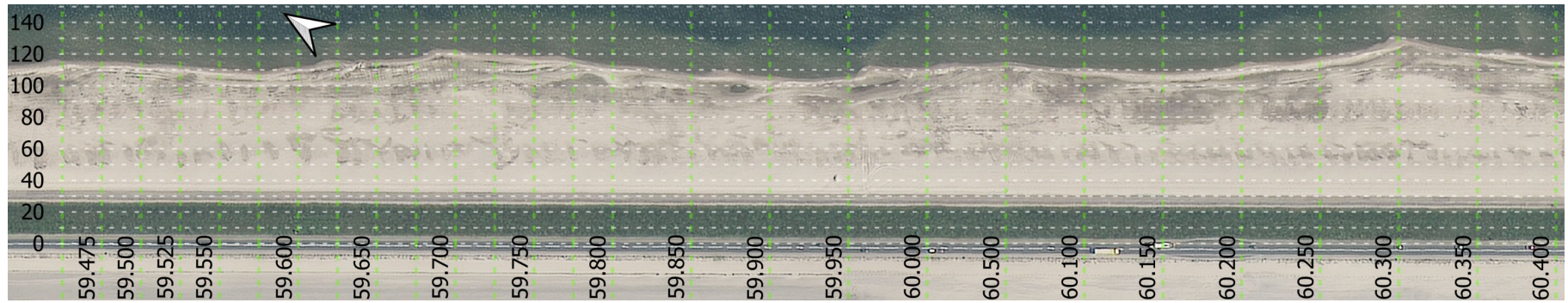
D.2 FL69: 22 June 2019 (satellite)
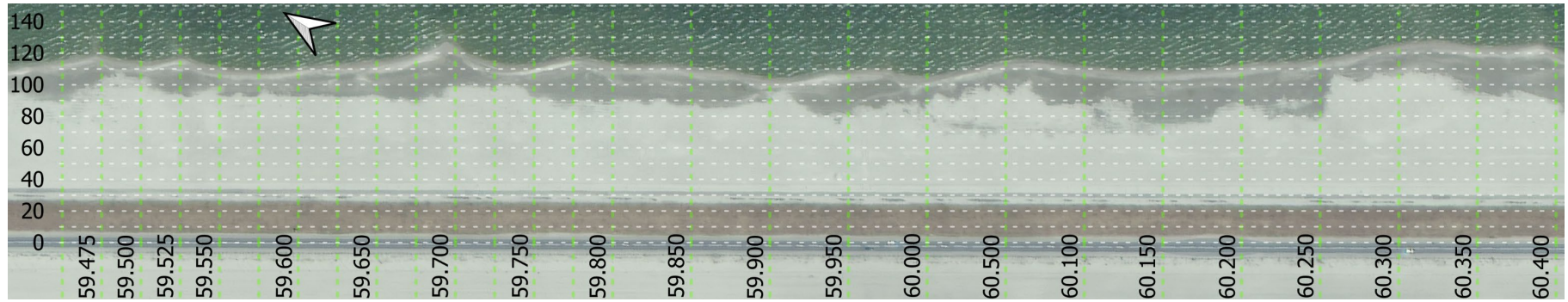
D.3 FL69: 29 June 2019 (satellite)
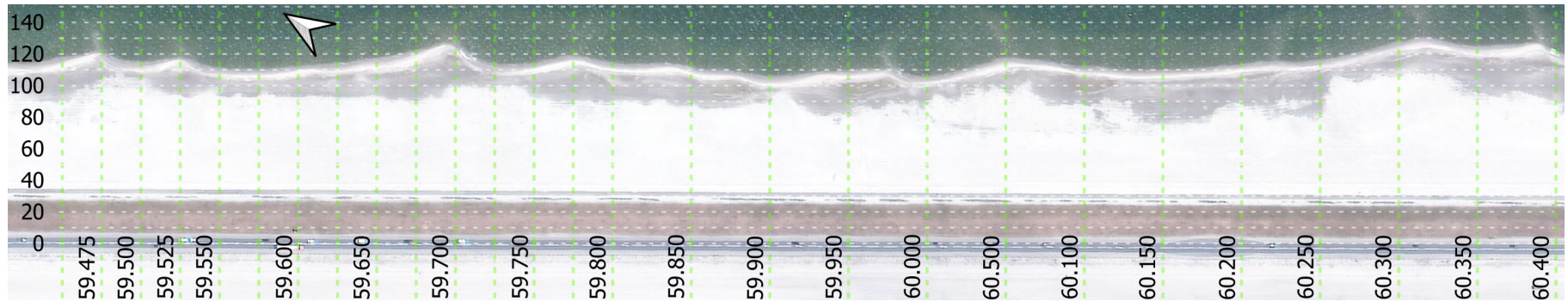
D.4   FL69: 28 July 2019 (satellite)
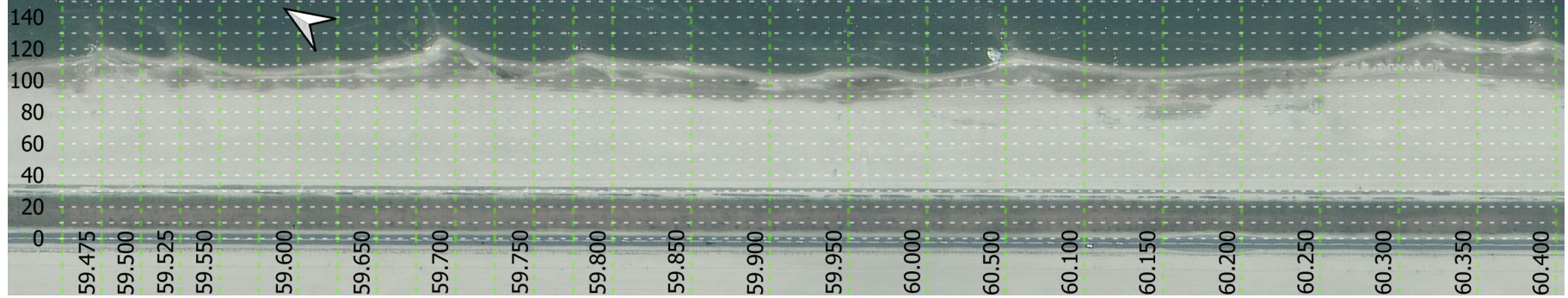
D.5   FL69: 19 September 2019 (satellite)

D.6   FL69: 16 November 2019 (orthogonal)
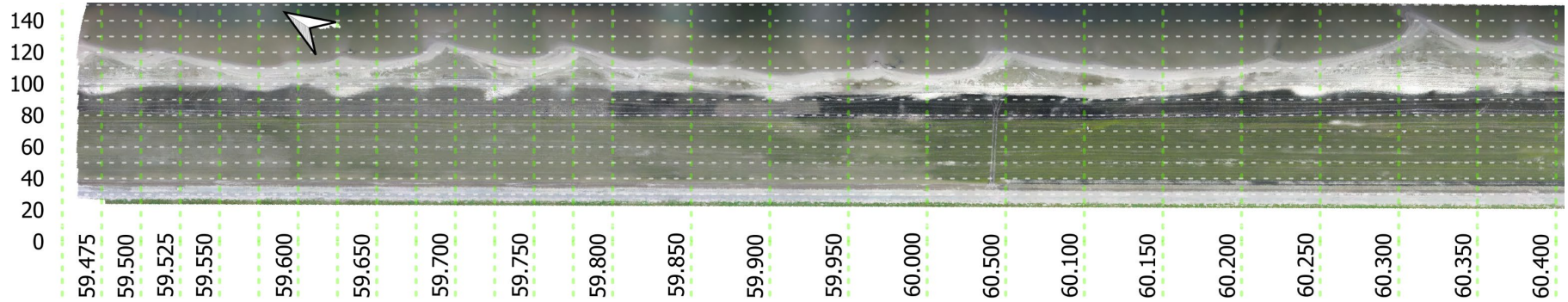
D.7   FL69: 4 December 2019 (orthogonal)
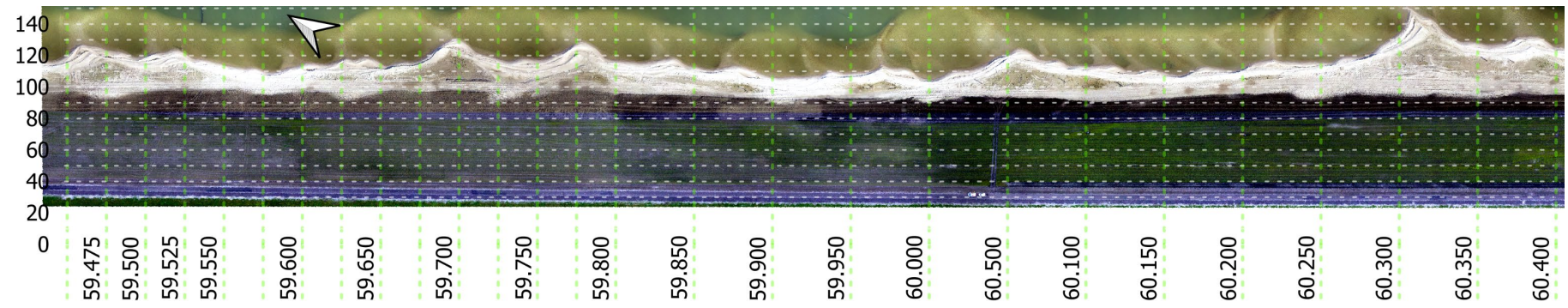
D.8   FL69: 14 December 2019 (satellite)
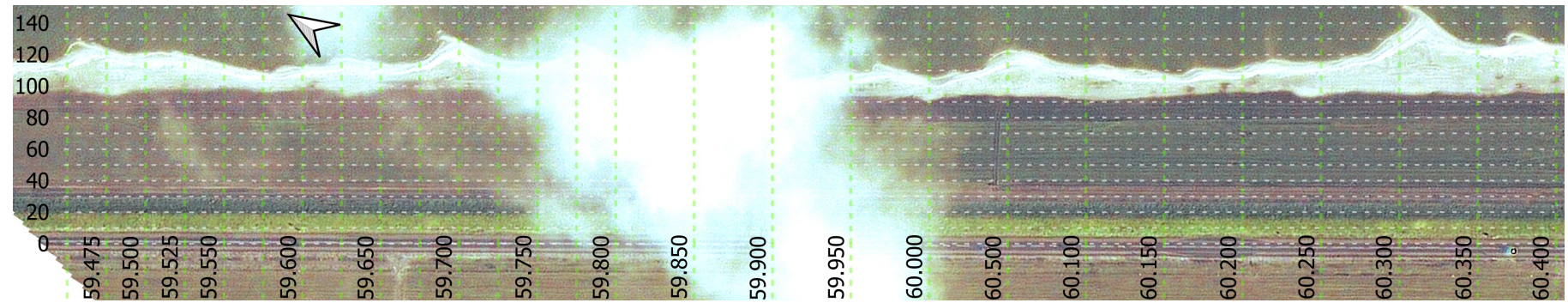
D.9   FL69: 16 January 2020 (orthogonal)
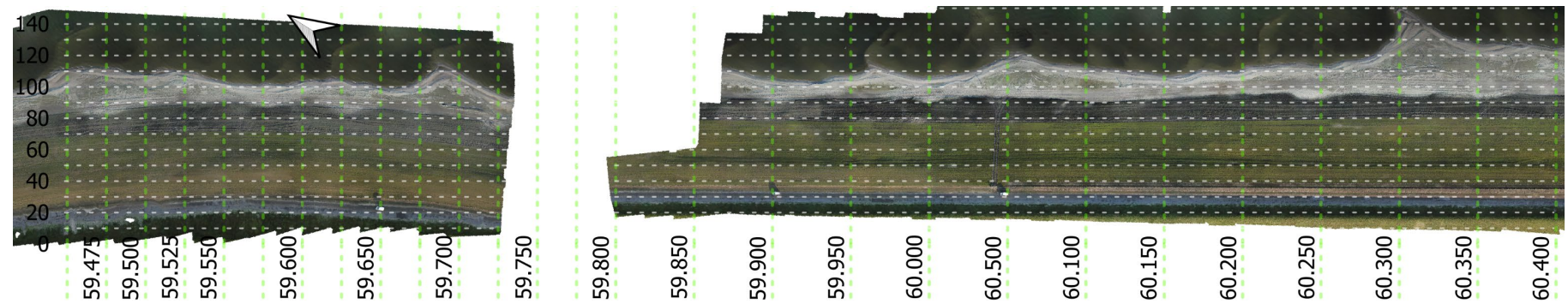
D.10 FL69: 28 February 2020 (orthogonal)
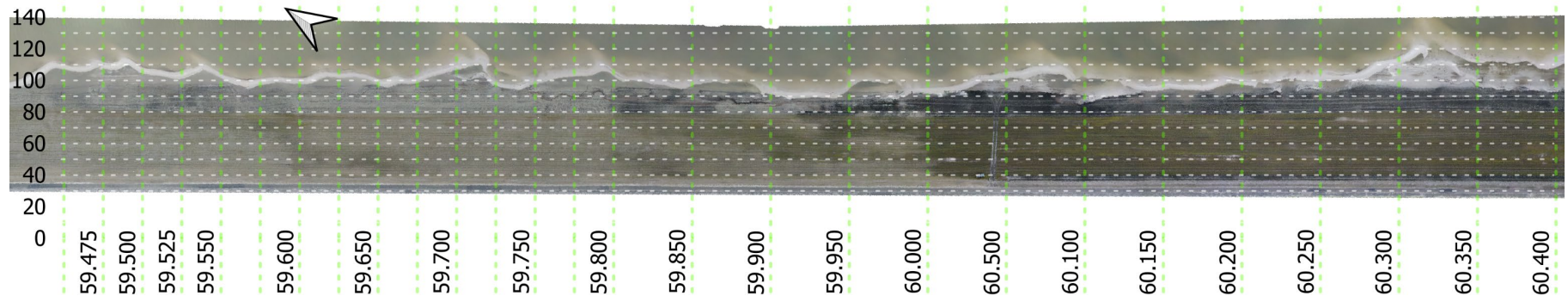
D.11 FL69: 1 April 2020 (orthogonal)
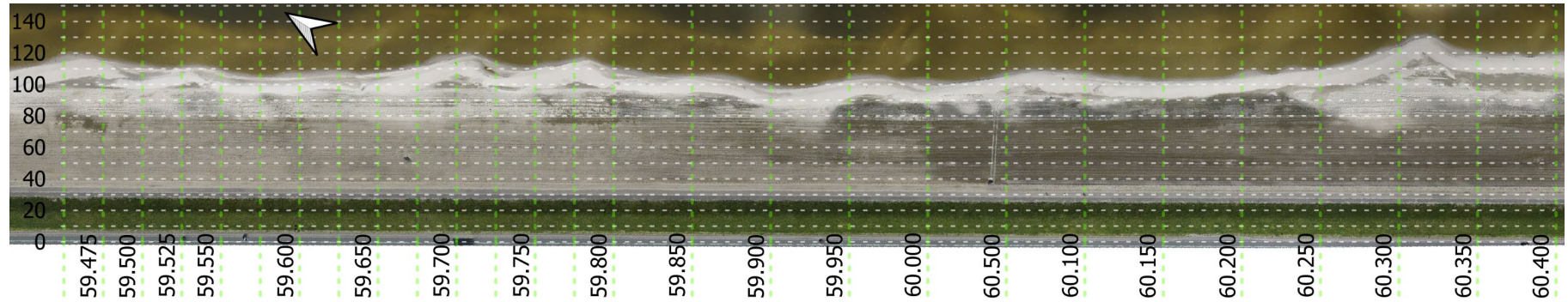
D.12 FL69: 26 April 2020 (satellite)
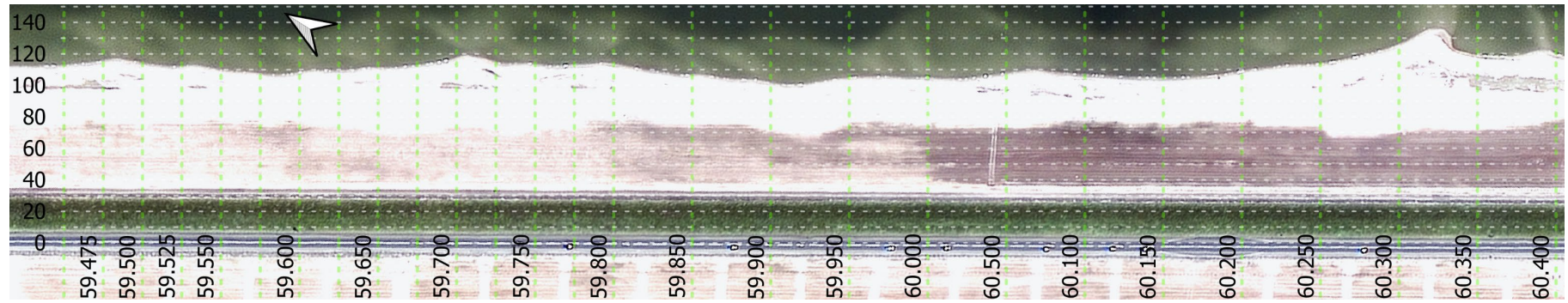
D.13 FL69: 25 May 2020 (orthogonal)
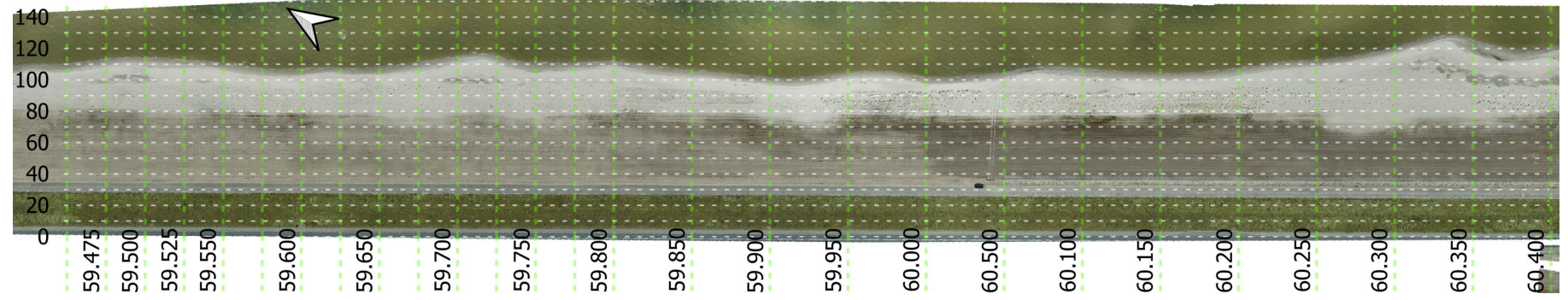
D.14 FL69: 17 July 2020 (orthogonal)
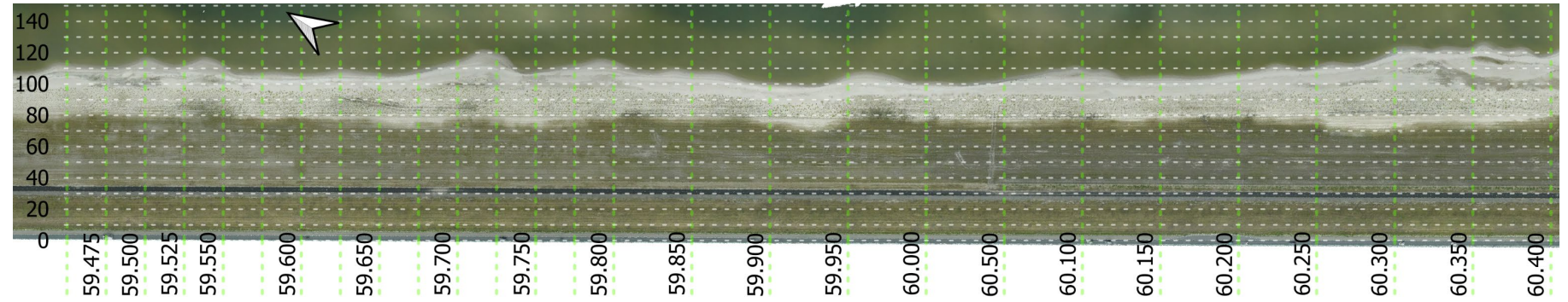
D.15 FL70: 24 April 2019 (satellite)
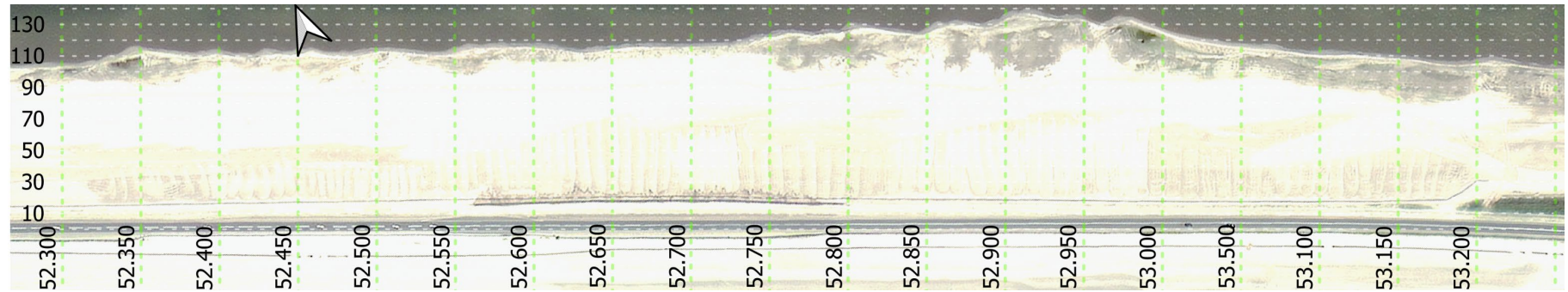
D.16 FL70: 22 June 2019 (satellite)
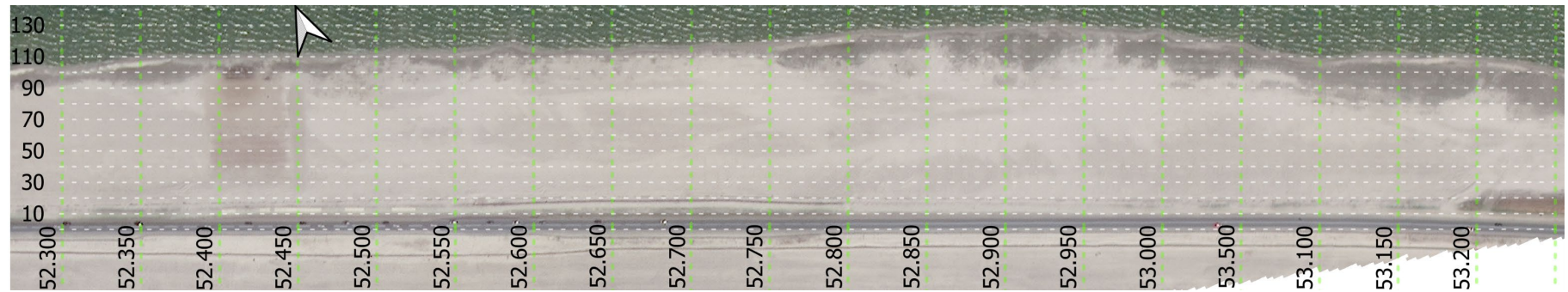
D.17 FL70: 29 June 2019 (satellite)
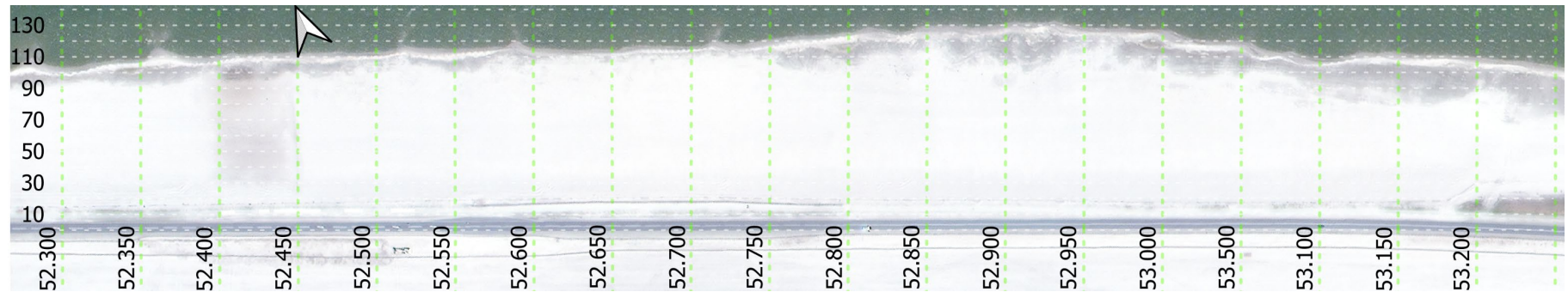
D.18 FL70: 16 November 2019 (orthogonal)
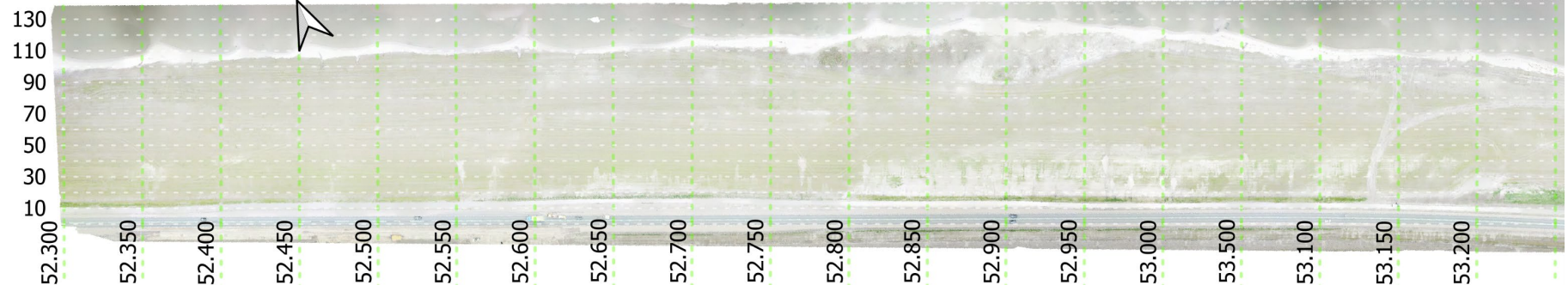
D.19 FL70: 4 December 2019 (orthogonal)
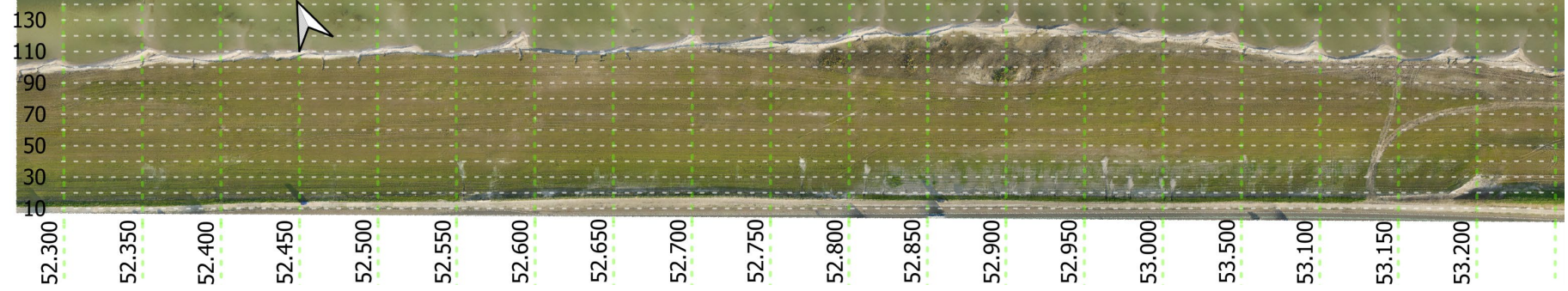
D.20 FL70: 16 January 2020 (orthogonal)
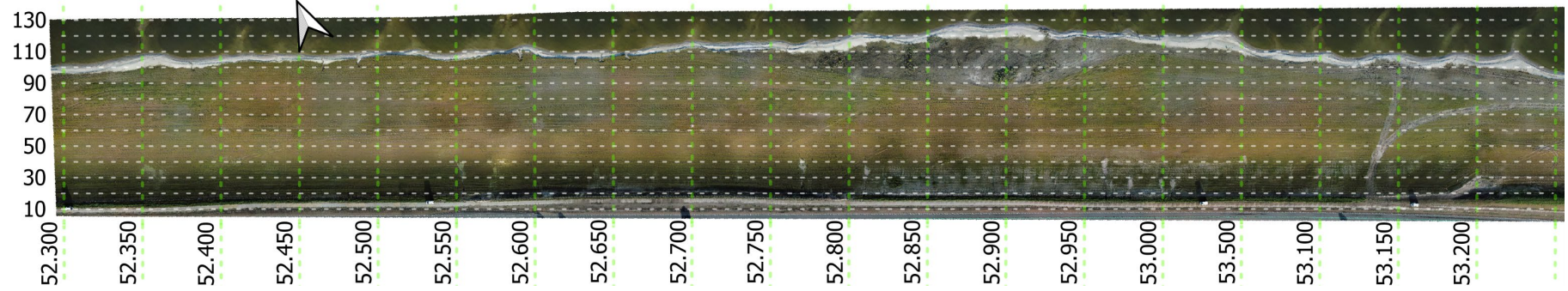
D.21 FL70: 28 February 2020 (orthogonal)
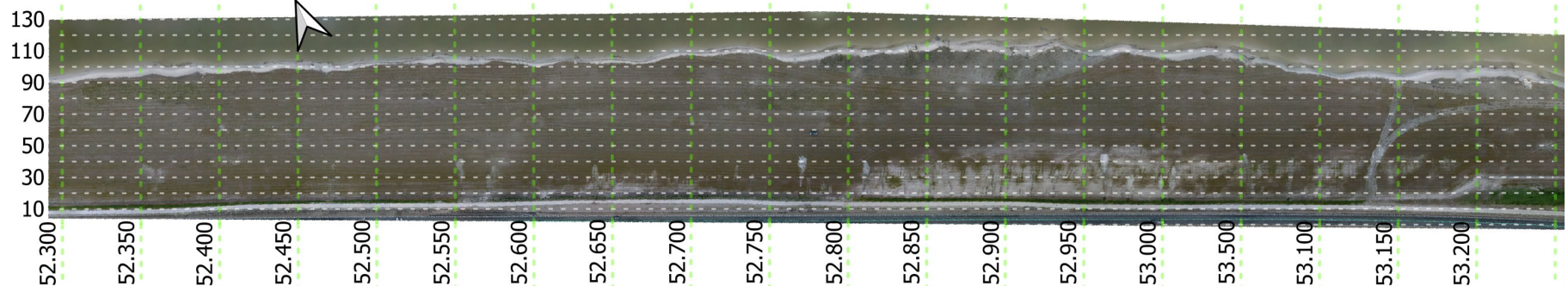
D.22 FL70: 24 March 2020 (satellite)
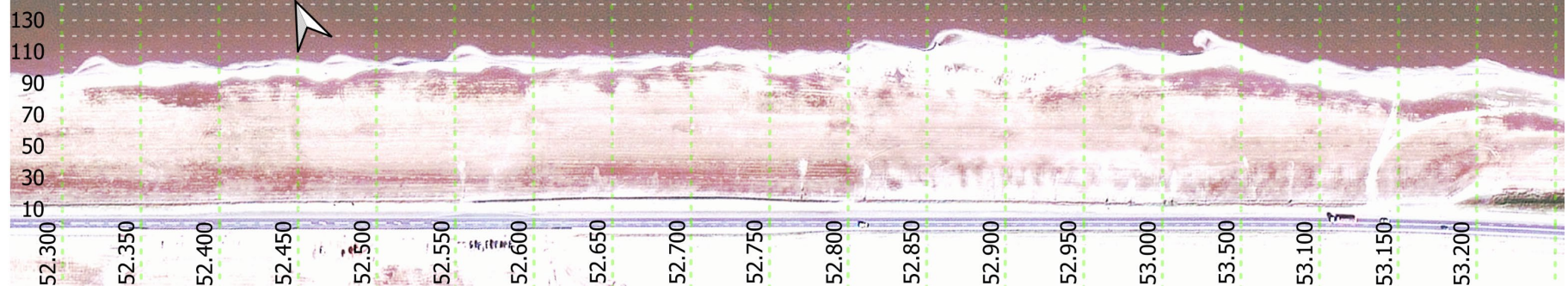
D.23 FL70: 27 March 2020 (satellite)
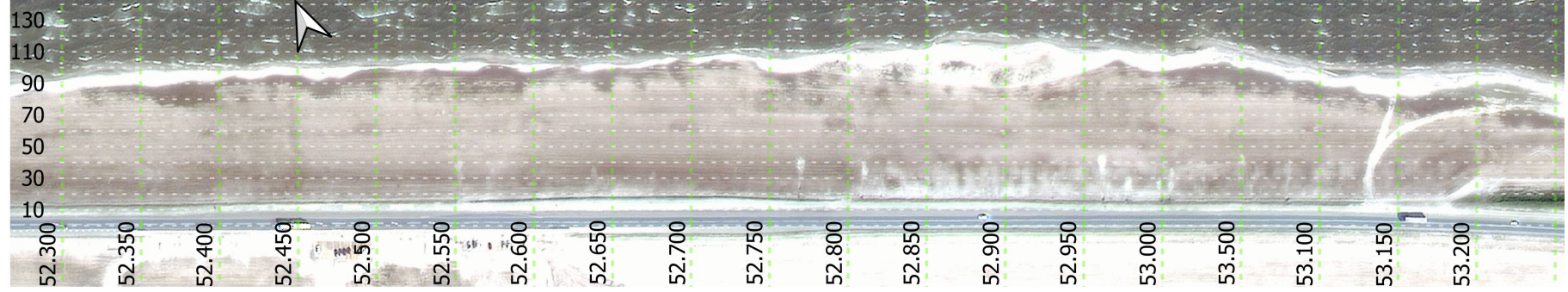
D.24 FL70: 1 April 2020 (orthogonal)
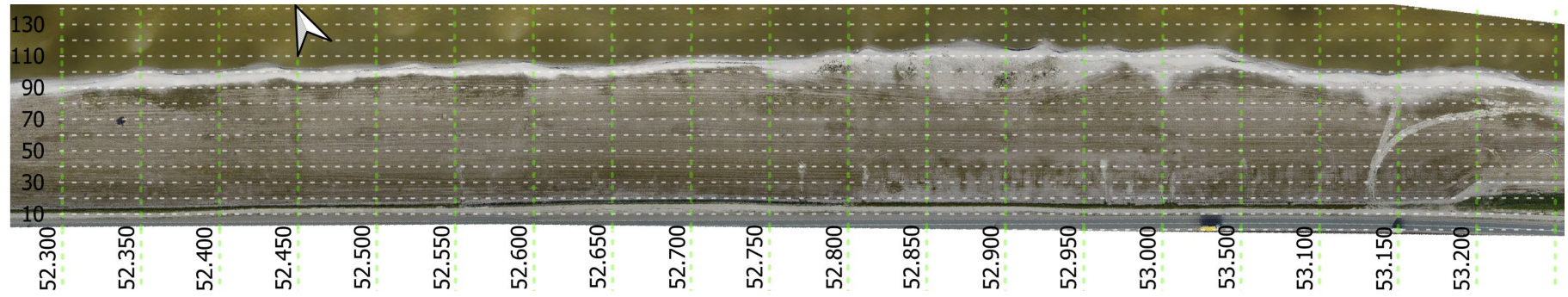
D.25 FL70: 24 April 2020 (satellite)
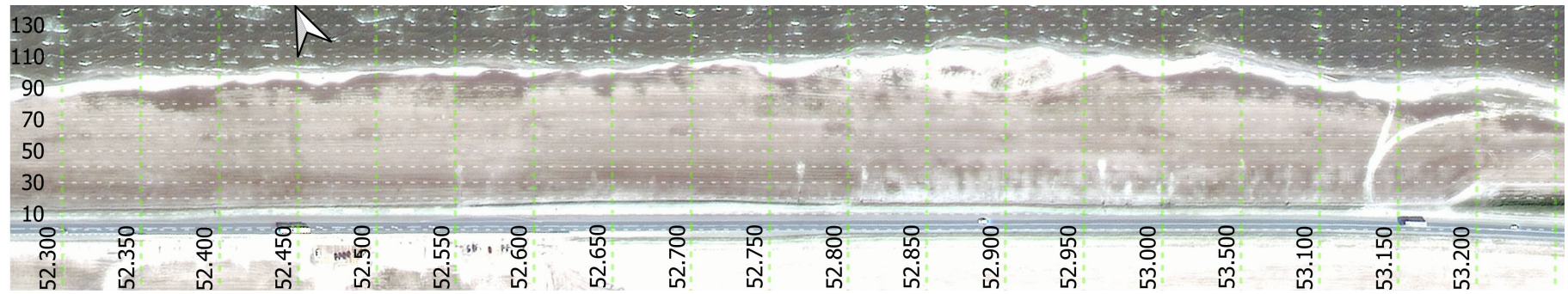
D.26 FL70: 25 May 2020 (orthogonal)
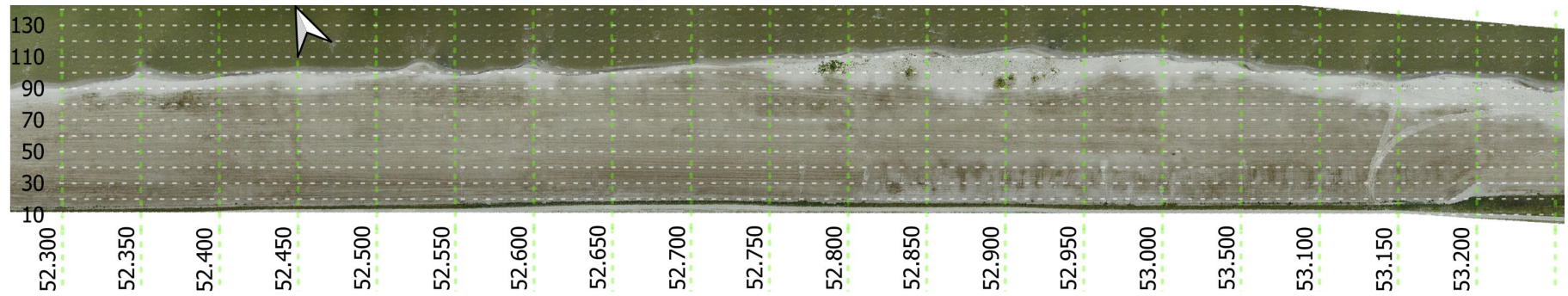
D.27 FL70: 21 June 2020 (satellite)

130
110
90
70
50
30
10

52.300 52.350 52.400 52.450 52.500 52.550 52.600 52.650 52.700 52.750 52.800 52.850 52.900 52.950 53.000 53.500 53.100 53.150 53.200
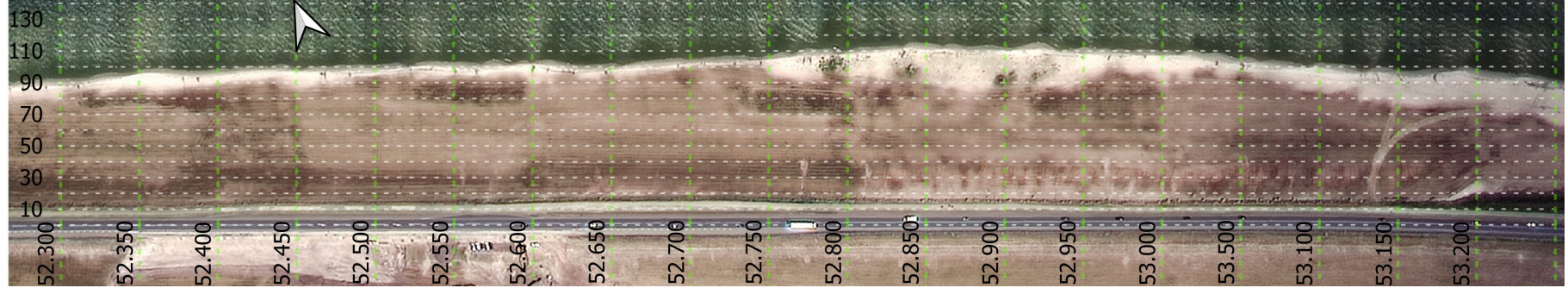
D.28 FL70: 17 July 2020 (orthogonal)

130
110
90
70
50
30
10

52.300 52.350 52.400 52.450 52.500 52.550 52.600 52.650 52.700 52.750 52.800 52.850 52.900 52.950 53.000 53.500 53.100 53.150 53.200
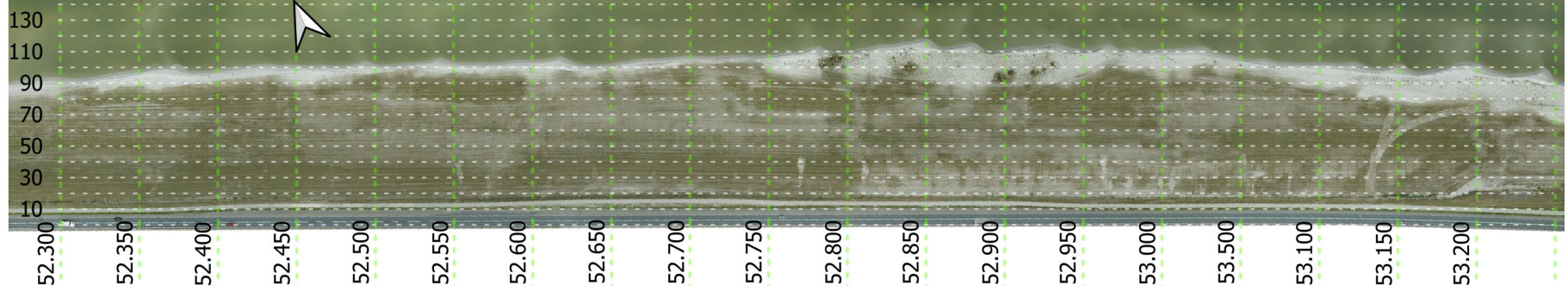
Appendix E: Conceptual model evaluation

The results of applying the conceptual model to our waterlines are given below, in a pairwise comparison of the morphological periods. Quantities used to describe them are the number of cusps (N_c), wavelength (L_c), amplitude (A_c) and shape asymmetry (As). The layout is as follows; the top figure shows the orthogonal photo of the last of the indicated periods (for example, Appendix E.1 shows the photo of T1). Waterlines of the start and end of these periods are indicated by red and blue, respectively, and are evaluated approximately at the water level at the start and end of these periods. The x-axis indicates the transects of the Houtribdijk, the y-axis the cross-shore distance to Shore's reference line.

The lower left graphs show relevant hydrodynamics for this period, like the origin of the waves, the wave height, and the water level. The top of these three graphs, the solid red line indicates the beach orientation, the solid green line the shore normal, and the dashed green lines the 45° critical angles for high-angle wave instabilities. Stormy conditions are indicated by parts of the data that are colored red. In these three graphs, the sections that are shaded in yellow indicate the representative hydrodynamic period, as found using the conceptual model.

On the middle right, we see the wave roses for both stormy and calm conditions. The bars indicate the wave origins, in the same way as the graph to the left of them. Similarly, the lines indicate beach orientation, shore normal and the critical angle. The roses are rotated towards the beach orientation, so that we may see more clearly where the waves are coming from.

The graph below the roses shows the change in the quantities mentioned above, for all measurement periods. The periods we are currently looking at are indicated by a yellow shading. The text below this graph presents a short summary of our observations and the reason why the representative hydrodynamics were chosen. Unless specified, the first line of observations always describes changes in average values of the quantities. In the text we use terms explained in the macro scale conceptual model theory (Section 5.4). As a result of the theoretical background and our storm analysis (Section 4.1), we will only look for representative hydrodynamics that can be considered stormy.
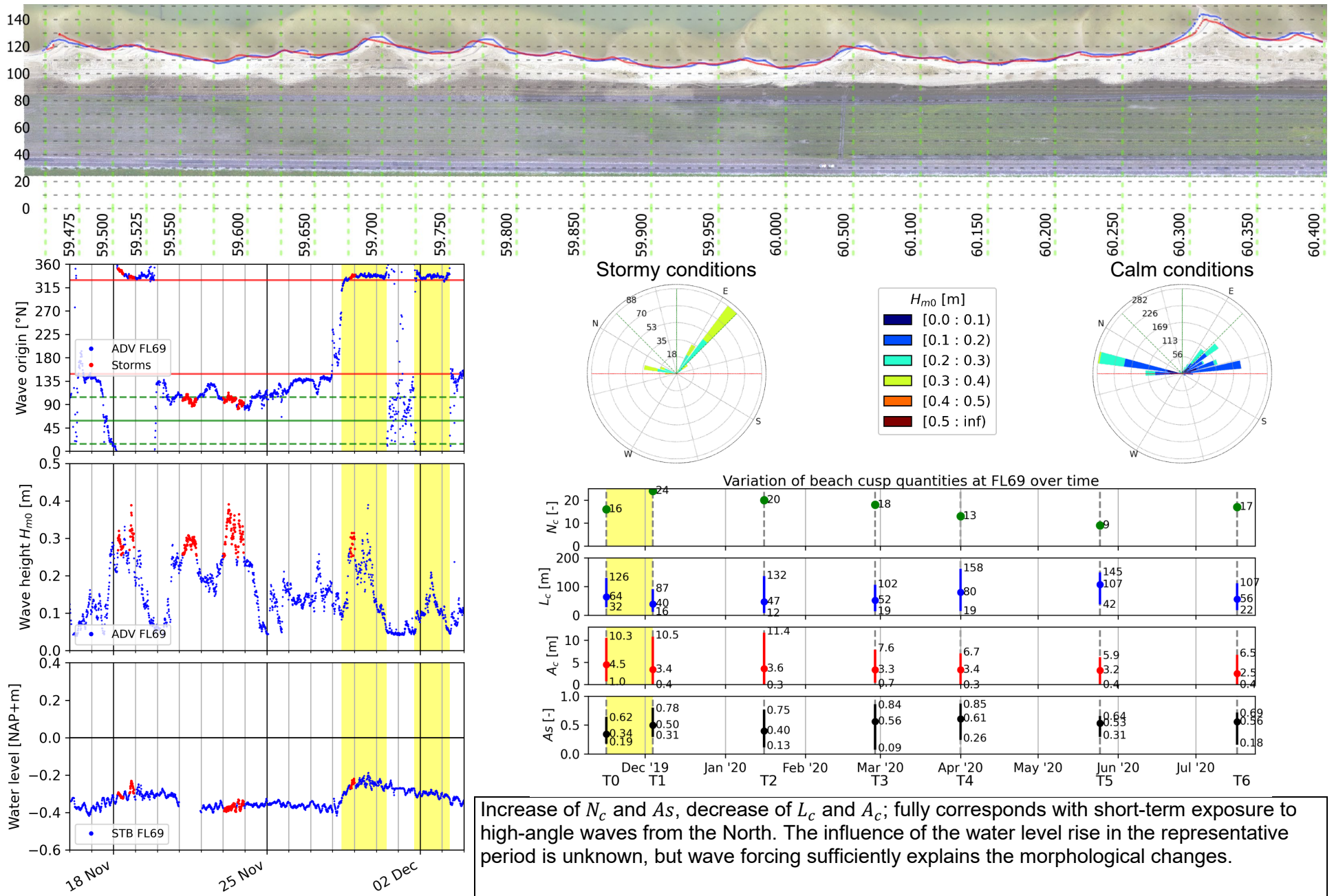
Stormy conditions

Calm conditions

H_{m0} [m]
- [0.0 : 0.1)
- [0.1 : 0.2)
- [0.2 : 0.3)
- [0.3 : 0.4)
- [0.4 : 0.5)
- [0.5 : inf)

Variation of beach cusp quantities at FL69 over time

Increase of N_c and As, decrease of L_c and A_c; fully corresponds with short-term exposure to high-angle waves from the North. The influence of the water level rise in the representative period is unknown, but wave forcing sufficiently explains the morphological changes.
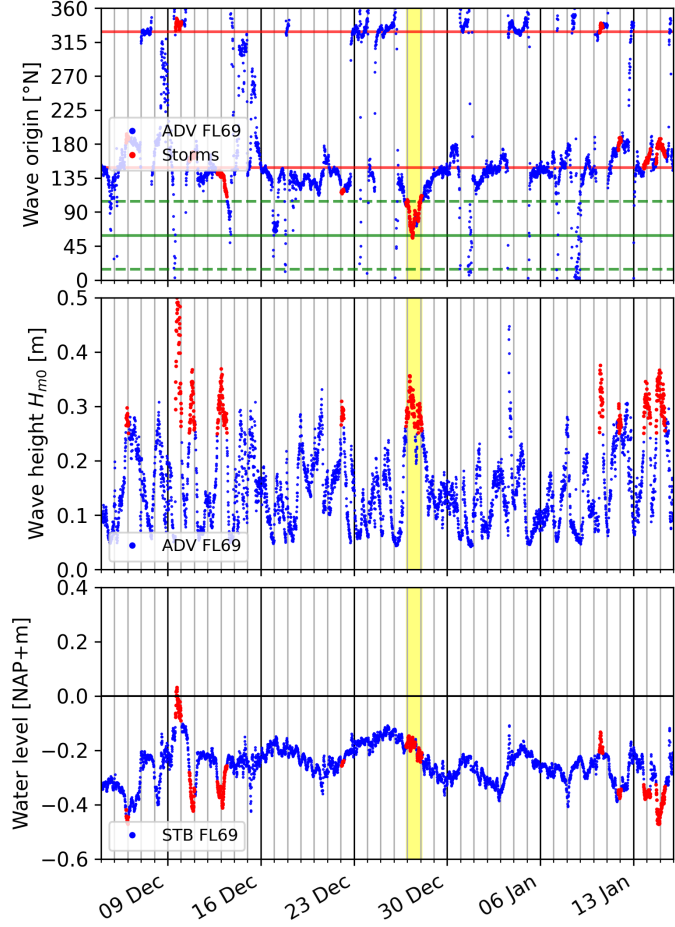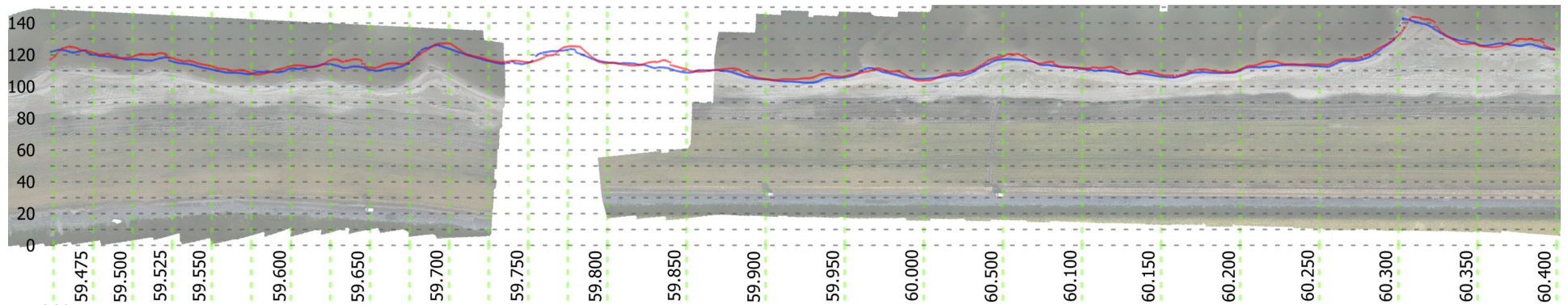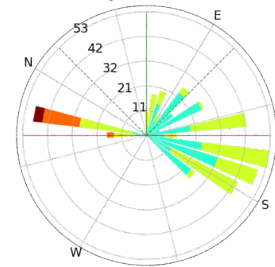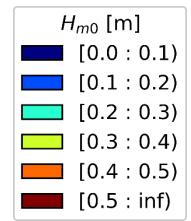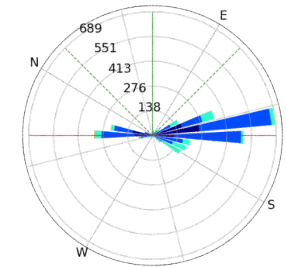
Variation of beach cusp quantities at FL69 over time
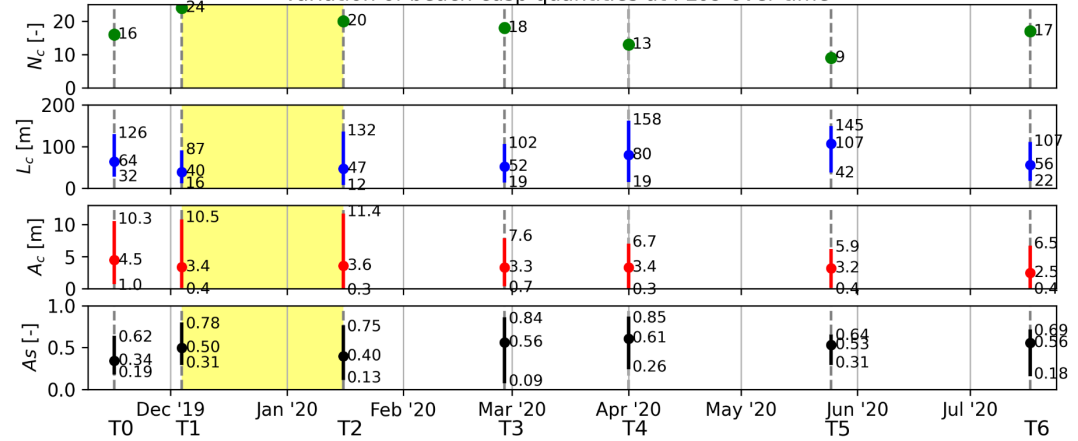
Decrease of N_c and As, increase of L_c and A_c; fully corresponds with short-term exposure to low-angle waves from the East. Despite the short duration, a decrease in water level near the end of this period (even though waves are travelling offshore) may have aided in the dissipation of some of the smaller features, leading to an increase in the average amplitude.
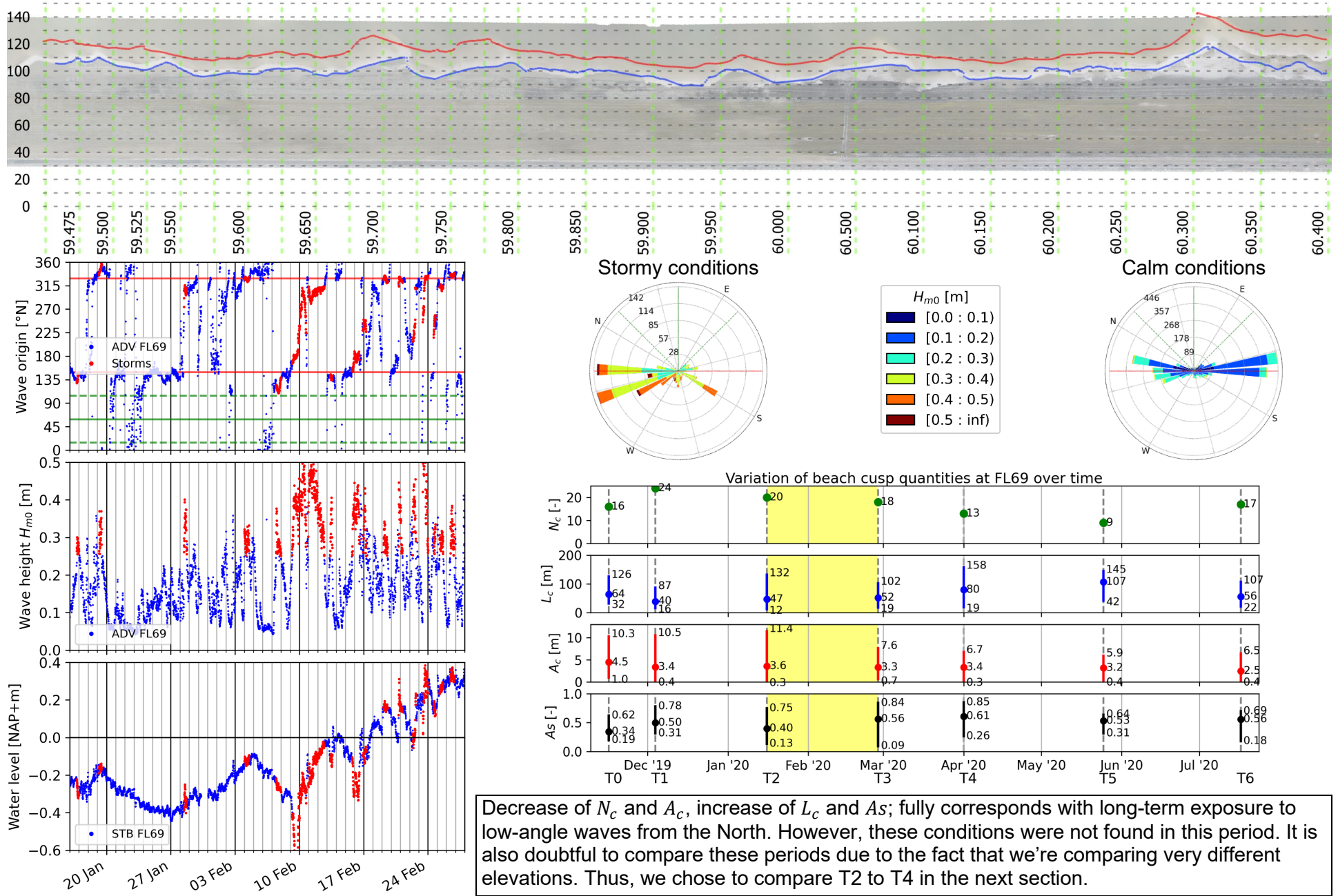
Decrease of N_c and A_c, increase of L_c and As; fully corresponds with long-term exposure to low-angle waves from the North. However, these conditions were not found in this period. It is also doubtful to compare these periods due to the fact that we're comparing very different elevations. Thus, we chose to compare T2 to T4 in the next section.
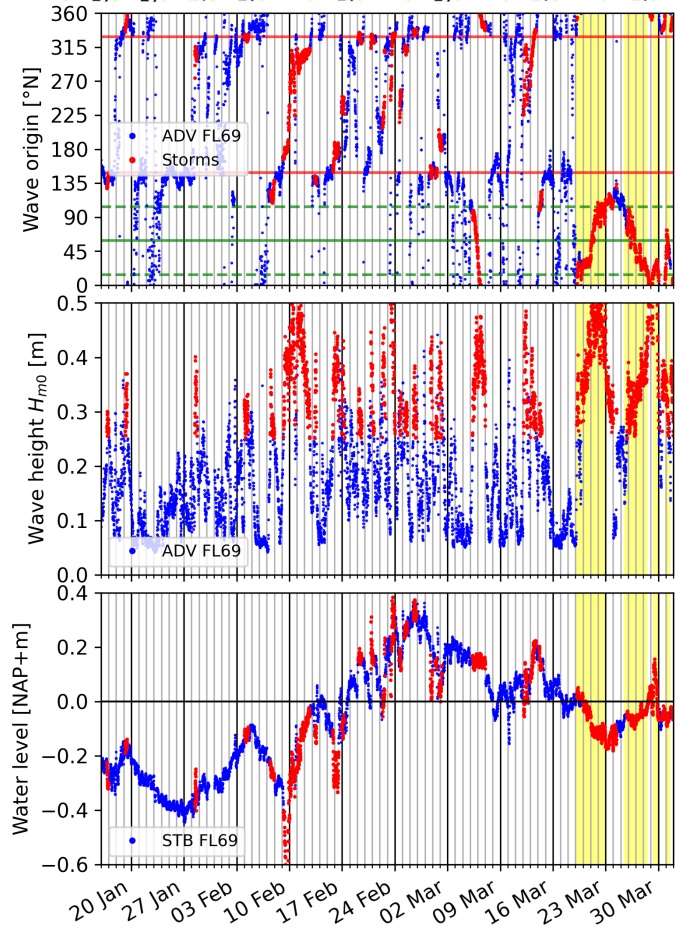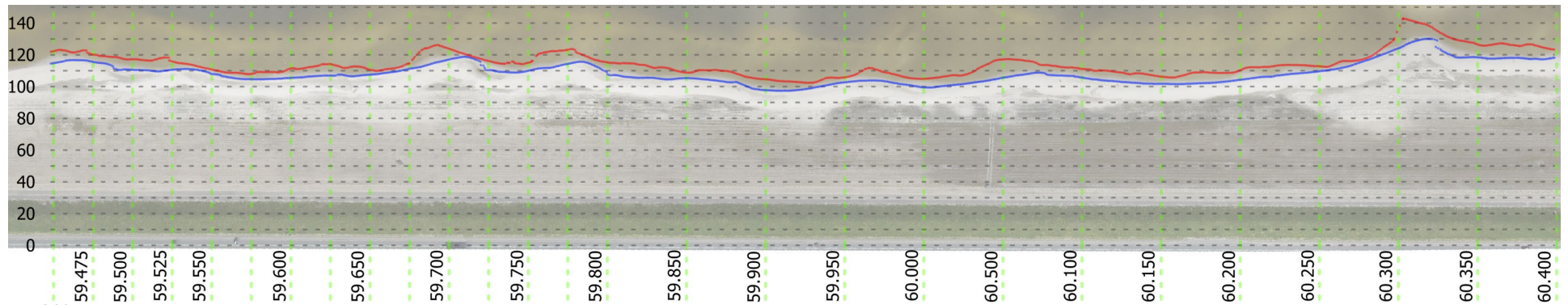
Stormy conditions

Calm conditions

H_{m0} [m]

[0.0 : 0.1)
[0.1 : 0.2)
[0.2 : 0.3)
[0.3 : 0.4)
[0.4 : 0.5)
[0.5 : inf)
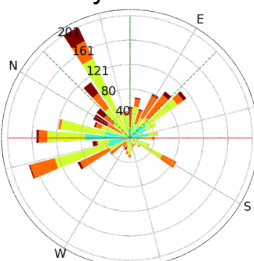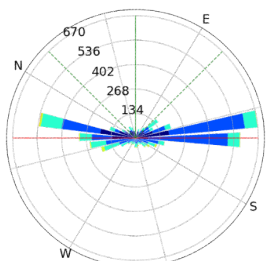
Variation of beach cusp quantities at FL69 over time
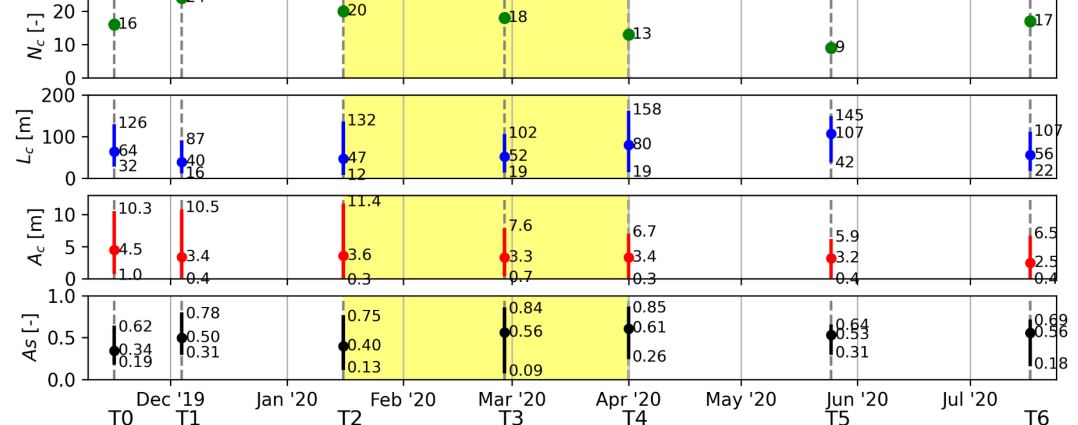
Decrease of N_c and A_c, increase of L_c and As; fully corresponds with long-term exposure to low-angle waves from the North. Water levels fluctuated a lot over the course of this period, which could have helped in decreasing the amplitude. However, it may still be doubtfull whether the waterline are comparable, due to the large difference in reference elevation.
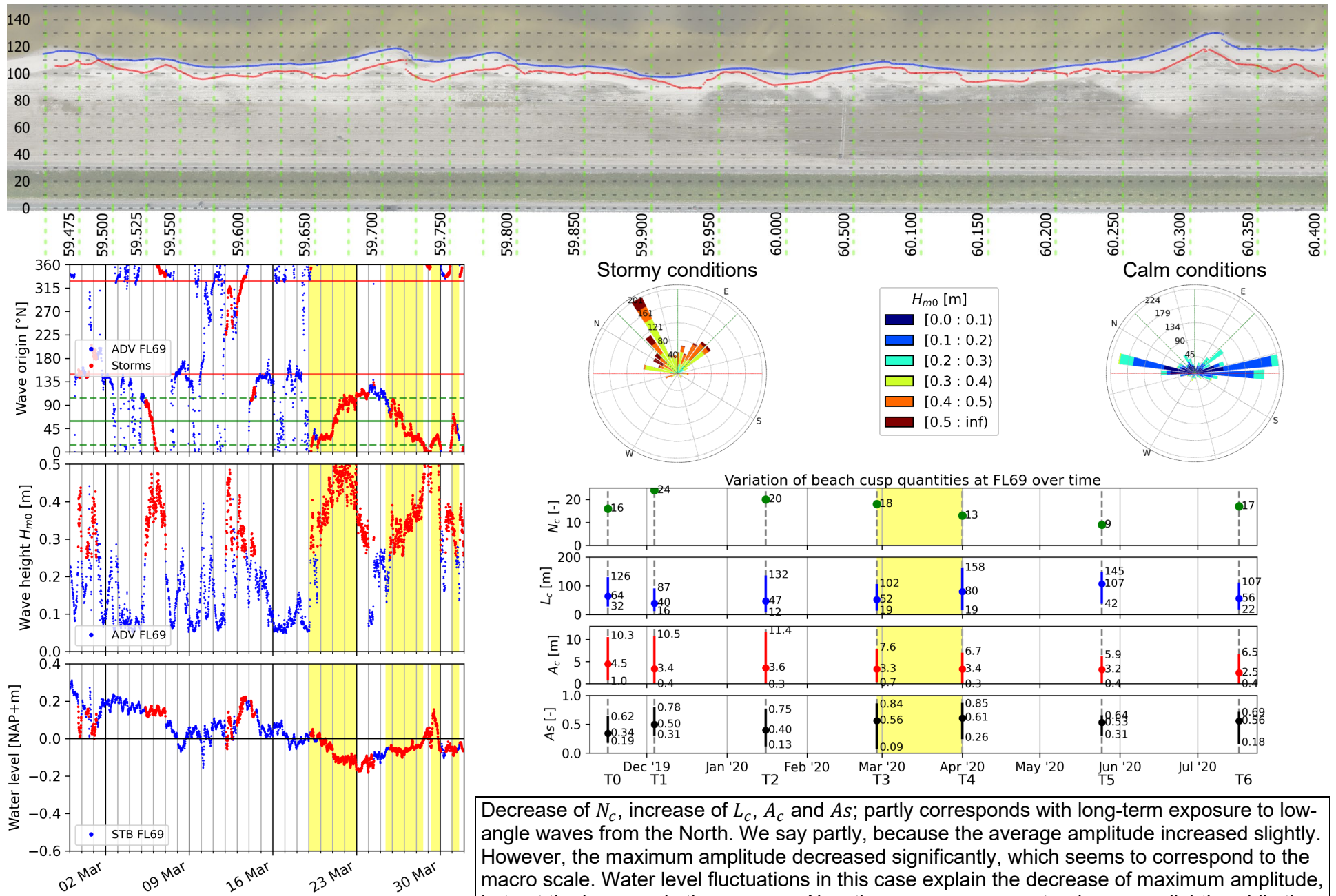
Decrease of N_c, increase of L_c, A_c and As; partly corresponds with long-term exposure to low-angle waves from the North. We say partly, because the average amplitude increased slightly. However, the maximum amplitude decreased significantly, which seems to correspond to the macro scale. Water level fluctuations in this case explain the decrease of maximum amplitude, but not the increase in the average. Also, the average asymmetry decrease slightly, while the minimum and maximum both increased.
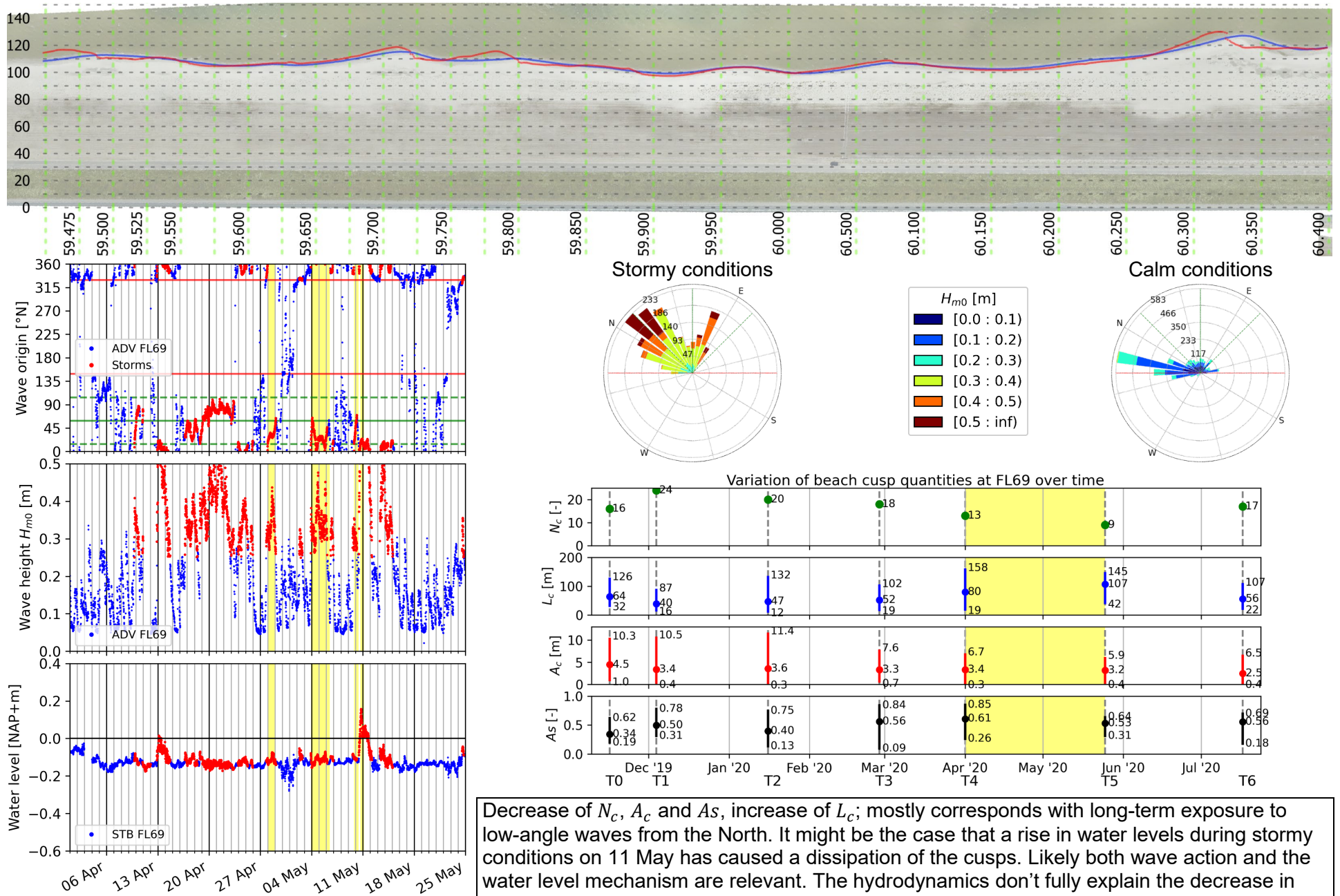
Decrease of N_c, A_c and As, increase of L_c; mostly corresponds with long-term exposure to low-angle waves from the North. It might be the case that a rise in water levels during stormy conditions on 11 May has caused a dissipation of the cusps. Likely both wave action and the water level mechanism are relevant. The hydrodynamics don't fully explain the decrease in asymmetry here, but asymmetry probably also decreases as cusps fully dampen out, which is substantiated by the decrease in range of asymmetries.
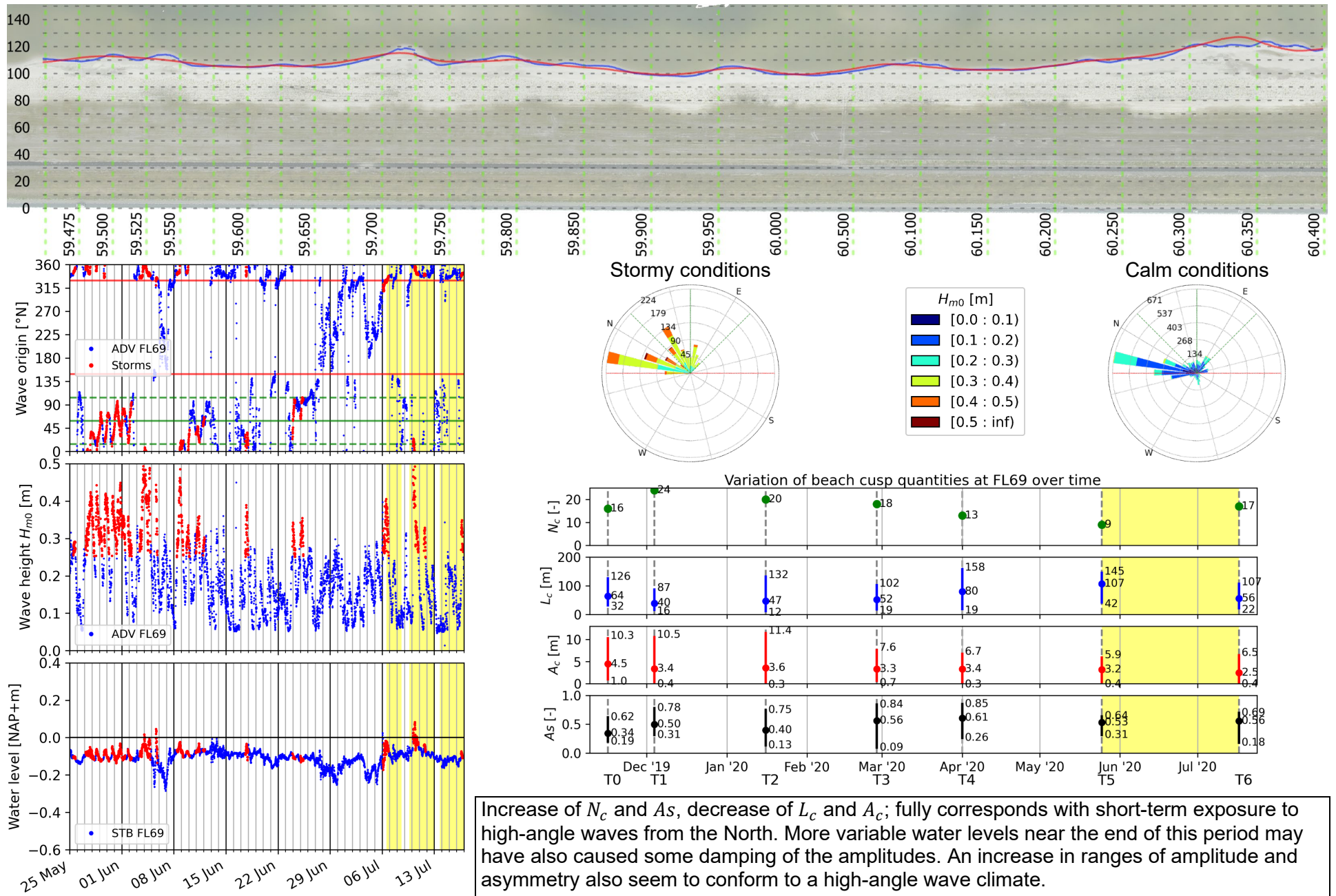
Increase of N_c and As, decrease of L_c and A_c; fully corresponds with short-term exposure to high-angle waves from the North. More variable water levels near the end of this period may have also caused some damping of the amplitudes. An increase in ranges of amplitude and asymmetry also seem to conform to a high-angle wave climate.
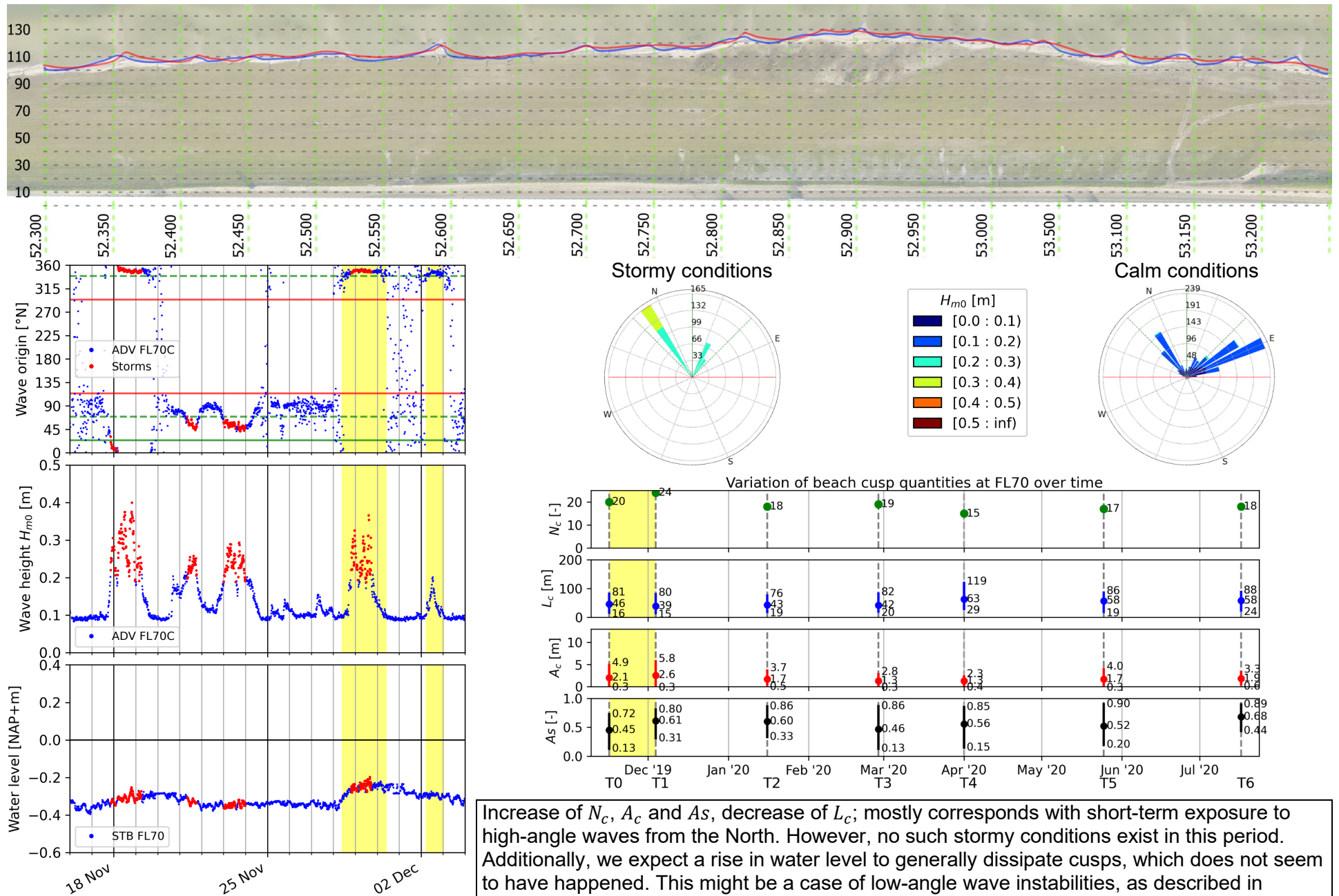
Increase of N_c, A_c and As, decrease of L_c; mostly corresponds with short-term exposure to high-angle waves from the North. However, no such stormy conditions exist in this period. Additionally, we expect a rise in water level to generally dissipate cusps, which does not seem to have happened. This might be a case of low-angle wave instabilities, as described in Section 2.2.3.
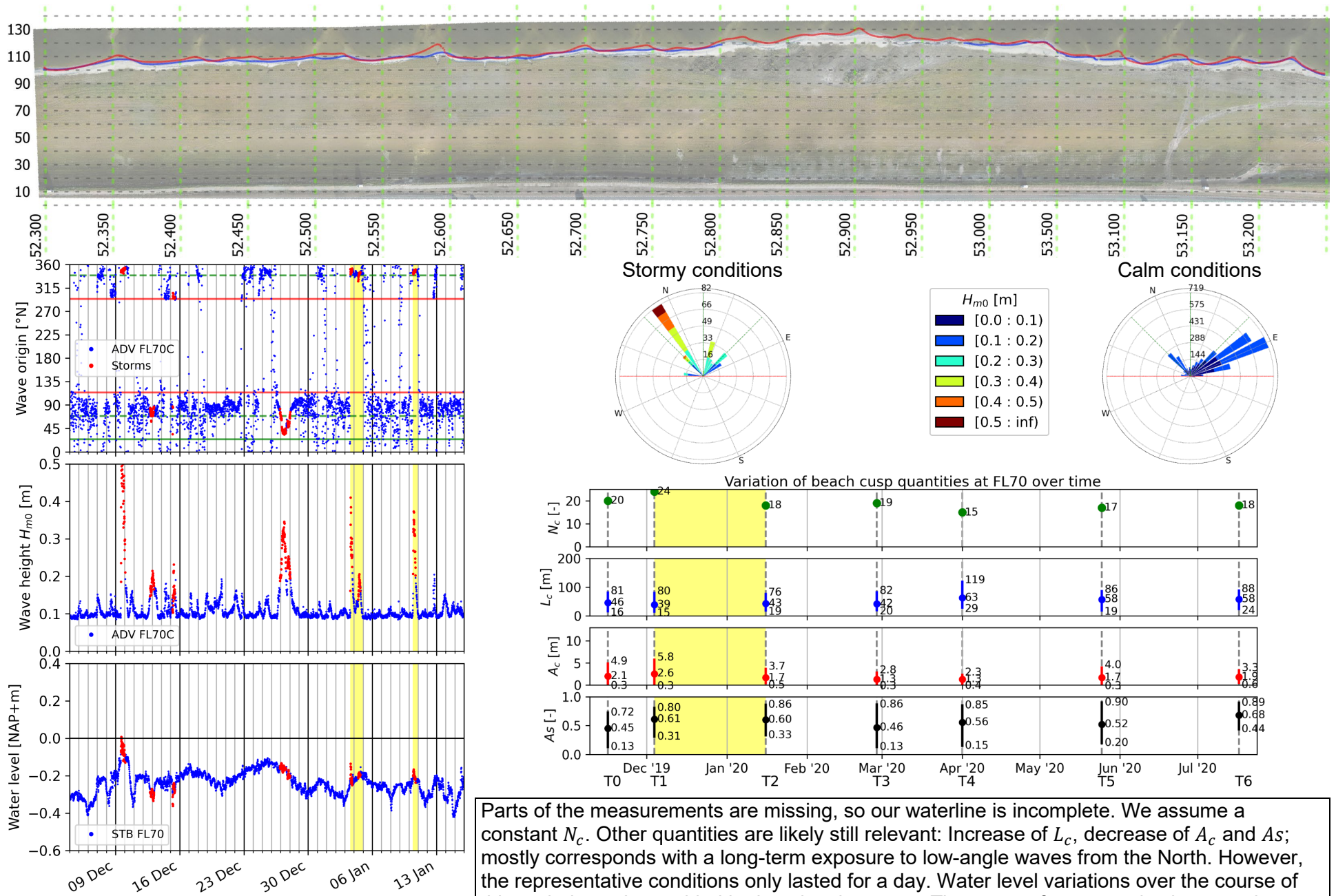
Parts of the measurements are missing, so our waterline is incomplete. We assume a constant N_c. Other quantities are likely still relevant: Increase of L_c, decrease of A_c and As; mostly corresponds with a long-term exposure to low-angle waves from the North. However, the representative conditions only lasted for a day. Water level variations over the course of this period may have aided in damping the cusps. The range of asymmetries increased, substantiating the representative conditions.

E.10   FL70: 16 January to 28 February 2020 (T2 to T3)
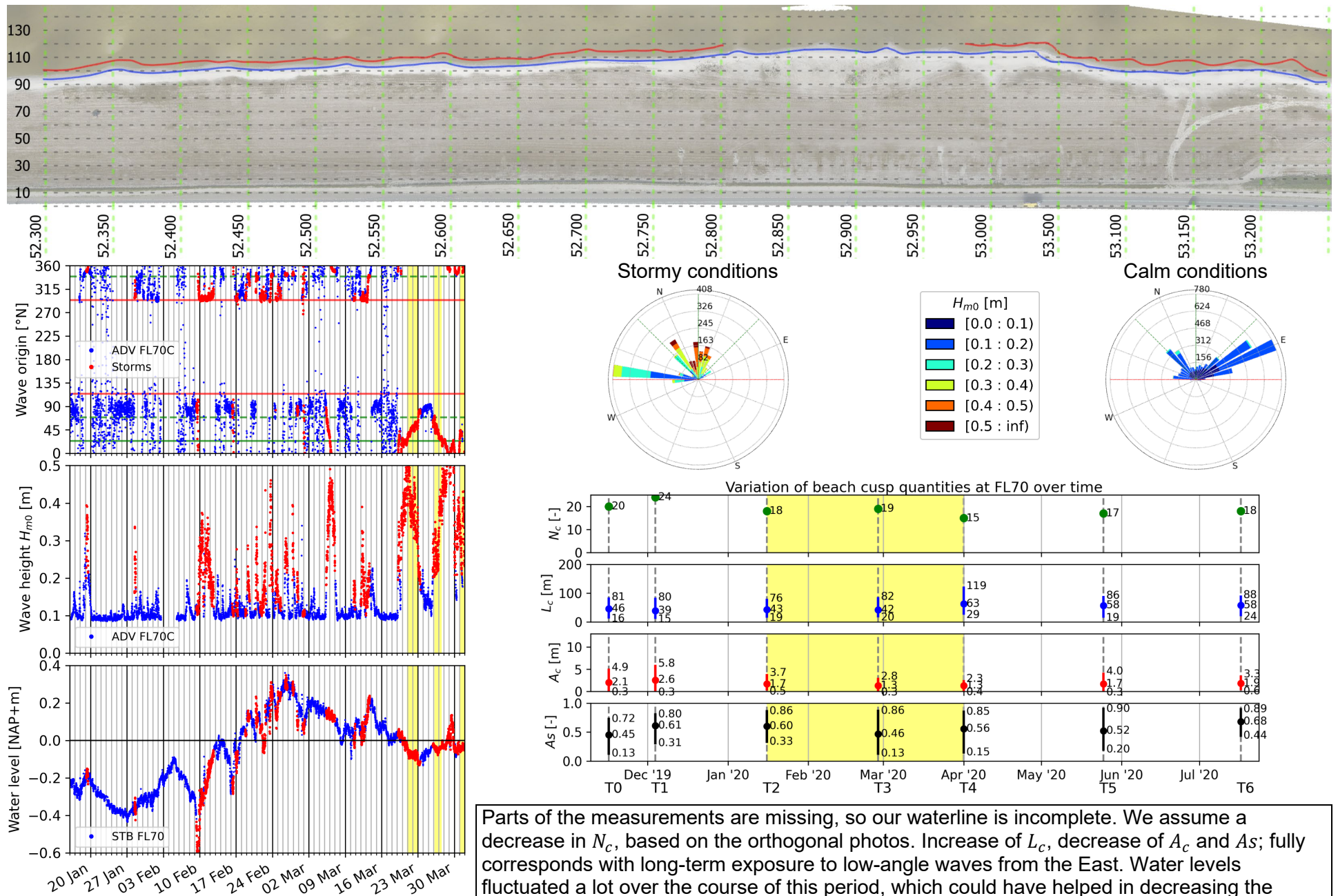
Increase of N_c, decrease of L_c, A_c and As; fully corresponds with short-term exposure to high-angle waves from the East. However, these conditions were not found in this period. It is also doubtful to compare these periods due to the fact that we're comparing very different elevations. Thus, we chose again to compare T2 to T4 in the next section.

Parts of the measurements are missing, so our waterline is incomplete. We assume a decrease in N_c, based on the orthogonal photos. Increase of L_c, decrease of A_c and As; fully corresponds with long-term exposure to low-angle waves from the East. Water levels fluctuated a lot over the course of this period, which could have helped in decreasing the amplitude. However, it may still be doubtfull whether the waterline are comparable, due to the large difference in reference elevation.

E.12 FL70: 28 February to 1 April 2020 (T3 to T4)
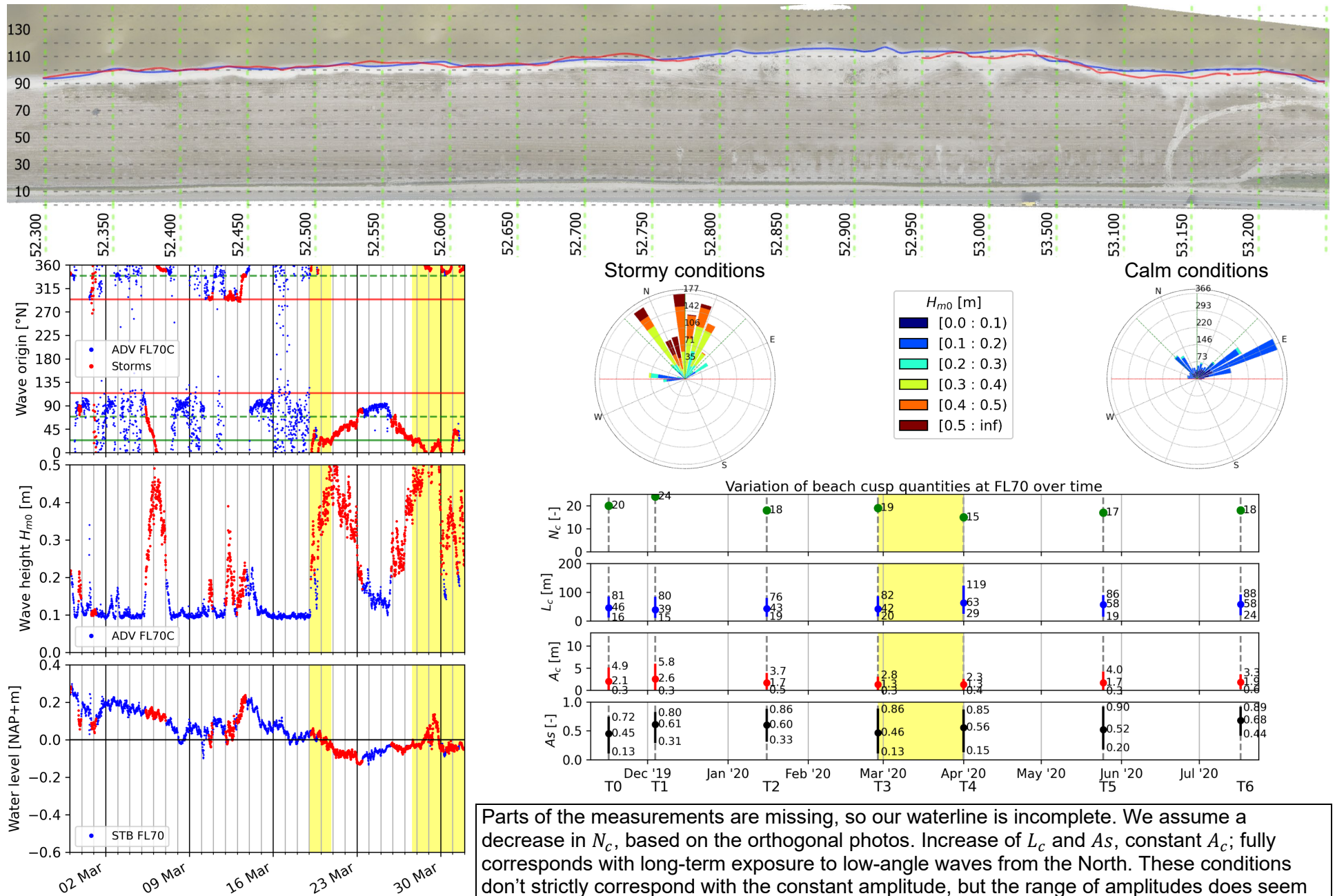
Parts of the measurements are missing, so our waterline is incomplete. We assume a decrease in N_c, based on the orthogonal photos. Increase of L_c and As, constant A_c; fully corresponds with long-term exposure to low-angle waves from the North. These conditions don't strictly correspond with the constant amplitude, but the range of amplitudes does seem to have decreased. However, this might mean that water level fluctuations had no effect on decreasing the amplitude.
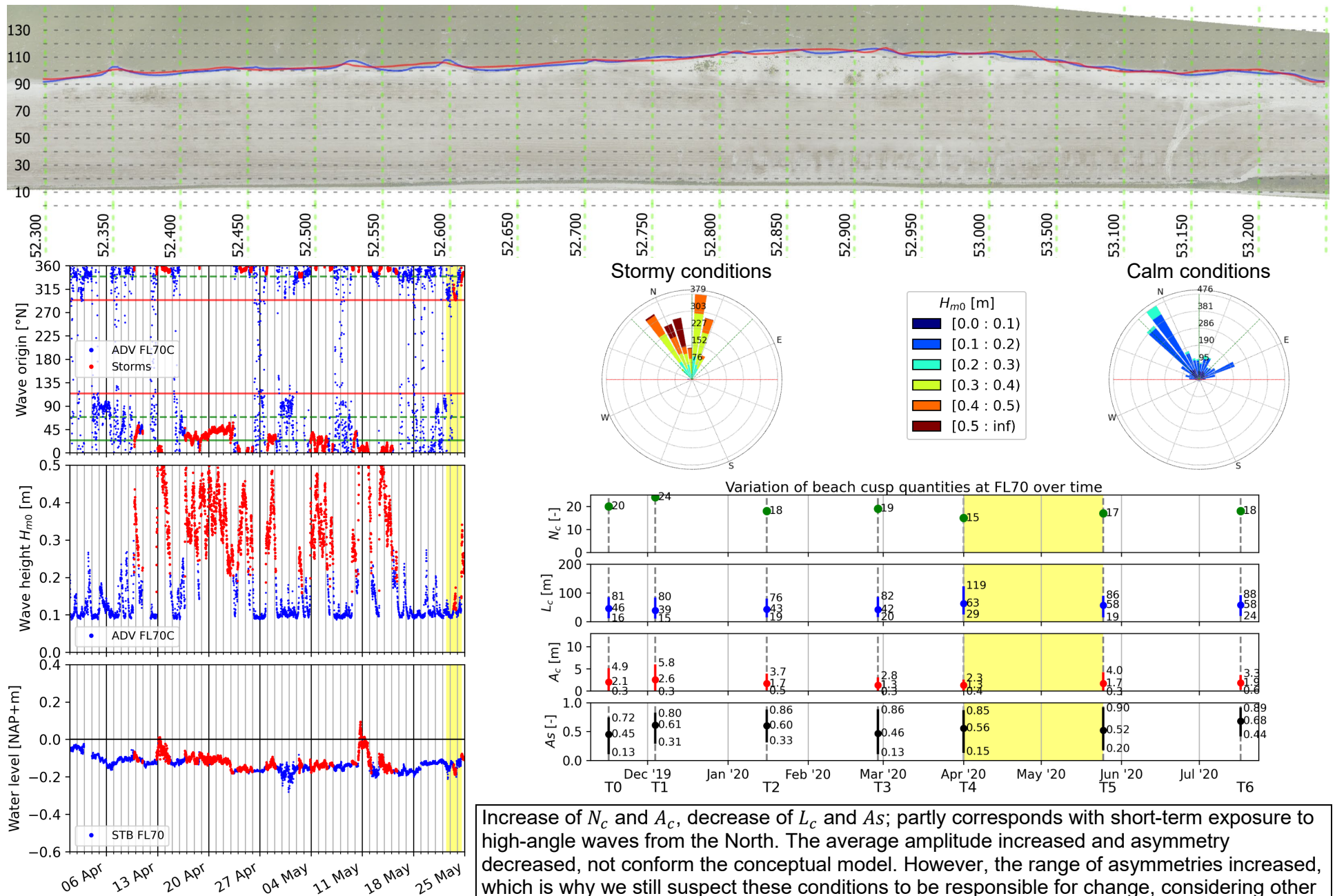
Stormy conditions

Calm conditions

Variation of beach cusp quantities at FL70 over time

Increase of N_c and A_c, decrease of L_c and As; partly corresponds with short-term exposure to high-angle waves from the North. The average amplitude increased and asymmetry decreased, not conform the conceptual model. However, the range of asymmetries increased, which is why we still suspect these conditions to be responsible for change, considering other conditions in this period are even less relevant. The increase in amplitude may be caused by a transition from short- to long-term exposure to the hydrodynamics.
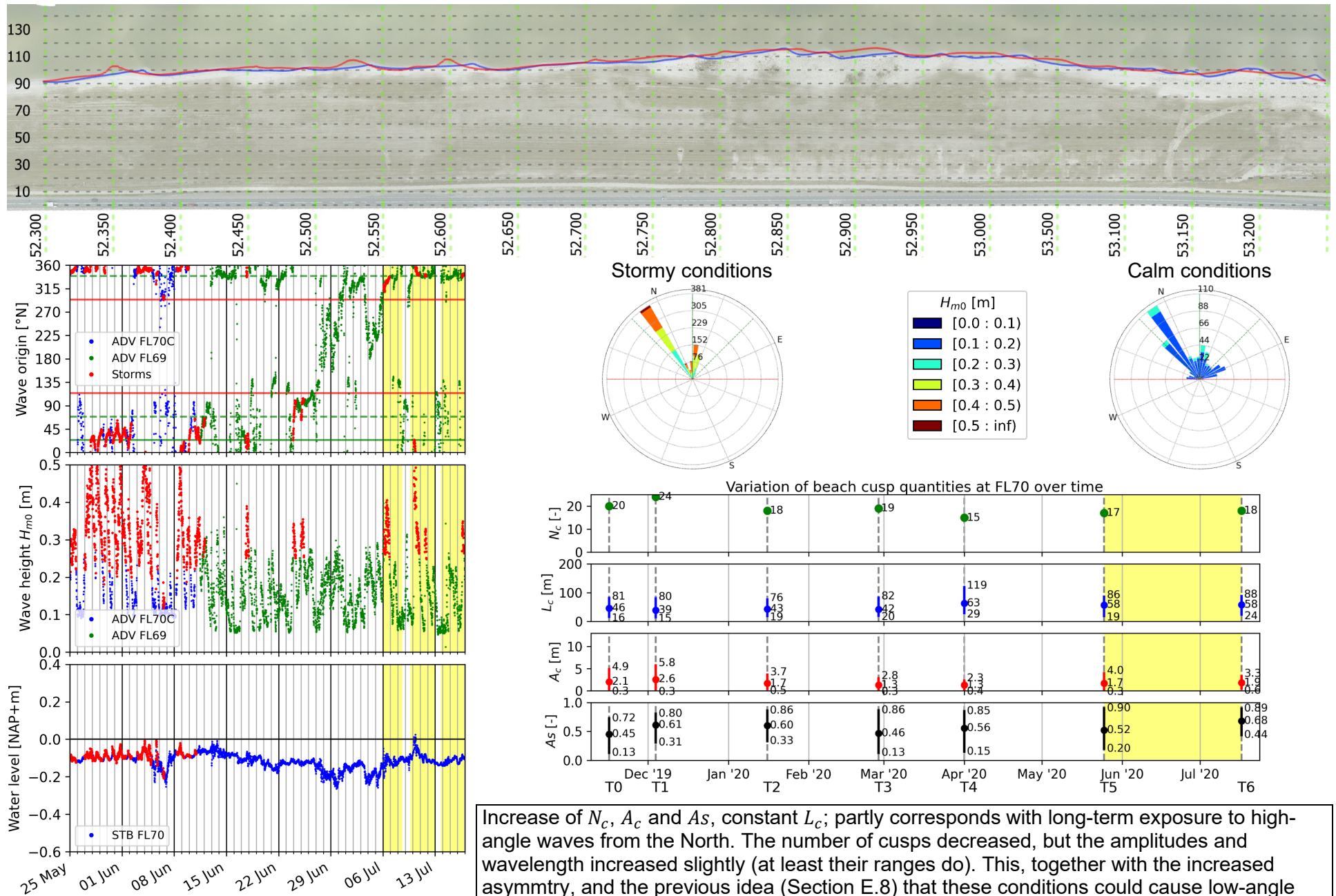
Stormy conditions

Calm conditions

H_{m0} [m]
- [0.0 : 0.1)
- [0.1 : 0.2)
- [0.2 : 0.3)
- [0.3 : 0.4)
- [0.4 : 0.5)
- [0.5 : inf)

Variation of beach cusp quantities at FL70 over time

Increase of N_c, A_c and As, constant L_c; partly corresponds with long-term exposure to high-angle waves from the North. The number of cusps decreased, but the amplitudes and wavelength increased slightly (at least their ranges do). This, together with the increased asymmtry, and the previous idea (Section E.8) that these conditions could cause low-angle wave instabilities, has led us to the indicated representative hydrodynamics. However, using ADV data of location FL69 might be less representative for the actual conditions at FL70C.

Appendix F: Persistent cusps at location FL69

Some of the cusps that have persisted at location FL69 for an extended period of time are more closely analyzed below. Quantities used to describe them are the longshore position (x_c), amplitude (A_c) and shape asymmetry (As). Different colors indicate the date of measurement of the cusp. The longshore position is defined by the position of the horn, which is indicated by a dashed line of the corresponding color. As described in the methodology (Section 3.3.2), cusps are rotated such that they all appear horizontal. The y-axis indicates the approximate cross-shore distances to the leftmost bay locations.

Cusps for each of the measurement periods are compared in a pairwise fashion (e.g. T0 with T1, T1 with T2, etc.). For each of these compared periods, we list the micro scale case (Section 2.4, also briefly described below) corresponding to the representative hydrodynamics (Section 5.5.1 and Appendix E). How this case conforms to the measured morphological change is indicated for all quantities in the next columns. A 'v' (green) indicates that the hydrodynamics led to the expected change in quantity, a '?' (yellow) that it is unsure, and a 'x' (red) that it did not. The final column indicates our overall judgement of how well the cusps conform to the conceptual model. If all quantities conform, we assign a 'v'. If one or two quantities do not conform, we assign a '?'. When none of them conform, we assign a 'x'. This overall column is the one included in the conclusion of Chapter 5.

Micro cases B, C, D and E are observed. Cases B and C correspond to a high-angle wave climate with a preference for wave coming from an indicated direction, where C is the case with a fully unidirectional wave climate. Case D concerns a low-angle wave climate with no clear preference for wave direction. Case E is a low-angle wave climate with a preference for the indicated direction.

F.1 Cusps at transect 59.700
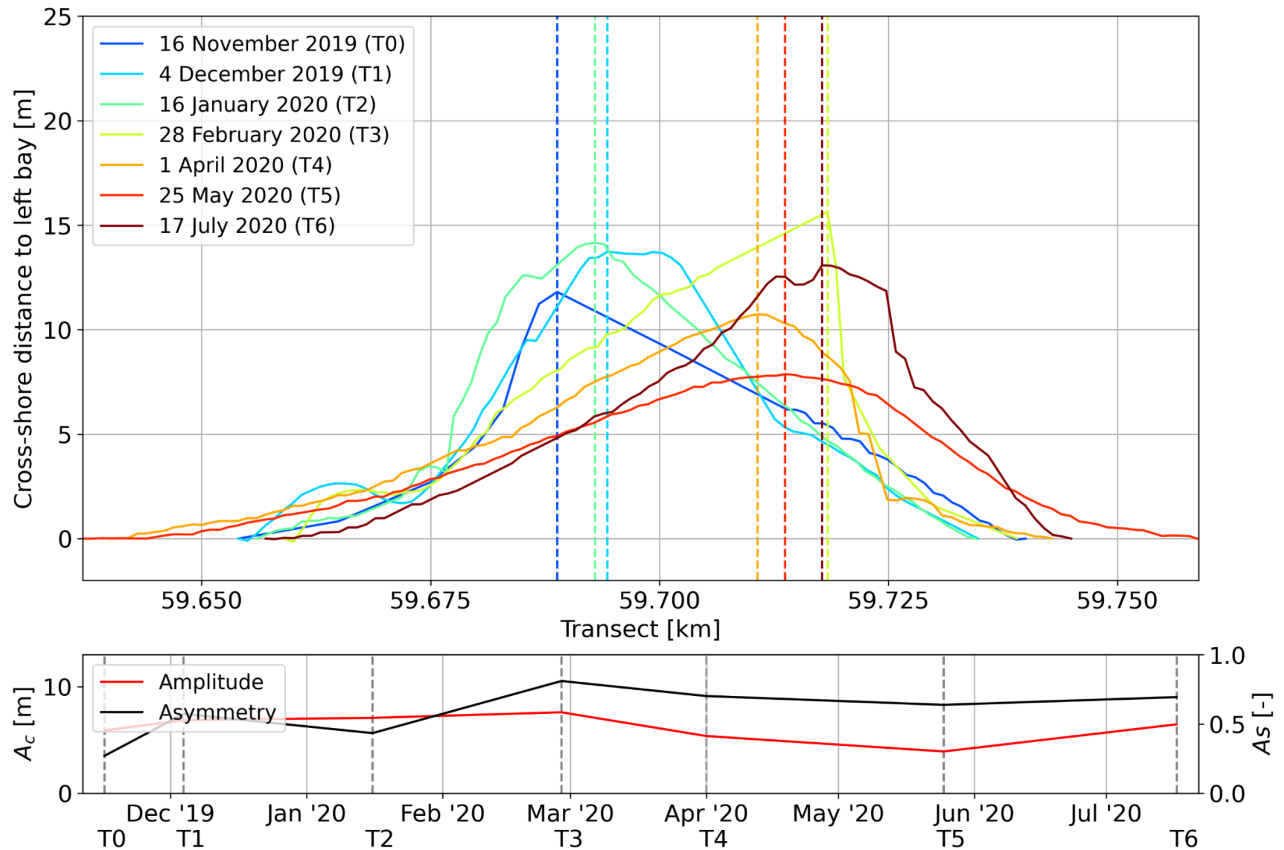
Period	Micro scale case	x_c	A_c	As	Overall
T0 to T1	B/C from the left	v	v	v	v
T1 to T2	E from the right	v	x	v	?
T2 to T3	E from the left	v	x	v	?
T2 to T4	E from the left	v	v	v	v
T3 to T4	E from the left	x	v	x	?
T4 to T5	E from the left	v	v	x	?
T5 to T6	B/C from the left	v	v	v	v

F.2   Cusps at transect 59.775
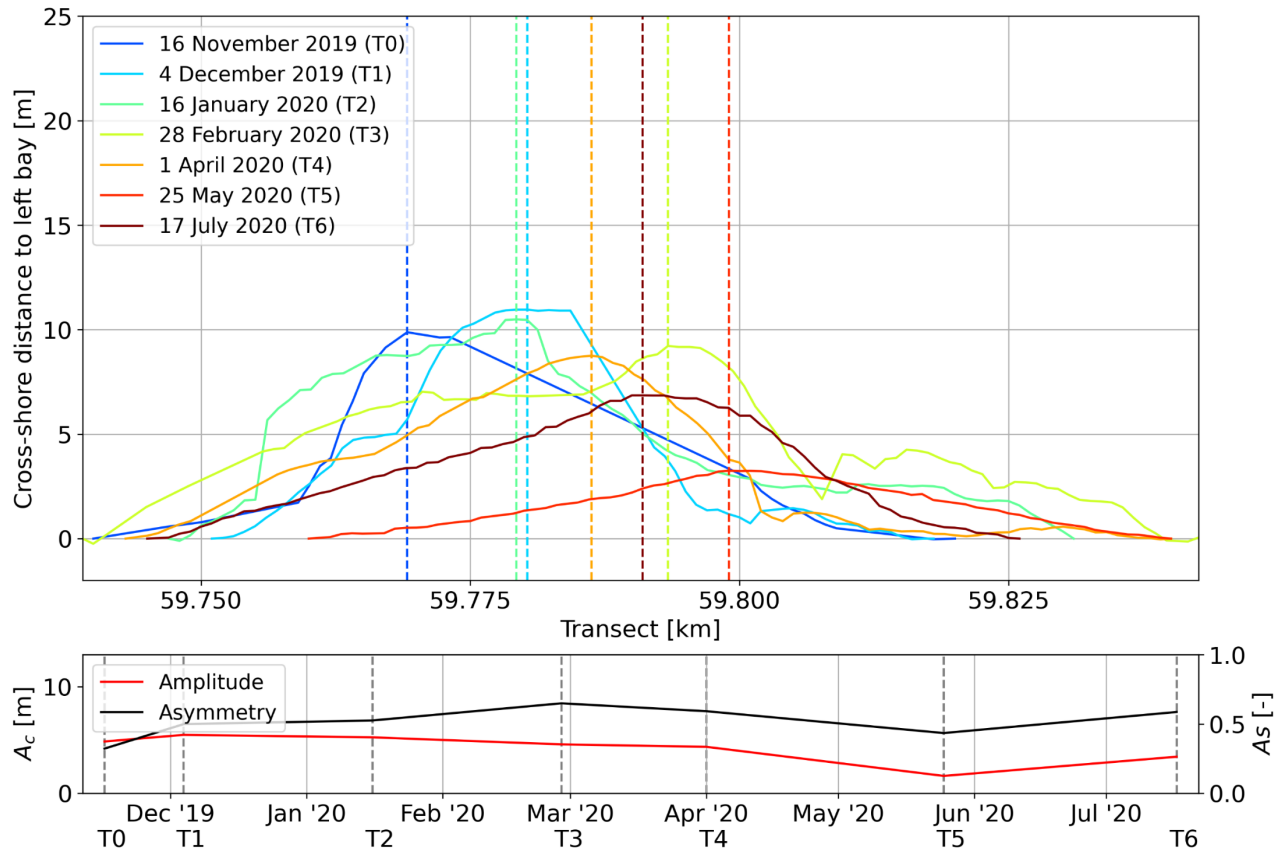
Period	Micro scale case	x_c	A_c	As	Overall
T0 to T1	B/C from the left	v	v	v	v
T1 to T2	E from the right	v	v	x	?
T2 to T3	E from the left	v	v	v	v
T2 to T4	E from the left	v	v	v	v
T3 to T4	E from the left	x	v	v	?
T4 to T5	E from the left	v	v	x	?
T5 to T6	B/C from the left	x	v	v	?

F.3 Cusps at transect 60.050
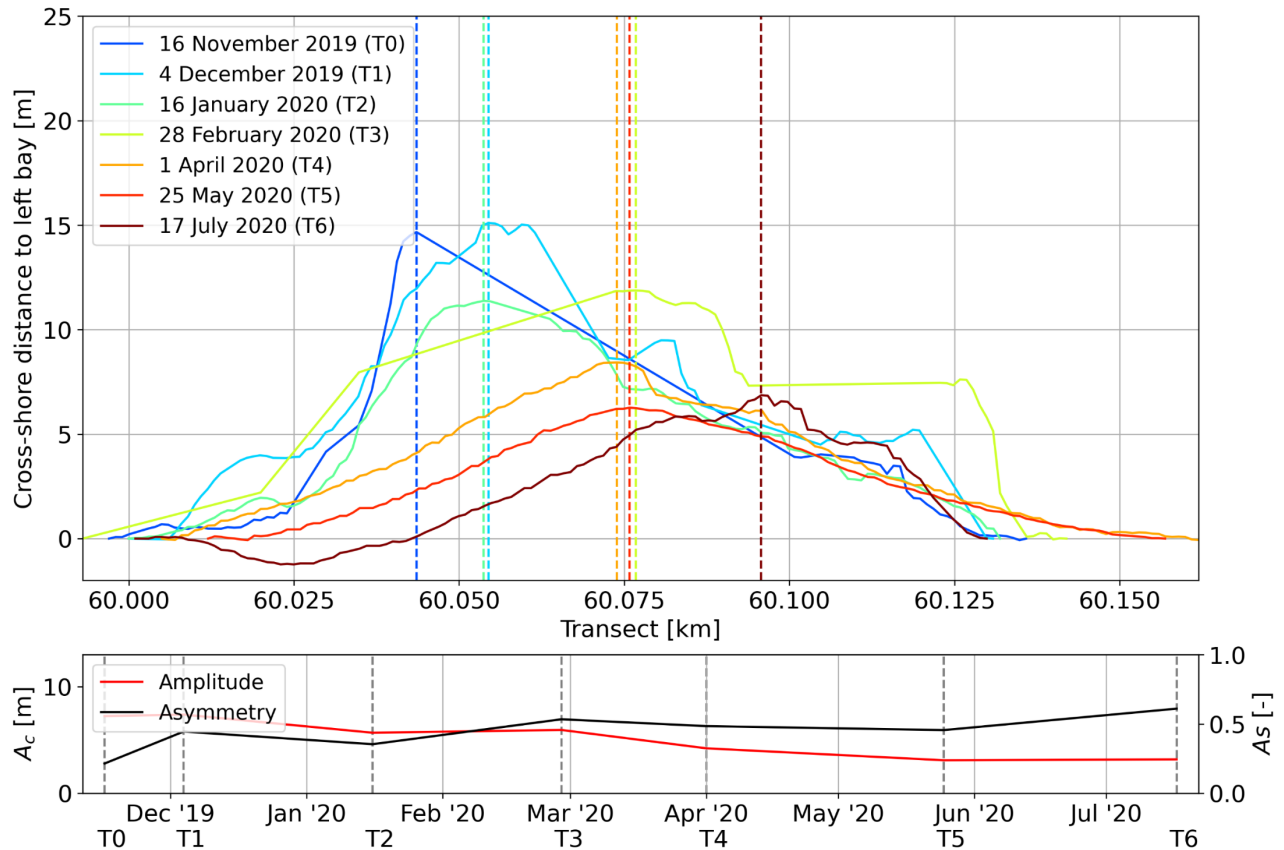
Period	Micro scale case	x_c	A_c	As	Overall
T0 to T1	B/C from the left	v	v	v	v
T1 to T2	E from the right	v	v	v	v
T2 to T3	E from the left	v	x	v	?
T2 to T4	E from the left	v	v	v	v
T3 to T4	E from the left	x	v	x	?
T4 to T5	E from the left	v	v	x	?
T5 to T6	B/C from the left	v	v	v	v

F.4 Cusps at transect 60.300
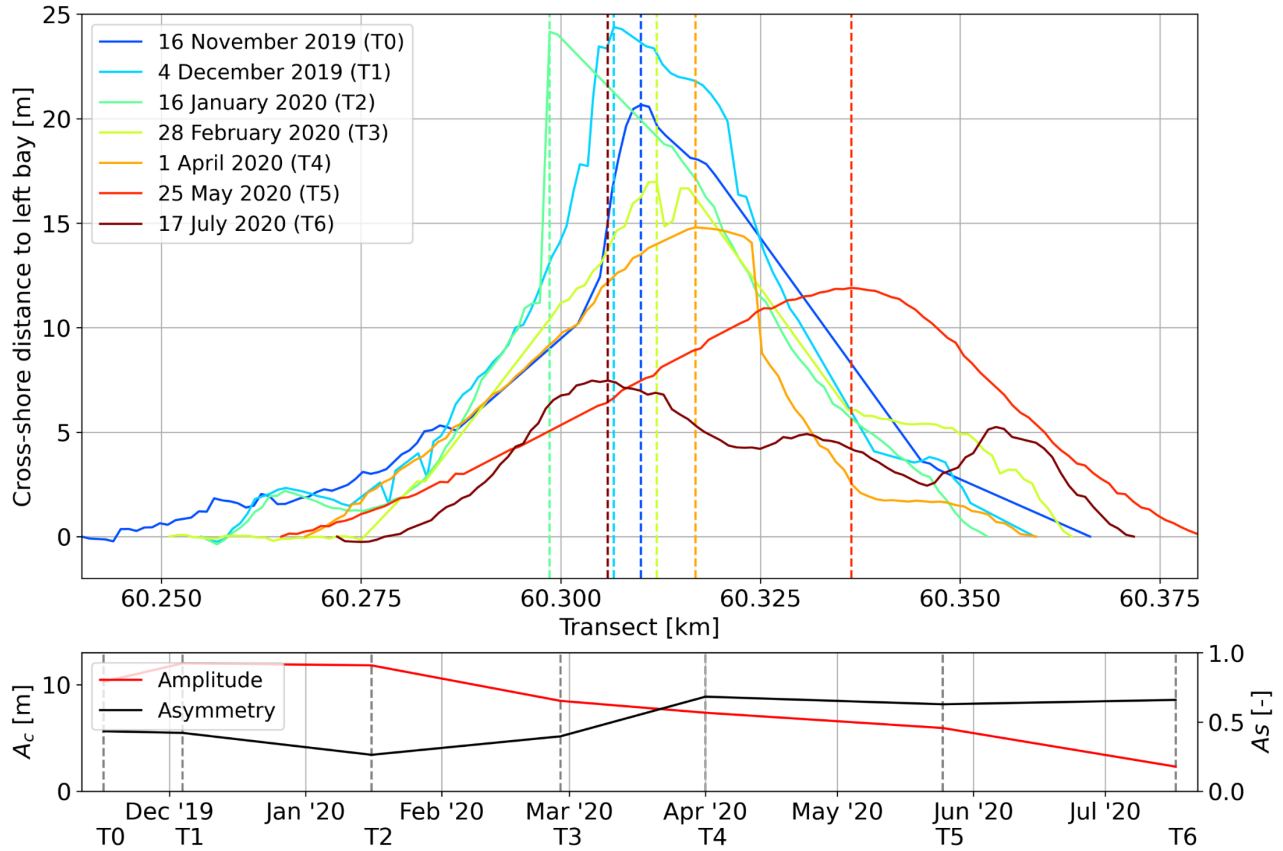
Period	Micro scale case	x_c	A_c	As	Overall
T0 to T1	B/C from the left	x	v	x	?
T1 to T2	E from the right	v	x	v	?
T2 to T3	E from the left	v	v	v	v
T2 to T4	E from the left	v	v	v	v
T3 to T4	E from the left	v	v	v	v
T4 to T5	E from the left	v	v	x	?
T5 to T6	B/C from the left	x	x	v	?

Appendix G: ShorelineS model exploration

Before we started using this new model, we explored its functionalities and capabilities. This was mostly done to see what settings could be used to best reproduce the physical process of high-angle waves instabilities, specifically for our environment at the Houtribdijk. Section G.1 shows the results of the verification of the micro scale conceptual model (Section 2.4). In Section G.2 we elaborate on some testing with the different transport formulations implemented in ShorelineS. Sections G.3 and G.4 concern some simulations showing the effects of waves on random waterlines. The former discusses the principle of self-organization, the latter shows the effect of a Northern storm on each of these random waterlines. In Section G.5 various ways to implement a representative profile were explored. Lastly, in Section G.6 we briefly illustrate the effect of changing the breaking wave parameter (γ) on modeling results. Several properties and assumptions of the model that are relevant to our research are described below (Roelvink et al., 2020):

- The model applies a simplified sediment conservation equation as governing equation:
$$\frac{\partial n}{\partial t} = -\frac{1}{D_c}\frac{\partial Q_s}{\partial s}$$
  Where:
  - n [m]: Cross-shore coordinate, perpendicular to the coastline.
  - s [m]: Longshore coordinate.
  - t [y]: Time.
  - D_c [m]: Active profile height.
  - Q_s [m³/y]: Longshore transport of sediment.

- Several well-known formulations for the longshore transport are included. Two of which being the simplified and original CERC formulas as used by the USACE (United States Army Corps of Engineers, 1984). Another being an adaptation of the original CERC formula by Ashton & Murray (2006a). These all contain some form of expression for the wave height (wave energy) and the wave angle of incidence (relative to the shore-normal), where some of them include a (peak) wave period. The last expression is the one by Kamphuis (1991), which in addition to the previous, includes grain size diameter and average profile slope.

Table G-1: Overview of ShorelineS transport formulations (adapted from Roelvink et al., 2020).

Author	Notation	Formula
USACE (1984) (simplified)	CERC1	$Q_s = bH_{s0}^{5/2}\sin(2\phi_{loc})$
Ashton & Murray (2006a)	CERC2	$Q_s = K_2 H_{s0}^{12/5}T^{1/5}\cos^{6/5}(\phi_{loc})\sin(\phi_{loc})$
USACE (1984)	CERC3	$Q_s = bH_{sb}^{5/2}\sin(2\phi_{locb})$
Kamphuis (1991)	KAMP	$Q_s = 2.33H_{sb}^2 T^{1.5}m_b^{0.75}D_{50}^{-0.25}\sin^{0.6}(2\phi_{locb})$

  Where:
  - b, K_2 and m_b: Calibration coefficients.
  - H_{s0} and H_{sb} [m]: Offshore and breaking wave heights, respectively.
  - ϕ_{loc} and ϕ_{locb} [°]: Local offshore and breaking wave angle, respectively.
  - T [s]: Peak wave period.
  - D_{50} [m]: Median grain diameter.

- In the paper, the assumption was made that sufficient time had passed for the profile to be in equilibrium, which means the distance from the top and bottom of the active profile to MSL is equal. ShorelineS models the line around MSL, which is therefore roughly located at this equidistant elevation, the middle of the active profile. This is different from earlier models, which usually take the top of the active profile. The method that is applied in ShorelineS allows one to neglect complex curvature corrections to the sediment balance, leading to a faster computation. Appendix A of the Supplementary Images (Roelvink et al., 2020) explains the mathematical derivation, showing that this is indeed the case whenever we model the middle of the active profile.

- In practice, they use the above derivation to argue that neglecting the complex curvature correction yields similar results as when it is included. Namely, it shows that for cases where there is equilibrium, the sediment balance above conserves dry area and sediment volume. They concluded that this correction term can thus be neglected, considering other model uncertainties. Therefore, a linear profile should suffice in most cases. However, for the case of the Houtribdijk, this is likely less valid. We have briefly investigated several options for a different profile in Section G.3.

- Refraction, required by some of the transport formulations, is calculated through Snel's law. This implies that we assume a longshore uniform bathymetry. For the cases of more complex bathymetry, refraction may be performed through 2D refraction model, as described in the paper. This, however, requires external modeling or measurements. Also, it reduces the light-weight aspect of ShorelineS, and is therefore disabled by default. We have therefore included is only as a recommendation (Section 9.2).

G.1 Conceptual model verification

To verify our micro scale conceptual model (Section 2.4), several simulations were run with ShorelineS. The results of them are presented for each of the cases mentioned (A through E), in Figure G-1 up to and including Figure G-5. The solid blue line indicates the initial perturbations, having a length of 40 m and an amplitude of 5 m. The wave height for all cases was 0.5 m. We made use of the simple CERC formula (Table G-1) to illustrate the principle of high-angle wave instabilities.

The figures show that most cases correspond relatively well to our expectations. The micro scale conceptual model predicts amplitudes to be smaller, and we assumed the bays to retain their position, which was different from the ShorelineS results. However, the CERC formula applied is not meant to be used quantitatively, and should only be used to illustrate principles (Roelvink et al., 2020).

Qualitative changes, like a general increase in amplitude for the high-angle cases, seems to correspond to our expectations. However, judging the change in wavelength for high-angle cases seems difficult, seeing as the surrounding instabilities seem to interact with each other. For both high-angle cases B and C we see a displacement of the horn to the right, and a clear change in shape asymmetry, conforming to what we expected. The low-angle cases seem hard to assess, as for both cases the decrease in amplitude seems to dominate the bump deformation. However, in both these cases we see an increase in wavelength, as per our expectations.

Since these results correspond relatively well to our conceptual model, we have assumed that we correctly interpreted the theory on high-angle wave instabilities. In turn, this provides confidence in our theorized macro scale conceptual model, and the ability of ShorelineS to reproduce our beach cusps.
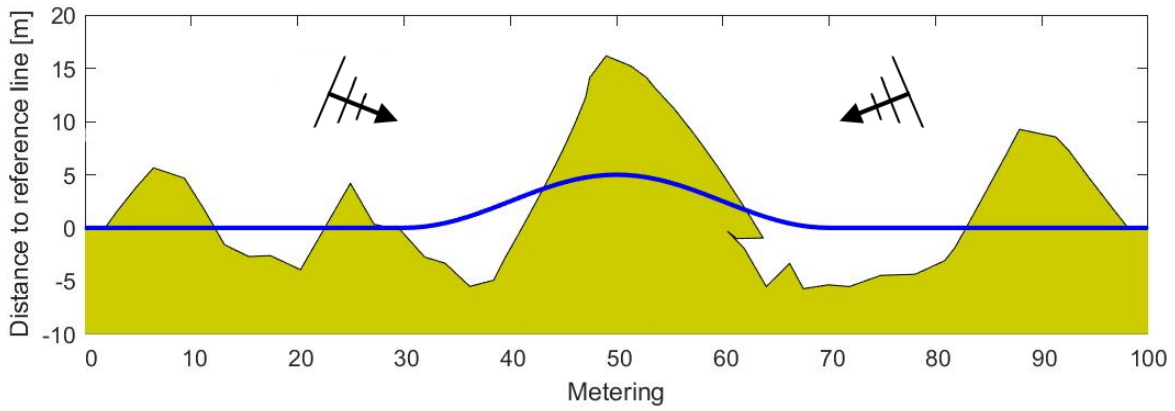
Figure G-1: Conceptual model high-angle case A ShorelineS simulation.
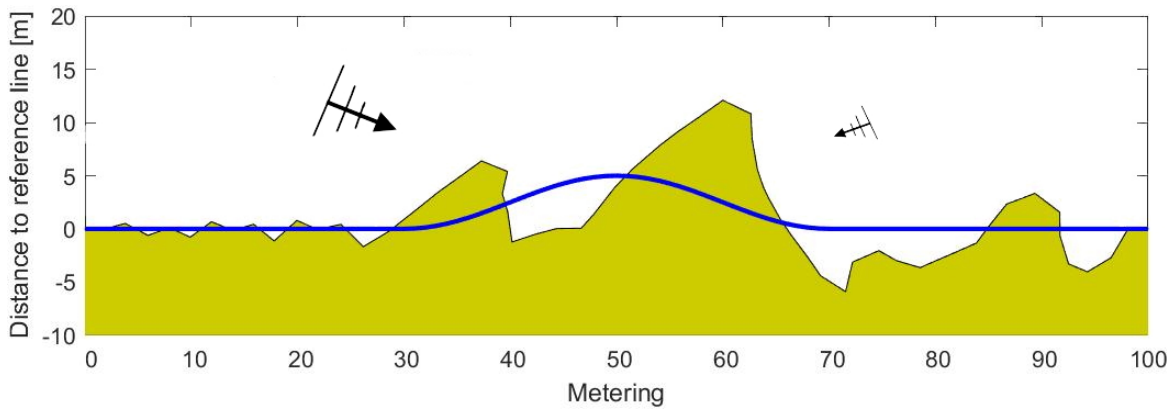
Figure G-2: Conceptual model high-angle case B ShorelineS simulation.
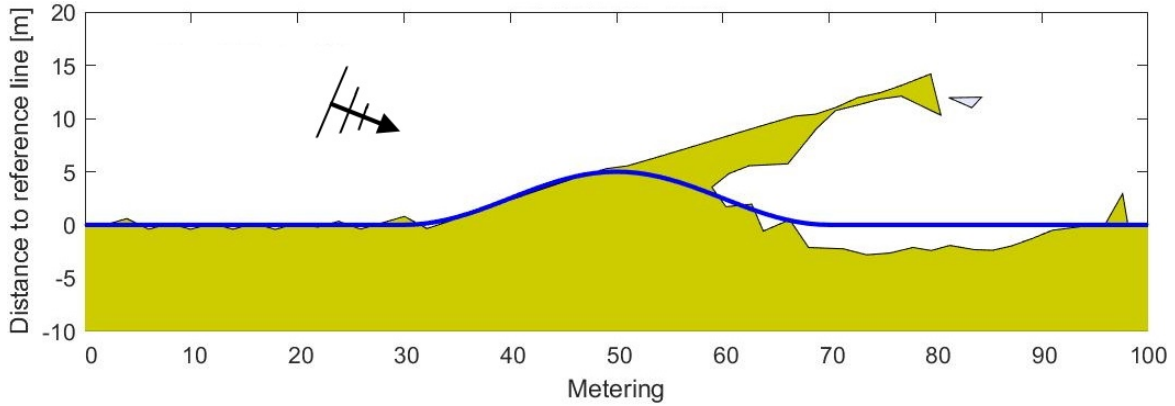
Figure G-3: Conceptual model high-angle case C ShorelineS simulation.
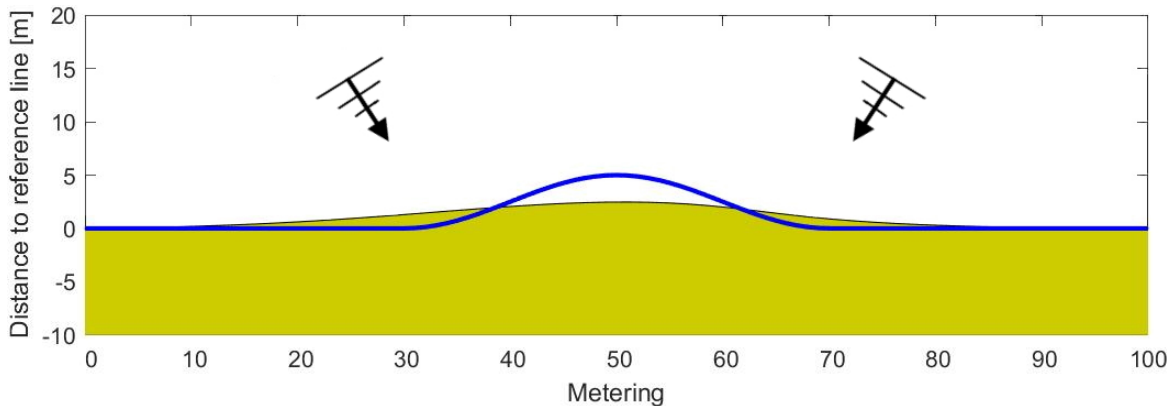
Figure G-4: Conceptual model low-angle case D ShorelineS simulation.
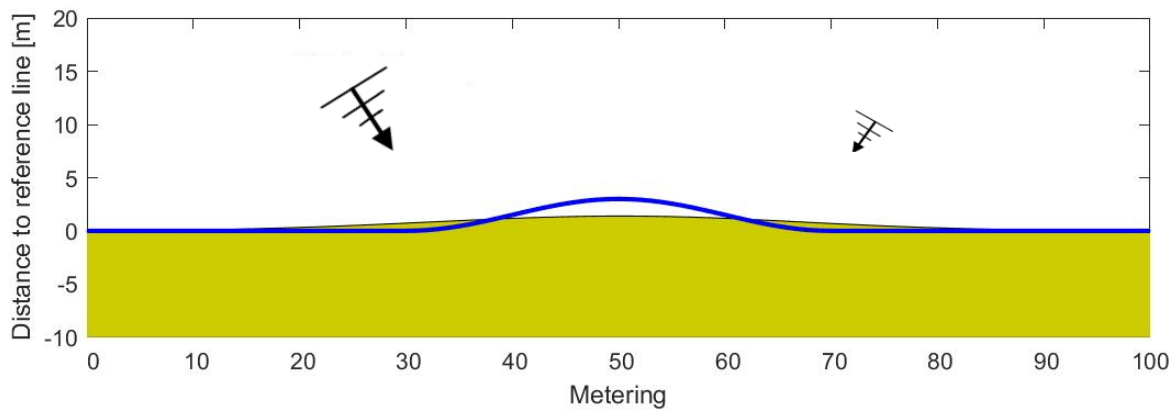
Figure G-5: Conceptual model low-angle case E ShorelineS simulation.

G.2 Transport formulations and smoothing factor

ShorelineS was extensively tested in order to find a way to calibrate the model so that it best represents the physical process of high-angle wave instabilities. A few of the most relevant simulations are presented in this section. Figure G-6 up to and including Figure G-11 show a close-up of transects 60.100 to 60.350, modeled using different transport formulations (Table G-1) and smoothing factors.

In the figures presented in this section, the blue line indicates the starting period (T0). The black line, including the yellow shading, indicate the model results. The first set of two figures shows the application of the KAMP formulation, the second set shows CERC2 and the third shows CERC3. For each set, the first was run without smoothing, the second with a smoothing factor of 0.2. This smoothing factor was defined as follows (Roelvink et al., 2020):

$$s_{i,smooth} = f s_{i-1} + (1 - 2f)s_i + f s_{i+1}$$

Where:

  o s_i [m]: Longshore coordinate at node i.
  o f [-]: Smoothing factor.

Wave conditions were the same for all simulations, with wave heights of 0.25 m, peak periods of 2.51 s, and local wave incidence angles of 82°. Runtime in all cases was one day, spatial steps approximately 2 m, deep water depth was 2.3 m, and nearshore water depth was 0.85 m. In the case of KAMP, the median grain diameter was 300 µm and the mean bed slope ($\tan \beta$) was 0.046.

What we see, is that KAMP and CERC3 simulations generally show larger transports. Besides that, the location where perturbations emerge seems to be more or less the same for all simulations. Also, the smoothing factor seems to prevent the forming of 'wiggles' (e.g. at 60.250 in Figure G-6). The differences between the KAMP and CERC3 results, with smoothing, seemed to be comparable. For this reason, we have chosen the one that contained most of the physics we expected to be relevant, the KAMP formulation. Also, we applied a smoothing factor of 0.05 to the simulations discussed in Chapter 6 (and Appendix H), to reduce wiggles.
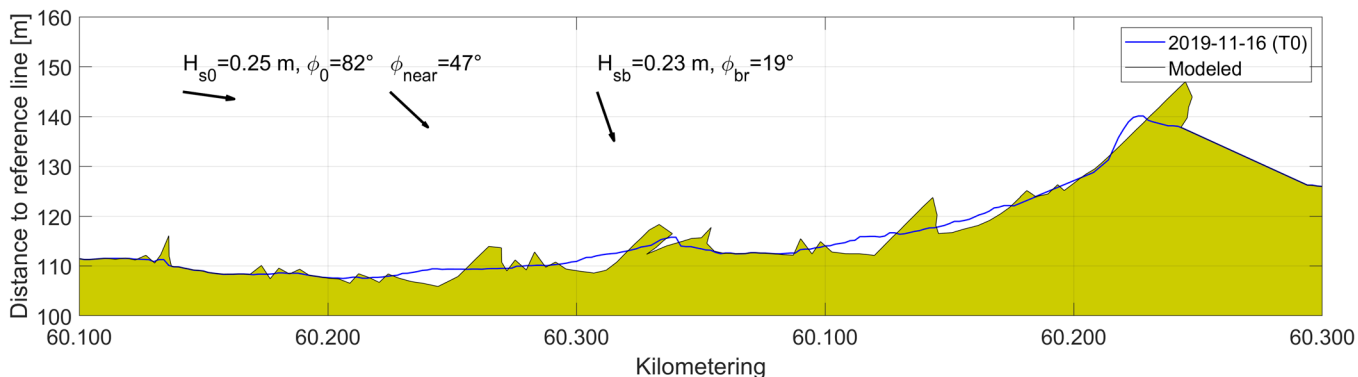
Figure G-6: ShorelineS testing of KAMP formulation at transect 60.100 to 60.350 at FL69, no smoothing.
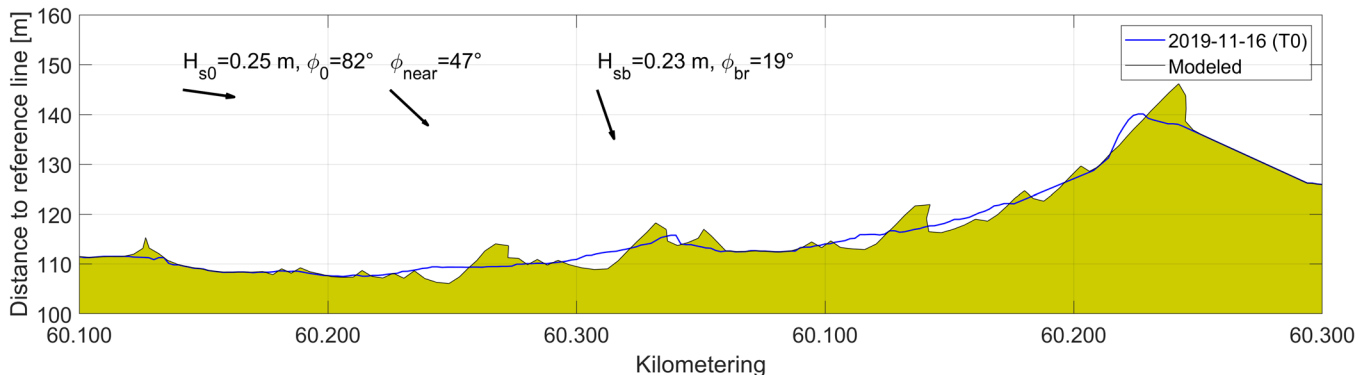
Figure G-7: ShorelineS testing of KAMP formulation at transect 60.100 to 60.350 at FL69, smoothing factor of 0.2.
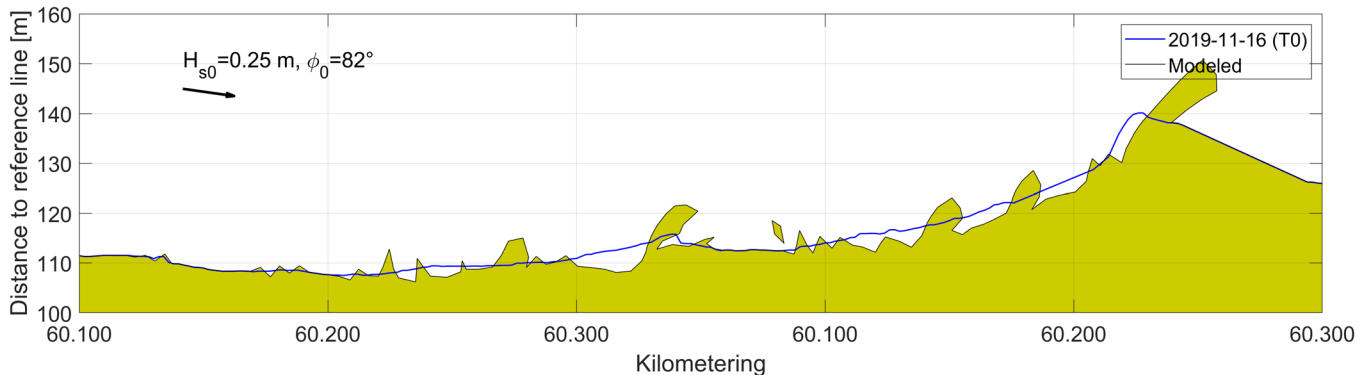
Figure G-8: ShorelineS testing of CERC2 formulation at km 60.100 to 60.350 at FL69, no smoothing.
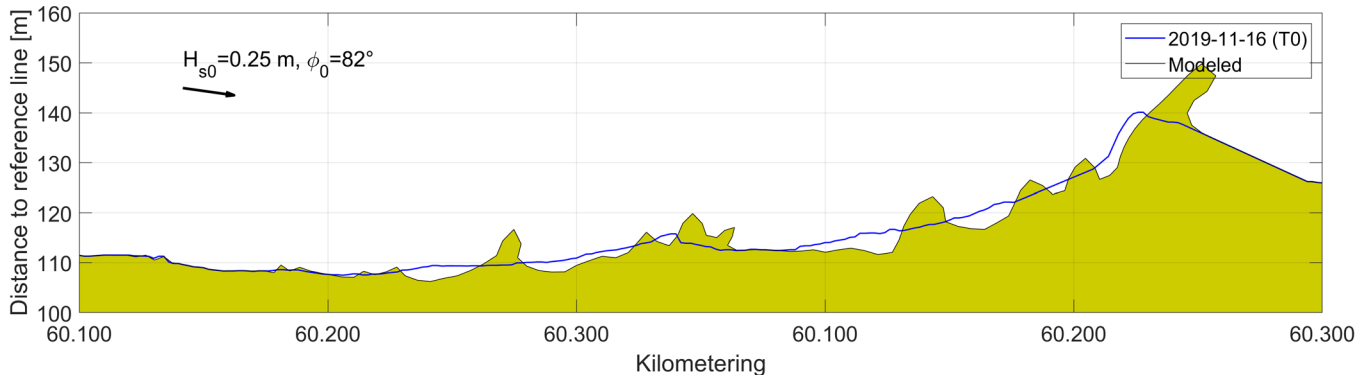
Figure G-9: ShorelineS testing of CERC2 formulation at transect 60.100 to 60.350 at FL69, smoothing factor of 0.2.
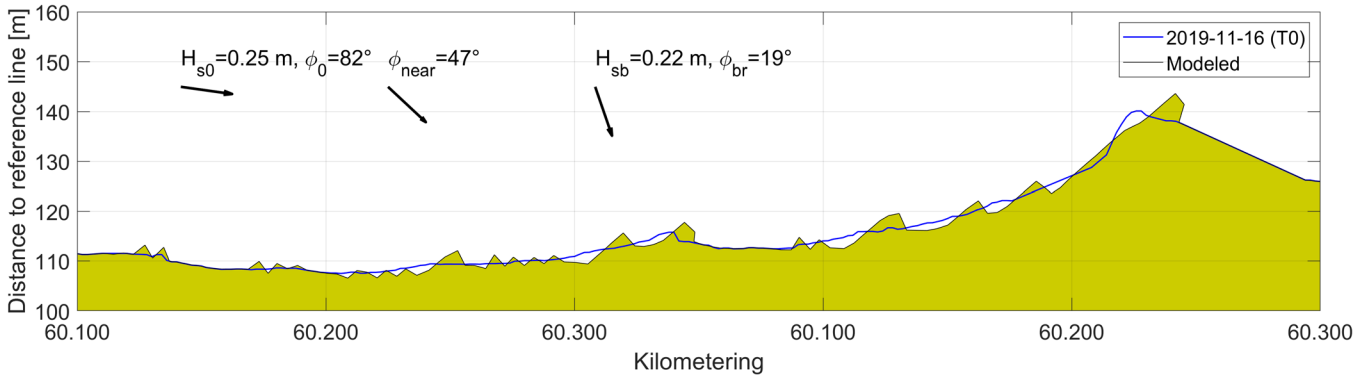
Figure G-10: ShorelineS testing of CERC3 formulation at transects 60.100 to 60.350 at FL69, no smoothing.
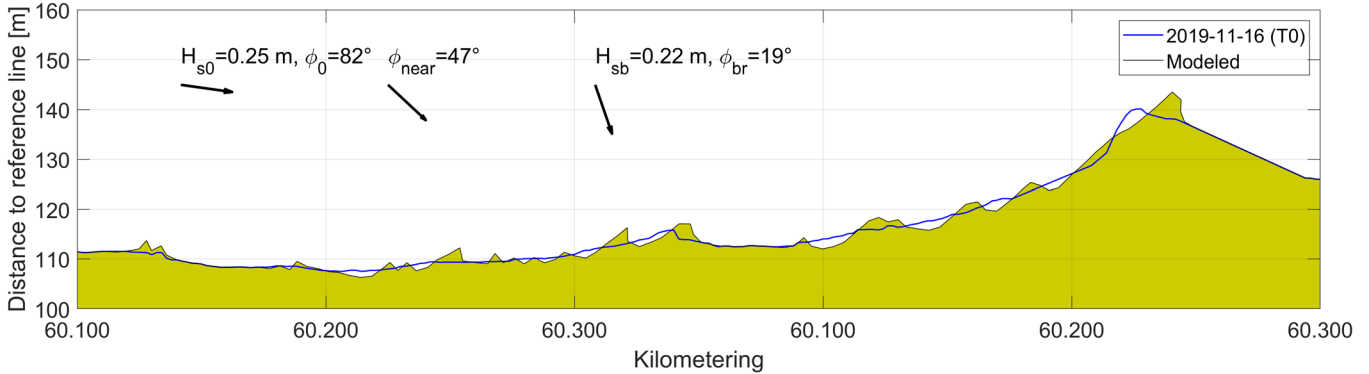
Figure G-11: ShorelineS testing of CERC3 formulation at transects 60.100 to 60.350 at FL69, smoothing factor of 0.2.

G.3   Self-organization

In Section 6.1 we described that we would prefer a numerical model that implements the self-organization principle (see Section 2.2.1). Below, we have shown that ShorelineS applies this principle well. This was done by running five simulations with a randomized initial waterline, all with the same forcing, and looking at the scales of the emerging features. Simulations were run for stormy and calm conditions (see Table G-2), with wave heights (H_{m0}), peak wave periods (T_p), local angles of incidence ($\phi_{0,loc}$), nearshore calibration water depths (d_n), and wave spreading (α, as found in Appendix B.3). Runtimes for all simulations is approximately seven days. We also treat the influence of extreme events on these random waterlines in Section G.4.

Table G-2: Wave conditions used in the random waterlines test simulations, with wave height (H_{m0}), peak wave period (T_p), offshore local wave angle of incidence ($\phi_{0,loc}$), nearshore water depth (d_n), and wave directional spreading (s_0).

Conditions	H_{m0} [m]	T_p [s]	$\phi_{0,loc}$ [°]	d_n [m]	s_0 [°]
Calm	0.15	2.10	75	0.31	41
Stormy	0.35	1.50	75	0.57	30

Figure G-12 through Figure G-16 (numbered runs 1 to 5) show the results of the five random waterline simulations with stormy hydrodynamic forcing (see Table G-2). We see that the results of all runs seem quite similar, with an estimated cusp (or spit) spacing between 10 to 30 m. Amplitudes all seem to be in the range of approximately 2 to 8 m, and there is a clear 'leaning' in the direction the waves are going.

Timescales, however, are slightly different. The figures all show the last time-step, so after approximately seven days. The point where we say beach cusps are visible, is defined as the time-step at which the initial 'wiggles' (as pointed out in Section G.2) have damped out. This point was

126

found to be different between some of the simulations. Runs 1, 2 and 5 clearly showed beach cusps after one to two days, with the days after that showing spit-like formations. The other runs (3 and 4) showed beach cusps after five to seven days.

The length-scales seem to conform to the smaller cusps we sometimes see forming (e.g. photo (G) in the observations of Section 5.1.1, or Appendix D.7). Also, the timescales, despite being more variable, seem to agree with the order of days we assumed in the conceptual model (Section 5.4) and were found from observations.
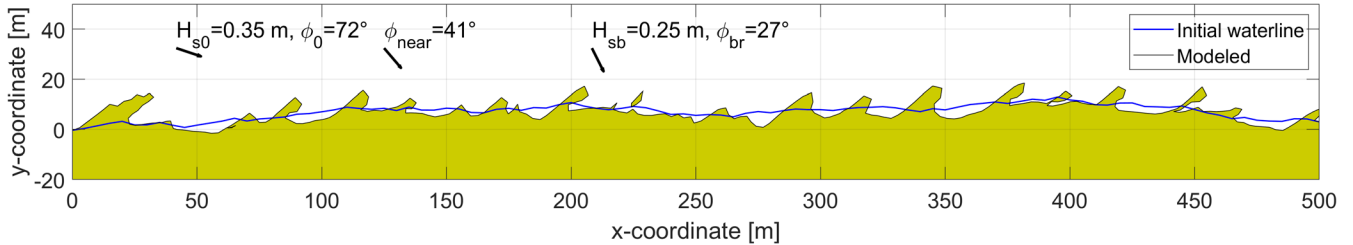
Figure G-12: Test run for finding self-organizing behavior under stormy conditions with random waterline 1.
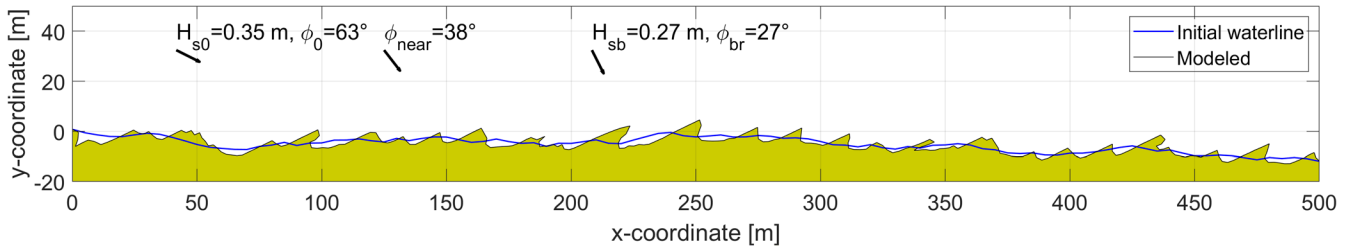
Figure G-13: Test run for finding self-organizing behavior under stormy conditions with random waterline 2.
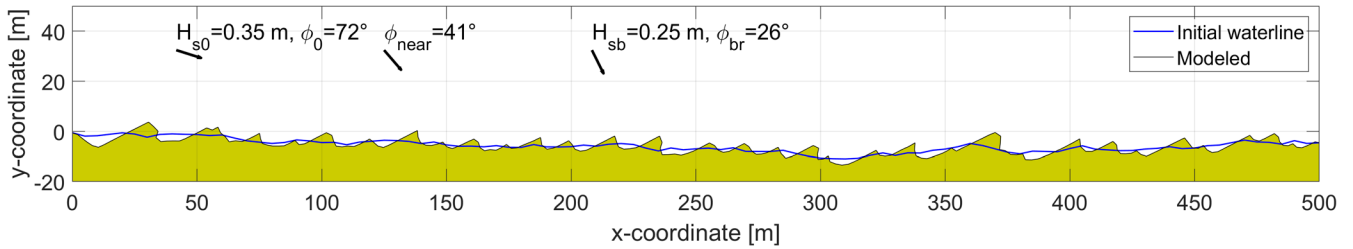
Figure G-14: Test run for finding self-organizing behavior under stormy conditions with random waterline 3.
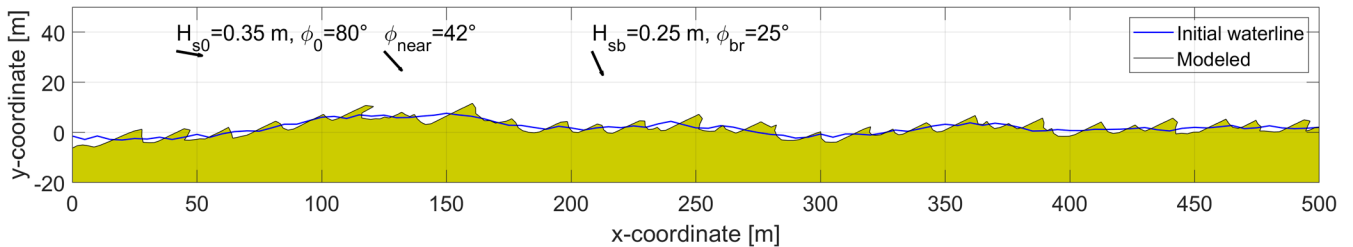
Figure G-15: Test run for finding self-organizing behavior under stormy conditions with random waterline 4.
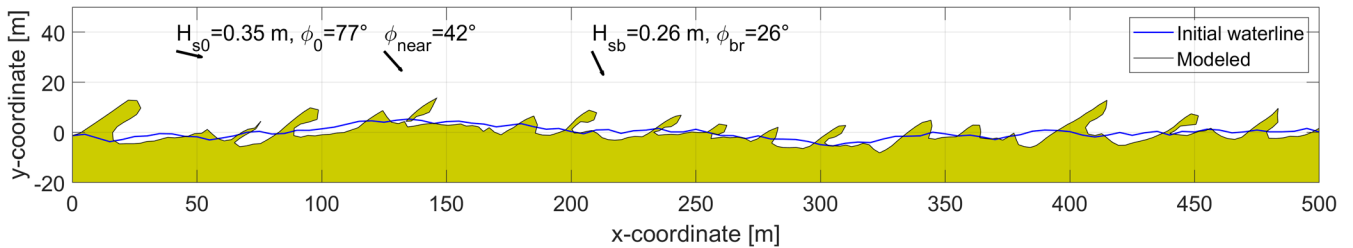
Figure G-16: Test run for finding self-organizing behavior under stormy conditions with random waterline 5.

Figure G-17 through Figure G-21 (similarly numbered from 1 to 5) show the simulation results of the same random waterlines as for stormy conditions, but now with a milder hydrodynamic forcing (see Table G-2). Cusp spacing seems to be slightly less than for stormy conditions, now in the range of 10 to 20 m, but amplitude is significantly less, now in the range of approximately 1 to 3 m.

Timescales seem to behave in a similar way as for stormy conditions, where we see that runs 1, 2 and 5 have more pronounced features than runs 3 and 4. So far, it seems that stormy conditions can cause the emergence of features in the order of days, while calm conditions take at least a week for similar results.
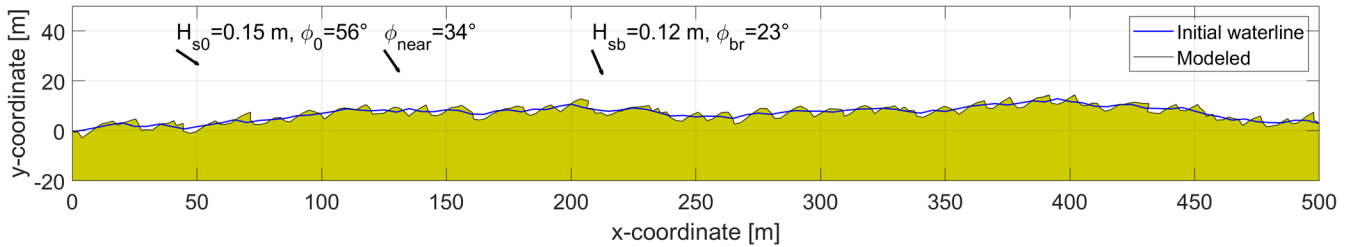
Figure G-17: Test run for finding self-organizing behavior under calm conditions with random waterline 1.
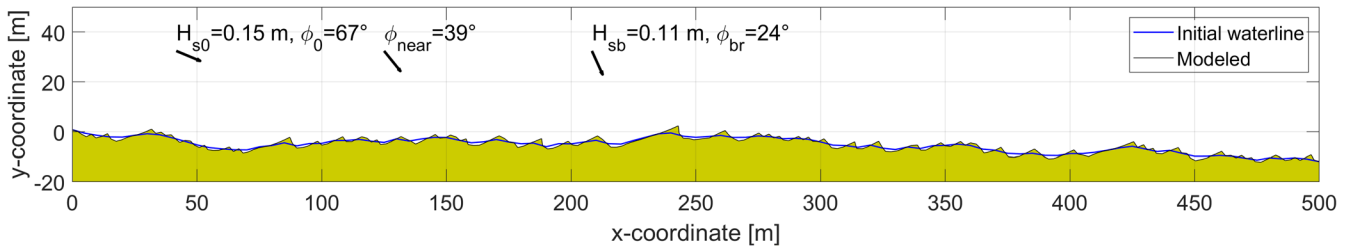
Figure G-18: Test run for finding self-organizing behavior under calm conditions with random waterline 2.
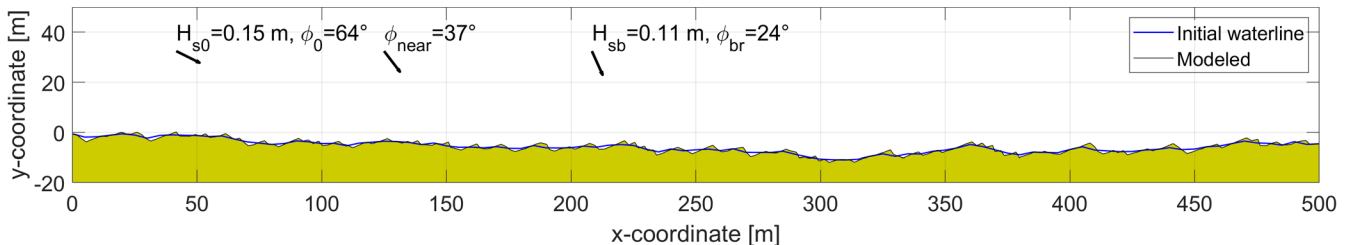
Figure G-19: Test run for finding self-organizing behavior under calm conditions with random waterline 3.
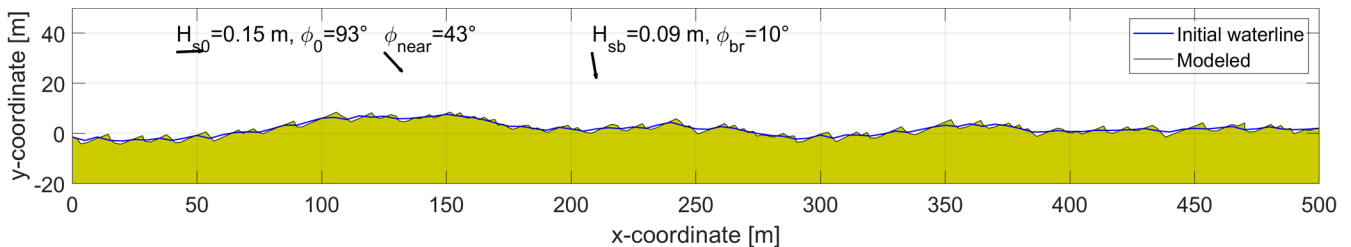
Figure G-20: Test run for finding self-organizing behavior under calm conditions with random waterline 4.
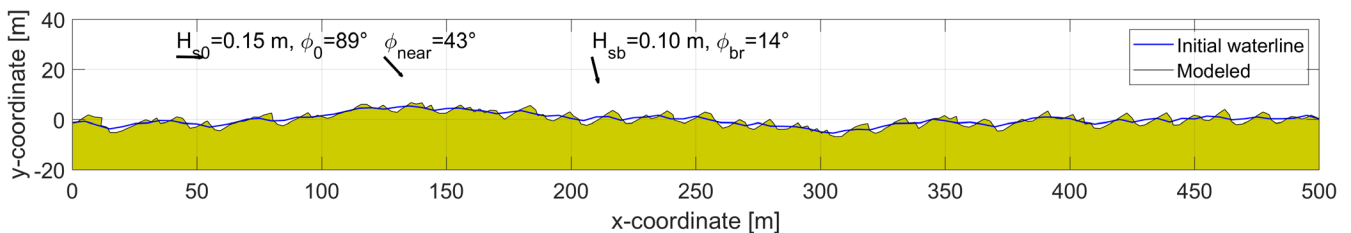
Figure G-21: Test run for finding self-organizing behavior under calm conditions with random waterline 5.

These results seem to substantiate the assumptions in literature that calm conditions have much less effect on the waterline than stormy conditions. Additionally, we see that no matter the initial waterline, clear cusp dimensions can be distinguished that are suspected to have configured themselves from a balance between hydrodynamic forcing and negative feedback from the morphology. In each of the runs, it was clear that initial perturbations grew quickly, which eventually slowed down upon reaching their new configuration. The simulations also show that smaller features emerge along the larger waterline shapes. These larger shapes were not damped out during calm conditions, but did change under the influence of stormy conditions. Altogether, the typical length- and timescales we found seem to be conform the self-organization principle. Also, the simulations seem to agree with the idea the initial waterline leads to the more prominent cusps, but the smaller cusps are largely independent of this initial state.

G.4   Northern storms

An interesting question, one which was not addressed in our data and modeling analyses, is what would happen to the waterline when forced by a Northern storm, arriving both at a high-angle and with a large wave height.

We applied a wave height of twice the wave height for stormy conditions used in the previous section (so $H_{m0} = 0.70$ m). This may not be considered quite extreme, but due to unstable simulations this was about as high as we could go given the limited amount of time. Our other hydrodynamic conditions are the peak wave period ($T_p = 4.30$ s), local angles of incidence ($\phi_{0,loc} = 75°$), nearshore calibration water depths ($d_n = 0.95$ m), and wave spreading ($\alpha = 30°$, same as stormy conditions from Appendix B.3). Simulations were run for approximately a week.

Figure G-22 through Figure G-26 (numbered runs 1 to 5) show the simulation results after a runtime of a week. We clearly see spit formation, with less clearly distinguishable cusps. These spits were already visible after one day, with beach cusps having formed after the first timestep (about an hour).

Even though these responses may seem a little extreme, spit formation has already been observed before in Section 5.1. They can be seen more clearly at km 60.300 in Appendices D.6 through D.9, and km 53.025 in Appendix D.22. We relate these simulation results back to the case of the Houtribdijk, where it seems less likely that feature like this will form so easily, mostly due to the sudden increase in depth at the edge of the submerged platform. However, assuming that features like this will try to form under such conditions, this does hint at the possibility of permanent loss of material, as eroded sediment is deposited over the platform edge. Despite this, it is probably best to perform a more in-depth analysis on the effects of such events on the morphological behavior of the waterline.
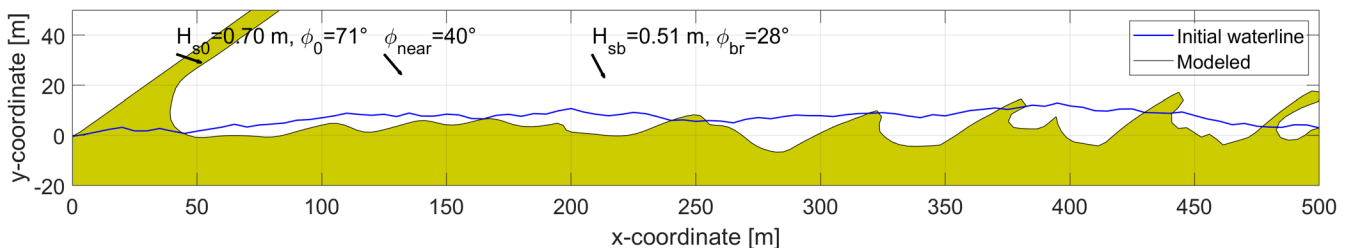
Figure G-22: Test run for finding self-organizing behavior under extreme conditions with random waterline 1.
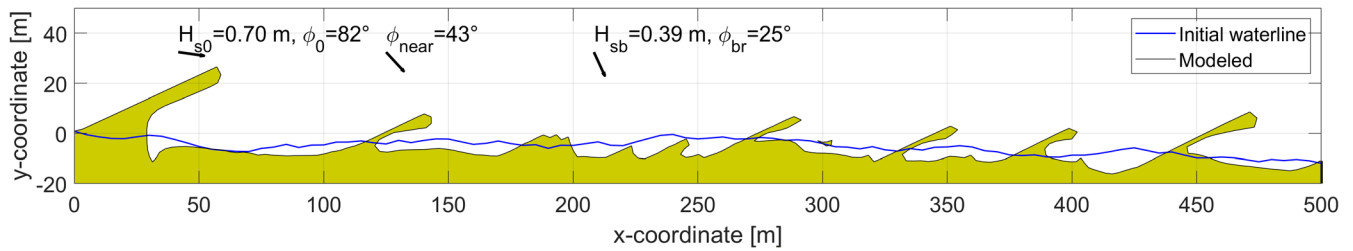
Figure G-23: Test run for finding self-organizing behavior under extreme conditions with random waterline 2.
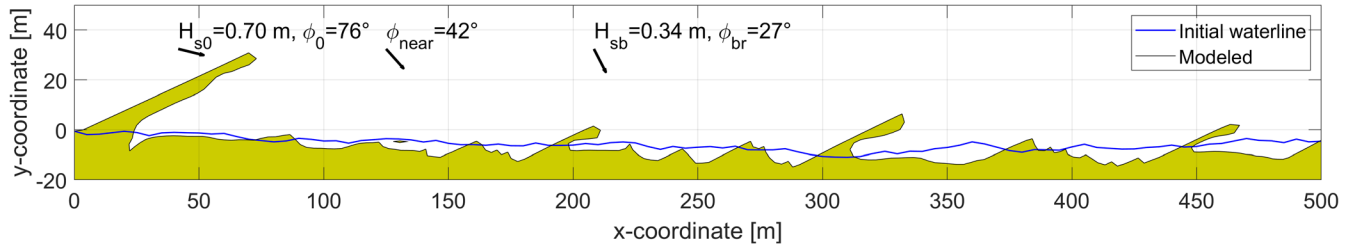
Figure G-24: Test run for finding self-organizing behavior under extreme conditions with random waterline 3.
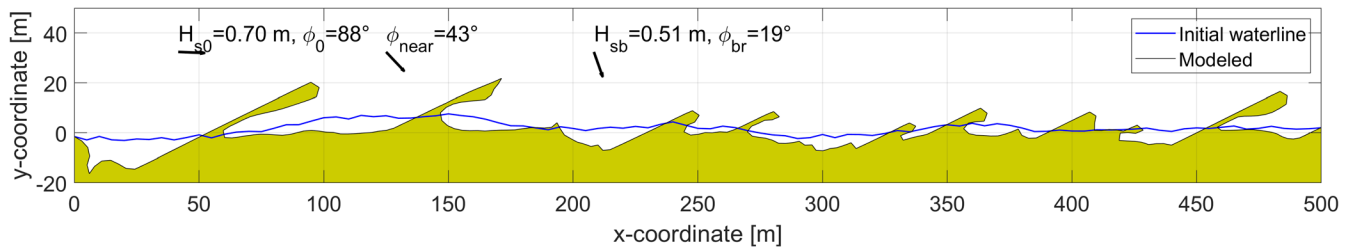
Figure G-25: Test run for finding self-organizing behavior under extreme conditions with random waterline 4.
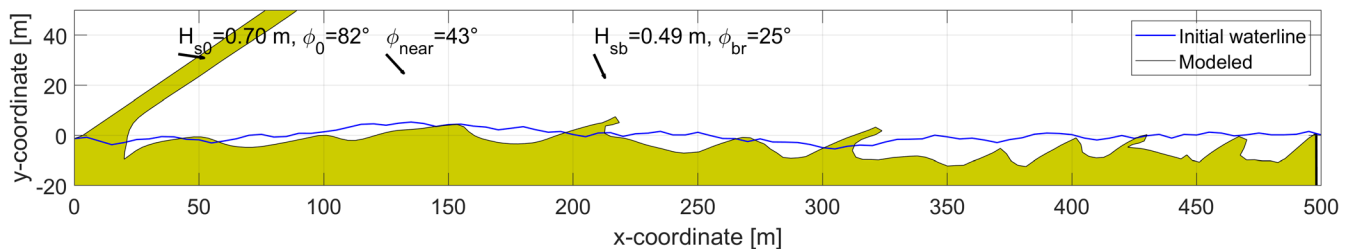
Figure G-26: Test run for finding self-organizing behavior under extreme conditions with random waterline 5.

G.5   Profile corrections

In this section we have considered the linear profile assumption, and how it is assumed not valid for our low-energy environment. As mentioned at the start, Appendix A of the Supplementary Images by Roelvink et al. (2020) provided a mathematical derivation of why this assumption has little impact when a coastline has had sufficient time to adapt to forcing. Seeing as this is likely not the case for our environment, we have experimented with some adjustments to the linear profile, to see whether changes indeed have limited effect, even in our case.

The adjustment implied a correction that we may apply due to the curvature to the coastline. To clarify, lower parts of a profile, when going around a curve, contain more volume than the upper parts of the profile. A correction term can be included in ShorelineS, that takes this difference into account. This, as mentioned at the start of this appendix, is mostly relevant when distances from the toe and crest of the profile to MSL are not equal. If equidistant, the correction term equals zero.

Figure G-28 shows the standard implementation in ShorelineS, a linear profile without curvature correction. Figure G-29 presents the linear profile with curvature correction, and Figure G-30 shows the logarithmic profile with curvature correction. The linear profile with curvature correction is copied from (Roelvink et al., 2020), the logarithmic profile with curvature correction was based on the

characteristic profile at location FL69 (Figure G-27). In the figures showing the modeling results, the blue line indicates the starting period (T0). The black line, including the yellow shading, indicate the model results.

$$\Delta n_{lin,c} = \Delta V \bigg/ \left(\Delta s (z_{crest} - z_{toe}) - \frac{\Delta s}{R} \left[\frac{z_{crest}^2 - z_{toe}^2}{2\tan(\beta)} \right] \right)$$

$$\Delta n_{log,c} = \Delta V \bigg/ \left(\Delta s (z_{crest} - z_{toe}) - \frac{\Delta s}{R} \left[\frac{z_{crest} - z_{toe}}{c_1} \right] (-1)^{\frac{1}{c_2}} \Gamma \left(\frac{c_2 + 1}{c_2} \right) \right)$$

Where:
   - $\Delta n_{lin,c}$ [m]: Change in the cross-shore coordinate for linear curvature corrected profile.
   - $\Delta n_{log,c}$ [m]: Change in the cross-shore coordinate for logarithmic curvature corrected profile.
   - ΔV [m³]: Change in volume for the considered time-step Δt.
   - Δs [m]: Change in the longshore coordinate for the respective profile.
   - z_{crest} [NAP+m]: Elevation of the crest of the swash berm ($= -0.11$ m+NAP).
   - z_{toe} [NAP+m]: Elevation of the toe of the platform ($= -0.89$ m+NAP).
   - $\tan(\beta)$ [-]: Mean profile slope.
   - R [m]: Radius of curvature of the respective coastline section.
   - c_1 and c_2 [-]: Factors for the curvature of the logarithmic profile (0.56 and 0.50, respectively).

Wave conditions were the same as in the previous section, with wave heights of 0.25 m, peak periods of 2.51 s, and local wave incidence angles of 82°. Runtime in all cases was two days, spatial steps approximately 2 m, deep water depth was 2.3 m, and nearshore water depth was 0.85 m. All simulations were run with the KAMP transport formulation, meaning we set the median grain diameter at 300 μm and the mean bed slope ($\tan\beta$) at 0.046.

The figures show that runs with a curvature correction yield lower magnitudes of response, visible by the lower amplitudes of the cusps. Besides that, both curvature corrected profiles yield similar results. Whether the curvature corrections yield more realistic results, was not verified.
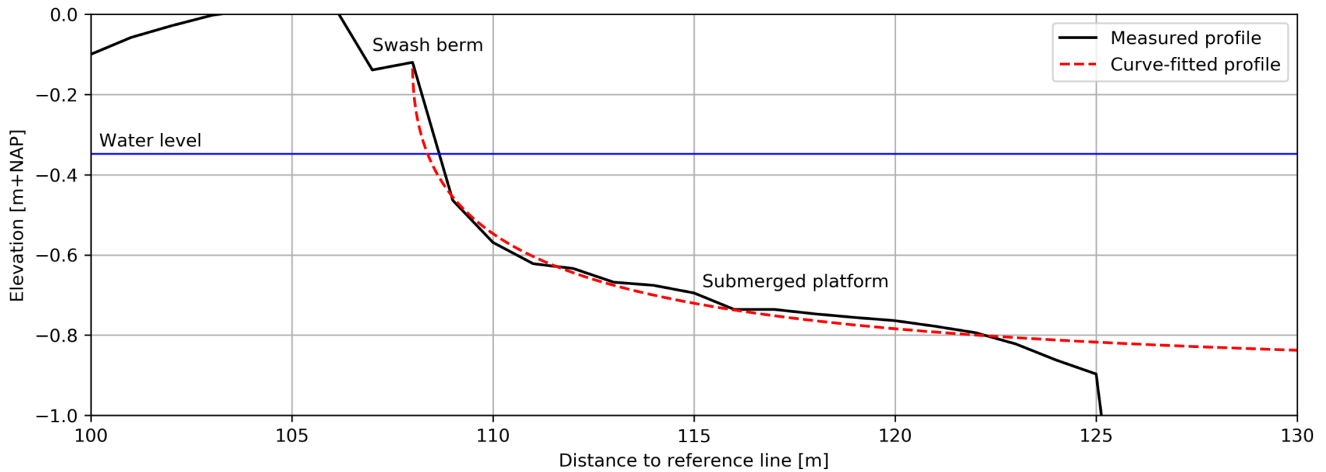
Figure G-27: Logarithmic fit to a representative profile at location FL69.
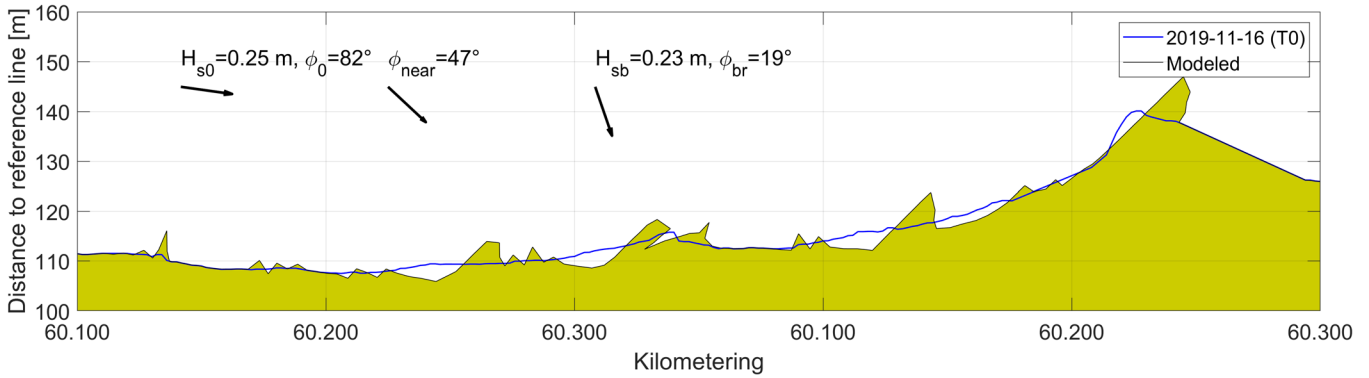
Figure G-28: ShorelineS testing of linear profile for transects 60.100 to 60.350 at location FL69.
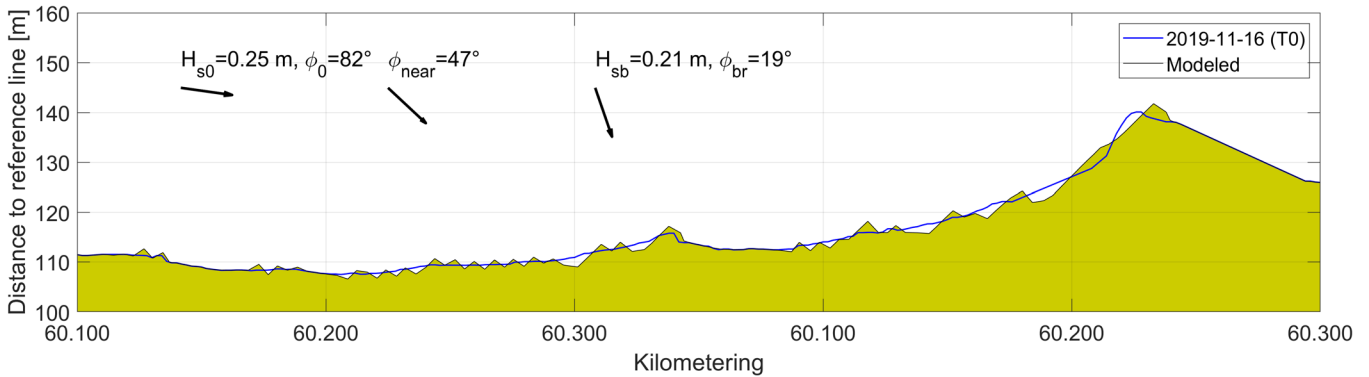
Figure G-29: ShorelineS testing of linear profile with curvature correction for transects 60.100 to 60.350 at location FL69.
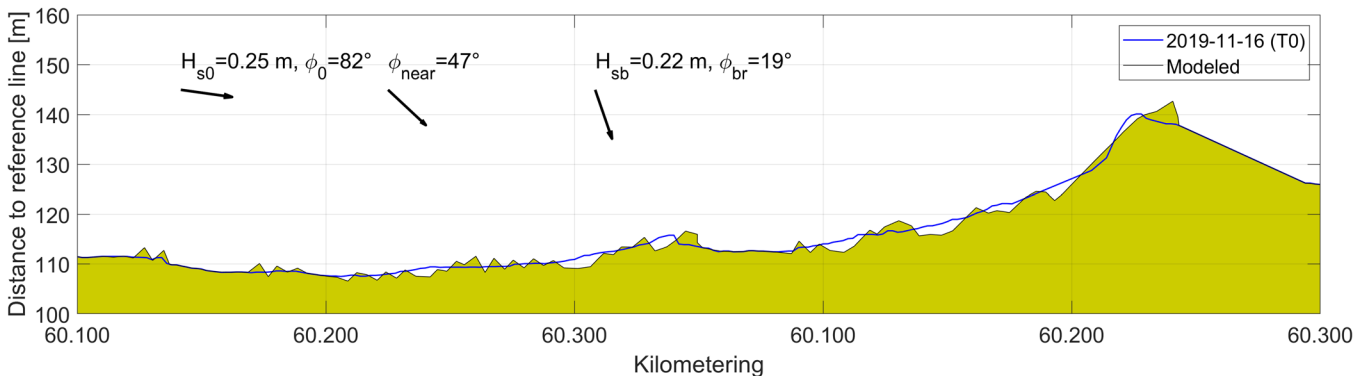
Figure G-30: ShorelineS testing of logarithmic profile with curvature correction for transects 60.100 to 60.350 at location FL69.

G.6   Breaking wave parameters

ShorelineS includes a couple of transport formulations that evaluate the breaking wave conditions. It does so in a couple of steps. First, the offshore conditions are transformed to nearshore conditions, either by Snel's law, or a 2D refraction model. Second, the nearshore conditions are transformed to breaking conditions. This last step is done using the following definitions:

$$h_{br} = \left[\frac{H_{s0}^2 c_1 \cos(\phi_{loc})}{\alpha \gamma^2 \sqrt{g}}\right]^{0.4} \qquad \text{and} \qquad H_{sb} = h_{br}\gamma$$

Where:

- h_{br} [m]: Water depth at breaking.
- H_{s0} and H_{sb} [m]: Deep-water and breaking wave height, respectively.
- c_1 [m/s]: Nearshore wave celerity.

- ○ $\phi_{0,loc}$ [°]: Local offshore wave angle of incidence.
- ○ α [-]: Calibration factor for point of breaking.
- ○ γ [-]: Breaking coefficient with 5% breaking waves.
- ○ g [m/s^2]: Gravitational acceleration (= 9.81 m/s^2).

This formulation shows that our breaking wave conditions are dependent on two calibration parameters (α and γ). These are generally calibrated by measurement of the nearshore conditions. A similar effort was made near the beach at the IJsselmeer, but the general consensus was that the value of the γ-parameter ($\sim$1.5) was likely not realistic. To illustrate the effect of changing this parameter, Figure G-31 and Figure G-32 below compare results for location FL69, starting at T0, for a γ-value of 0.72 (default) and 1.5, respectively. In the figures presented in this section, the blue line indicates the starting period (T0). The black line, including the yellow shading, indicate the model results.

As we can see from the figures, the breaking wave height and angle of incidence changed relatively much. There do not seem to be significant changes to the modeled coastline when changing γ. However, the validity of this application is doubtful because we assumed a longshore uniform bathymetry (through Snel's law). This means that we assume the waves have sufficient space to refract to their new orientations. For a linear profile (see Figure G-33), we therefor assume that distances L_1 and L_2 are sufficiently large to refract the waves from deep water to nearshore depths (h_d to h_n), and from nearshore to breaking depths (h_n to h_{br}). For the profile at the Houtribdijk this is probably not the case, because of the abrupt changes in depth (see Figure G-34). Both from deep water to nearshore depths (h_d to h_{n1}), and from nearshore to breaking depths (h_{n2} to h_{br}), we see that these distances are smaller. Of course, there is also refraction from h_{n1} to h_{n2}, but it is considered relatively small due to the low gradient of the platform.

Exact quantification is difficult, so 2D refraction computations are likely required to accurately predict refraction. However, as previously shown in Figure 4-4 (repeated in Figure G-35), refraction was observed to occur only very close to the waterline. Breaking wave angles in the model are therefore likely underestimated, and might in reality be even larger. Since modeled waterlines are often already exaggerated responses of the beach, having even larger nearshore angles of incidence may not yield accurate results. Despite this, predictive analyses should probably take this mechanism into account, if we want to correctly simulate the physical process.
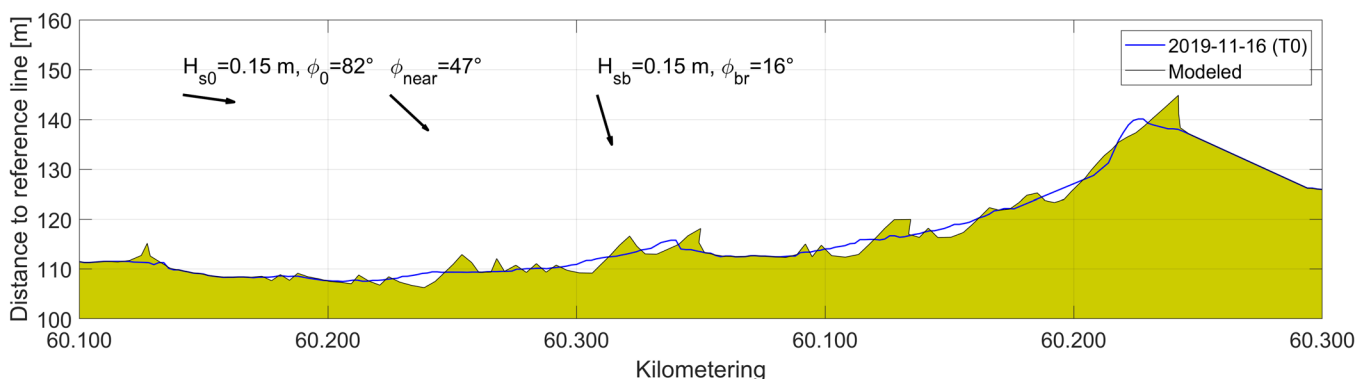
Figure G-31: ShorelineS testing of breaking wave conditions ($\gamma = 0.72$) for transects 60.100 to 60.350 at location FL69.
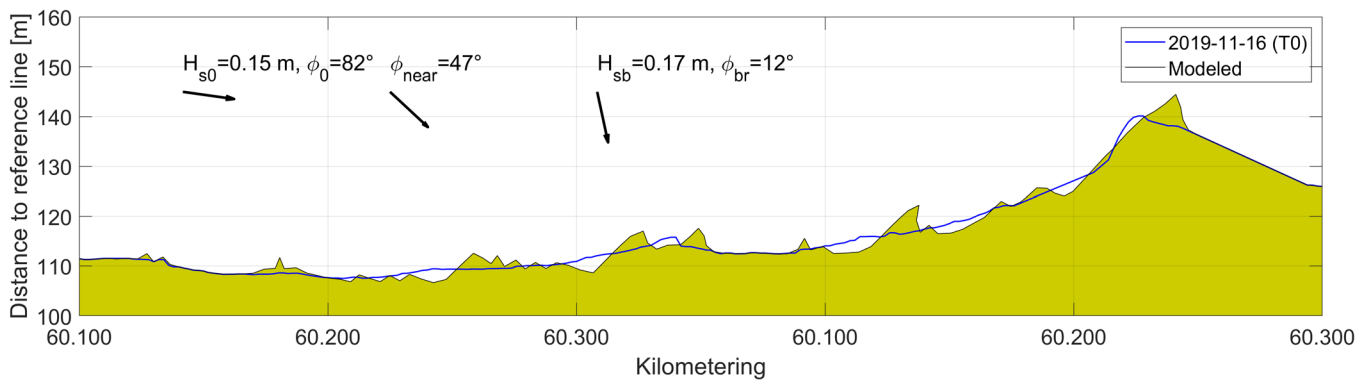
Figure G-32: ShorelineS testing of breaking wave conditions ($\gamma = 1.5$) for transects 60.100 to 60.350 at location FL69.
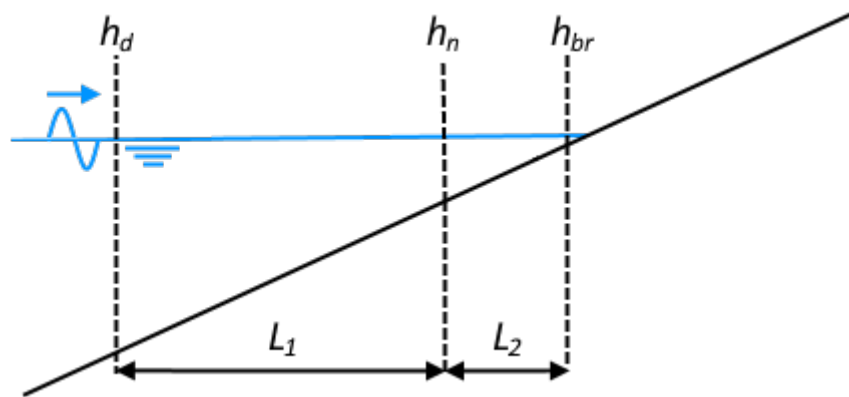
Figure G-33: Refraction path under linear profile assumptions, with deep water depth (h_d), nearshore water depth (h_n), breaking water depth (h_{br}), and refraction distances (L_1 and L_2).
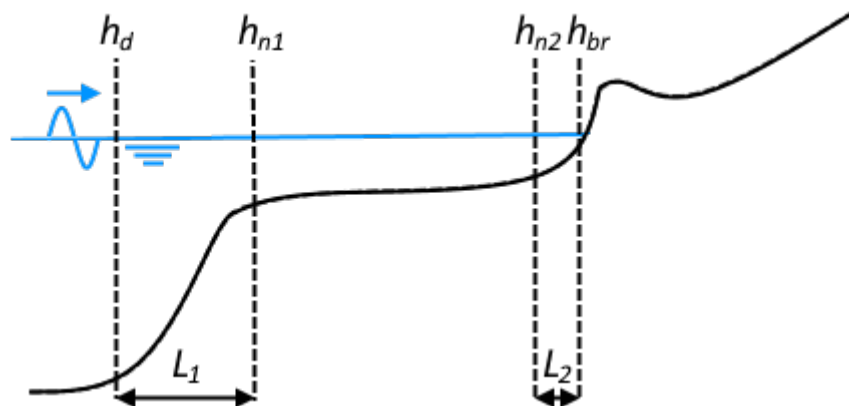
Figure G-34: Refraction path under logarithmic profile assumptions, with deep water depth (h_d), nearshore water depth (h_{n1} and h_{n2}), breaking water depth (h_{br}), and refraction distances (L_1 and L_2).

Figure G-35: Aerial photo near location FL69, taken on 22nd February 2020 (Bureau Start the Future, 2020).

Appendix H: ShorelineS modeling results

In order to strengthen the claim that high-angle waves are the dominant cause for morphological changes, the numerical model ShorelineS was used to try and reproduce the measured waterlines. A complete overview of the simulations is presented in this appendix, along with a comparison of the results to the measured waterline. In Section 6.2 we described the settings we used to do this. The results of the simulations may be found in Section 6.3, and the conclusions in Section 6.4.

Quantities used to describe the comparisons are the number of cusps (N_c), wavelength (L_c), amplitude (A_c) and shape asymmetry (As). The layout is as follows; the top two graphs indicate the beach sections at either FL69 or FL70. Contrary to Appendix E, we split each of the beach sections up in two parts. In black we have the waterline simulated using the representative hydrodynamics, where the dry part of the beach is colored yellow. Waterlines from the measured data at the start and end of the indicated periods are colored red and blue, respectively. The x-axis indicates the transects of the Houtribdijk, the y-axis the cross-shore distance to Shore's reference line.

The lower left graphs shows relevant hydrodynamics for this period, as was done in Appendix E, like the origin of the waves, the wave height, and the water level. The top of these three graphs, the solid red line indicates the beach orientation, the solid green line the shore normal, and the dashed green lines the 45° critical angles for high-angle wave instabilities. Stormy conditions are indicated by parts of the data that are colored red. In these three graphs, the sections that are shaded in yellow indicate the representative hydrodynamic period, as found using the conceptual model. Different from the graphs in Appendix E, we now indicated the average values of the representative hydrodynamics in purple.

Since we are now comparing the actual cusp quantities with the modeled quantities, we need to compare two different results in a single figure. The figures showing the variation of model cusp quantities will only show two sets of values. The first being the measured cusp quantities at the start of the period, the second being the cusp quantities from simulating to the end of the period. For example: From period T0 to T1, we show the number of cusps from Appendix E for the first period (at T0, light green), and then the modeled number of cusps for the second period (at T1, dark green). Since this is a qualitative comparison, we have not included the exact quantities of the measured cusps at the end of the period (T1 in the example). Instead, the texts at the bottom of the pages repeat the observations from Appendix E. We then compare this to the results we get when applying the conceptual model to our modeled waterline. Unless specified, the first line of observations always describes changes in average values of the quantities. Since there were no representative conditions found for period T2 to T3, this comparison is omitted.
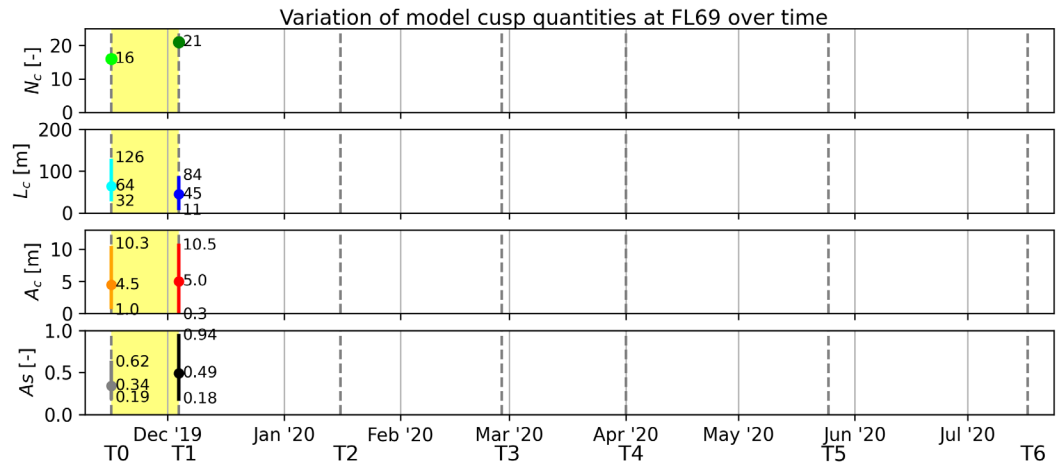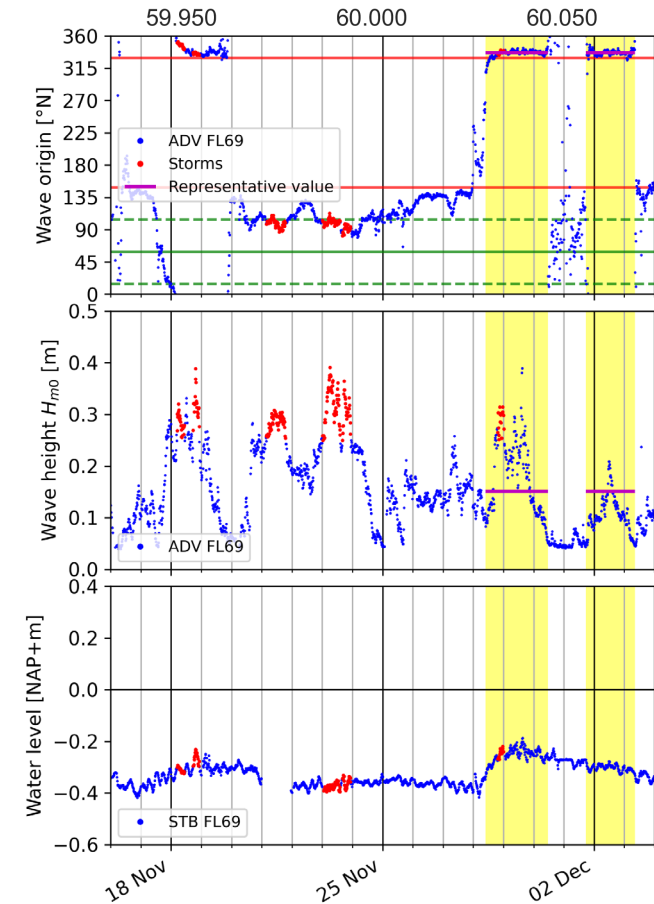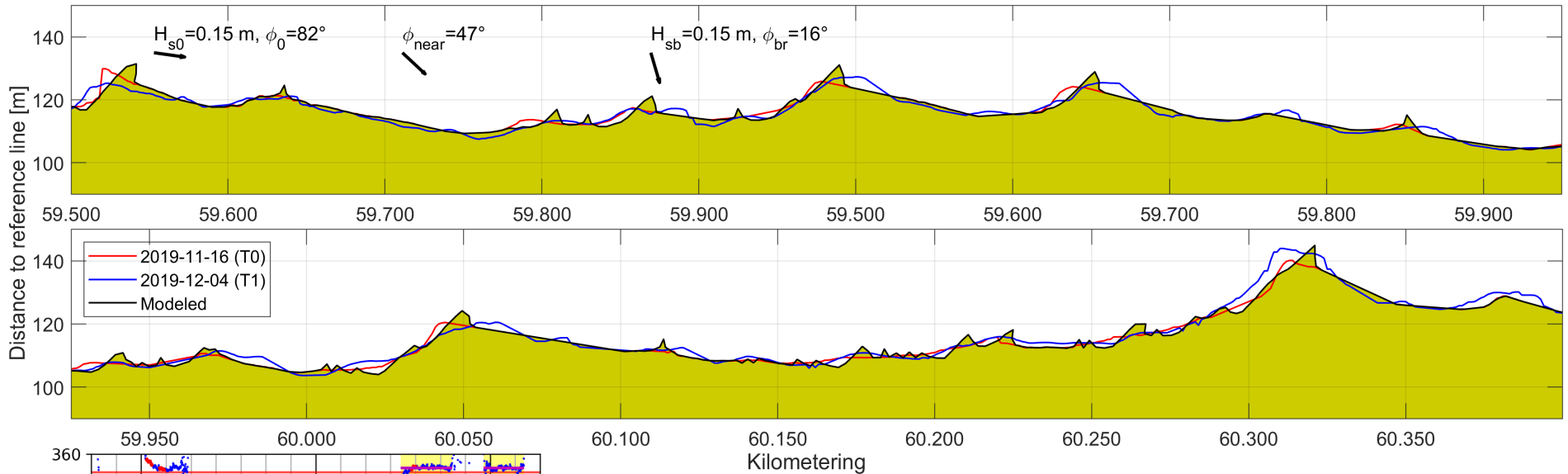
Measured waterline:
Increase of N_c and As, decrease of L_c and A_c; fully corresponds with short-term exposure to high-angle waves from the North.

Modeled waterline:
Increase of N_c, A_c and As, decrease of L_c; mostly corresponds with short-term exposure to high-angle waves from the North. Qualitative changes mostly agree, except for the early increase in amplitude, which is something we expect from a long-term exposure to high-angle waves. In contrast to our expectations, the water level rise near the end of this period does not seem to have decreased the amplitudes.
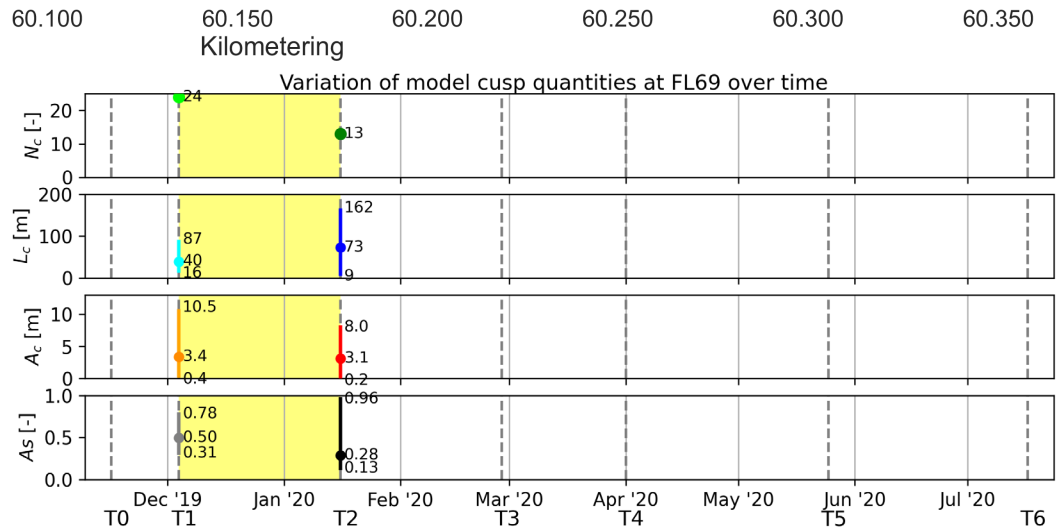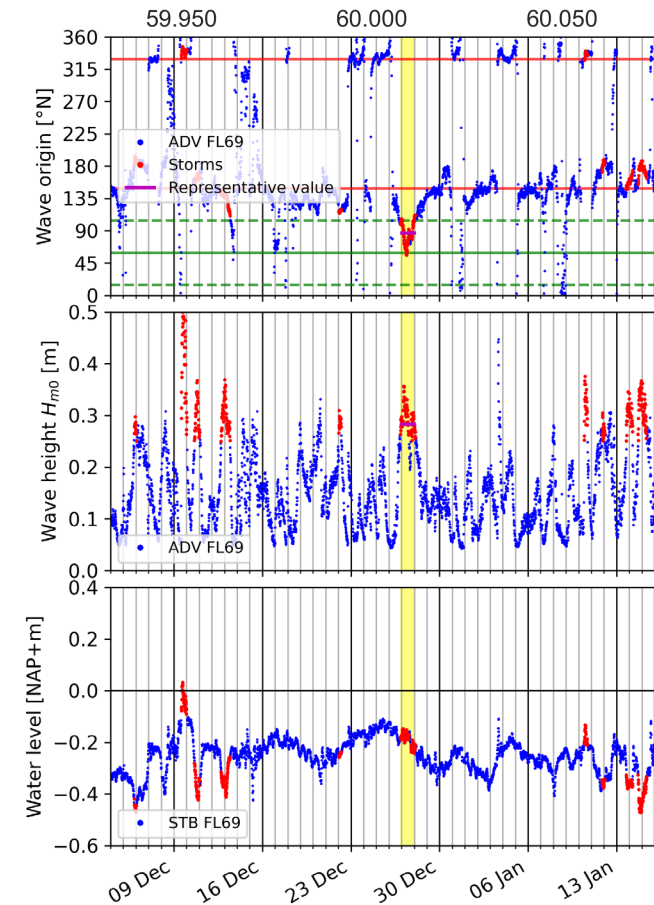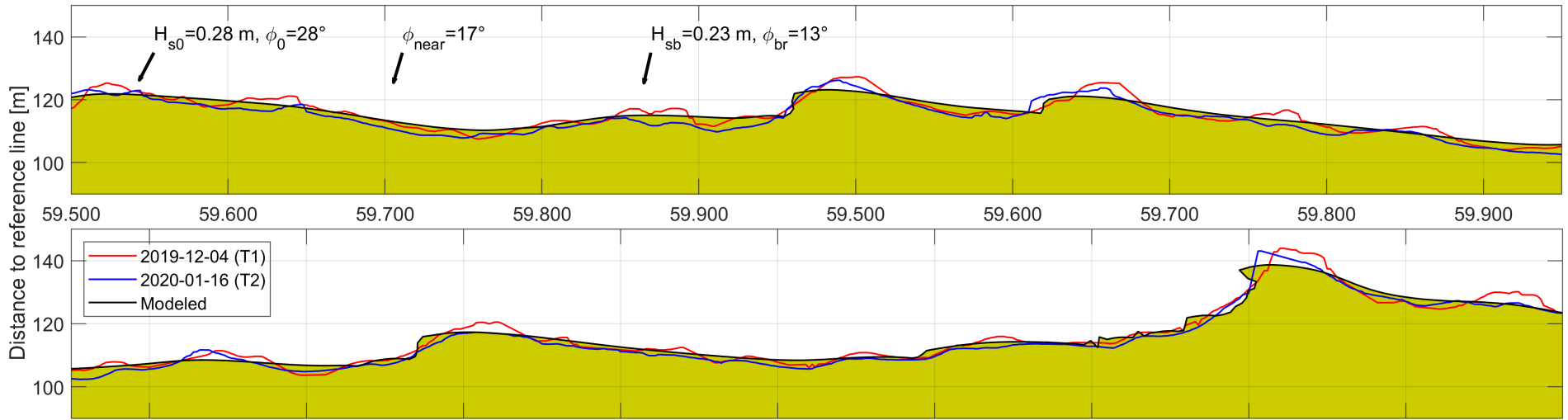
Measured waterline:

Decrease of N_c and As, increase of L_c and A_c; fully corresponds with short-term exposure to low-angle waves from the East.

Modeled waterline:

Decrease of N_c, A_c and As, increase of L_c; fully corresponds with long-term exposure to low-angle waves from the East, meaning it mostly corresponds to what the conceptual model predicts (short-term low-angle waves). Even though the representative period is only a day, the simulation results indicate a long-term exposure. Our expectations are that this rapid response, as seen by the decrease in amplitude, are caused by the relatively large wave height used in the simulation.
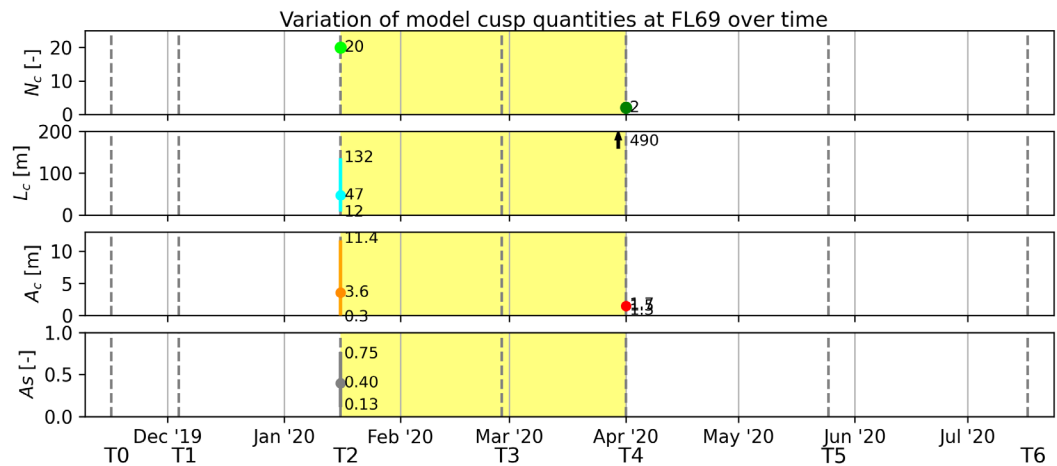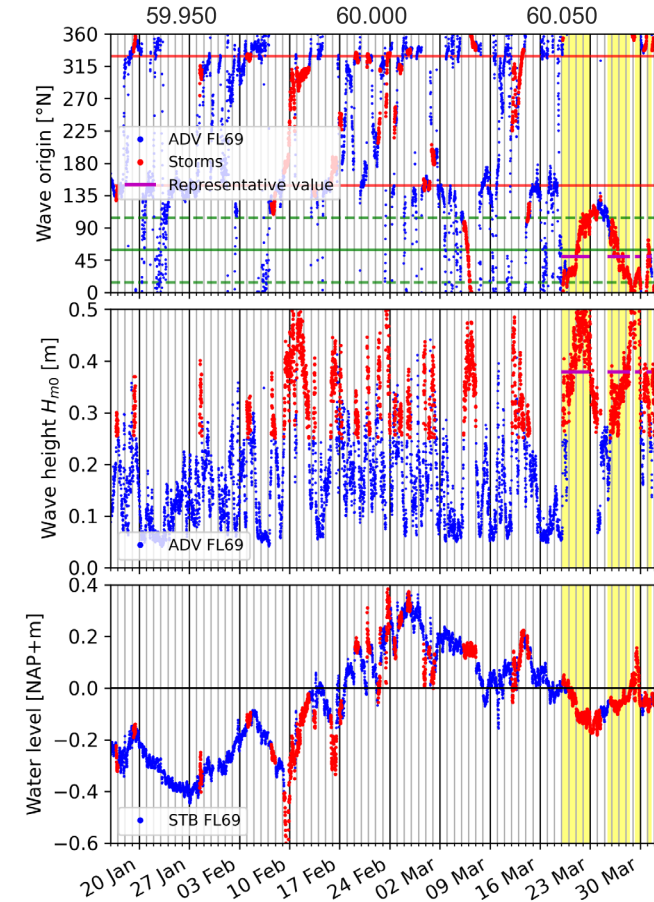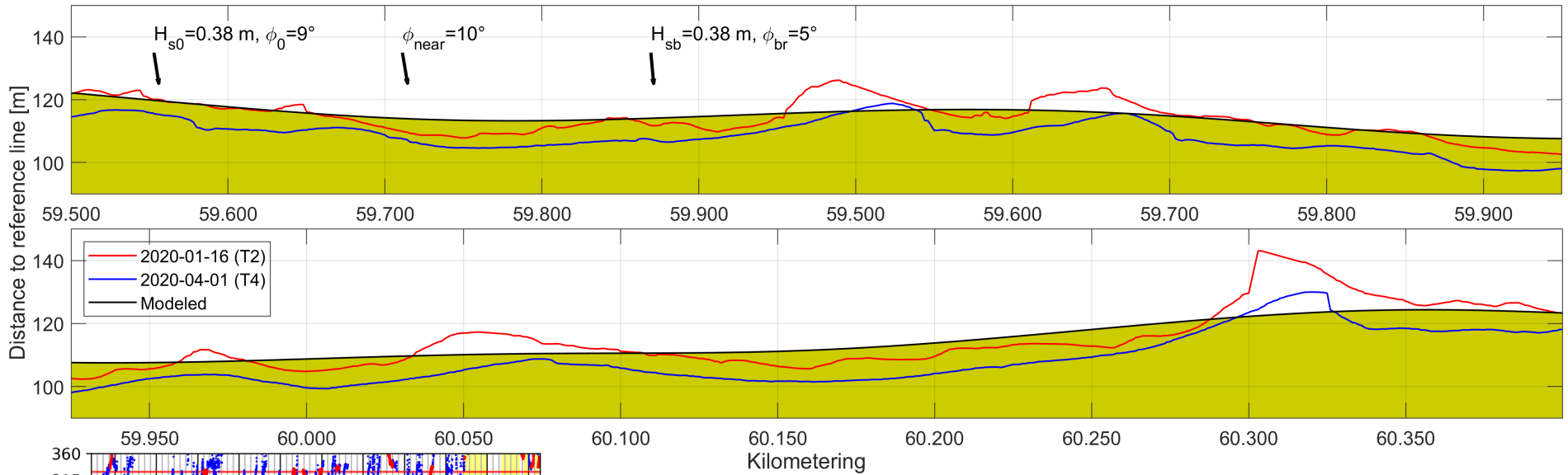
Measured waterline:

Decrease of N_c and A_c, increase of L_c and As; fully corresponds with long-term exposure to low-angle waves from the North.

Modeled waterline:

Decrease of N_c and A_c, increase of L_c; mostly corresponds with long-term exposure to low-angle waves from the North. Even though we were unable to quantify asymmetry, due to the flatness of the waterline, it seems that the changes are qualitatively fully explained, despite the relatively large variations in water levels.
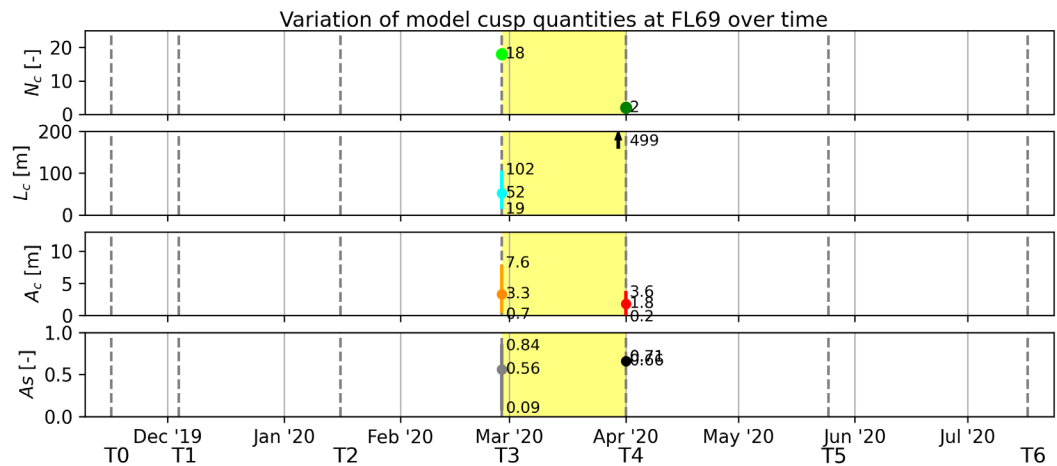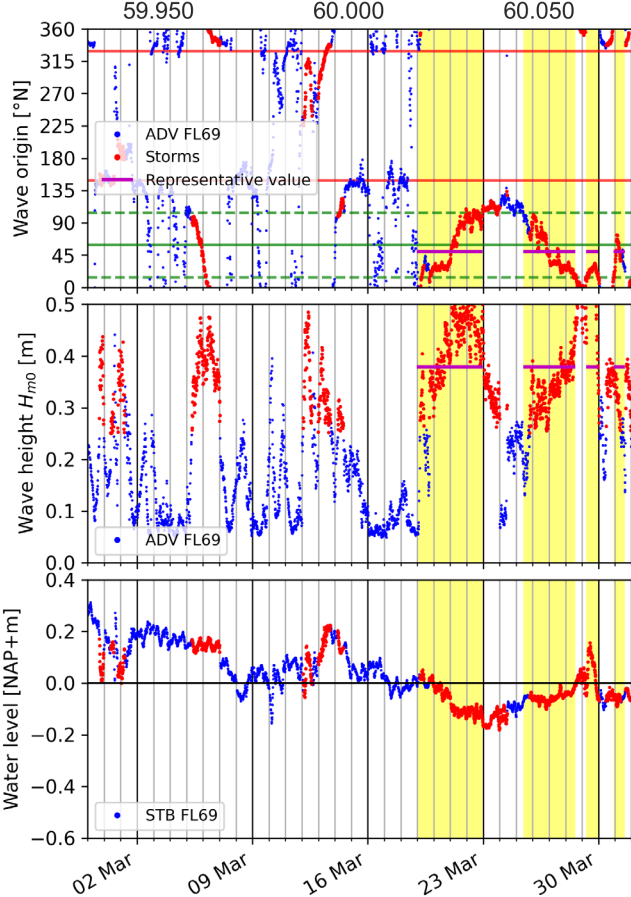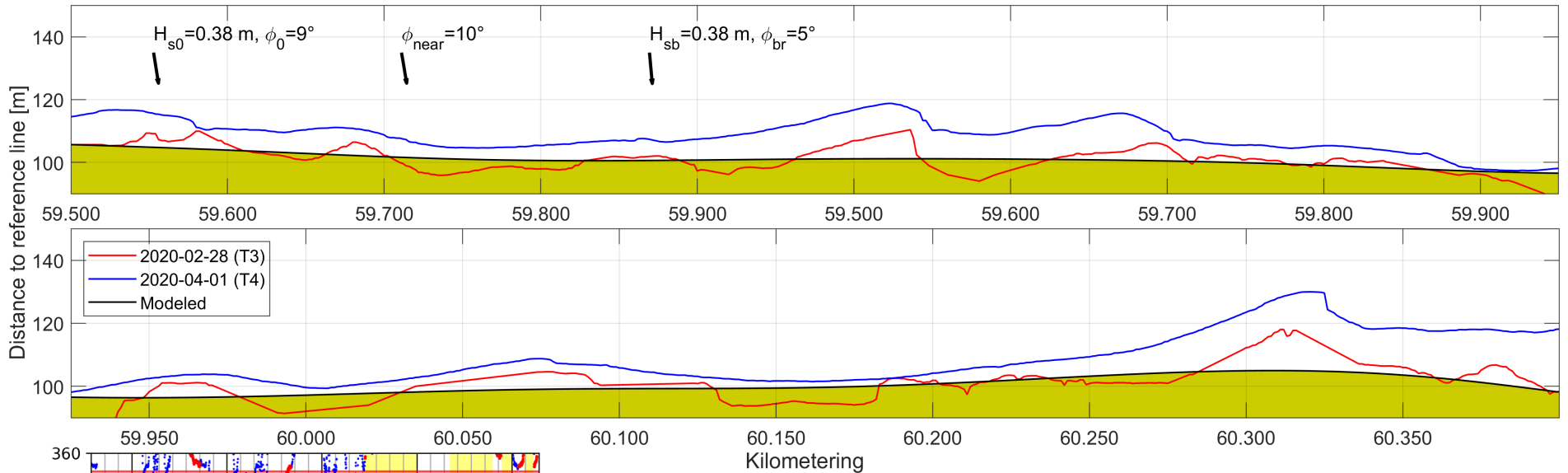
Measured waterline:

Decrease of N_c, increase of L_c, A_c and As; partly corresponds with long-term exposure to low-angle waves from the North.

Modeled waterline:

Decrease of N_c and A_c, increase of L_c and As; fully corresponds with long-term exposure to low-angle waves from the North. The model simulations seem to fully conform to the expectations. However, we are unsure of the validity, due to a relatively large difference in water levels between T3 and T4.
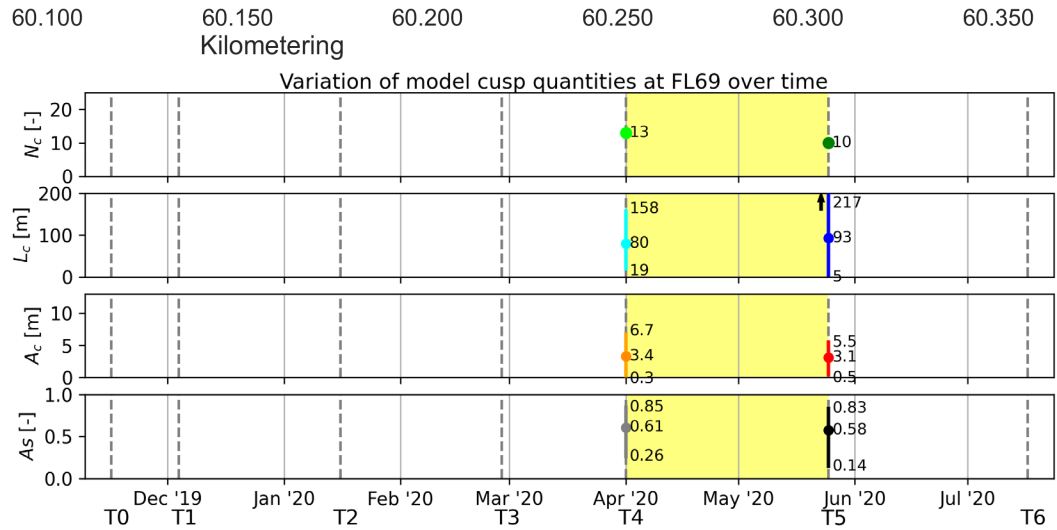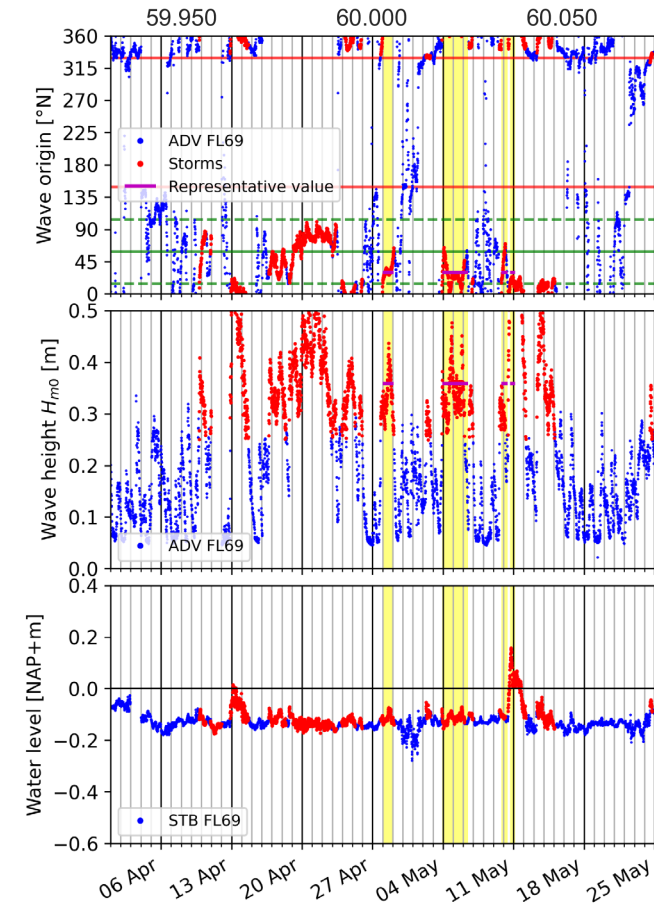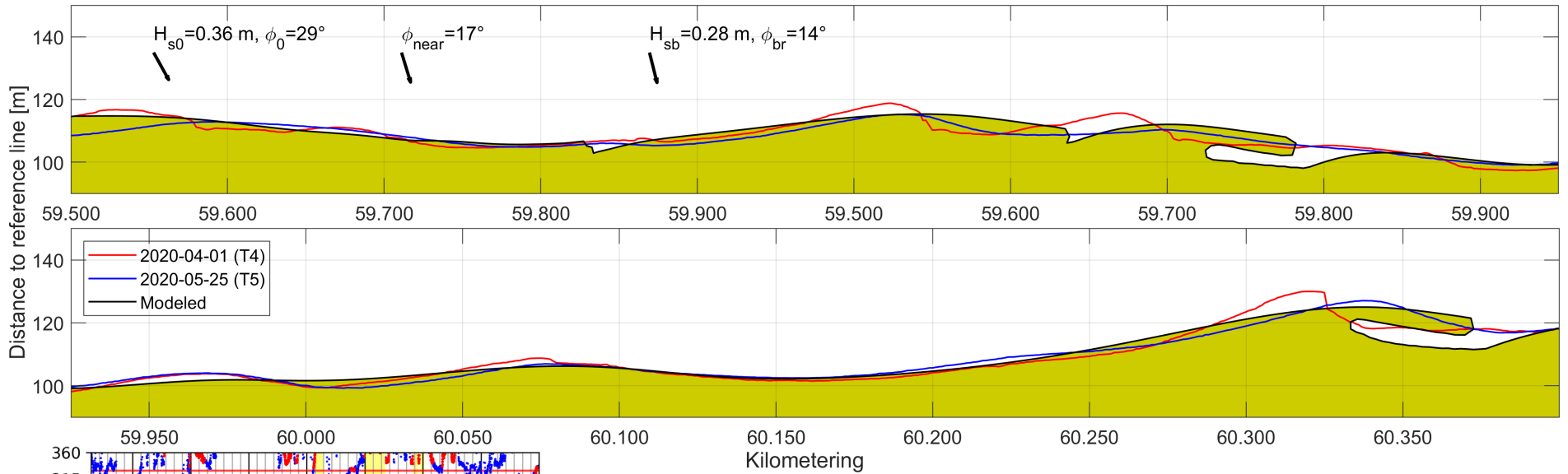
Measured waterline:

Decrease of N_c, A_c and As, increase of L_c; mostly corresponds with long-term exposure to low-angle waves from the North.

Modeled waterline:

Decrease of N_c, A_c and As, increase of L_c; mostly corresponds with long-term exposure to low-angle waves from the North. The asymmetry seems to decrease, which is the same issue with the corresponding period in Appendix E.6. Even though it was not what we were looking for, this low-angle case also seems to quantitatively match the measured waterlines.
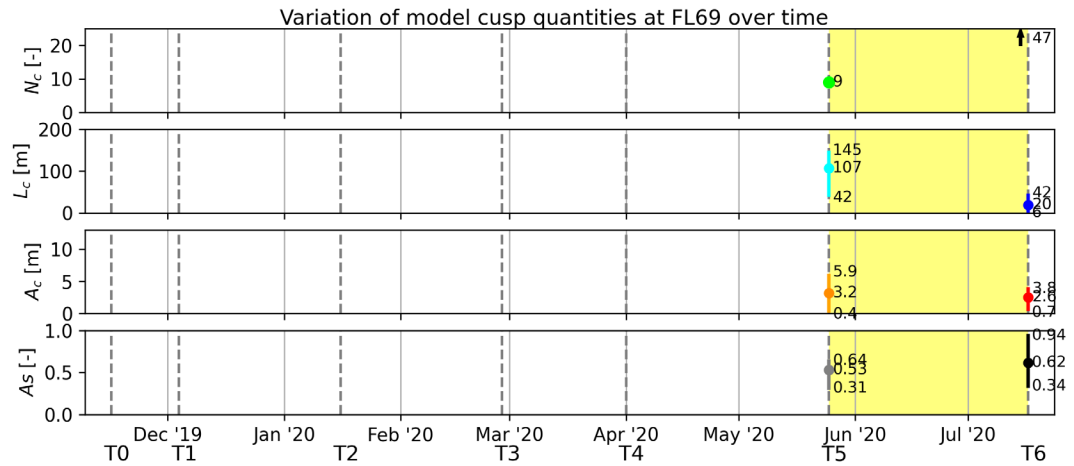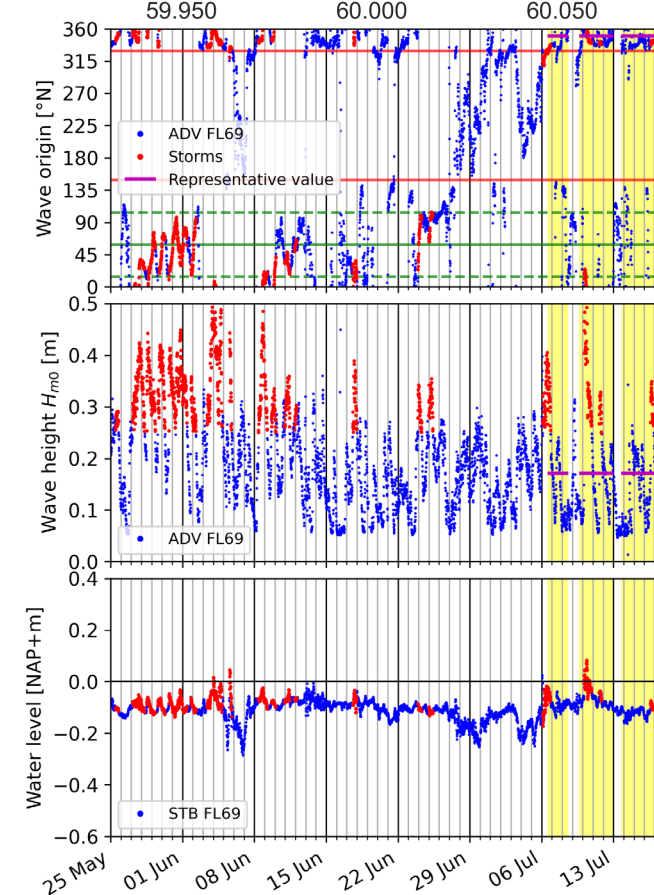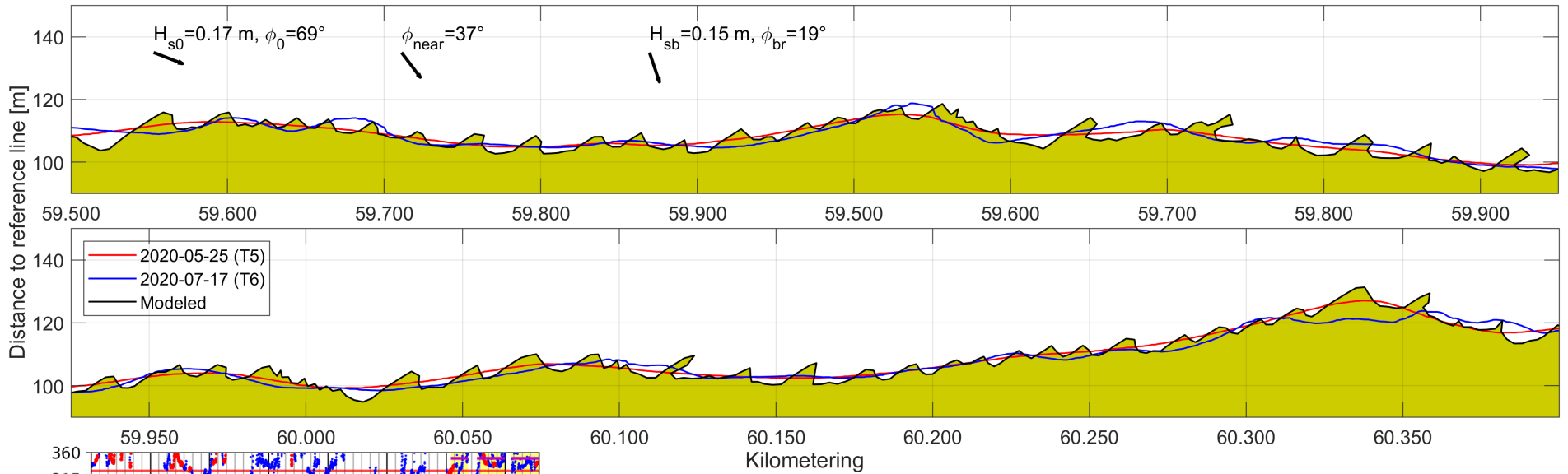
Measured waterline:

Increase of N_c and As, decrease of L_c and A_c; fully corresponds with short-term exposure to high-angle waves from the North.

Modeled waterline:

Increase of N_c and As, decrease of L_c and A_c; fully corresponds with short-term exposure to high-angle waves from the North. Even though this case seems to exaggerate the number of cusps, the qualitative changes fully corresponds with the measured changes.

H.7 FL70: 16 November to 4 December 2019 (T0 to T1)
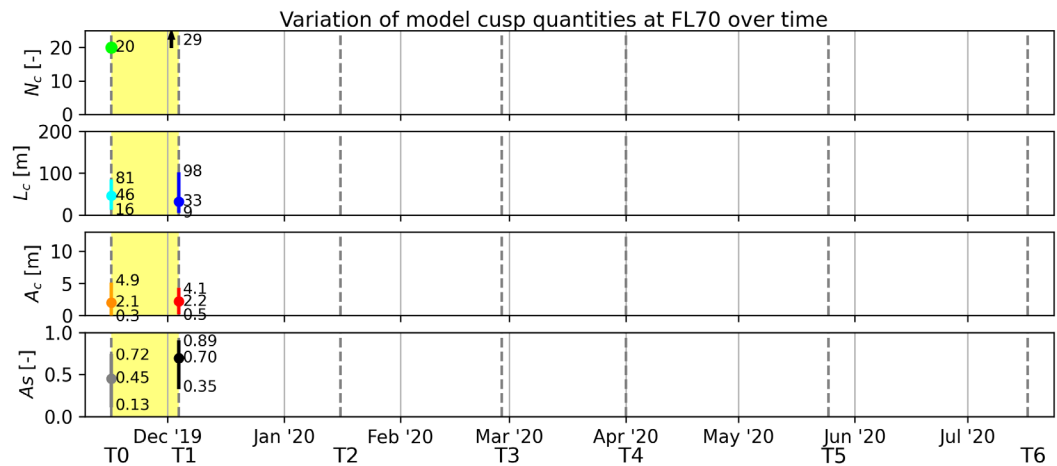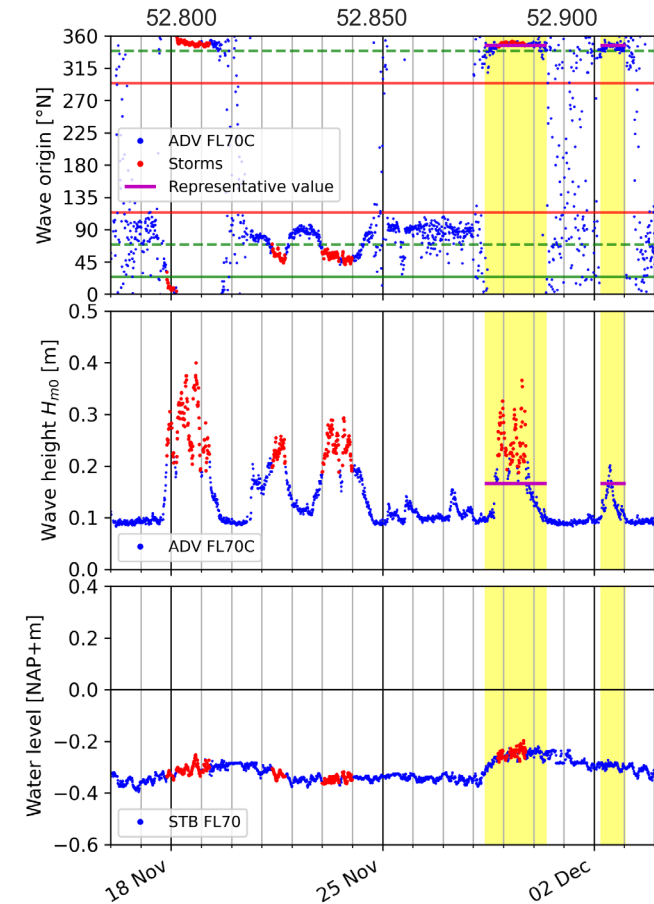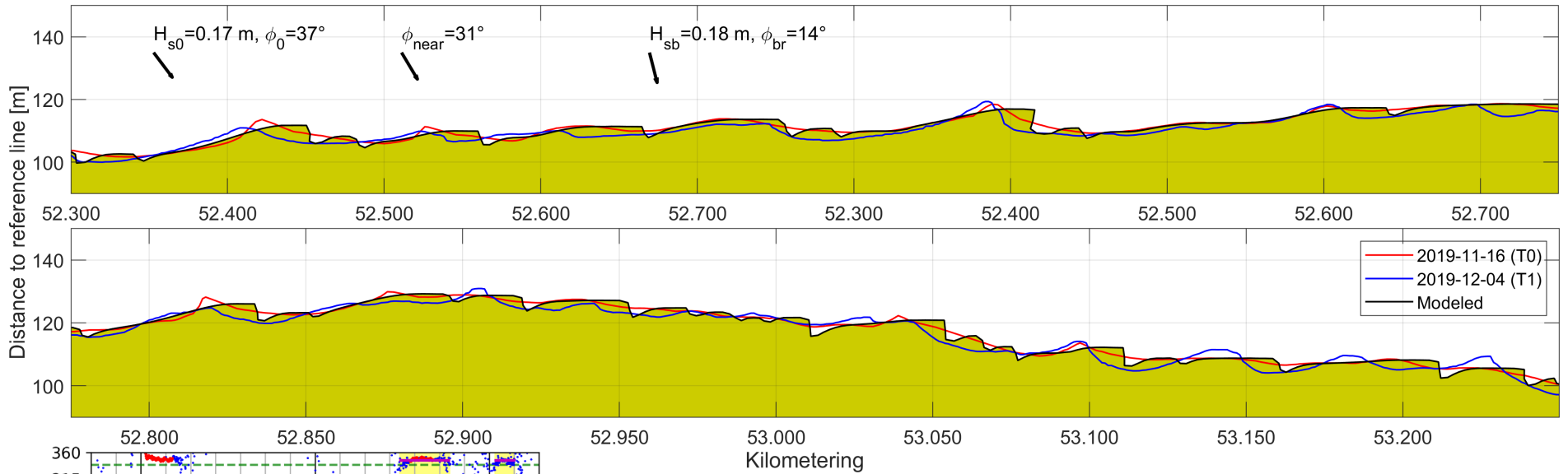
Measured waterline:

Increase of N_c, A_c and As, decrease of L_c; mostly corresponds with short-term exposure to high-angle waves from the North. We suspected the representative conditions to act as high-angle.

Modeled waterline:

Increase of N_c, A_c and As, decrease of L_c; mostly corresponds with short-term exposure to high-angle waves from the North. This simulation seems to also quantitatively look similar to the measured waterline of T1. Additionally, we see the emergence of new cusps, corresponding to the low-angle wave instability mechanism (Section 2.2.3).
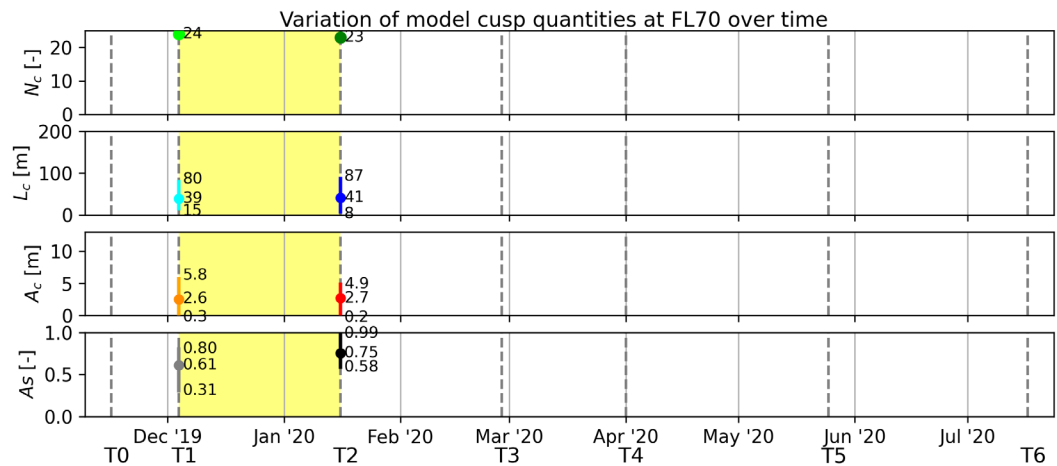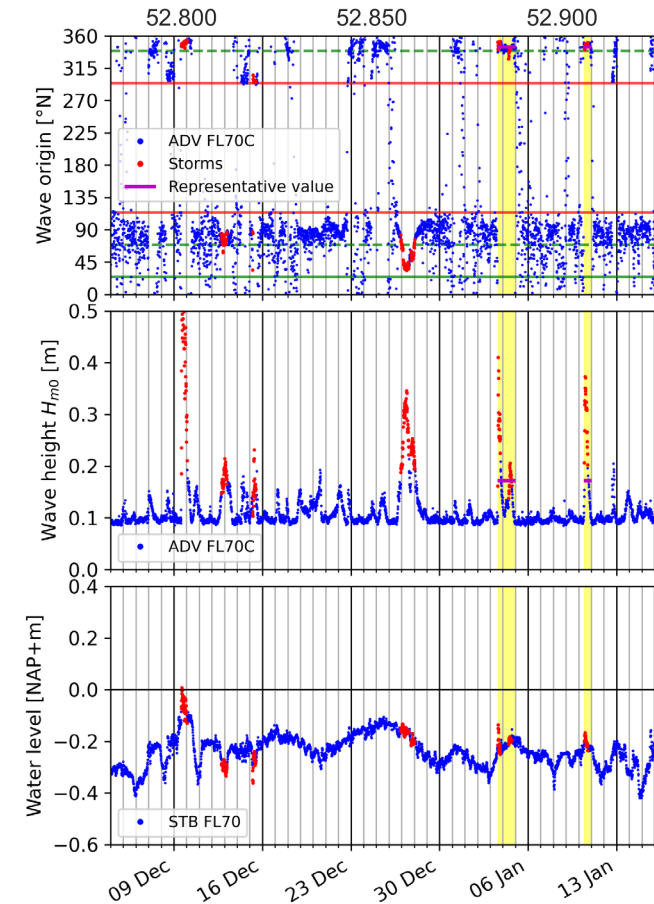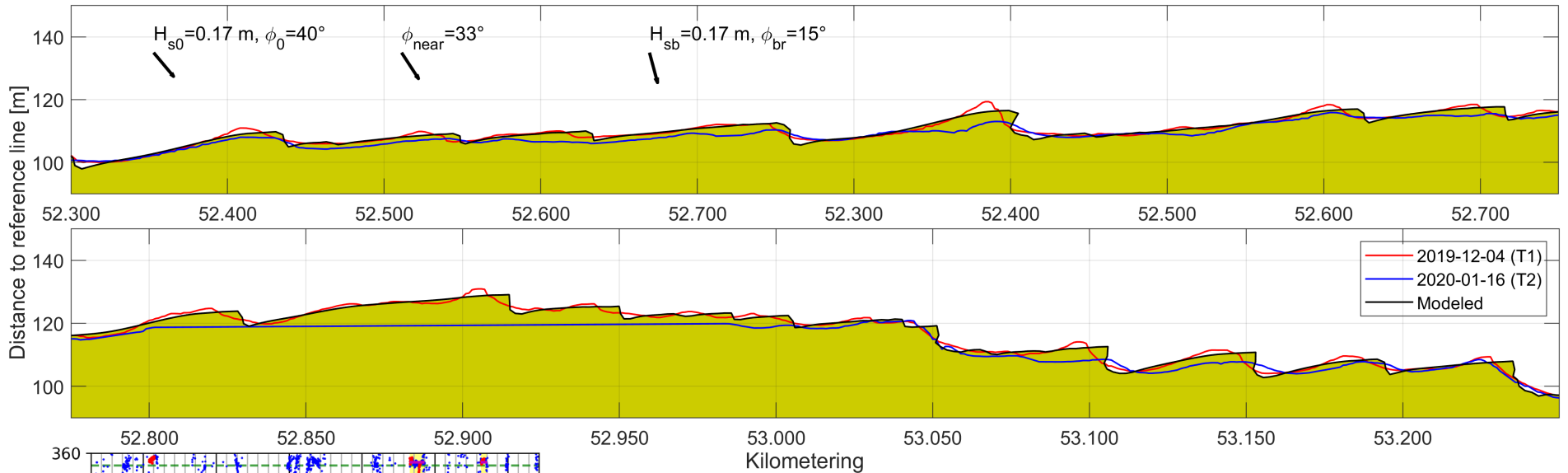
Measured waterline:
We assume a constant N_c. Other quantities are likely still relevant: Increase of L_c, decrease of A_c and As; mostly corresponds with a long-term exposure to low-angle waves from the North.

Modeled waterline:
Decrease of N_c, increase of L_c, A_c and As; fully corresponds with a short-term exposure to low-angle waves from the North, meaning it mostly corresponds to what the conceptual model predicts (long-term low-angle waves). We expected (Appendix E.9) the measured waterline to mostly be damped out by the water level fluctuations. The short-term response of the model results seem to agree with that, showing us that more is indeed needed for these changes to be considered long-term.
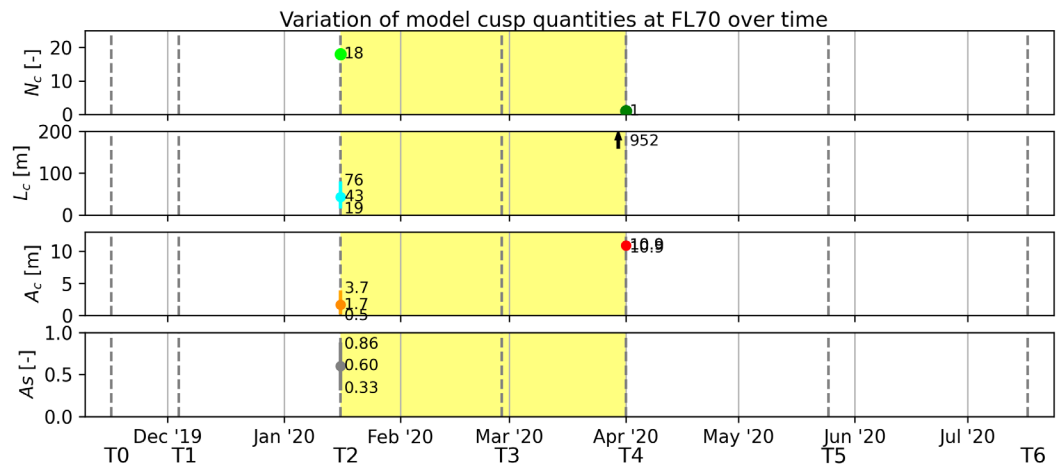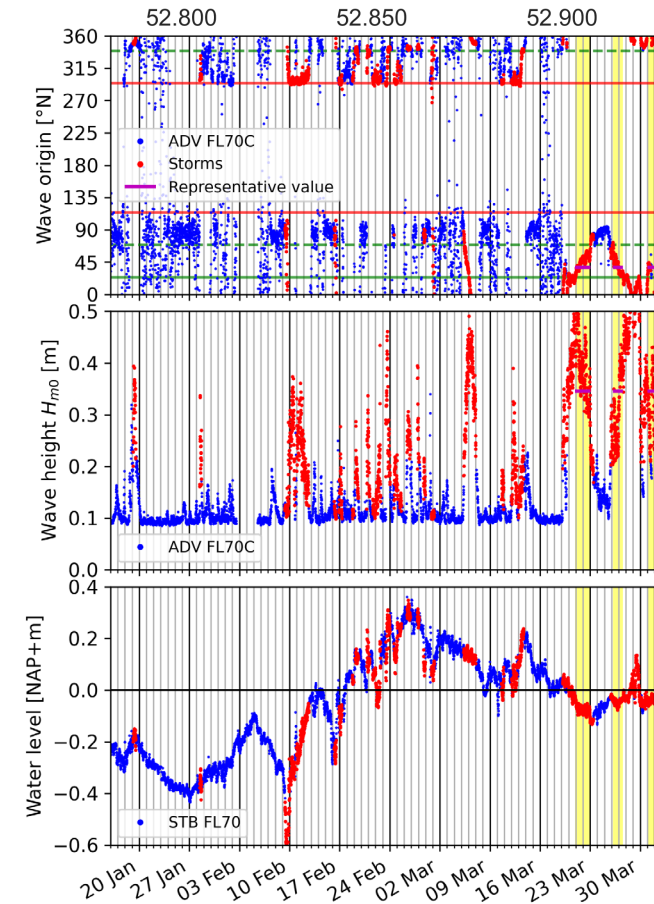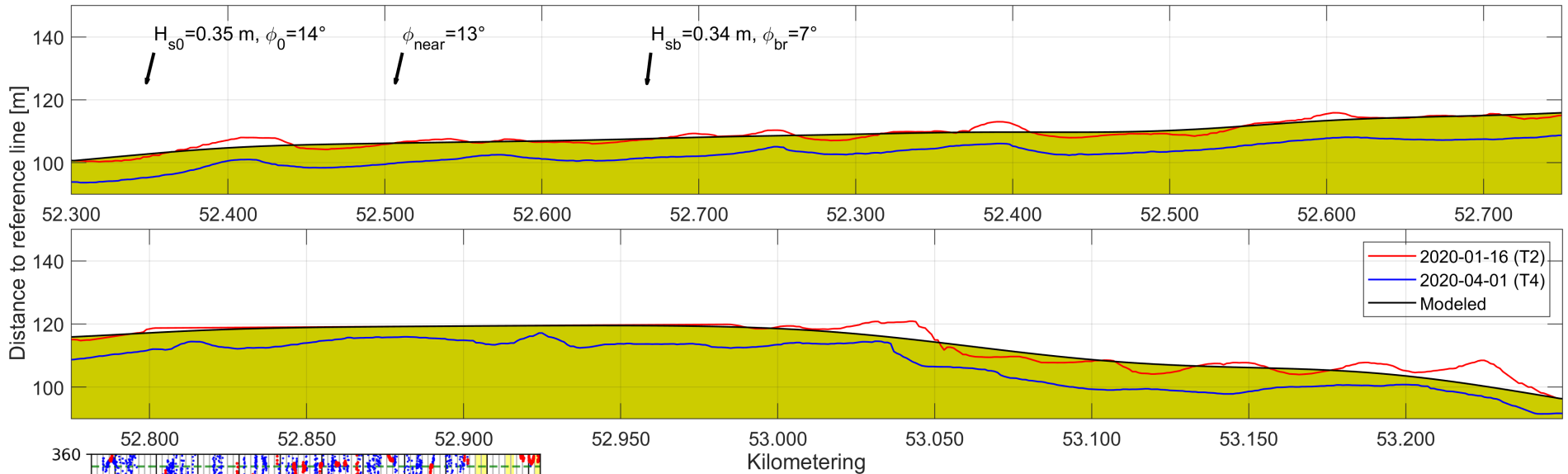
Measured waterline:

We assume a decrease in N_c. Increase of L_c, decrease of A_c and As; fully corresponds with long-term exposure to low-angle waves from the East.

Modeled waterline:

Decrease of N_c, increase of L_c and A_c; fully corresponds with short-term exposure to low-angle waves from the East, meaning it mostly corresponds to what the conceptual model predicts (long-term low-angle waves). Even though we were unable to quantify asymmetry, due to the flatness of the waterline, it seems that our representative period is considered short-term in the model results. It might be the case that the relatively large water level variations have played a role in making the measured response act long-term.
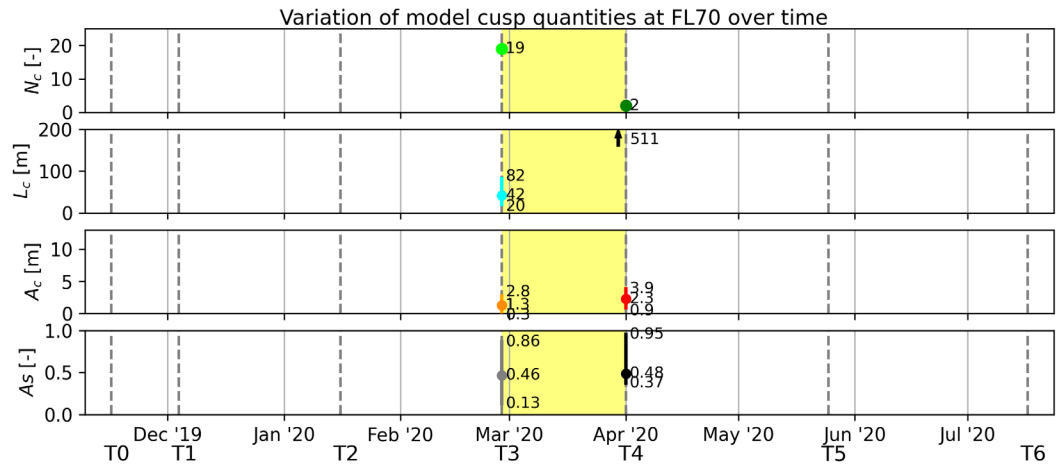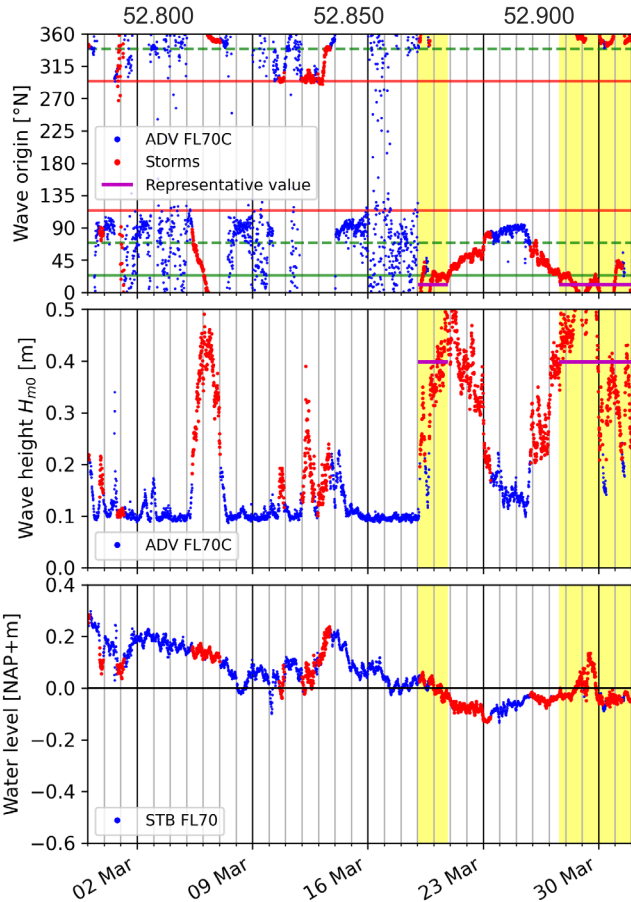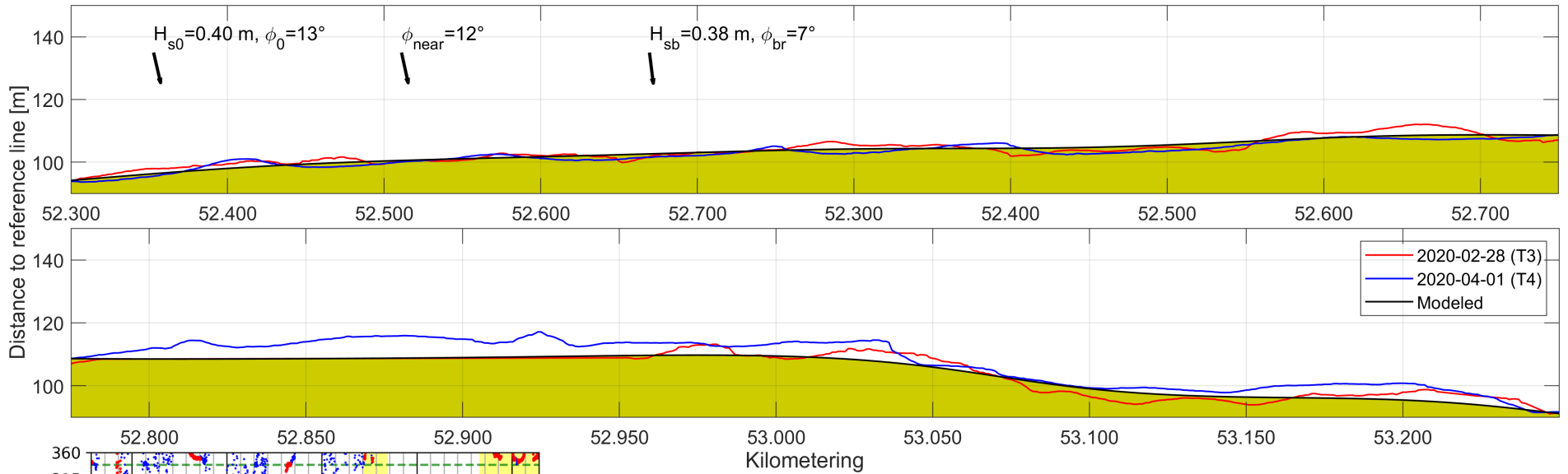
Measured waterline:
We assume a decrease in N_c. Increase of L_c and As, constant A_c; fully corresponds with long-term exposure to low-angle waves from the North.

Modeled waterline:
Decrease of N_c, increase of L_c, A_c and As; fully corresponds with short-term exposure to low-angle waves from the North, meaning it mostly corresponds to what the conceptual model predicts (long-term low-angle waves). Similar to the previous case, we suspect that the water level variations in this period caused the measured waterline to behave long-term.
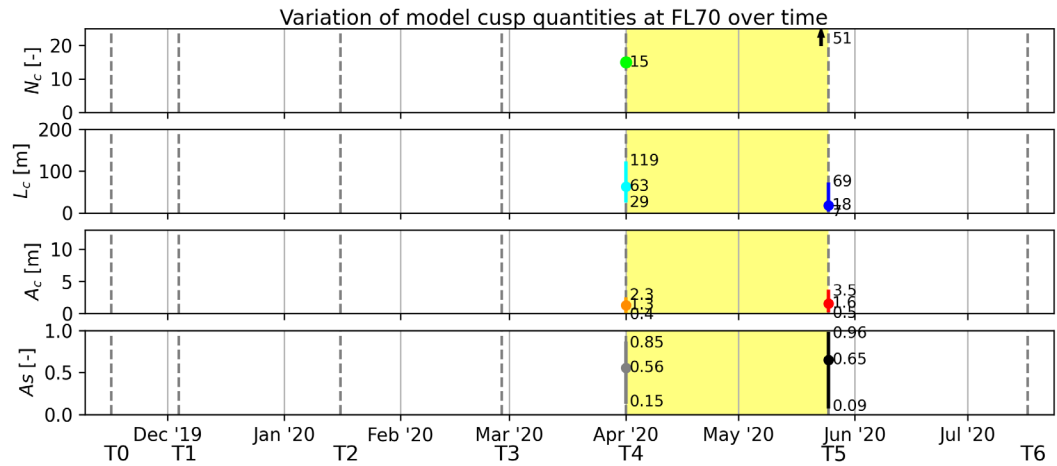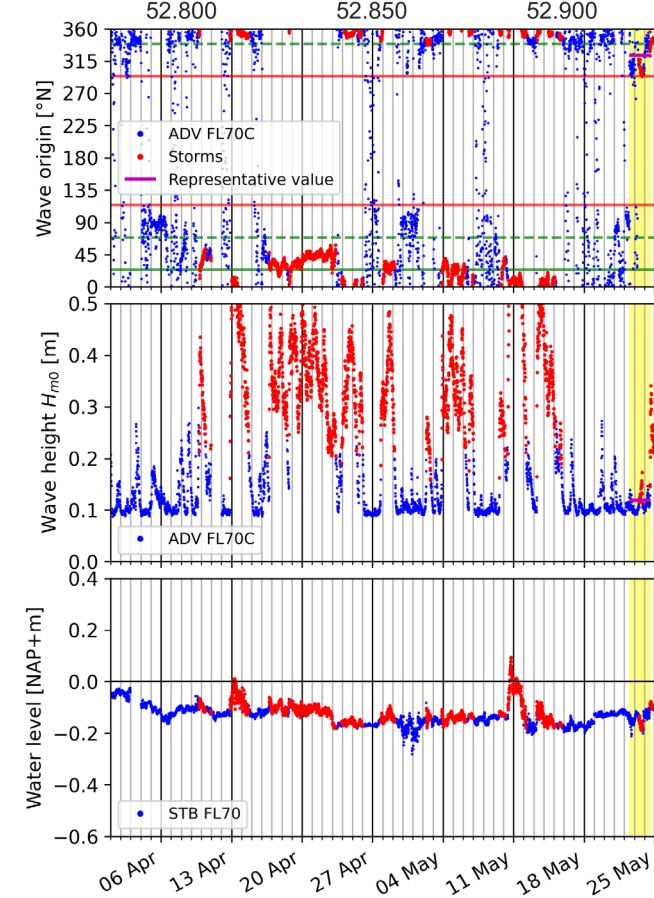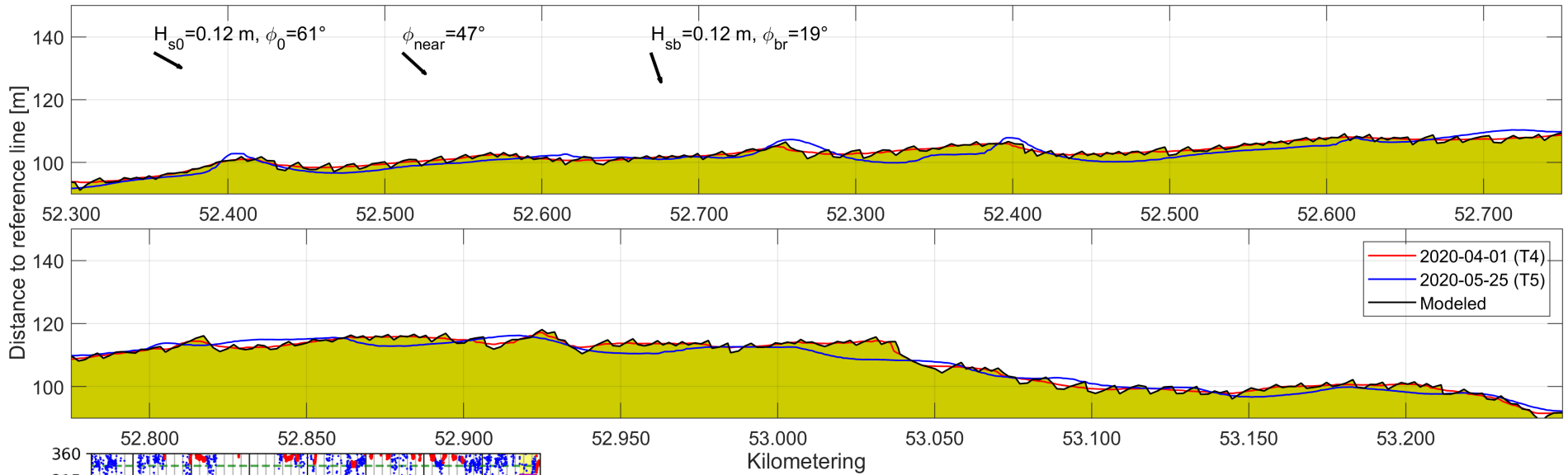
Measured waterline:

Increase of N_c and A_c, decrease of L_c and As; partly corresponds with short-term exposure to high-angle waves from the North.

Modeled waterline:

Increase of N_c and A_c and As, decrease of L_c; partly corresponds with short-term exposure to high-angle waves from the North. Given the representative high-angle hydrodynamics, we expect these results are in the transition from short-term to long-term exposure to high-angle waves (since the duration is about two and a half days). The amplitude has started to rise, and the next step will likely be the cusps absorbing each other and increase the average wavelength.
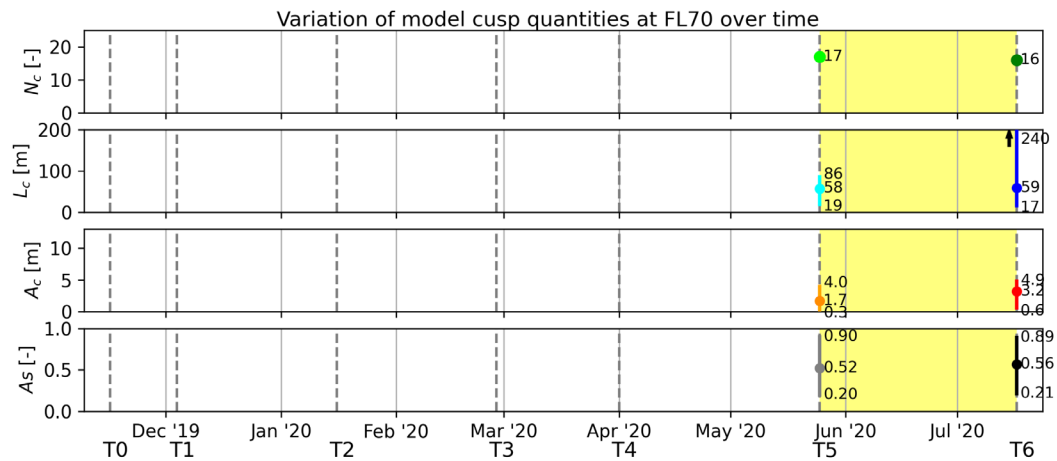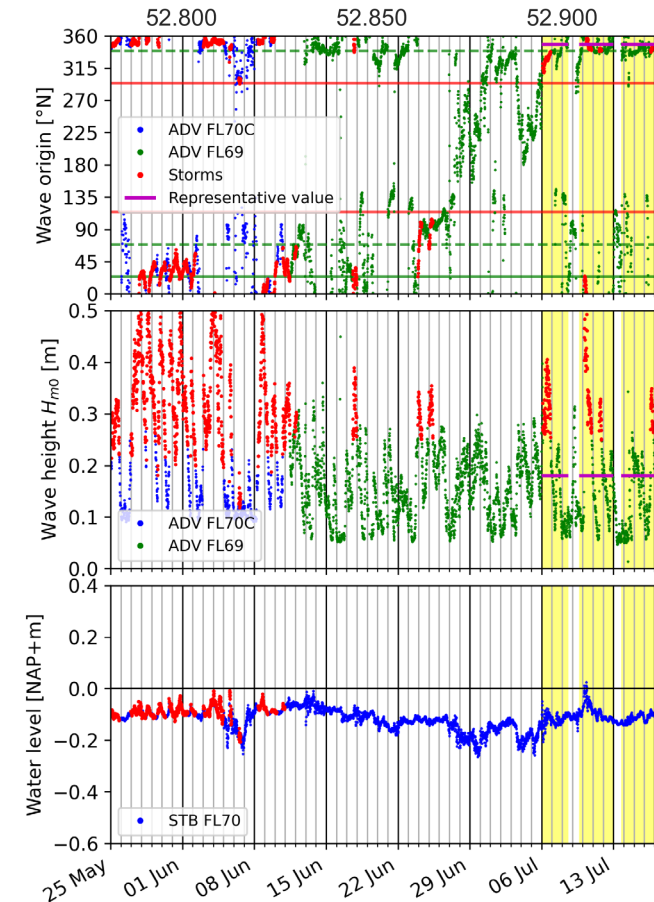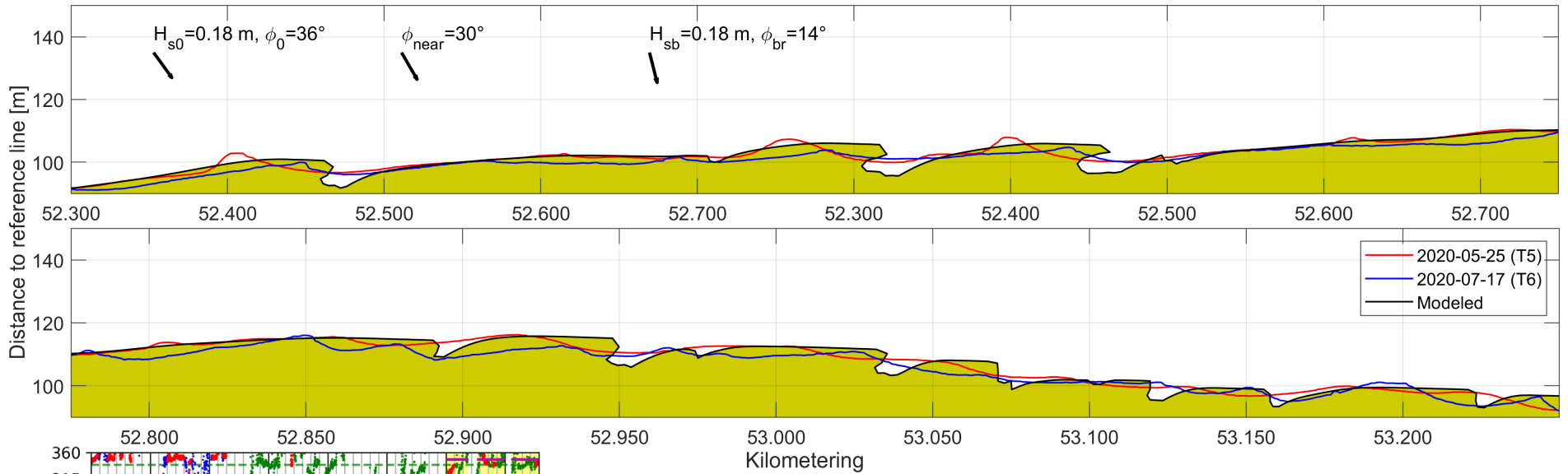
Measured waterline:

Increase of N_c, A_c and As, constant L_c; partly corresponds with long-term exposure to high-angle waves from the North.

Modeled waterline:

Decrease of N_c, increase of L_c, A_c and As; fully corresponds with long-term exposure to high-angle waves from the North. The representative hydrodynamics indicate low-angle conditions, but the response seems high-angle. The response seems to substantiate low-angle wave instabilities, but is likely simply numerical.